REPORT NO.
UCB/EERC-84/01
JANUARY 1984

EARTHQUAKE ENGINEERING RESEARCH CENTER

PSEUDODYNAMIC TEST METHOD FOR SEISMIC PERFORMANCE EVALUATION: THEORY AND IMPLEMENTATION

by

PUI-SHUM B. SHING
STEPHEN A. MAHIN

Report to the National Science Foundation

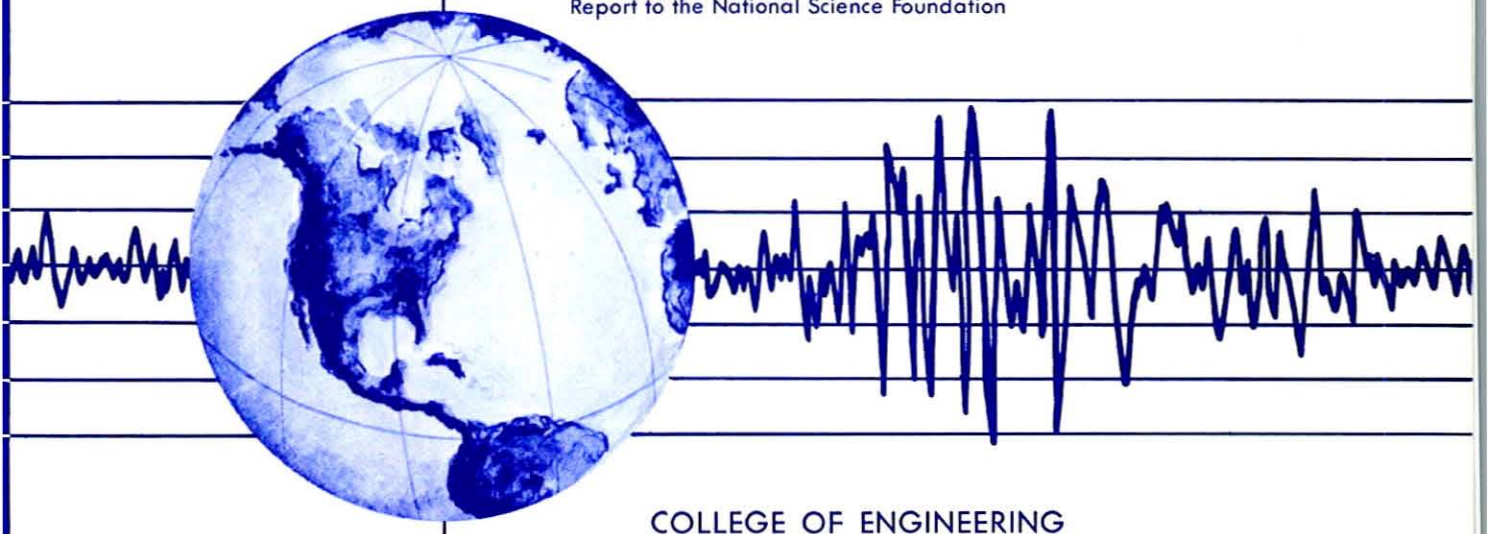

COLLEGE OF ENGINEERING

UNIVERSITY OF CALIFORNIA · Berkeley, California

50272-101

REPORT DOCUMENTATION PAGE	1. REPORT NO. NSF/CEE - 84016	2.	3. Recipient's Accession No. PB84 190644

4. Title and Subtitle

Pseudodynamic Test Method for Seismic Performance Evaluation: Theory and Implementation

5. Report Date January 1984

6.

7. Author(s)

P.-S. B. Shing and S.A. Mahin

8. Performing Organization Rept. No. UCB/EERC-84/01

9. Performing Organization Name and Address

Earthquake Engineering Research Center
University of California
1301 South 46th Street
Richmond, CA 94804

10. Project/Task/Work Unit No.

11. Contract(C) or Grant(G) No.

(C)

(G) CEE80-08584

12. Sponsoring Organization Name and Address

National Science Foundation
1800 "G" Street, NW
Washington, DC 20550

13. Type of Report & Period Covered

14.

15. Supplementary Notes

16. Abstract (Limit: 200 words)

The pseudodynamic test method is a relatively new experimental technique for evaluating the seismic performance of structural models in a laboratory by means of on-line computer control simulation. It is especially efficient for testing structures that are too large, heavy, or strong to be tested on available shaking tables. In the first part of this report, the fundamental theory of the pseudodynamic test method is examined. The adequacy of the analytical assumptions, and the reliability of the numerical methods are evaluated. The results of these studies provide useful guidelines for the selection of appropriate test specimens and realistic analytical models. The stability, accuracy, and error-propagation characteristics of numerical integration methods used in pseudodynamic testing are investigated, and guidelines for selecting appropriate integration time steps are obtained. Numerical techniques for suppressing error-propagation effects are presented. The second part discusses an implementation scheme for the pseudodynamic method. Some useful features of computer software are mentioned. The performance characteristics of necessary equipment are described and instrumentation precautions are pointed out. The last part presents the results of pseudodynamic tests recently performed at Berkeley. The results of these tests are correlated with analytical and shaking table test results for verifying the capability and reliability of the method.

17. Document Analysis a. Descriptors

b. Identifiers/Open-Ended Terms

c. COSATI Field/Group

18. Availability Statement:

Release Unlimited

19. Security Class (This Report)	21. No. of Pages 172
20. Security Class (This Page)	22. Price

(See ANSI-Z39.18) *See Instructions on Reverse*

OPTIONAL FORM 272 (4-77)
(Formerly NTIS-35)
Department of Commerce

PSEUDODYNAMIC TEST METHOD FOR SEISMIC PERFORMANCE EVALUATION: THEORY AND IMPLEMENTATION

by

Pui-shum B. Shing

and

Stephen A. Mahin

A Report to Sponsor
National Science Foundation

Report No. UCB/EERC-84/01
Earthquake Engineering Research Center
College of Engineering
University of California
Berkeley, California

January 1984

ABSTRACT

The pseudodynamic test method is a relatively new experimental technique for evaluating the seismic performance of structural models in a laboratory by means of on-line computer control simulation. It is especially efficient for testing structures that are too large, heavy, or strong to be tested on available shaking tables. This report presents the results of analytical and experimental studies that are carried out at Berkeley for evaluating the capabilities and limitations of the pseudodynamic test method. A method of implementation and results of several verification tests are presented and discussed as well.

The pseudodynamic test method combines well-established analytical techniques in structural dynamics with experimental testing. A test structure must be first idealized as a discrete-parameter system, so that the equations of motion for the system can be represented by second-order ordinary differential equations. Based on analytically prescribed inertial and viscous damping characteristics of the system, as well as on structural restoring forces directly measured during the test, the governing equations of motion for the test specimen can be solved by a step-by-step numerical integration method. The displacement response computed, based on a specific earthquake excitation record, is then imposed on the test structure by means of electro-hydraulic actuators. Thus, the quasi-statically imposed displacements of the test structure will resemble those that would actually be developed if the structure were tested dynamically.

Based on the above procedure, three major sources of errors can be introduced into a pseudodynamic test. First, the accuracy of the pseudodynamic method is limited by the reliability of the analytical techniques employed. A discrete-parameter model may not realistically reflect the actual dynamic characteristics of a continuous test specimen; and analytically prescribed viscous damping may be a highly idealized energy dissipation mechanism. Second, numerical integration can only yield an approximate solution to the equations of motion. Numerical errors introduced can distort the actual dynamic response characteristics of a system. Third, control and feedback errors are inevitable in most experiments. Since these errors are

introduced into numerical computations through displacement control and restoring-force feedback, significant cumulative errors can be induced in pseudodynamic test results.

The above problems will be investigated in this report, which can be divided into three major parts. In the first part, the fundamental theory of the pseudodynamic test method is examined. The adequacy of the analytical assumptions, and the reliability of the numerical methods are evaluated. The results of these studies provide useful guidelines for the selection of appropriate test specimens and realistic analytical models. The stability, accuracy, and error-propagation characteristics of numerical integration methods used in pseudodynamic testing are investigated, and guidelines for selecting appropriate integration time steps are obtained. Numerical techniques for suppressing error-propagation effects are presented. The second part discusses an implementation scheme for the pseudodynamic method. Some useful features of computer software are mentioned. The performance characteristics of necessary equipment are described and instrumentation precautions are pointed out. The last part presents the results of pseudodynamic tests recently performed at Berkeley. The results of these tests are correlated with analytical and shaking table test results for verifying the capability and reliability of the method.

In spite of certain limitations, the results of these studies indicate that the pseudodynamic test method can be as realistic and reliable as shaking table tests. However, to obtain accurate test results, high precision instruments and reliable numerical integration methods should be used. The experimental error-propagation effects can be estimated by mathematical equations and can be efficiently mitigated by numerical means. In addition, it has been shown that the method can provide better controlled experimental conditions than shaking table tests for large and heavy specimens.

ACKNOWLEDGEMENTS

The financial support provided by the National Science Foundation for the studies presented in this report and for the development of the pseudodynamic test system at Berkeley is gratefully acknowledged. Some support was also provided by the University of California Committee on Research for the purchase of computer graphics equipment in the laboratory.

Many persons have contributed their efforts to the development of the pseudodynamic test system at Berkeley. The authors are particularly in debt to Dr. Jerry Dimsdale for building the function generator and his assistance in the development of computer software. Chris Thewalt developed the computer graphics program and added several useful features to the pseudodynamic test program. The authors would also like to thank Stavros Dermitzakis for his assistance in the design and performance of experimental testing, and Amir Javadian-Gilani for doing the data reduction and analytical correlation for the tubular frame tests. Dave Steere was especially helpful in the system development. Albert Lawrence of the Machine Shop offered valuable advice and assistance in the experimental setup.

The work of Gail Feazell in preparing the figures of this reported is also appreciated.

Any opinions, findings, and conclusions or recommendations expressed in his report are those of the authors, and do not necessary reflect the views of the National Science Foundation.

TABLE OF CONTENTS

CHAPTER 1
INTRODUCTION

1.1. Seismic Performance Tests

During a severe seismic event, a structure should be able to sustain large deformations without collapse and be capable of dissipating substantial energy by inelastic deformations. By taking advantage of the inelastic load-resistance and energy-dissipation capabilities of a structure, it may be possible to reduce construction costs considerably without sacrificing the safety of the structure. Moreover, a ductile system provides a margin of safety against unusually severe seismic events. The inelastic performance of a structure is, however, complex and varies according to the intensity and frequency characteristics of seismic excitations, the dynamic and restoring force characteristics of the structure as a whole, the detailing of local critical regions within the structure, and the workmanship during construction. Although various analytical methods are available to predict the inelastic response of a structure, the confidence that can be placed in results obtained with them is severely limited by the uncertainties introduced by the simplified mathematical idealization of the structure and of its nonlinear member properties. For these reasons, experimental testing remains the most reliable means to evaluate the inelastic behavior of structural systems and to devise structural details to improve seismic performance. Various experimental methods are available for this purpose, such as shaking table tests, forced-vibration tests, and quasi-static tests. In addition, an on-line computer-control (or pseudodynamic) method has recently been developed [1] for assessing the inelastic seismic performance of large-scale structural models which cannot be tested realistically or efficiently by conventional methods.

Shaking table testing is one of the most realistic and reliable experimental methods for evaluating the inelastic seismic performance of a particular structure. Nevertheless, the size, weight, and strength of structures which can be subjected to simulated earthquake excitations are significantly limited by the capacity of available tables [2,3]. Installing a new shaking table facility or increasing the capacity of an existing one is generally a very costly option. These

limitations also require most structures to be tested at significantly reduced scales, and thus, raise the problem of dynamic and material similitude [2,3]. In addition, problems of table-structure interaction [4] may develop for heavy specimens. This leads to tremendous difficulties in interpreting test results and in correlating them with analytical predictions.

Dynamic tests into the inelastic range can also be performed using mechanical excitors [5a], pulse generators [5b], or blast-induced ground motions [6]. The excitations imposed by a few excitors will probably result in different inertia-force distributions on structures than earthquake motions. Since the inelastic seismic response of a structure is sensitive to the distribution and history of inertia forces, it may be difficult to interpret the results in terms of the actual seismic performance of the test structure during earthquake excitations. However, such methods are useful for evaluating the dynamic characteristics of a structure and for predicting its elastic structural response. Blast induced ground motions can be similar in character to seismic excitations. Nevertheless, the high costs required for these and other innovative dynamic test methods might limit their use to special structures or complex problems involving soil-foundation-structure interaction.

In view of these difficulties, quasi-static testing remains the most economical and versatile experimental method for assessing and comparing the inelastic energy-dissipation capabilities and failure mechanisms of different structural designs. In quasi-static tests, small structural systems or basic subassemblages from large structures are subjected to a prescribed load or deformation history. Such tests utilize conventional equipment that is available in most structural laboratories and allow for detailed observation of structural behavior during tests. To determine appropriate loading histories in these tests, an inelastic dynamic computer analysis can be performed for the structure in question. The displacements computed at various locations in the structure can then be used to control the experiment [7]. Unfortunately most mathematical idealizations are much simpler than actual structural behavior, so that computed loading histories are not likely to be realistic. Because of this, it is more common to assume *a priori* a highly idealized deformation history that is characteristic of the general cyclic nature of seismic

response [8]. Such prescribed displacement histories can be particularly valuable in: (i) assessing the effect of different structural details on the inelastic behavior of structures by subjecting different specimens to identical deformation histories; and (ii) studying the basic mechanisms that affect the inelastic behavior of a particular structure by varying the amplitude, rate or pattern of the applied deformation histories. However, it is not possible to directly relate the energy-dissipation capacity of a specimen measured in this type of test with that required for seismic safety. Consequently, questions continually arise with such experiments as to whether the specimen is under- or over-tested.

To facilitate the formulation of more rational and reliable seismic-resistant design methods, it is desirable to develop methods for prescribing more realistic displacement histories for quasi-static tests. One potential method for doing this would be use of on-line computer control methods. This so-called pseudodynamic test method has the potential for combining the economy and versatility of conventional quasi-static testing with the realism of shaking table tests.

1.2. The Pseudodynamic Test Method

The pseudodynamic test method uses the same basic equipment as conventional quasi-static tests. It differs from the conventional quasi-static method in that the displacement history imposed on a test specimen is determined by a computer during a test based on the measured dynamic characteristics of the specimen and a specified seismic excitation record. These histories are imposed on the specimen quasi-statically and should closely resemble those that would be developed if the specimen were tested dynamically. To accomplish this, a test structure is first idealized as a discrete-parameter system, the inertial and damping characteristics of which are analytically prescribed. The displacement response of the test specimen to a prescribed seismic excitation is then evaluated by solving the governing equations of motion for the system using well-established, step-by-step numerical integration algorithms. Based on the measured restoring-force characteristics of the structure from the previous step or steps and the

prescribed inertial and damping characteristics, the displacement response in each step of a test is computed and imposed on the specimen using hydraulic actuators. This method, therefore, utilizes the same numerical approach generally used in nonlinear structural dynamics, except that structural restoring force characteristics are based directly on experimental feedback rather than on idealized mathematical models.

Consequently, the pseudodynamic method can simulate the realistic seismic response of structural specimens in a laboratory without the uncertainties associated with nonlinear mathematical models of structures. The method provides more informative results, regarding seismic performance of a structure, than conventional quasi-static testing by taking into account the dynamic characteristics of a test specimen and of the excitation. However, it retains the simplicity and versatility of quasi-static tests, provides well-controlled experimental conditions, and allows for detailed observation of structural behavior during a test. Thus, the pseudodynamic method offers a good alternative for seismic performance testing when shaking table facilities are not available or the test requirements exceed the capabilities of available tables.

The pseudodynamic method has been successfully applied by Japanese researchers to tests of various structural systems, including single-degree-of-freedom (SDOF) and multiple-degree-of-freedom (MDOF) steel and reinforced concrete structures [9-11]. The results of these tests correlated well with analytical and shaking table test results [10,11]. However, certain mechanical and numerical problems have been experienced in testing stiff systems which have large numbers of degrees of freedom [12,13]. The major problems in these tests were identified to be caused by errors in displacement control using electro-hydraulic actuator systems and the sensitivity of numerical computations to experimental errors. To reduce displacement control errors, improved actuator-control techniques are currently under development at the University of Michigan, Ann Arbor [14]. The propagation of experimental errors in numerical computations has been investigated and methods for eliminating or suppressing the error effects have been developed at the University of California, Berkeley [15]. Experimental studies at Berkeley also indicate that precise displacement control can be achieved if the electrical and mechanical

components of an actuator-controller system are appropriately adjusted and if the load and velocity applied are within the capacities of the system.

According to the previous studies, one can obtain very reliable pseudodynamic test results by using high performance test equipment, and appropriate instrumentation and numerical techniques. However, problems related to the fundamental principles of the pseudodynamic method have to be clearly understood by the user before it can be applied with confidence. It must be realized that the structural discretization and numerical integration techniques used in pseudodynamic testing only provide an approximate solution for the dynamic response of a test structure. The accuracy of test results depends largely on the selection of appropriate test specimens, the determination of realistic discrete-parameter models, and the use of reliable numerical methods. For example, a structure which has very uniformly distributed mass may require such a large number of degrees of freedom in a discrete-parameter idealization that pseudodynamic testing is no longer efficient. In order to insure accurate numerical results, the stability and accuracy of the step-by-step integration method should be fully understood, especially with regards to the selection of appropriate integration time intervals. Additionally, viscous damping, strain-rate effects, and the performance of loading apparatus may all affect the results of pseudodynamic tests and must be carefully considered in planning a test. These problems need to be identified and carefully examined before the pseudodynamic method can be applied with confidence.

1.3. Objectives and Scope

The main objectives of this report are to examine the underlying theory for the pseudodynamic test method and to evaluate its capabilities and limitations. In doing that, the fundamental problems related to structural idealization and numerical integration are investigated. The implementation of the method is discussed as well to illustrate the development of necessary experimental equipment and computer software. The performance characteristics of the test equipment are examined to offer some guidelines for proper instrumentation and test

preparation. Finally, the practicability and reliability of the pseudodynamic method will be verified by correlating the results of several pseudodynamic tests recently performed at Berkeley with analytical and shaking table test results.

In Chapter 2 of this report, we review some of the well-established analytical techniques in structural dynamics and seek the theoretical justification for the pseudodynamic approach. Furthermore, factors to be considered in selecting numerical integration algorithms applicable to pseudodynamic testing, and methods for their implementation are discussed. In Chapter 3, the numerical properties of the selected integration methods are examined. The stability and accuracy of the methods in computing the dynamic response of linear and nonlinear systems are considered, and suggestions are offered for the selection of the most desirable method and the determination of appropriate integration time intervals. The effects of experimental errors on numerical computations, and numerical techniques for suppressing error-propagation effects are briefly summarized from a previous study [15]. In Chapter 4, the adequacy of discrete-parameter models in idealizing test structures is investigated. The determination of viscous damping properties and the significance of strain-rate effects are also considered. In Chapter 5, the implementation of the pseudodynamic method is briefly discussed based on the recently installed facility at Berkeley. The characteristics of various experimental equipment are examined, and proper instrumentation techniques and error checking procedures are recommended. The results of pseudodynamic tests on a simple SDOF system are presented and correlated with analytical predictions. In Chapter 6, we presents the pseudodynamic test results of a tubular steel frame which was previously tested on a shaking table. The results of the two experiments are compared. The advantages and disadvantages of the two experimental methods are discussed. In Chapter 7, we offer general conclusions regarding the practicability and limitations of the pseudodynamic method, as well as potential future applications, based on the analytical and experimental studies presented herein.

CHAPTER 2
THEORETICAL BACKGROUND

2.1. The Pseudodynamic Test Procedure

The pseudodynamic method combines well-established analytical techniques in structural dynamics with experimental testing. A test structure is first idealized as a discrete-parameter system such that the equations of motion for the system can be represented by a family of second-order ordinary differential equations. The inertial and viscous damping characteristics of the system are analytically prescribed, such that the dynamic characteristics of the test structure are accurately represented. During a test, the equations of motion are solved by means of direct step-by-step numerical integration. The displacement response computed in each step of a test is imposed quasi-statically on the test structure by hydraulic actuators. The restoring forces developed by structural deformations are, then, physically measured with load transducers, and fed back to a numerical algorithm for the computation of displacement response in the next step. A digital computer is used for all the numerical computations and experimental control.

In this chapter, theoretical justifications of the above procedure will be examined. The implementation of different integration algorithms for pseudodynamic testing will be discussed. The numerical characteristics of these algorithms and their adequacy for the experimental application will be considered. Based on these understandings, we will identify the possible sources of inaccuracies in pseudodynamic experiments.

2.2. Discrete-Parameter Structural Model

In a dynamic analysis, a structural system can be considered as an assemblage of structural elements interconnected at a finite number of nodal points, at which the mass of the system is assumed to be concentrated. The deformation state of this idealized discrete-parameter system is completely determined by the degrees of freedom at the nodal points. This discretization method is intended to simplify the analytical procedure for a structural system which actually has uniformly distributed mass and an infinite number of degrees of freedom. The analyses of

such continuous systems involve the solution of partial differential equations, which can be a formidable task even for a very simple structure. However, the equations of motion for a discrete-parameter system can be represented by a family of second-order ordinary differential equations, which can be expressed in a matrix form as

$$\mathbf{m}\,\mathbf{a} + \mathbf{c}\,\mathbf{v} + \mathbf{k}\,\mathbf{d} = \mathbf{f} \tag{2.1}$$

where **m**, **c**, and **k** are the mass, viscous damping, and stiffness matrices of the system; **d** is a vector representing nodal displacements; **v** and **a** are the velocity and acceleration vectors, which are, respectively, the first- and second-order time derivatives of **d**; and **f** is an external force excitation vector. As in the above equation, all vector and matrix quantities are represented by boldfaced variables in this report. This matrix equation can be conveniently solved by numerical methods with the help of a digital computer.

The equations of motion for a discrete-parameter system can be formulated by the finite element method [16]. Using this analytical method, we can formulate the mass and stiffness matrices of structural elements, from which we can assemble the global stiffness and mass matrices of a structure by the direct stiffness method. The viscous damping matrix is usually constructed based on some idealized modal damping properties of a system, e.g., the damping can be conveniently assumed to be stiffness or mass proportional, or both. The total number of degrees of freedom in such a system is the sum of degrees of freedom at all nodal points. Consequently, a discrete-parameter model can only represent a finite number of degrees of freedom of a continuous system, and the higher mode effects of the system are neglected. It is, therefore, natural to realize that better solutions can be obtained by increasing the number of nodal points or degrees of freedom of a model. In general, a small number of degrees of freedom will be sufficient to provide an accurate solution because the higher frequency responses of a structure are usually insignificant under seismic excitations. The selection of nodal points or the number of degrees of freedom depends on the physical properties of the structure and the characteristics of external excitations.

Consequently, the adequacy of a discrete-parameter model depends on how well the dynamic behavior of a continuous system is represented by the vibration modes of the model under a specific type of external excitation. Consider, for example, a steel braced frame shown in Fig. 2.1a. The frame can be idealized as an assemblage of 36 elements interconnected at 20 nodal points (see Fig. 2.1b). Since each node can have three independent displacement components, the frame has a total of 54 degrees of freedom after excluding the two fixed nodes at the base. If the beam and column members of the frame are relatively stiff in axial deformations, then the total number of degrees of freedom can be reduced to 30 (see Fig. 2.1c). The corresponding 30×30 stiffness and mass matrices of the frame can be obtained by the finite element method. However, further simplification is possible if most of the mass is concentrated at the story levels, such as the dead loads contributed by floor systems, and if the frame is excited by horizontal ground accelerations dominated by relatively low frequencies. In that case, only the six lateral degrees of freedom need to be considered in response computations (see Fig. 2.1d). The stiffness of the reduced system can be derived from the original 30×30 matrix by static condensation. Since the rotational inertia at the nodal points is neglected and the translational inertial effects at the floor levels can be considered as uncoupled, the mass matrix becomes diagonal representing only the mass lumped at each story level.

It is apparent that significant computational effort is saved by the static condensation procedure. Even though the higher frequency responses of a system are lost in a reduced model, a lumped-mass idealization (as the one in Fig. 2.2d) is, very often, preferred by an analyst because of the computational efficiency and the fact that the higher frequency responses are usually insignificant.

In pseudodynamic testing, a test structure has to be idealized as a discrete-parameter system with the same considerations as above. Based on an idealized model, the mass and damping matrices of a test structure are analytically constructed. Nevertheless, the restoring forces developed by structural deformations at the selected nodal points are experimentally measured during a test, such that analytical formulation of the stiffness matrix is not required. Although

the pseudodynamic method is not restricted to any specific type of structural models, a lumped-mass idealization can tremendously simplify the experimental setup and numerical formulation. In addition, since structural displacements and restoring forces are imposed and measured, respectively, at a selected set of degrees of freedom, and the mass matrix is constructed accordingly, a static condensation procedure is implicitly applied to a structure during a pseudodynamic test. Therefore, the result of a pseudodynamic test should be considered as a quasi-statically simulated dynamic response of a reduced structural model. This result should closely represent the actual dynamic behavior of the test structure as long as the higher frequency responses neglected by the model are insignificant.

Consequently, pseudodynamic testing should be theoretically as reliable as those general analytical techniques. In addition to that, the stiffness property of a structure is experimentally measured during a test, so that the uncertainties associated with the modeling of nonlinear material behavior in structural analyses are avoided.

2.3. Numerical Schemes

2.3.1. General Step-By-Step Integration Methods

The equations of motion for a nonlinear structural system can be most conveniently solved by a direct step-by-step integration method under any arbitrary external excitations. In step-by-step integration, the duration T for which the structural response is to be evaluated is divided into N equal time intervals Δt, i.e., $\Delta t = T/N$. By considering the equilibrium equations (Eq. (2.1)) at time equal to 0, Δt, $2\Delta t$,....., and $N\Delta t$, and assuming that the solution in each step is a function of those in the previous step or steps, we can obtain an approximate solution of the equations of motion. These numerical methods can, generally, be classified into two types: explicit and implicit methods. We adopt the definition that an integration method is explicit if the displacement solution in each step is assumed to be a function of previous step solutions only. Otherwise, the method is considered as implicit.

The stability and accuracy of an integration method are two important criteria for determining the reliability of the method. A stable method is defined as one by which the numerical solution of a free-vibration response will not grow without bound for any arbitrary initial conditions [17]. If a method is stable and if the numerical solution will approach the exact solution as Δt approaches zero, then the method is convergent. This is an essential condition for obtaining reliable numerical solutions. Many implicit methods are unconditionally stable, i.e., they are stable for any value of $\omega\Delta t$, where ω is a natural frequency of the system analyzed. Explicit methods are, generally, conditionally stable, but are computationally more efficient. In that case, numerical solutions become unstable when $\omega\Delta t$ exceeds a certain value. In spite of that, explicit methods are usually more preferable than implicit methods when the number of degrees of freedom of a structure is small, such that the magnitude of Δt is not severely restrained by the stability condition on the highest frequency mode of the structure.

One of the most general integration methods in structural dynamics is the Newmark Algorithm [18], which assumes that

$$\mathbf{m}\,\mathbf{a}_{i+1} + \mathbf{c}\,\mathbf{v}_{i+1} + \mathbf{k}\,\mathbf{d}_{i+1} = \mathbf{f}_{i+1} \tag{2.2}$$

$$\mathbf{d}_{i+1} = \mathbf{d}_i + \Delta t\,\mathbf{v}_i + \Delta t^2\left[\left(\frac{1}{2} - \beta\right)\mathbf{a}_i + \beta\,\mathbf{a}_{i+1}\right] \tag{2.3}$$

$$\mathbf{v}_{i+1} = \mathbf{v}_i + \Delta t\,[(1-\gamma)\,\mathbf{a}_i + \gamma\,\mathbf{a}_{i+1}] \tag{2.4}$$

in which $\mathbf{a}_{i+1}$, $\mathbf{v}_{i+1}$, and $\mathbf{d}_{i+1}$ are the acceleration, velocity, and displacement vectors, respectively, at time equal to $(i+1)\Delta t$; and β and γ are parameters selected by the user to achieve desirable stability and accuracy properties. For example, by letting β equal to 1/4 and γ equal to 1/2, we have the constant-average-acceleration method, which is implicit and unconditionally stable. When β is zero, the $\mathbf{a}_{i+1}$ term in Eq. (2.3) disappears and the method becomes explicit.

2.3.2. Algorithms for Pseudodynamic Application

From Eqs. (2.2) to (2.4), we can observe that the determination of $\mathbf{d}_{i+1}$ in terms of $\mathbf{d}_i$, $\mathbf{v}_i$, and $\mathbf{a}_i$ by an implicit integration method requires the explicit knowledge of stiffness matrix $\mathbf{k}$. Nevertheless, in pseudodynamic testing, only the product $\mathbf{k}\cdot\mathbf{d}_{i+1}$ can be measured experimentally as a restoring force vector $\mathbf{r}_{i+1}$ after $\mathbf{d}_{i+1}$ is computed and physically imposed on a test structure. In general, the stiffness matrix of a nonlinear system cannot be accurately determined during a pseudodynamic test. Even though $\mathbf{r}_i$ and $\mathbf{d}_i$ are known in each step of a test, we usually do not have sufficient information to compute the instantaneous tangent stiffness $\mathbf{k}_i$ for a highly coupled MDOF nonlinear system. Where a method for determining the tangent stiffness can be devised, the resulting values may be overly sensitive to errors in experimental measurements. Furthermore, due to the change of tangent stiffness from one integration step to the next, the solution of nonlinear differential equations by an implicit method usually requires iterative corrections, which are highly undesirable for testing inelastic systems because the inelastic restoring forces developed depend very much on the displacement history of the structure. The internal displacement cycles carried through during iterative corrections may result in an erroneous convergence. To avoid these problems, explicit integration methods are recommended for pseudodynamic testing.

Since only a limited number of structural degrees of freedom are generally involved in a pseudodynamic test, the stability criterion imposed by an explicit integration method will not usually affect the efficiency of the test method. Furthermore, explicit methods are generally as accurate as implicit ones. In the following, the formulations and implementation schemes of four different explicit methods which have been recommended for pseudodynamic testing are discussed. The adequacy of the methods for the experimental application is evaluated and compared as well.

(i) The Basic Central Difference Method

The central difference method is one of the most widely used integration technique in dynamic analysis. It was initially selected by Japanese researchers for pseudodynamic testing [19] because of its efficiency and accuracy. In the central difference method, the velocity and acceleration are assumed to be represented by the following difference equations:

$$\mathbf{v}_i = \frac{\mathbf{d}_{i+1} - \mathbf{d}_{i-1}}{2\,\Delta t} \tag{2.5}$$

$$\mathbf{a}_i = \frac{\mathbf{d}_{i+1} - 2\,\mathbf{d}_i + \mathbf{d}_{i-1}}{\Delta t^2} \tag{2.6}$$

By substituting these equations into the equilibrium equation

$$\mathbf{m}\,\mathbf{a}_i + \mathbf{c}\,\mathbf{v}_i + \mathbf{r}_i = \mathbf{f}_i \tag{2.7}$$

where $\mathbf{r}_i$ is the restoring force directly measured in a pseudodynamic test, we can solve for $\mathbf{d}_{i+1}$ in terms of $\mathbf{d}_i$, $\mathbf{d}_{i-1}$, and $\mathbf{r}_i$. It is, therefore, a two-step method. The application of this algorithm to pseudodynamic testing is illustrated by the flow diagram in Fig. 2.2a.

(ii) The Summed-Form Central Difference Method

The summed form of the central difference method can reduce unfavorable rounding errors which may occur in the basic central difference method when Δt is very small [20]. This method was suggested by Powers [21] for pseudodynamic testing. In this method, we define $\mathbf{z}_i = (\mathbf{d}_{i+1} - \mathbf{d}_i) / \Delta t$. Consequently, we have $\mathbf{z}_{i+1} - \mathbf{z}_i = \Delta t\ \mathbf{a}_{i+1}$ and $\mathbf{z}_{i+1} + \mathbf{z}_i = 2\,\mathbf{v}_{i+1}$, according to Eqs. (2.5) and (2.6). By substituting these relations into the equilibrium equation

$$\mathbf{m}\,\mathbf{a}_{i+1} + \mathbf{c}\,\mathbf{v}_{i+1} + \mathbf{r}_{i+1} = \mathbf{f}_{i+1} \tag{2.8}$$

we obtain

$$\mathbf{z}_{i+1} = \left(\frac{\mathbf{m}}{\Delta t} + \frac{\mathbf{c}}{2}\right)^{-1} \left[\mathbf{f}_{i+1} - \mathbf{r}_{i+1} + \mathbf{z}_i \left(\frac{\mathbf{m}}{\Delta t} - \frac{\mathbf{c}}{2}\right)\right] \tag{2.9}$$

Although this method has a different numerical formulation, it is mathematically identical to the basic central difference method. The implementation of the method for pseudodynamic testing is shown in Fig. 2.2b.

(iii) The Newmark Explicit Method

An explicit form of the Newmark integration method can be obtained by letting $\beta = 0$ and $\gamma = 1/2$ in Eqs. (2.3) and (2.4). Although this is a one step method, the algorithm is, again, mathematically equivalent to the basic central difference method. The application of this algorithm to pseudodynamic testing is suggested by Mahin and Williams [22], and is illustrated in Fig. 2.2c.

(iv) The Modified Newmark Algorithm

The three explicit algorithms discussed above do not have a numerical dissipation property. As will be shown later, numerical dissipation is useful for suppressing the spurious growth of high frequency responses due to experimental errors in a MDOF test. A modified Newmark explicit method was proposed by Shing and Mahin [15]. The numerical damping in this algorithm is approximately frequency-proportional. This modified method has the following formulation:

$$\mathbf{m}\,\mathbf{a}_{i+1} + \left[\left(1+\alpha\right)\mathbf{k} + \frac{\rho}{\Delta t^2}\,\mathbf{m}\right]\mathbf{d}_{i+1} = \mathbf{f}_{i+1} + \left[\alpha\,\mathbf{k} + \frac{\rho}{\Delta t^2}\,\mathbf{m}\right]\mathbf{d}_i \tag{2.10}$$

$$\mathbf{d}_{i+1} = \mathbf{d}_i + \Delta t\;\mathbf{v}_i + \frac{\Delta t^2}{2}\,\mathbf{d}_i \tag{2.11}$$

$$\mathbf{v}_{i+1} = \mathbf{v}_i + \frac{\Delta t}{2}\,(\mathbf{a}_i + \mathbf{a}_{i+1}) \tag{2.12}$$

in which $\mathbf{k}\,\mathbf{d}_{i+1}$ and $\mathbf{k}\,\mathbf{d}_i$ are replaced by $\mathbf{r}_{i+1}$ and $\mathbf{r}_i$, respectively, in pseudodynamic testing. By substituting Eq. (2.11) into Eq. (2.10) and solving for $\mathbf{a}_{i+1}$, we can obtain a test algorithm as shown in Fig. 2.2d. In this algorithm, damping is implicitly included in the numerical formulation such that the specification of a damping matrix $\mathbf{c}$ is not required. The parameters α and ρ,

which are selected by the user, determine the magnitude of numerical damping for each vibration mode of a system. We can see that the modified algorithm becomes the Newmark explicit method by letting α and ρ equal to zero. The selection of values for the parameters will be discussed in more detail in the next chapter.

The first three algorithms discussed above are mathematically equivalent to one another [15]. Therefore, they have identical stability and accuracy properties. However, their numerical characteristics can be different. For example, the basic central difference method will have significant error-propagation effects when erroneous displacement feedback values are used in the computations, while the other two methods are less sensitive to displacement feedback errors [15]. In general, the modified Newmark algorithm is highly recommended for MDOF testing where experimental error propagation can be significant in the higher modes.

2.4. Sources of Pseudodynamic Test Errors

We can observe from the above discussions that errors can occur from various sources in a pseudodynamic test. A discrete-parameter model may not accurately reflect the actual dynamic behavior of a continuous test specimen which has uniformly distributed mass. The exact damping characteristics of a structure are difficult to model since viscous, Coulomb, and other types of damping mechanisms may all exist in reality. In addition, because of the quasi-static load application in pseudodynamic testing, strain-rate effects may influence the inelastic response of a structure. Besides these problems, numerical integration can only yield approximate solutions to the equations of motion. Furthermore, since experimental feedback is used in the numerical computations and a large number of computation steps may be involved in a single test, significant cumulative errors can occur in the final test result. The significance of these problems will be examined in the following two chapters; and limitations of the method will be identified. Based on these studies, experimental and numerical guidelines can be established to ensure reliable test results.

CHAPTER 3
STEP-BY-STEP INTEGRATION METHODS

3.1. Sources of Numerical Errors

As pointed out in the previous chapter, numerical integration will only give an approximate solution to the equations of motion due to simplifying assumptions used in the numerical procedure. An integration algorithm is considered as reliable if stability and accuracy can be achieved with a reasonably small integration time interval Δt. Errors in numerical solutions are often manifested in the form of frequency distortion and energy dissipation, as well as the growth of a spurious root. Besides these intrinsic numerical problems, errors are inevitable in experimental measurements. Errors in experimentally measured restoring forces are introduced into numerical computations during pseudodynamic testing. Since these errors are usually significantly larger than numerical errors caused by floating-point computations, severe cumulative error growth can occur in a pseudodynamic test; and test results can be rendered unreliable even though the integration method used is stable and accurate.

In this chapter, we will investigate the numerical properties, as well as the reliability, of the four explicit integration methods which have been recommended for pseudodynamic application. Analytical techniques for evaluating the stability and accuracy of numerical integration methods in solving linear differential equations have been well established. The approach used by Hilber, et al. [23] will be followed here because of its consistency with structural dynamics problems. The reliability of the integration methods in solving nonlinear equations will be considered as well. The results of these studies are illustrated with numerical examples. Effects of numerical errors on seismic response computations will be studied, so that practical guidelines can be obtained for the selection of appropriate integration time intervals in pseudodynamic testing. Furthermore, experimental error propagation in numerical computations was investigated in a previous study [15], the results of which will be summarized in the last section of this chapter.

3.2. Numerical Stability and Accuracy

3.2.1. Linear Systems

In the following analysis, we consider a linear elastic SDOF system. However, the results obtained herein are applicable to linear MDOF systems in general by means of modal superposition. In solving the equation of motion for a linear elastic SDOF system, a step-by-step integration algorithm can be written in a recursive matrix form [17,23] as

$$\mathbf{x}_{i+1} = \mathbf{A}\,\mathbf{x}_i + \mathbf{L}\,f_{i+\nu} \tag{3.1}$$

where $\mathbf{x}_i$ is a solution vector which contains the appropriate displacement, velocity, and/or acceleration terms associated with step i or steps previous to that. The parameter ν is an integer which is equal to either 0 or 1, depending on the specific numerical method considered. The matrix $\mathbf{A}$ is called the amplification matrix and the vector $\mathbf{L}$ is the load vector. The scalar $f_{i+\nu}$ is the external force excitation applied.

In the case of a free-vibration response, we have

$$\mathbf{x}_n = \mathbf{A}\,\mathbf{x}_{n-1} = \mathbf{A}^n\,\mathbf{x}_0 \tag{3.2}$$

where $\mathbf{x}_0$ is the initial vector. If the integration method is stable and is applied to an underdamped system, then Eq. (3.2) should yield a bounded oscillatory response for any arbitrary initial vector $\mathbf{x}_0$, according to our definition of stability. If the matrix $\mathbf{A}$ is $N\times N$ in dimension and has N distinct eigenvalues, $\lambda_1, \lambda_2, \ldots\ldots$, and λ_N, then there exists a diagonal matrix $\mathbf{J}$ such that

$$\mathbf{J}^n = \mathbf{\Phi}^{-1}\,\mathbf{A}^n\,\mathbf{\Phi} \tag{3.3}$$

in which $\mathbf{\Phi} = [\boldsymbol{\phi}_1, \boldsymbol{\phi}_2, \ldots\ldots, \boldsymbol{\phi}_N]$ and $\mathbf{J} = \text{diag}\ (\lambda_1, \lambda_2, \ldots\ldots, \lambda_N)$; the vectors $\boldsymbol{\phi}_i$ are the eigenvectors of $\mathbf{A}$ corresponding to the eigenvalues λ_i. Hence, we can obtain from Eqs. (3.2) and (3.3) a numerical solution of the free-vibration response as

$$d_n = c_1 \lambda_1^n + c_2 \lambda_2^n + ... + c_N \lambda_N^n \tag{3.4}$$

where d_n is the displacement value at step n and is an element of $\mathbf{x}_n$, and c_1, c_2,..... are constants determined from initial conditions. For most one- and two-step algorithms, the matrix **A** can be formulated as a 2×2 or 3×3 matrix. Consequently, in order that Eq. (3.4) represents a bounded oscillatory response, two of the eigenvalues of **A**, $\lambda_{1,2}$, should be complex conjugates and $|\lambda_3| < |\lambda_{1,2}| \leqslant 1$. These are the stability conditions for an integration algorithm. The third eigenvalue λ_3 (if it exists) is called the spurious root since it does not stand for a realistic numerical solution of free vibration. Therefore, if the stability conditions are satisfied, λ_1 and λ_2 can be represented as

$$\lambda_{1,2} = A \pm i\, B = e^{(-\bar{\xi} \pm i)\bar{\Omega}} \tag{3.5}$$

where $i = \sqrt{-1}$, and A and B are real numbers such that $(A^2 + B^2) \leqslant 1$. In addition, $\bar{\xi}$ and $\bar{\Omega}$ are defined as follows:

$$\bar{\xi} = -\frac{\ln (A^2 + B^2)}{2\,\bar{\Omega}} \tag{3.6}$$

$$\bar{\Omega} = \arctan\left(\frac{B}{A}\right) \tag{3.7}$$

By substituting Eq. (3.5) into Eq. (3.4) and assuming $N = 3$, we can obtain

$$d_n = e^{-\bar{\xi}\bar{\omega}\Delta tn}\ (c_1 \cos \bar{\omega}\Delta tn + c_2 \sin \bar{\omega}\Delta tn) + c_3 \lambda_3^n \tag{3.8}$$

in which $\bar{\omega} = \bar{\Omega}/\Delta t$. Since the closed-form solution of an underdamped free-vibration response is

$$d(t) = e^{-\xi\omega t}\ (c_1 \cos \omega_D t + c_2 \sin \omega_D t) \tag{3.9}$$

where ξ is the viscous damping ratio and ω_D is the natural response frequency with damping, we can physically interpret that $\bar{\xi}$ and $\bar{\omega}$ are the corresponding quantities in a numerical

solution. If no damping is considered in the equation of motion, then $\bar{\xi}$ is purely a numerically induced phenomenon. Therefore, the magnitude of numerical damping $\bar{\xi}$ and the percentage of frequency distortion $(\bar{\omega} - \omega)/\bar{\omega}$ in an undamped free vibration can be considered as measures of numerical inaccuracies. These numerical properties will be considered for each of the explicit integration methods in the following.

(i) The Basic Central Difference Method

From Eqs. (2.5) to (2.7), we can write the numerical solution of an underdamped free-vibration response using the basic central difference method as

$$d_{i+1} = (2 - \omega^2 \Delta t^2)\, d_i - d_{i-1} \tag{3.10}$$

This equation can be represented in the recursive form:

$$\mathbf{x}_{i+1} = \mathbf{A}\, \mathbf{x}_i \tag{3.11}$$

with

$$\mathbf{x}_i = \begin{Bmatrix} d_i \\ d_{i-1} \end{Bmatrix}$$

and

$$\mathbf{A} = \begin{bmatrix} 2-\omega^2\Delta t^2 & -1 \\ 1 & 0 \end{bmatrix}$$

By solving the eigenvalue problem $(\mathbf{A} - \lambda\, \mathbf{I}) = 0$, we have

$$\lambda_{1,2} = A \pm i\, B \tag{3.12}$$

where

$$A = 1 - \frac{\omega^2\, \Delta t^2}{2}$$

$$B = \frac{\sqrt{4 - (\omega^2 \Delta t^2 - 2)^2}}{2}$$

Stability. The stability conditions require that $(A^2 + B^2) \leqslant 1$ and that B is a real number. Since $(A^2 + B^2)$ is always equal to 1 here, according to Eq. (3.12), we have numerical stability governed by the condition that

$$(\omega^2 \Delta t^2 - 2)^2 \leqslant 4 \tag{3.13}$$

which requires

$$0 \leqslant \omega \Delta t \leqslant 2 \tag{3.14}$$

Consequently, the central difference method is stable as long as $\omega \Delta t$ is less than 2.

Accuracy. By substituting the values of A and B in Eq. (3.12) into Eqs. (3.6) and (3.7), we have

$$\bar{\xi} = 0 \tag{3.15}$$

and

$$\bar{\omega} = \frac{1}{\Delta t} \arctan \left(\frac{\sqrt{4 - (\omega^2 \Delta t^2 - 2)^2}}{2 - \omega^2 \Delta t^2} \right)$$

Therefore, the numerical solution by the central difference method is energy conserved when no external force or damping is present. The only source of numerical inaccuracy is the frequency or period distortion introduced by the method. The percentage of frequency distortion is a function of $\omega \Delta t$ according to Eq. (3.15). In Fig. 3.1, we plot the percentage of period distortion $(T - \bar{T})/T$ against $\Delta t/T$, where T $(= 2\pi/\omega)$ is the real natural period of a system and $\bar{T}$ $(= 2\pi/\bar{\omega})$ is the apparent period of the numerical solution. We can observe that period distortion will approach zero as $\Delta t/T$ goes to zero, and that a reasonably accurate solution can be obtained (less than 1% distortion) when $\Delta t/T$ is less than 0.05. This level of accuracy is

comparable to those of the most reliable implicit methods.

Based on these stability and accuracy properties, the central difference method is adequate for pseudodynamic application.

(ii) The Summed-Form Central Difference Method

The summed form of the central difference method has the following solution scheme for an underdamped free-vibration response:

$$d_{i+1} = d_i + \Delta t \; z_i \tag{3.16}$$

$$z_{i+1} = z_i - \omega^2 \, \Delta t \; d_{i+1}$$

which can be represented in a recursive form as Eq. (3.11) with

$$\mathbf{x}_i = \begin{Bmatrix} d_i \\ z_i \end{Bmatrix} \tag{3.17}$$

and

$$\mathbf{A} = \begin{bmatrix} 1 & \Delta t \\ -\omega^2 \Delta t & 1 - \omega^2 \Delta t^2 \end{bmatrix}$$

It can be shown that the eigenvalues of matrix **A** are identical to those of the basic central difference method. Therefore, its stability and accuracy properties are identical to those of the basic formulation.

(iii) The Newmark Explicit Method

The Newmark explicit method has the following solution scheme for a free-vibration response:

$$d_{i+1} = d_i + \Delta t \; v_i + \frac{\Delta t^2}{2} \, a_i$$

$$v_{i+1} = v_i + \frac{\Delta t}{2} \, (a_i + a_{i+1}) \tag{3.18}$$

$$a_{i+1} = -\omega^2 d_{i+1}$$

which can be expressed in a recursive form as Eq. (3.11) with

$$\mathbf{x}_i = \begin{Bmatrix} d_i \\ v_i \\ a_i \end{Bmatrix} \tag{3.19}$$

and

$$\mathbf{A} = \begin{bmatrix} 1 & \Delta t & \frac{\Delta t^2}{2} \\ \frac{-\omega^2 \Delta t}{2} & 1-\frac{\omega^2 \Delta t^2}{2} & \frac{\Delta t - \omega^2 \Delta t^3}{2} \\ -\omega^2 & -\omega^2 \Delta t & \frac{-\omega^2 \Delta t^2}{2} \end{bmatrix}$$

Again, the first two eigenvalues, $\lambda_{1,2}$, of matrix **A** here are identical to those of the previous two methods; and $\lambda_3 = 0$. Therefore, its stability and accuracy properties are identical to those of the previous methods as well. These results agree with the fact that the three numerical methods are mathematically identical [15].

(iv) The Modified Newmark Algorithm

Based on Eqs. (2.10) to (2.12), the modified Newmark explicit algorithm can be written in a recursive matrix form with

$$\mathbf{x}_i = \begin{Bmatrix} d_i \\ \Delta t\ v_i \\ \Delta t^2\ a_i \end{Bmatrix} \tag{3.20}$$

and

$$\mathbf{A} = \begin{bmatrix} 1 & 1 & \frac{1}{2} \\ -\frac{\Omega^2}{2} & 1-(1+\alpha)\frac{\Omega^2}{2}-\frac{\rho}{2} & \frac{1}{2}-(1+\alpha)\frac{\Omega^2}{4}-\frac{\rho}{4} \\ -\Omega^2 & -(1+\alpha)\Omega^2-\rho & -(1+\alpha)\frac{\Omega^2}{2}-\frac{\rho}{2} \end{bmatrix}$$

in which $\Omega = \omega \, \Delta t$.

Stability. Matrix **A** has eigenvalues

$$\lambda_{1,2} = A_1 \pm (A_1^2 - A_2)^{1/2} \tag{3.21}$$

and

$$\lambda_3 = 0$$

where

$$A_1 = 1 - (1 + \alpha) \frac{\Omega^2}{2} - \frac{\rho}{2}$$

$$A_2 = 1 - \alpha \, \Omega^2 - \rho$$

To satisfy the stable oscillatory condition, we must have $A_1^2 < A_2 \leqslant 1$, such that $\lambda_{1,2}$ are complex conjugates and $|\lambda_{1,2}| \leqslant 1$. When $A_1^2 = A_2$, the algorithm will have a non-oscillatory solution, but the solution will remain stable as long as $A_2 \leqslant 1$. The condition $A_1^2 \leqslant A_2$ implies that

$$\frac{-1 + \sqrt{1 - (1 + \alpha) \rho}}{1 + \alpha} \leqslant \Omega \leqslant \frac{1 + \sqrt{1 - (1 + \alpha) \rho}}{1 + \alpha} \tag{3.22}$$

and from $A_2 \leqslant 1$, we have

$$\Omega \geqslant \sqrt{-\frac{\rho}{\alpha}} \tag{3.23}$$

To obtain approximately frequency-proportional numerical damping, we should select ρ to be negative and α positive. Under these assumptions, the conditions in Eqs. (3.22) and (3.23) are equivalent to

$$\sqrt{-\frac{\rho}{\alpha}} \leqslant \Omega \leqslant \frac{1 + \sqrt{1 - (1 + \alpha) \rho}}{1 + \alpha} \tag{3.24}$$

This is the stability condition for the modified Newmark explicit algorithm. By letting α and ρ equal to zero, we have the same condition as Eq. (3.14).

Accuracy. According to Eqs. (3.6) and (3.7), the eigenvalues from Eq. (3.21) will give the following numerical properties:

$$\bar{\xi} = -\frac{\ln(1 - \alpha\,\Omega^2 - \rho)}{2\,\bar{\Omega}} \tag{3.25}$$

and

$$\bar{\omega} = \frac{1}{\Delta t} \arctan\left[\frac{B}{A}\right]$$

where

$$A = 1 - (1 + \alpha)\,\frac{\Omega^2}{2} - \frac{\rho}{2}$$

$$B = \left\{\Omega^2 - \left[(1 + \alpha)\,\frac{\Omega^2}{2} + \frac{\rho}{2}\right]^2\right\}^{1/2}$$

Therefore, this method is not energy-conserving if α and ρ are not equal to zero. From Eq. (3.25), we can see that $\bar{\xi} = 0$ when $\Omega = \sqrt{-\rho/\alpha}$. For $\Omega < \sqrt{-\rho/\alpha}$, damping is negative and the solution becomes unstable, i.e., energy is added into the numerical solution. In Fig. 3.2, we plot $\bar{\xi}$ against $\omega\Delta t$ for α equal to 0.1 and 0.5, respectively. In both curves, $\sqrt{-\rho/\alpha}$ is 0.1. We can see that damping increases with increasing α. Consequently, by an appropriate combination of α and ρ, one can have a zero or small damping for the fundamental mode while having a significantly greater damping for a higher frequency. This characteristic is very useful for suppressing the spurious growth of higher mode responses due to experimental errors in MDOF testing.

According to Eq. (3.25), the frequency distortion here is similar to those in the previously discussed methods when Ω is close to $\sqrt{-\rho/\alpha}$ or when numerical damping is small. Frequency

distortion will increase with larger numerical damping. However, large damping is only used for the insignificant higher frequency modes of a MDOF system. Consequently, reliable results can be obtained by the modified Newmark method if sufficiently small Δt is used and appropriate numerical damping characteristics are selected.

3.2.2. Nonlinear Systems

The stability and accuracy properties of numerical integration methods in solving nonlinear differential equations are not very well understood due to the lack of an analytical evaluation technique. These properties were usually evaluated via numerical experiments in past studies, which sometimes brought contradictory results. However, it can be shown that unconditionally stable implicit methods can become unstable when applied to nonlinear problems with large integration time intervals [24]. The cause of this instability can be attributed to two factors. First, solving a nonlinear equation by means of an implicit integration method usually requires an approximate solution procedure, such as iterative correction, tangent-modulus or pseudo-force approximation. The additional errors introduced by an approximate solution procedure will affect the stability and accuracy of the solution acquired. Consequently, the stability and accuracy of a nonlinear solution can no longer be determined by the characteristics of the integration method alone [24]. Furthermore, a nonlinear solution can be unstable even though a converged solution is attained by iterative corrections in each integration step. This can be explained by a spurious energy growth which may occur in numerical solutions of nonlinear equations [25]. To visualize this fact, we must realize that the force-deformation relation of a nonlinear system cannot be exactly traced with discretized displacement increments during a step-by-step integration procedure, as shown in Fig. 3.3. As integration time interval increases, the discrepancy will grow such that significant erroneous energy effects will be introduced into the solution. If energy is continuously added into a system, then numerical instability will result. Based on these observations, the difficulties involved in evaluating the numerical properties of nonlinear solution techniques can be easily recognized.

Since explicit integration methods can provide a direct solution for a nonlinear equation, the problem associated with an approximate solution procedure does not exist here. However, for nonlinear systems, the integration time interval selected should always be sufficiently small so that the nonlinear behavior can be accurately traced with the discretized displacement increments. Disregarding the energy effects, the stability and accuracy characteristics of the explicit methods for linear systems are locally valid for nonlinear systems by the fact that a nonlinear system can always be considered as a piecewise linear system, in which the tangent stiffness will dictate the numerical characteristics. This implies that the Δt selected for a linear system will remain conservative if the system becomes nonlinear and if the nonlinearity is of the softening type, as long as the nonlinear behavior can be accurately traced with the Δt selected. This is because the effective $\Delta t/T$ ratio will be smaller as a system becomes less stiff. The opposite will be true for a hardening system.

3.2.3. Numerical Examples

To illustrate the previous discussions, the Newmark explicit method was used for computing the free-vibration response of several SDOF systems. Three types of stiffness properties were used: linear elastic, nonlinear elastic, and inelastic force-deformation relations, which are shown in Fig. 3.4. The linear elastic system had a unit mass and a stiffness of $4\pi^2$ kip/in. such that the natural period was 1 sec. The nonlinearities of the other two systems were modeled by the Menegotto-Pinto relation (see Fig. 3.4). They had initial asymptotic stiffnesses of $4\pi^2$ kip/in. such that their natural periods would approach 1 sec as vibration amplitudes decreased. In these simulations, free-vibration response was induced by releasing the system from rest at a 1 in. deformation from the initial zero force position.

The numerical results for the linear elastic system are shown in Fig. 3.5. At Δt equal to 0.01 sec, the numerical solution was very accurate and could be considered as the exact solution of the problem, according to Fig. 3.1. At Δt equal to 0.10 sec, a small period shrinkage could be observed. The period shrinkage increased when Δt was increased to 0.20 sec. The solution

became unstable when Δt was 0.32 sec, as predicted by Eq. (3.14). In Fig. 3.5, the response curves at the large integration time intervals were smoothed by cubic spline interpolations. It should be noted that the Newmark explicit method is energy conserving for linear systems. In this example, the vibration amplitudes always remained at 1 in. no matter what integration time interval was used, as long as $\omega\Delta t$ was within the stability limit.

The results for the nonlinear elastic system are shown in Fig. 3.6. At Δt equal to 0.1 sec, the solution was less accurate than that for the linear system. More significant frequency shrinkage and amplitude loss could be observed in the free-vibration response. Furthermore, large alternating amplitude changes were observed at Δt equal to 0.20 sec, indicating both energy growth and energy decay in the oscillations. However, the solution remained stable even when Δt was increased to 0.40 sec. These phenomena are consistent with our discussions in the previous section. The erroneous energy effects in solving the nonlinear problem are the major source of inaccuracies as shown by the hysteretic curves in Fig. 3.7. We can observe from the figure that significant energy changes were introduced by the apparent force-deformation relations when Δt was large.

The results for the inelastic system are shown in Fig. 3.8, from which we can see that the vibration amplitudes increased as Δt was increased. Therefore, more energy was added into the system when a larger Δt was used (see Fig. 2.3 b). However, the solution still remained stable when Δt was 0.32 sec.

From these numerical experiments, we can summarize that nonlinear solutions are usually less accurate than linear solutions when integration time intervals are large, due to the energy effects introduced by the discretized displacement increments. However, the stability limit will increase if the nonlinearity is of the softening type and if continuous energy growth does not occur, since the effective $\Delta t/T$ ratio is reduced.

3.3. Effects of Numerical Errors on Seismic Response

As we have already seen, numerical integration introduces frequency distortion such that a numerically computed response always has a frequency slightly different from that of the original system. The effect of frequency distortion on seismic response solutions can be observed from a typical linear elastic response spectrum of the El Centro 1940 earthquake (NS component) in Fig. 3.9a. The spectral curve with zero viscous damping shows that the maximum response amplitude varies drastically with structural period. Within the period range of most structures (i.e., from 0 to 1 sec.), a slight period shift can bring the maximum response amplitude from a peak to a trough or vice versa in the spectrum. This suggests that even a slight period distortion introduced by a numerical algorithm can significantly change the magnitude of seismic response of a linear elastic system which has little or no damping. In Fig. 3.9b, the effect of period shrinkage on the maximum response amplitude is graphed for three different structural periods. The error index ϵ on the y-axis is defined as the ratio of the maximum displacement which is obtained by an exact solution after a period shift over that obtained at the exact period. It is apparent that a structure with a period of 0.35 sec. can have more than 20% error even though the period shrinkage is less than 1%. However, the effect of period shrinkage varies with structural period and depends on the frequency characteristics of the input spectrum as well. The plots in Fig. 3.9b are consistent with the results of numerical experiments, such as the response envelopes shown in Fig. 3.10. These envelopes of displacement amplitudes were computed by the central difference method based on the El Centro record. It can be seen that a more accurate solution can be obtained with the structural period of 0.45 sec than with the period of 0.35 sec when the $\Delta t/T$ ratios are less than 0.06. This is, of course, only true for the El Centro record. Different trends might be observed if a different earthquake record is used.

Fortunately, structural response will not be so sensitive to period change when viscous damping exists (see Fig. 3.9a) or when inelastic structural deformation occurs. This is illustrated by the error spectra in Fig. 3.11. The error index ϵ here is the ratio of the peak

displacement amplitude computed by the central difference method over the exact value. The error spectrum for the linear elastic system with 5% viscous damping shows smaller errors than the one without damping. Similarly, errors are smaller in the spectrum of elasto-plastic systems. It should also be pointed out that the energy effects introduced by the discretized displacement increments are smaller in elasto-plastic systems than in general nonlinear systems.

Since structural specimens will usually deform beyond their elastic limits in pseudodynamic testing and damping is very often included, a small frequency distortion introduced by numerical integration can generally be neglected. In general, the selection of a $\Delta t/T$ ratio for a pseudodynamic test should follow three criteria. First, the Δt selected should locally satisfy the stability condition of an integration algorithm during nonlinear structural testing. Second, large frequency distortion should be avoided by using a reasonably small $\Delta t/T$ ratio. Lastly, the Δt selected should be able to produce sufficiently small displacement increments so that the nonlinear force-deformation relation of a test structure can be traced accurately.

3.4. Experimental Error Propagation

In addition to the numerical errors mentioned above, experimental feedback errors are introduced into numerical computations during pseudodynamic testing. The cumulative effect of these errors can be realized by the fact that incorrect displacements imposed on a test structure will result in erroneous force feedback; and the errors in force feedback will in turn lead to erroneous displacements being computed in the next step. Due to this error cumulation, a pseudodynamic test result can be rendered unreliable even though the experimental errors introduced in each step are relatively small.

3.4.1. Sources and Effects of Experimental Errors

Experimental errors are introduced into a pseudodynamic result during the control and feedback processes of a test as shown in Fig. 3.12. A computed displacement response usually cannot be exactly imposed on a test structure. The displacement control errors can be caused by

instability or lack of sensitivity of the actuator-controller system, miscalibration of displacement transducers, or real-to-integer and digital-to-analog (D/A) conversions of control signals. The displacements or restoring forces measured from a test structure may also be different from the actual quantities due to measurement errors, e.g., the frictional force in actuator connections may influence the restoring-force measurements. If the erroneous displacement and force feedback values are used in the numerical computations, then the computed response will be in error as well. This can be illustrated by a numerical simulation using a SDOF linear elastic system. In the simulation, random errors were introduced into the numerically computed displacements and restoring forces in each step, and the erroneous values were used to compute the displacement response in the next step. The errors introduced into the displacement feedback had a standard deviation of σ_d and those into the force feedback had a standard deviation of $k \cdot \sigma_d$ where k was the stiffness of the system. Without any external excitation to the system, spurious displacement responses (i.e., cumulative errors) due to random errors were obtained by the central difference and Newmark explicit methods, respectively, as shown in Fig. 3.13. It can be observed that the central difference method is very sensitive to random errors as the maximum cumulative errors obtained were approximately $100\sigma_d$ in this example. However, the cumulative errors produced by the Newmark explicit method were much smaller.

3.4.2. Error-Propagation Characteristics

The above example illustrates that the mathematically identical methods can have different experimental error-propagation characteristics due to the different numerical formulations. The results of a previous study [15] indicate that the Newmark explicit and the summed-form central difference methods have identical error-propagation properties which are different from those of the basic central difference method. The basic central difference method can become unstable when displacement-feedback errors are introduced into the numerical computations and when $\omega\Delta t$ is very small. This is shown in Fig. 3.14 where error amplification factors $|C|$ and $|D|$ are plotted against $\omega\Delta t$ for the three explicit integration methods. The absolute

value $|C|$ is an amplification factor for cumulative displacement-feedback errors, while the value $|D|$ is the factor for cumulative force-feedback errors. These factors are functions $\omega\Delta t$ only. From Fig. 3.14, we can observe that $|D|$ is always much smaller than $|C|$ when $\omega\Delta t$ is less than 0.5, and that $|C|$ will approach infinity as $\omega\Delta t$ goes to zero in the basic central difference method. Therefore, we can conclude that numerical results will always be more accurate if the computed displacements are used instead of the measured ones in the step-by-step computations. By using the computed displacements, displacement-feedback errors are eliminated and all three explicit methods will have identical error-propagation characteristics as shown in Fig. 3.14.

Even if the computed displacements are used in the step-by-step integration, displacement control errors are still introduced into the numerical computations through the resulting force-feedback errors (Fig. 3.12). Force-feedback errors can have significant effects on experimental results depending on whether the errors are random or systematic in nature. Systematic errors, which often result from poor performance of experimental equipment or improper instrumentation techniques, can induce a significant cumulative error growth due to resonance-like effects. Random errors may result from electrical noise or other less well-defined sources. Their effects are less severe. The cumulative error bounds for the two types of experimental errors have been derived for linear elastic systems [15], and are shown in Figs. 3.15 and 3.16, respectively. In both cases, cumulative errors increase with the number of integration steps. However, reducing the integration time interval Δt can significantly reduce the cumulative growth of random errors. For example, if we reduce Δt by half while keeping the total analysis duration constant, as indicated by moving from point A to point B in Fig. 3.15, the cumulative errors can be reduced by more than 40%. In the case of systematic errors, the same reduction in Δt would only reduce cumulative errors by approximately 10%, as shown in Fig. 3.16. In general, if systematic errors are present, cumulative errors will approach a relatively significant lower bound as Δt goes to zero. The undesirable properties of systematic errors can be attributed to some consistent energy increasing or dissipating effects. Figs. 3.15 and 3.16 also indicate that the

larger $\omega\Delta t$ is, the faster will be the rate of cumulative error growth with respect to the number of integration steps. Therefore, the higher modes of a MDOF system will be more sensitive to experimental errors than the lower ones.

To illustrate the error-propagation phenomenon, analytical simulations were performed with a 2-degree-of-freedom system shown in Fig. 3.17a. The exact response of the system to the El Centro ground motion was dominated by its fundamental frequency (see Fig. 3.17b). Random and systematic errors were then introduced into the computations by round-off and truncation, respectively, in the real-to-integer conversions of displacement control signals. It can be shown that truncation errors are energy increasing [15]. In both cases, the numerical results are contaminated with the second mode frequency (see Figs. 3.17c and 3.17d). In the case of systematic errors, the spurious second mode effect grew very rapidly. In general, the higher mode effects induced by energy increasing systematic errors are the major threats to numerical stability in MDOF testing.

3.4.3. Improvement Methods

Due to the error-propagation effects, experimental errors should be eliminated or reduced to insignificant levels in any test. This may not be always possible, especially in systems which have many degrees of freedom. In such systems, even small errors can propagate very rapidly in the higher modes. Under that circumstance, numerical methods can be used to mitigate the error-propagation effects [15]. The most efficient method to remove the spurious higher mode effects is to introduce frequency-proportional numerical damping, e.g., by using the modified Newmark algorithm (Fig. 3.2). As an example, a two-story shear building with inelastic inter-story force-deformation relations was numerical simulated by using the Menegotto-Pinto model. Under the influence of energy increasing systematic errors, the numerically computed response of the system to the El Centro excitation had a significant second mode effect (see Fig. 3.18). The modified Newmark algorithm was, then, used to damp out the spurious higher mode response. The α and ρ parameters selected were 0.4 and -0.016, respectively, such that the

numerical damping was about 0.9% for the first mode and 13.6% for the second if the system remained approximately linear. As a result, the second mode response was efficiently removed by the large numerical damping, while the fundamental mode was only slightly affected (Fig. 3.19). A method based on conservation of energy has also been developed to compensate for the energy changes caused by systematic errors [15]. This method is especially efficient for correcting force-measurement errors due to large frictional effects which are more or less constant throughout a test.

In general, inelastic systems have less severe error-propagation problems than linear systems. Furthermore, most of the systematic errors in pseudodynamic testing can be eliminated or significantly reduced by using high performance equipment, and proper instrumentation and test techniques. These experimental errors can be easily detected in a test system by monitoring the displacement error signals or the unusual energy changes during some preliminary tests [15].

CHAPTER 4
STRUCTURAL IDEALIZATIONS

4.1. Structural Idealization Errors

In addition to the numerical and experimental errors discussed before, the reliability of pseudodynamic test results basically depends on the realism of an idealized test model. An unrealistic model will not accurately reflect the actual dynamic characteristics of a test structure. As pointed out in Chapter 2, structural idealization involves analytical modeling of the inertial and viscous damping characteristics of a test specimen. In doing that, a continuous structural system is considered as a discrete-parameter system which has the mass concentrated at a limited number of degrees of freedom. The dynamic characteristics of a discrete-parameter model may not closely resemble those of a continuous structure since only a limited number of vibration modes are considered in the model. The higher mode effects of a continuous system are lost and the lower frequencies may be distorted. Besides that, the nonlinear properties of structural materials are, very often, dependent on the rate of loading. Therefore, the nonlinear behavior of a structure tested quasi-statically may not be the same as that under actual dynamic excitations. Furthermore, damping is a difficult property to model since various damping mechanisms may exist in a real structure, such as viscous, Coulomb, and hysteretic dampings. Coulomb and hysteretic dampings are automatically taken into account in a pseudodynamic test, while viscous damping is specified in the numerical equation. Because of the difficulties in identifying one damping effect from the other in a real vibration test, the determination of the exact viscous damping property of a structure is not possible.

The significance of the above problems will be examined in this chapter. Certain evaluation criteria will be established to assess the accuracy of discrete-parameter models in pseudodynamic testing. The significance of strain-rate and viscous damping effects on inelastic seismic response will be studied with numerical simulations. Although the pseudodynamic test method has its limitations, it is possible to show that accurate test results can be obtained if adequate considerations are given to the selection of a test specimen and of structural model

characteristics.

Other inaccuracies may also exist in a pseudodynamic test, such as the concentration of load application through hydraulic actuators, and the geometric effects on force and displacement measurements during large deformations. However, most of these problems can be avoided by a careful design of test apparatus and by the use of proper testing techniques.

4.2. Accuracy of Discrete-Parameter Models

A structure has to be idealized as a discrete-parameter model in order to be tested pseudodynamically. The stiffness properties of a test structure are directly measured during a test in terms of restoring forces developed by structural deformations at specified degrees of freedom. However, the mass matrix of the system has to be constructed with analytical assumptions. Consequently, the reliability of a test model depends entirely on the realism of the inertial properties assumed.

The mass matrix of a structure is usually assembled from mass matrices of structural elements by the direct stiffness method. Two general approaches are available for constructing element mass matrices [16]. One is by simple lumping of element mass at nodal points, and the other is by a finite element method using displacement shape functions of structural elements. These two methods are shown in Fig. 4.1 for a uniform beam element which has mass $\overline{m}$ per unit length. The consistent-mass matrix formed by the finite element method includes the rotational, as well as the translational, inertia of a beam; and the inertial effects are coupled between the different degrees of freedom. The lumped-mass matrix is based on a simple assumption that the total mass of a beam is equally divided and concentrated at the two end nodes; the inertial effects are not coupled. Consequently, the former is a more rational approach than the later. In general, the consistent-mass formulation is more accurate than the lumped-mass method, if identical nodal points are selected in both cases, because of the larger number of degrees of freedom considered at each nodal point in a consistent-mass model. Nevertheless, the rotational inertia considered in a consistent-mass formulation not only

requires a greater computational effort, but also impose loading and instrumentation difficulties on pseudodynamic experiments. For this reason, lumped-mass formulations are usually preferred in the experiments.

It is generally true that the accuracy of discrete-parameter models can be improved by increasing the number of degrees of freedom. However, a small number of degrees of freedom can very often provide sufficient accuracy if the structure considered has a significant amount of mass actually concentrated at the selected nodal points. Therefore, to assess the reliability of the lumped-mass approach in pseudodynamic testing, we will consider structures which have various degrees of mass concentration. Simple, but representative, structural examples will be used in these studies. As a result, approximate guidelines can be established for evaluating the adequacy of a structure for pseudodynamic testing.

4.2.1. Evaluation Criteria

To evaluate the reliability of discrete-parameter models, we consider a uniform cantilever column which has a length L and a concentrated mass m at the top (Fig.4.2a). The column itself has a uniform mass $\bar{m}$ per unit length. The elastic modulus and cross-sectional moment of inertia of the column are E and I, respectively. The equation of motion for the system under a horizontal base acceleration a_g can be represented by a partial differential equation as

$$EI \frac{\partial^4 u}{\partial y^4} + \bar{m} \frac{\partial^2 u}{\partial t^2} = - \bar{m} a_g \tag{4.1}$$

in which the lateral displacement u of the column is a function of the y-coordinate along the length of the column, and time t. The free-vibration response of the system, i.e., the response when $a_g = 0$, can be solved from Eq. (4.1) by separation of variables with the following boundary conditions:

$$u(0,t) = u'(0,t) = 0$$

$$u''(L,t) = 0 \tag{4.2}$$

$$EI\ u'''(L,t) = m\ \ddot{u}(L,t)$$

where the primes and dots represent differentiations with respect to y and t, respectively. The resulting ordinary differential equations can then solved to obtain the natural frequencies ω_i and mode shapes $\phi_i(y)$ of the system. To find the response of the system to seismic excitations, we can express the closed-form solution of Eq. (4.1) in the following form by means of modal superposition:

$$u(y,t) = \sum_{i=1}^{\infty} \phi_i(y)\ Y_i(t) \tag{4.3}$$

in which the $Y_i(t)$'s are the displacement response in the modal coordinates. It should be noted that a continuous system has an infinite number of vibration modes. The above equation is true because of the orthogonality properties of the mode shape functions $\phi_i(y)$ [16]. For a uniform column, the $\phi_i(y)$'s satisfy the following orthogonality conditions:

$$\int_0^L \phi_m(y)\ \phi_n(y)\ dy = 0 \tag{4.4}$$

$$\int_0^L \phi_m(y)\ \phi_n^{iv}(y)\ dy = 0$$

for $m \neq n$. By substituting Eq. (4.3) into Eq. (4.1) and using the above conditions, we can obtain a system of uncoupled equations of motion:

$$\ddot{Y}_n(t) + \omega_n^2\ Y_n(t) = -\frac{L_n}{M_n}\ a_g(t) \tag{4.5}$$

where

$$L_n = \bar{m} \int_0^L \phi_n(y)\ dy + m\ \phi_n(L) \tag{4.6}$$

$$M_n = \bar{m} \int_0^L \phi_n^2(y)\ dy + m\ \phi_n^2(L)$$

for $n = 1, 2, \ldots, \infty$. The value M_n is considered as the generalized mass for vibration mode n, and L_n is a load modification factor. Consequently, the solution of Eq. (4.1) can be easily obtained by solving the individual modal equations and superimposing the results as indicated in Eq. (4.3). Based on this approach, we can write

$$u(y,t) = \sum_{i=1}^{\infty} \frac{L_i}{M_i\ \omega_i}\ \phi_i(y)\ V_i(t) \tag{4.7}$$

where

$$V_i(t) = \int_0^t a_g(t)\ \sin \omega_i(t-\tau)\ d\tau$$

The last equation is called the Duhamel integral. The quantity $V_i(t)$, which is usually called the spectral pseudo-velocity response, depends on the characteristics of the excitation $a_g(t)$ and the natural frequency ω_i. In addition, the bending moment developed in the column will be

$$m_b(y,t) = EI \sum_{i=1}^{\infty} \frac{L_i}{M_i\ \omega_i}\ \phi_i''(y)\ V_i(t) \tag{4.8}$$

Therefore, in the absence of resonance effects or when disregarding the value of $V_i(t)$, modal participations in the displacement response are determined by the $L_i/(M_i\omega_i)$ factor. In the case of bending moment, the frequency ω_i in $L_i/(M_i\omega_i)$ is canceled out by an identical term in $\phi_i''(y)$. In this respect, modal participations depend mainly on the load factors L_i/M_i. According to Eqs. (4.7) and (4.8), it is true that the bending moment response will have a larger participation of higher mode effects than the displacement response. In general, if the L_i/M_i's are negligibly small for the higher frequency modes, the infinite series representing the displacement and bending moment in Eqs. (4.7) and (4.8) can be truncated without affecting the accuracy of the solutions.

Similarly, the displacement response of a N-DOF discrete-parameter model can be written as

$$\mathbf{u} = \sum_{i=1}^{N} \frac{L_i}{M_i\,\omega_i}\,\boldsymbol{\phi}_i\,V_i(t) \tag{4.9}$$

where

$$L_i = \boldsymbol{\phi}_i^T\,\mathbf{m}\,\mathbf{r} \tag{4.10}$$

$$M_i = \boldsymbol{\phi}_i^T\,\mathbf{m}\,\boldsymbol{\phi}_i$$

In this case, the displacement and mode-shape functions are replaced by vector quantities $\mathbf{u}$ and $\boldsymbol{\phi}_i$, respectively; and $\mathbf{r}$ is an influence coefficient vector which represents structural displacements due to a unit base displacement. By comparing Eq. (4.9) with Eq. (4.7), we can conclude that the accuracy of a discrete-parameter model depends on: (i) the realism of the load factors L_i/M_i represented by the discrete-parameter model (Eq. (4.10)) with respect to the values obtained from the continuous system (Eq. (4.6)); (ii) the significance of the higher mode effects neglected by the discrete-parameter model, i.e., the magnitudes of L_i/M_i for $i > N$; (iii) the accuracy of the lower frequencies ω_i represented by the discrete-parameter model; and (iv) the accuracy of the mode shape vectors $\boldsymbol{\phi}_i$ with respect to the true mode shapes $\phi_i(y)$. These will be our evaluation criteria in the following studies. The influence of higher mode effects also depends on the frequency content of the external excitations. This can be safely neglected here since $V_i(t)$ will generally decrease with higher modes.

4.2.2. Lumped-Mass Models

The uniform cantilever column considered previously (Fig. 4.2a) can be modeled as a SDOF or MDOF lumped-mass system (see Fig. 4.2b - 4.2e). As the number of DOF increases, the behavior of a discrete-parameter model will approach that of a continuous system. This can be illustrated by considering a uniform system without mass concentration, i.e., a column with $m = 0$. The load factors L_i/M_i, computed by means of Eq. (4.6) for the uniform column, are plotted as a solid line in Fig. 4.3a. We can observe that modal participations drop significantly at

the higher modes and the vibration modes greater than the 6th have a negligible influence. This implies that the truncation of the higher mode effects by using a discrete-parameter model is justifiable. The load factors L_i/M_i, obtained by means of Eq. (4.10) for discrete-parameter models shown in Figs. 4.2b to 4.2e, are plotted in Fig. 4.3a as well. It is apparent that the larger the number of degrees of freedom is, the more realistic are the modal participations represented by a model. When the number of degrees of freedom is very large (e.g., by using a 24-DOF consistent-mass model shown in Fig. 2.4f), the load factors represented by a discrete-parameter model are very close to those of the continuous system. Similarly, significant improvements can be observed in the lower mode frequencies as the number of degrees of freedom increases (see Fig. 4.3b). Although the higher mode frequencies are less accurate than the lower ones, the participations of the higher modes are less significant. From these observations, we can conclude that a discrete-parameter model can be very reliable if the number of degrees of freedom considered is sufficiently large.

In general, we are interested in the seismic performance of buildings or other load carrying structures which have a significant amount of mass concentrated at specific locations. Lumped-mass models can be very realistic in representing such structures. For example, consider a column with a concentrated mass at the top (Fig. 4.2a). The load factors L_i/M_i, obtained by means of Eq. (4.6), are plotted in Fig. 4.4a at various ratios of mass concentration. The x-axis of the figure represents the ratio of the concentrated mass at the top of the column over the mass of the column alone. We can observe that the higher mode participations drop rapidly to insignificant levels as mass concentration increases. At 90% mass concentration (i.e., a mass ratio of 10), the column can be accurately viewed as a SDOF system. Similarly, the frequency errors in a SDOF lumped-mass model are very small at high mass concentration levels, as shown in Fig. 4.4b.

Similar improvements can be observed in systems with multiple concentrated masses. Figs. 4.5 to 4.7 show the results for columns which have two, three, and four equal masses, respectively, concentrated at equal distances. A 24-DOF consistent-mass model (see Fig. 4.2f)

is used as the evaluation criterion. In these figures, the x-axis represents the ratio of the total concentrated mass over the mass of the column alone. From these results, we can conclude that the dynamic characteristics of a system which has N concentrated masses can be accurately represented by a N-DOF lumped-mass model when the ratio of the total concentrated mass is high. The variation of frequency errors of the highest mode of a system with respect to mass concentration is similar to that of the single concentrated mass example, while the frequency errors in the lower modes are much smaller, as shown in Figs. 4.5b to 4.7b. Furthermore, the larger the number of concentrated masses is, the more accurate are the lower frequencies and the less significant are the higher modes. Consequently, a system with a large number of concentrated masses can be modeled very accurately by the mass lumping method.

The accuracy of mode-shape vectors $\boldsymbol{\phi}_i$ of a discrete-parameter model can be indicated by the bending curvatures of a column due to modal deformations. In Fig. 4.8, we compare the first mode frequency errors with the base curvature errors due to the first mode deformation of the columns with various mass concentrations. It can be seen that the curvature errors are smaller than the frequency errors.

According to the above examples, we can conclude that lumped-mass models can be reliably used for load carrying structures if the total concentrated mass constitutes more than 80% of the total system mass. This criterion can be satisfied by most building systems, which carry a significant amount of dead load at each floor level.

4.2.3. Simplified Consistent-Mass Models

The consistent-mass formulation in Fig. 4.1a includes the rotational inertia of a beam. This is usually insignificant, and increases both the computational effort and the complexity of the loading apparatus in pseudodynamic experiments. On the other hand, the lumped-mass formulation is not very accurate for systems which have uniformly distributed masses, unless large numbers of degrees of freedom are used. A simplified consistent-mass approach which neglects the rotational inertia can avoid the implementation problems and improve the accuracy of a

discrete-parameter model. This approach uses the same consistent-mass matrix shown in Fig. 4.1a, but assumes that the terms related to the rotational inertia are zero. In this way, the 4×4 consistent-mass matrix for a beam element is reduced to a 2×2 tri-diagonal matrix.

Fig. 4.9a shows a 3-DOF system with the simplified consistent-mass formulation. The number of degrees of freedom involved is the same as the lumped-mass model. However, the more rational treatment of the inertial properties (by including the coupling of inertia forces) in this case improves the accuracy of the discrete-parameter model, as shown by the frequency errors in Fig. 4.9b. The improved accuracy of the simplified consistent-mass formulation can also be observed by comparing the load factors and frequency errors in Fig. 4.10 with those in Fig. 4.3. In Fig. 4.10, only the lateral degrees of freedom are considered as in the lumped-mass case.

4.3. Strain-Rate Effects

Due to different rates of loading, the inelastic behavior of a structure in a pseudodynamic test may differ from that in an actual seismic response. Most structural materials exhibit strain-rate dependent inelastic properties. However, strain-rate effects vary from one material to another. In general, the larger the strain-rate is, the higher will be the inelastic strength. Since loads are applied quasi-statically in a pseudodynamic test, a test structure will usually exhibit a lower inelastic strength.

For mild steel, the yield and ultimate stresses increase with the rate of loading. Manjoine [26] showed that the yield and ultimate stresses of mild steel increase by 170% and 40%, respectively, when the strain rate is increased from 10^{-6}/sec to 10^{3}/sec at room temperature. Fortunately, the seismic response of most structures is dominated by the fundamental structural periods which generally vary from 0.1 sec to 1 sec. These response periods will not induce significant strain-rate effects in steel structures. Consider, for example, that the variation of strain in a structural member during a seismic response is governed by

$$\epsilon = a\ \epsilon_y \sin \omega t \tag{4.11}$$

where a is a constant indicating the maximum inelastic deformation (or ductility) experienced by the member, ϵ_y is the yield strain, and ω is the fundamental frequency of the structure. The rate of change of strain would, therefore, be

$$\dot{\epsilon} = a\ \epsilon_y\ \omega \cos \omega t \tag{4.12}$$

Thus, the maximum strain rate $\dot{\epsilon}_{max}$ is $a\epsilon_y\omega$. Since most structures are designed such that a is less than 10 and ω is less than 60/sec (i.e., period $>$ 0.1 sec), $\dot{\epsilon}_{max}$ is usually smaller than 0.6/sec by assuming that $\epsilon_y = 0.0012$ (i.e., A36 steel). According to Manjoine's results, this will cause no more than 30% increase in yield stress and 10% increase in ultimate strength. In addition, the yielding of structural members will not occur simultaneously and the maximum strain rates usually occur at very small strain levels, where the deformation is basically elastic, as shown by Eqs. (4.11) and (4.12). Since strain rates have a negligible influence on elastic properties, the highest strain rates often occur where they have the least effect. At large inelastic deformations where strain-rate effects can be significant, strain rates are usually reduced to insignificant levels. Consequently, strain-rate effects are generally insignificant on the global behavior of steel structures. Forced-vibration tests performed by Hanson [27] on tubular steel columns showed that the dynamic force-deflection hysteresis curves of the columns were very close to the static curves when the vibration periods were about 0.3 sec and the maximum deflections were 2 times the yield deflection.

The effects of strain rates on the seismic response of a structure can be illustrated with numerical simulations. Fig. 4.11 shows a SDOF system which has the nonlinear behavior modeled by the Menegotto-Pinto relation. The increased inelastic resistance due to a high strain rate can be simulated by shifting the asymptotic bound of the nonlinearity curve upward, as shown in Fig. 4.11b. The results in Fig. 4.12 indicate that a 10% increase in inelastic resistance has very little influence on the response history.

Consequently, the strain-rate effects are generally negligible in testing steel structures. In spite of that, a pseudodynamic test should be performed at a reasonable rate. If the time of a

test is too long, strain-aging can occur. On the other hand, if a test is too fast, the real inertial effects enter into the restoring-force measurements. Neither of these is desirable. The pause between displacement increments should be small as well so that no stress relaxation will occur. In general, strain-rate effects are material dependent. The strength and deformation of reinforced-concrete structures might be more sensitive to strain rates due to the cracking of concrete materials. This phenomenon has not been well studied. Probably, more experimental data are required to clarify this effect.

4.4. Energy Dissipation

Mechanical vibration of any real system will experience an amplitude decay when no external excitations are present. This energy dissipation is most conveniently modeled by a viscous damping mechanism in analytical simulations. However, other forms of energy dissipation mechanisms exist in real systems, such as Coulomb damping due to friction and hysteretic damping due to inelastic behavior of materials. These damping mechanisms have very different characteristics as will be discussed in the following.

Viscous damping can be represented by a dash-pot model (Fig. 4.13a) in which the damping force is proportional to the velocity of motion. The equation of motion for a SDOF system with viscous damping can be written as

$$m\ a(t) + c\ v(t) + k\ d(t) = f(t) \tag{4.13}$$

in which c is the damping coefficient. The magnitude of viscous damping in an analytical model is usually specified in terms of a damping ratio ξ which is equal to $c/(2m\omega)$. If damping is less than the critical, i.e., $\xi < 1$, the free-vibration amplitude of a viscously damped system has a logarithmic decay:

$$d_{n+1} = d_1\ e^{2\pi\xi n} \tag{4.14}$$

in which d_1 is the vibration amplitude at time t_1 and d_{n+1} is the amplitude after n cycles (Fig. 4.13b).

Coulomb damping is due to friction. The magnitude of friction depends on the texture of contact surfaces and the normal force applied onto the surfaces. For a SDOF system in Fig. 4.14a, the frictional force F is $W\mu_f$ where W is the weight of the block and μ_f is the coefficient of dynamic friction for the contact surfaces. The frictional resistance in this case is, therefore, of constant magnitude and is opposite to the direction of motion. Consequently, the equation of motion for such a system is

$$m\ a(t)\ + F\ \text{sign}(v) + k\ d(t) = f(t) \tag{4.15}$$

where sign(v) is the sign of velocity at any time instant t. The decay of free-vibration amplitude due to Coulomb damping (Fig. 4.14b) is linear:

$$d_{n+1} = d_n - \frac{4F}{k} \tag{4.16}$$

This also implies that the influence of Coulomb damping becomes insignificant if the response amplitude is relatively large or if the stiffness of a system is high, i.e., $\frac{F}{k} << d_n$.

Hysteretic damping is another form of energy dissipation, due to the inelastic behavior of structural materials (Fig. 4.15). This can occur even if the deformation of a structure is within the expected elastic limit because of localized yieldings which can be caused by residual stresses in steel, stress concentrations at joints, and premature yielding due to combined axial and bending stresses in a truss for example. In addition, some materials do not have a clearly defined yield point.

In a real vibration test, all three energy dissipation mechanisms may exist. Therefore, it is difficult to define the damping properties of a structure in terms of any single form. It is a common practice to measure structural damping in terms of an equivalent viscous damping ratio ξ_{eq}. This is realistic, of course, only if the effects of Coulomb and hysteretic dampings are

relatively small, and it may not be adequate for other vibration amplitudes.

In a pseudodynamic test, Coulomb and hysteretic dampings are automatically included in response computations by using the actual restoring forces measured from the test structure. However, viscous damping has to be analytically specified. Care should be taken in selecting an adequate viscous damping ratio for a test structure, in order to prevent over- or under-estimation of the damping effect. This can usually be done by comparing the pseudodynamic free-vibration response simulation which does not include viscous damping with the actual free-vibration response of the structure. The difference between the equivalent viscous dampings measured in the two cases indicates an approximate amount of viscous damping required to be considered in a pseudodynamic test.

Sometimes, unrealistically high Coulomb damping may exist in a pseudodynamic test due to unusually high frictional forces in hydraulic actuator connections or in special structure supporting apparatus. These are generally negligible if the frictional forces are small with respect to the stiffness of the structure. Other erroneous energy effects (either energy adding or energy dissipating) may occur in a pseudodynamic test due to experimental errors (Sec. 3.4). These should be carefully checked, and eliminated or compensated for before any major test [15].

The viscous damping properties may change as a structure deforms inelastically. Nevertheless, the energy dissipation becomes dominated by hysteretic damping as soon as significant inelastic deformations occur (see Chapter 6 for example). Therefore, the change of viscous damping in inelastic testing can often be neglected. This can be illustrated by the results of numerical simulations in Fig. 4.16. We can observe that a 2% viscous damping has a significant influence on the elastic response (Fig. 4.16a), but it has negligible effects in an inelastic system (Fig. 4.16b).

Finally, we can conclude that although the exact damping properties of a structure are difficult to measure, reasonable viscous damping values can be assigned to a pseudodynamic test structure through careful considerations of various damping mechanisms. Since equivalent structural dampings measured from most vibration tests vary between 1 and 2%, a small discrepancy in damping will not affect the reliability of inelastic testing.

CHAPTER 5
IMPLEMENTATION AND VERIFICATION TESTS

5.1. Introduction

The theoretical background and analytical evaluations of the pseudodynamic test method have been presented in the previous chapters. The feasibility of the method has been verified based on theoretical considerations, which indicate that the reliability of pseudodynamic results depends on the mechanical properties of the test structure, the adequacy of the modeling assumptions used, and the accuracy of the numerical method selected. However, according to the error-propagation properties of the numerical algorithms, it is obvious that the accuracy of the experimental results also depends largely on the experimental techniques adopted, the design of the test apparatus, as well as on the performance of the test equipment. Reliable test results can be obtained only if appropriate considerations are given to each of the above items. This chapter is devoted to the practical implementation of the pseudodynamic method. A typical implementation scheme will be discussed by referring to the system recently installed at the Structural Engineering Laboratory at Berkeley. Some desirable features of the computer software will be mentioned. In addition, the precision and the performance characteristics of the necessary test equipment will be examined. As a result, precautions for instrumentation and test performance can be identified. By utilizing the experimental system installed at Berkeley, verification tests were performed on a simple SDOF steel specimen. The results of these tests will be presented and correlated with analytical simulations.

5.2. Implementation Method

5.2.1. Experimental System and Procedure

As discussed in Chapter 2, the discretization of a structure for pseudodynamic testing involves the selection of structural degrees of freedom which can realistically describe the dynamic behavior of the specimen. These structural degrees of freedom are usually specified at

locations where most of the system mass is concentrated. Following the discretization procedure, we can write the equations of motion for a general MDOF test structure in a matrix form:

$$\mathbf{m}\,\mathbf{a} + \mathbf{c}\,\mathbf{v} + \mathbf{r} = \mathbf{f} \tag{5.1}$$

where **m** and **c** are the analytically constructed mass and viscous damping matrices of the structure; and **r** is the linear or nonlinear restoring-force vector related to the structural deformations developed at the specified degrees of freedom. Using one of the explicit step-by-step integration algorithms illustrated in Fig. 2.2, we can readily solve Eq. (5.1) for the dynamic response of a structure to any external excitation **f** specified in a pseudodynamic test.

During a pseudodynamic test, the displacement response computed in each step is quasi-statically imposed on a test structure by means of electro-hydraulic actuators, which are physically attached to the structure at locations where the structural degrees of freedom are defined. The restoring forces developed by the structure, due to the deformations applied, are then measured by load transducers and returned to the main computer through a data acquisition unit. Based on the displacements computed in the previous step or steps, as well as on the corresponding restoring forces measured during the test, the displacement response in the next step is computed by means of a step-by-step integration method. This procedure is repeated until the test is completed. Thus, a pseudodynamic test proceeds in a stepwise manner, through which the dynamic response of a structure is quasi-statically simulated by using a numerical algorithm, and appropriate loading and data acquisition apparatus that are available in most structural laboratories.

In reality, the experimental setup for pseudodynamic testing is very similar to that for conventional quasi-static tests. The same test equipment required by conventional quasi-static testing is used here, such as actuator-controller systems which impose specified displacements on a test structure, a data acquisition unit which collects data from measurement instruments, and a mini-computer that stores the acquired data. However, a computer is also used for the

computation of displacement response during a pseudodynamic test. Therefore, the conversion of the conventional quasi-static testing technique to the pseudodynamic method requires the development of computer software which computes the structural response and automates the displacement control and data acquisition processes during a test. A ramp generator must also be built to transfer the displacement signals from the computer.

A typical implementation scheme of the pseudodynamic method, which is used at Berkeley, is shown in Fig. 5.1. The test algorithm is implemented in a mini-computer, which performs the following major functions in each step of a test: (i) read the data channels of the data acquisition unit and store the data in a disc file; (ii) calculate the displacement response using step-by-step integration; and (iii) send the displacement signals to actuator controllers, so that correct dispacements will be imposed on a test structure. The structural displacements computed in each step are sent as voltage signals through a multi-channel ramp generator (D/A converter) to actuator controllers, each of which commands a hydraulic actuator to impose the specified displacement at each structural degree of freedom. The ramp speeds for all channels are so proportioned that the displacement increments for all degrees of freedom of a structure are reached simultaneously. The restoring forces developed by the specimen, as well as other measurements of structural behavior, are then returned to the computer as voltage signals through a high speed data acquisition unit (A/D converter).

The above procedure is repeated in every step of a test. The total time required for a single test is the sum of the time intervals ΔT taken by each of these steps. Each time interval can be subdivided into two phases: the hold period and the ramp period, during which various tasks are being performed, as shown in Fig. 5.2. These tasks are properly synchronized so that long pauses between displacement increments are avoided and correct data are acquired at the end of the ramps. During the hold period of the interval, data acquisition and numerical computations are performed. Data acquisition starts immediately after the ramps stop. The displacements computed are checked so that they will not exceed the ramp limits. The hold period is usually a small fraction of a second if a high speed data acquisition system is used. For a 20

kHz and 128 data channel unit, which is currently used at Berkeley, all channels can be read in 6.4 milliseconds. The ramps start if all the displacements computed are within the limits. During this second half of the interval, several tasks are performed concurrently: (i) the acquired data are recorded in a disc file; (ii) the excitation record is read; (iii) all data are checked to make sure that they are within the calibrated limits; and (iv) selected data channels are plotted for graphical display. Therefore, the ramp speed should be selected such that the ramps stop after all these tasks are completed. This will minimize the hold period and ensure that successive displacement increments are applied more or less continuously, and thus preventing stress relaxation problems. The ramp speed required depends mainly on the amount of data being plotted during a test and the operation speed of plotters. It varies from a fraction of a second, which is the base rate of the system clock, to a few seconds. The maximum ramp speed is also limited by the sensitivity of the actuator-controller system which follows the ramp signals, and the actuator servo-valve flow capacity. On the whole, each step of a pseudodynamic test can be performed in less than one second.

5.2.2. Computer Software

Based on the implementation scheme shown in Fig. 5.1, a pseudodynamic test program has been developed at Berkeley. The program can be divided into two separate execution modes: (i) the operation mode; and (ii) the test mode. Besides the basic functions discussed before, the program also includes several useful features which can improve the reliability as well as the capabilities of the pseudodynamic test method. The main features of the program are shown in Fig. 5.3, and will be discussed in the following.

(i) The Operation Mode

The operation mode comprises a set of macro commands by which all the available functions of the program can be called. The major functions of the program are the following:

(1) initialization of test parameters;

(2) measurement of structural stiffness;

(3) execution of the test mode;

(4) unloading of a tested structure;

(5) reduction of test data.

The test parameters which need to be initialized at the beginning of a test include: (a) the calibration factors of the measurement instruments; (b) the number of structural degrees of freedom considered; (c) the coefficients of the mass and viscous damping matrices; (d) the parameters for the integration algorithm used; and (e) the ramp speed. The structural stiffness can be measured automatically before and after a test by multiple sampling of the load-deformation relations of the structure at various degrees of freedom. A least square fit is performed on each set of sampled data to obtain the stiffness coefficients. Based on the measured stiffness and specified mass matrix, the natural frequencies and mode shapes of the structure can be computed. After a test, a structure can be automatically unloaded by an iterative approach using the initial elastic stiffness of the structure. This is especially convenient for MDOF testing. Finally, experimental data can be immediately reduced and plotted after a test. Arithmetic operations can be performed among the data collected from various channels to extract meaningful results.

(ii) The Test Mode

Pseudodynamic testing can be started by calling the test mode from the operation mode. The test mode performs all the necessary tasks, shown in Fig. 5.2, in each step of a pseudodynamic test. These include numerical integration, control of structural deformations, and collection of test data. Besides the basic operations, the following functions are also incorporated, as shown in Fig. 5.3:

(1) Test execution can be manually terminated or temporarily interrupted before completion, and restarted to continue the interrupted test. This allows readjustment of experimental apparatus or re-calibration of instruments during a test, or continuation of a test after an unexpected interruption.

(2) The discrepancy between the specified and measured displacements is monitored during a test. Spectral analysis can be performed on the displacement errors to detect the existence of systematic errors which are highly undesirable. Test execution will be automatically interrupted if the measured errors exceed a certain limit.

(3) Linear elastic testing can be performed by using the modal superposition method. The response of each mode can be calculated. The erroneous energy growth or decay in each mode can be monitored so that appropriate hysteretic energy compensation can be applied.

(4) The modified Newmark integration method which has numerical dissipation is implemented. Appropriate numerical dissipation can be selected (Sec. 2.3.2) to damp out the spurious growth of high frequency modes without significant effects on the lower ones.

(5) Hysteretic energy compensation is available for correcting energy growth or decay due to systematic experimental errors (Sec. 7.2, Reference 15). This is applicable to either SDOF or MDOF testing.

In addition to the above features, conventional quasi-static testing can be performed as a special case of the general pseudodynamic test method, during which data acquisition and displacement or load application are carried out automatically. Experimental data can be combined and plotted for graphical display during a test. Furthermore, multiple components of excitation, which are very common under real seismic conditions, can also be applied in a pseudodynamic test, so that tests on three-dimensional structural systems can be performed.

5.2.3. Test Equipment

The reliability of pseudodynamic testing depends very much on the quality and performance of the instruments used. Due to the error-propagation characteristics of the numerical integration algorithms, errors introduced into the displacement control and force measurement can induce a significant growth of cumulative errors during a test. For this reason, high precision control and measurement instruments are recommended for pseudodynamic testing. The performance features of these instruments and their error sources are briefly discussed here, as well as the means to minimize the errors.

(i) Measurement Transducers

The displacements imposed on a structure and the restoring forces developed are measured by displacement and load transducers, respectively. These are electronic devices which correlate the displacement or force variations with voltage changes. A perfect device will give an exactly linear correlation. Since the output of a displacement transducer is fed back to an actuator controller in the closed-loop displacement control, and the force measurement from a load transducer is used for the computation of displacement response, the accuracy of these devices is directly related to the reliability of pseudodynamic test results.

Errors associated with displacement transducers are commonly caused by: nonlinearities exhibited in the displacement-to-voltage conversions; lack of sensitivity, which impairs the stability of the closed-loop displacement control; and improper calibration. These errors are usually insignificant if good quality devices and proper calibration techniques are used. The accuracy of displacement control and measurement also depends on the installation of a transducer. If a transducer is installed to measure the actuator displacement instead of the direct structural displacement, then the flexibility of the actuator support will influence the actual displacement being imposed on the structure. Furthermore, geometric effects may become significant under large deformations.

Load transducers are mounted on actuator pistons. A well-designed and properly calibrated load transducer should be very reliable. However, the transducer readings may still be

in error if the actuators are not properly aligned or if the frictional forces in actuator clevises are relatively large. Geometric effects are, again, important if large displacements are imposed on a structure such that the measured force significantly differs from the component in the assumed direction of loading.

(ii) Actuator-Controller System

The response of an actuator-controller system (see Fig. 5.4) to a displacement command depends on the capacity of the servo-valve which drives the hydraulic actuator, and the gain setting on the controller which commands the servo-valve. If the gain is low, the system may respond sluggishly (Fig. 5.5a). If the gain is too high, the system may become unstable, and the actuator will overshoot and oscillate about the commanded displacement (Fig. 5.5b). Either of the above situations is undesirable in a pseudodynamic test because of the erroneous displacement and restoring-force values being fed back to the computer. Significant cumulative errors can occur in pseudodynamic results if the force feedback errors due to overshooting or undershooting are consistently introduced into the numerical computations. Therefore, an optimal gain should be selected such that the actuator response will closely follow the command signal (Fig. 5.5c). The maximum response speed of an actuator is limited by the capacity of the servo-valve (which is specified in terms of gallons of fluid flow per minute). In general, the selection of servo-valve capacity depends on the size of the actuator and the velocity requirement. Extensive experimental studies on actuator performance have been carried out at Berkeley; and problems related to the selection of controller and actuator parameters have been investigated. These are the topics of a future report. Some control theories have also been developed at the University of Michigan, Ann Arbor [14]. These studies provide valuable information for achieving accurate displacement control during a pseudodynamic test. Besides the precision of dispacement control, some other features of a controller system should also be looked upon. For example, an interlock unit which shuts off all actuators when displacements exceed certain limits or when large displacement errors are detected is very useful for preventing unintented damages to a test specimen.

(iii) Ramp Generator and Data Acquisition Unit

The ramp generator is a digital-to-analog (D/A) converter which transmits displacement commands from the computer to actuator controllers. Consequently, floating-point displacement values computed by the pseudodynamic algorithm have to be converted into integer numbers before they can be sent to the D/A converter, which translates binary integer numbers to analog voltage signals. A 12-bit binary D/A converter has a resolution limit of 1/2048 ($2/2^{12}$) of the full calibration range. In other words, displacement increments smaller than $d_{max}/2048$ are lost in the data transfer, where d_{max} is the maximum displacement for which the system is calibrated. This resolution error can be relatively significant if the maximum displacement calibrated for is substantially larger than that to be actually imposed. The ramp signal for each displacement increment can be sent as a linear (Fig. 5.6a), Haver-sine (Fig. 5.6b), or other function. According to the experimental studies, Haver-sine or other functions which have zero ramp terminal velocities can significantly improve the performance of an actuator. For a MDOF test, a multi-channel ramp generator is required. However, all ramps should start and stop simultaneously in spite of the different displacement increment for each ramp (Fig. 5.6c). The data acquisition unit is an A/D converter which translates analog feedback from measurement instruments to digital signals, which are returned to the main computer. The unit currently used at Berkeley (Fig. 5.7) is capable of scanning 128 data channels in 6.4 milliseconds. Again, resolution errors are produced during this A/D conversion.

The resolution errors in the displacement-command and force-feedback signals are introduced into the numerical computations. If truncations are used in the real-to-integer and A/D conversions, the resolution errors will be of systematic nature which can induce a significant error-propagation effect. Consequently, to minimize the effects of resolution errors, one should (i) calibrate the instruments close to the maximum values which would actually be expected during a test, and (ii) use round-off instead of truncation during the real-to-integer and A/D conversions.

The effects of instrumentation errors on pseudodynamic testing can be significant. Therefore, good instrumentation techniques and a careful error checking procedure should be followed in a pseudodynamic test (see Fig. 5.3). These are discussed in greater detail in Reference 15.

5.3. Verification Tests

5.3.1. Test Description

Verification tests were performed to examine the reliability of the pseudodynamic method. A SDOF cantilever system which had a concentrated mass at the top was selected for these tests (Fig. 5.8). The cantilever column was fabricated from a W6×16 I-section. One end of the column was welded to a thick plate which was bolted to a concrete reaction block; and the other end was attached to a hydraulic actuator piston through a clevis, representing the tip which carried the concentrated mass. A detailed test layout is shown in Fig. 5.9. The length of the column, from the fixed to the pinned end, was 48 in. It was assumed that the concentrated mass was 0.01305 kip·sec^2/in., and that the column itself had zero mass. The system was tested horizontally and the gravity effect of the mass was neglected. No viscous damping was included in the analytical formulation.

The displacement of the column top was monitored by an internal LVDT installed within the actuator. Since the reaction frame of the actuator was very stiff when compared with the column stiffness, the internal LVDT should give a very accurate measurement of the lateral displacement of the column. The restoring force was measured by a load cell mounted on the actuator piston. A 12-bit binary ramp generator was used to send out the displacement commands and a 14-bit data acquisition unit was used to collect the restoring force measurements. Because of the high speed data acquisition system used and the responsiveness of the actuator-controller system, a test with a 15 sec. excitation record and a 0.01 sec. integration time interval could be completed in about 25 min. It should also be mentioned that only two data

channels (displacement history and displacement errors) were being displayed by a digital plotter during the tests. The displacement and load transducers were carefully calibrated so that the maximum readings were close to the values actually experienced by the specimen during each test. Consequently, errors introduced by the real-to-integer and A/D conversions were negligibly small.

A sequence of pseudodynamic tests were performed with the SDOF system. A pseudodynamic free-vibration test was first carried out by introducing a short duration impulse excitation. This was followed by a linear elastic test using the El Centro 1940 (NS), 0.1g ground acceleration. Finally, the system was tested for inelastic response under the El Centro 0.8g and Miyagi Oki 0.45g ground motions. The results of these tests were compared with analytical simulations.

5.3.2. Test Results

(i) Linear Elastic Response

The elastic stiffness of the specimen was 3.56 kip/in. based on the nominal dimensions of the column. However, the actual stiffness measured in a static test was 3.75 kip/in. (which was 5% higher than the predicted value). According to the 0.01035 kip·sec^2/in. mass specified in the pseudodynamic formulation and the column stiffness measured, the system should have a natural period of 0.33 sec. Based on these properties, analytical simulations were performed (with zero viscous damping), the results of which are shown in Fig. 5.10. Fig. 5.10a shows the free-vibration response of the system under an impulse excitation, and Fig. 5.10b illustrates the linear response of the system to the El Centro 0.1g ground acceleration.

The free-vibration response obtained by pseudodynamic testing is shown in Fig. 5.11a. We can observe that the vibration period was almost identical to that predicted by analysis. Nevertheless, significant amplitude decay can be observed in the pseudodynamic result. This was apparently attributable to energy dissipation caused by the friction in the actuator clevis, as shown by the hysteretic loops in Fig. 5.11b. For the vibration amplitudes considered, this

Coulomb damping had an equivalent viscous damping ratio of 1.6%. This can be verified by comparing the pseudodynamic free-vibration response with the result of an analytical simulation using 1.6% viscous damping (Fig. 5.11a). Similarly, the pseudodynamic response of the system to the El Centro 0.1g ground acceleration closely matched the analytical result which had 1.6% viscous damping (Fig. 5.12).

(ii) Inelastic Response

The pseudodynamic response of the system to the El Centro 0.8g ground acceleration is shown in Fig. 5.13. Significant yielding was developed at the fixed end of the column, as can be observed from the displacement drift shown in the figure. The force-displacement hysteretic curves of the column shown in Fig. 5.14a indicate significant inelastic energy dissipation during the test. An analytical simulation was performed. The inelastic hysteretic behavior of the column was modeled by the Menegotto-Pinto relation as shown in Fig. 5.14b. By comparing the result of the nonlinear simulation with the pseudodynamic response (Fig. 5.13), we can observe that the correlation between the two results is good although no viscous damping was included in the analysis. It is obvious that Coulomb damping had a negligible effect on the inelastic response. The major discrepancy between the two results is that the analytical simulation had a slightly more significant displacement drift than the pseudodynamic response. This is most likely caused by analytical modeling defects. As shown in Fig. 5.14, the shapes of the hysteretic curves used for the nonlinear model are not exactly identical to those measured in the pseudo-dynamic test.

The inelastic response of the system to the 0.45g Miyagi Oki record is shown in Fig. 5.15. Again, the pseudodynamic response and the analytical simulation show good correlation.

5.3.3. Comments

The above test results show that the dynamic response of a structure can be reallistically simulated by pseudodynamic testing. Although an unrealistically high Coulomb damping was observed in the linear elastic test results, the damping effect became insignificant in the

inelastic response. This can be explained by two reasons. First, as we have discussed in the previous chapter, the influence of Coulomb damping depends on the relative magnitude of F/k with respect to the displacement amplitude. If the frictional force F and the structural stiffness k remain constant, the effect of Coulomb damping becomes less significant as the displacement amplitude increases. Second, as a structure yields, the energy dissipation in the response motion becomes dominated by hysteretic damping and the energy dissipated by frictional forces is comparatively small. Consequently, the effect of Coulomb damping is usually negligible if large inelastic deformations occur or if a system is relatively stiff.

To obtain more realistic damping characteristics in linear elastic tests, the energy dissipated by Coulomb damping can be appropriately compensated for by numerical means. This will be illustrated in the next chapter. As pointed out before, other experimental errors may also exist in pseudodynamic testing. Some errors may cause energy growth instead of energy decay in the response motions. These errors are highly disastrous to MDOF tests. However, most of these errors can be eliminated by using high precision instruments and proper instrumentation techniques.

CHAPTER 6

INELASTIC SEISMIC PERFORMANCE TESTS OF AN X-BRACED TUBULAR STEEL FRAME

6.1. Introduction

The reliability of the pseudodynamic method is further examined in this chapter by comparing the results of pseudodynamic testing with those of shaking table tests. An x-braced tubular steel frame which was previously tested on a shaking table by Ghanaat and Clough [4] was repaired and tested again by using the pseudodynamic method. The test frame was a 5/48 scale planar model of a representative tubular offshore tower designed according to the American Petroleum Institute (API) wave and earthquake criteria [28]. To correlate the results of the two experiments, the table accelerations recorded from the shaking table tests were used as input excitations in the pseudodynamic tests. Tests were performed sequentially with increasing magnitude of earthquake excitations corresponding to API "Strength" and "Ductility" level earthquakes as well as to a "Maximum Credible" event. Larger scale frame models of similar design were also tested quasi-statically by Zayas, et al. [8]. The results of these three experimental programs are compared here to evaluate the reliability and practicability of the pseudodynamic test method. In addition, the inelastic seismic performance of the similar test specimens under the different experimental conditions are examined, and implications for design and analysis of seismic-resistant structures are discussed.

6.2. Test Description

6.2.1. Features of the Test Frame

For correlation purpose, the frame selected for pseudodynamic testing had the same design as the one tested on a shaking table [4]. The geometric configurations and member size specifications of the two frames were identical. The 17 ft.-9 1/8 in. high and 75 in. wide tubular frame consisted of three braced panels (see Fig. 6.1). It represented a complete bent of a 5/48

scale model of a Southern California platform designed according to API wave and earthquake criteria [28]. The operation deck was simulated by a stiff beam. During the shaking table tests, a 40.4 kip dead load, which accounted for 99% of the total frame weight, was superimposed on the top of the frame to represent the weight of the deck appurtenance (see Fig. 6.2). The same mass distribution was assumed in the pseudodynamic tests.

Table 6.1 Member Sizes and Material Properties

Member No. or Description	Tube Dimensions Nominal Diameter (D) × Wall Thickness (t) (in.)	Yield Stress (ksi)	Ultimate Stress (ksi)
1,3	2 1/2 × 0.049	30.7	40.2
2,4	2 1/2 × 0.049	27.4	37.8
5,6,7,8	3 × 0.083	31.5	51.7
9,10	3 1/2 × 0.083	32.0	53.0
11,12,13	2 1/2 × 0.049	19.6	41.0
Jacket Legs	8 × 0.188	48.0	62.0

The section sizes of the frame members are listed in Table 6.1, with member identification numbers shown in Fig. 6.1. The upper-panel diagonal braces had a D/t (nominal diameter/wall thickness) ratio of 51; and that of the lower-panel braces was 36. All the braces were heat treated to obtain a yield stress similar to that of A36 steel. The average yield and ultimate stresses of the annealed materials, based on coupon tests, are shown in Table 6.1 as well. The variation of yield stresses in similar tubular sections was due to separate annealing processes.

The frame was so designed that the failure mechanism would be dominated by the yielding and buckling of the diagonal braces. For this reason, the cross-joints of the braces were reinforced with thick-walled inserts to prevent premature joint failures and the horizontal braces were over-designed.

6.2.2. Pseudodynamic Formulation

Since most of the mass was concentrated at the top of the frame, one could reasonably assume that the frame was a SDOF system in pseudodynamic testing (according to Sec 4.2). Moreover, the P-Δ effect of the dead load had to be numerically modeled because the frame was tested horizontally. With these considerations, the equation of motion for the test frame is

$$m\ a_{i+1} + c\ v_{i+1} + (k + k_g)\ d_{i+1} = f_{i+1} \tag{6.1}$$

where m is the mass at the frame top, c is the viscous damping coefficient, and k is the frame stiffness (force per unit lateral displacement of the deck); k_g is the geometric stiffness due to the P-Δ effect (i.e., weight/height); a_{i+1}, v_{i+1}, and d_{i+1} are the lateral acceleration, velocity, and displacement of the deck at time equal to $(i+1)\Delta t$; and f_{i+1} is the excitation force. With the 40.4 kip dead load, the geometric stiffness k_g was -0.196 kip/in. and the mass m was 0.105 kip sec^2/in. Viscous damping ratio was assumed to be 1.5%, which was an approximate value measured from the shaking table tests. For seismic excitations, $f_{i+1} = -\ m\ \bar{a}_{i+1}$, where $\bar{a}_{i+1}$ was the discretized ground acceleration at time $(i+1)\Delta t$.

Consequently, by using the Newmark explicit integration method (see Fig. 2.2c) and measuring the restoring force $r_{i+1} = k \cdot d_{i+1}$ directly from the test frame in each integration step, the displacement response could be solved from Eq. (6.1) and imposed on the frame in a stepwise manner.

6.2.3. Test Setup and Instrumentation

The pseudodynamic test setup is briefly described in Fig. 6.3. The frame base was attached to a stiff beam on a reaction block by clevises; and free horizontal movement was allowed at the frame top. A mini-computer was used for displacement computation, and for data acquisition and storage. The displacement increment computed at each step was transferred as a voltage signal to an actuator controller, which commanded a hydraulic actuator to impose

the specified displacement on the test frame. The actuator was connected to the frame top (or deck) by a clevis; and the displacement control loop was completed by a displacement-feedback transducer measuring the center point displacement of the deck in line with the actuator. After the correct displacement was imposed on the frame, the restoring force measured by a load transducer mounted on the actuator (as well as data from other measurement instruments) was collected and transferred to the computer by a high speed data acquisition system. The next displacement increment was, then, computed using the restoring-force feedback; and the whole process was repeated.

The yielding and buckling behavior of the diagonal braces was carefully monitored by linear potentiometers and load transducers. The out-of-plane displacements of the cross-joints and the lateral displacements of the frame at the horizontal brace levels were also measured. The movements of the base clevises were accurately monitored with LVDT's, so that the flexibility of the base support could be measured during the tests. The experimental setup and instrumentations are shown by the photographs in Fig. 6.4.

6.2.4. Test Sequence

The earthquake excitations used in the pseudodynamic tests were horizontal table accelerations recorded from the previous shaking table tests. They were derived from the Taft 1952 S69E earthquake record. Due to the filtering of high frequency components from the record used for the shaking table tests and the table-structure interaction phenomenon, the recorded accelerations differed slightly from the original Taft record. To obtain the dynamic similitude of the prototype, the time span of the acceleration record was scaled down by a factor of 0.48.

The test sequence is listed in Table 6.2. The magnitude of ground accelerations varied from $0.138g$ to $1.228g$. Tests 2 and 3 corresponded to the "Strength" and "Ductility" level earthquakes, respectively, according to the API criteria for seismic zone 4, while Tests 5 and 6 were extreme events. Tests 1 and 4 were half-"Strength Level" events used to study the change

Table 6.2 Test Sequence

Test No.	Earthquake Levels	Maximum Ground Acceleration (g)
1	Half-Strength	0.138
2	Strength	0.276
3	Ductility	0.581
4	Half-Strength	0.138
5	Max. Credible	1.228
6	Max. Credible	1.228

of dynamic behavior after significant structural damages. A typical Taft record is shown in Fig. 6.5.

6.3. Verification Tests

As pointed out before, pseudodynamic tests are susceptible to experimental errors. To ensure the credibility of test results, some preliminary tests were carried out to check the accuracy of the experimental apparatus.

A pseudodynamic free-vibration test was performed by introducing a short duration impulse excitation. Excessive energy decay was detected in the test because of the friction in the clevises and in the other frame support apparatus (Figs. 6.6a and 6.6b). This friction was numerically removed from the restoring-force measurements by a correction hysteretic loop, as shown in Fig. 6.6c. The corrected free-vibration responses are shown in Fig. 6.7a, with zero and 1.5% numerically specified viscous damping. The gradual decrease of displacement amplitudes in the zero damping case was caused by hysteretic energy dissipation related to localized yielding of the frame members due to residual stresses and stress concentrations at the joints. However, this was insignificant with respect to the 1.5% viscous damping. The natural period of the frame measured from the pseudodynamic free-vibrations was 0.402 sec., which indicated an elastic frame stiffness of 25.57 kip/in. This was consistent with the stiffness measured from static tests, but lower than the analytically computed stiffness (which is 32.4 kip/in.). This discrepancy was attributed to the base-support flexibility (0.007 in./kip) which was measured by

the LVDT's during the tests.

Finally, an elastic test was performed using a small magnitude Taft record ($0.069g$). An excellent correlation can be observed between the pseudodynamic and analytical results (see Fig. 6.7b). Again, the test result had a little more damping due to local nonlinearities.

6.4. Experimental Results

6.4.1. Inelastic Seismic Response

The global responses of the frame to the six consecutive Taft events are shown by the deck-level displacement time histories and the hysteretic loops of lateral frame load vs. deck displacement in Figs. 6.8 to 6.11. The change of response characteristics of the frame in each event, as observed from the figure, manifested the extent of structural damages developed. The most significant transitions of response characteristics appeared in the "Ductility Level" and the first "Maximum Credible" events as residual displacements and period elongations in the displacement time histories, which were accompanied by significant hysteretic energy dissipations. These corresponded to the first occurrence of severe yielding and buckling of the diagonal braces in the upper and lower panels, respectively. The load resistance and inelastic energy-dissipation capabilities of the frame were mainly offered by the diagonal braces. At the final stage, the upper-panel braces ruptured; and the frame lost more than 50% of its lateral stiffness but retained a good energy-dissipation capability.

The seismic behavior of the frame during the six events are briefly summarized in the followings:

(i) Half-"Strength Level" Event. During the half-"Strength Level" excitations, the frame experienced a maximum deck-level displacement and lateral load of 0.5 in. and 12.5 kips, respectively, at about 3.8 sec. of the 15 sec. record (Fig. 6.8a). A small nonlinearity was observed in the lateral load vs. deck displacement curves (6.8b). This was attributed to localized yielding in the braces. The most significant localized yielding was observed in brace 2.

(ii) "Strength Level" Event. During the "Strength Level" excitations, the maximum deck displacement and lateral load experienced by the frame were 0.8 in. and 18 kips, respectively (Fig. 6.9a). Considerable energy dissipation was observed in the frame hysteretic loops (Fig. 6.9b). All the diagonal braces showed limited local nonlinearities except braces 2 and 4, which had pronounced tensile and compressive yielding. This was in part due to a lower yield stress of the material for braces 2 and 4 (Table 6.1). At the end of the test, a small residual displacement was observed; the frame stiffness was reduced to 24.6 kip/in.

(iii) "Ductility Level" Event. The frame reached a peak displacement of 1.2 in. and a maximum load of 20 kips during the "Ductility Level" earthquake (Fig. 6.10a). The relatively small increase of lateral frame load was due to the development of significant frame nonlinearity. Sudden reductions of frame stiffness occurred at large displacement levels, as shown by the frame hysteretic loops in Fig. 6.10b. These corresponded to the compressive buckling and tensile yielding of braces 2 and 4. The buckling strengths of these braces deteriorated rapidly to about 1/3 of their original values during later displacement cycles. Tensile strength was also drastically reduced due to brace tearing in local buckling regions. Braces 1 and 3 remained essentially elastic throughout the test, while only localized yielding occurred at the lower-panel diagonal braces. After the test, the elastic frame stiffness measured was 23.6 kip/in.

(iv) Post-Damage Half-"Strength Level" Event. The displacement response of the frame in this test was much smaller than that in the initial half-"Strength Level" event. The peak displacement was 0.18 in. (Fig. 6.8a). Period elongation was observed in the displacement history, indicating a reduced frame stiffness.

(v) "Maximum Credible" Event. During the "Maximum Credible" event, the peak displacement of the frame was 2.4 in. (Fig. 6.11a). The lateral load reached a maximum frame capacity of 21 kips. Braces 2 and 4 ruptured, passing the lateral load resistance completely to the lower-panel diagonal braces by means of the jackets. However, the frame hysteretic loops showed stable energy dissipation throughout the test (Fig. 6.11b). Buckling occurred in all the four lower-panel diagonal braces, but braces 5 and 7 exhibited twice as much axial deformations as braces

6 and 8. After the test, the frame stiffness deteriorated to 11.74 kip/in. (i.e. 46% of the original value).

(vi) Second "Maximum Credible" Event. During the second "Maximum Credible" event, the displacement response of the frame was similar to the previous one except that some additional period elongation was observed (6.11a). Severe tensile yielding and compressive buckling were developed in braces 5 and 7, while braces 6 and 8 had relatively limited inelastic deformations. The buckling strengths of braces 5 and 7 were reduced by about 50% at later displacement cycles. The final stiffness of the frame was 10.41 kip/in. The energy-dissipation capability of the frame deteriorated slightly as shown by the hysteretic loops in Fig. 6.11b.

The damages suffered by the frame during these events are shown by the photographs in Fig. 6.12.

6.4.2. Effect of Structural Damage on Seismic Response

As shown by the response spectra of a Taft event in Fig. 6.13, the peak elastic response of a structure to the excitation record can vary within a considerable range, depending on its natural frequency and viscous damping. For the elastic responses in Fig. 6.8a, the tower initially had a period of about 0.4 sec. corresponding to a peak in the response spectra. Lengthening the period due to damages in the "Strength" and "Ductility" level events moved the period into a spectral valley thereby reducing the response considerably. This trend depends on the period shift but also on the particular record used.

The response of a damaged structure is usually different from that of an original one because of stiffness degradation and hysteretic energy dissipation. In Fig. 6.14, we compare the peak elastic displacement responses of the frame based on the original and post-damage frame stiffnesses, respectively, at each excitation level. These values were obtained from the elastic spectrum in Fig. 6.13, assuming 1.5% damping. The significance of effective hysteretic damping can be realized from the experimental data curve plotted in the same figure. The curve shows that the actual peak displacement response of the frame was about 60% of the value predicted

by the elastic spectrum during the "Maximum Credible" event due to hysteretic damping. Therefore, inelastic structural deformation is desirable during intense seismic excitations, as long as the structure remains stable and develops a good energy-dissipation capability.

6.4.3. Inelastic Brace Behavior

Lateral buckling of the load resisting braces concentrated mainly in one of the braces along a full diagonal; and the out-of-plane displacements of the cross-joints remained relatively small. The upper-panel braces, which had a smaller cross-sectional area and a larger D/t ratio than the lower-panel ones, buckled first. Their buckling strength deteriorated rapidly with cycling until the final rupture. The stability and the energy-dissipation capability of the frame during the "Maximum Credible" events were mainly contributed by the stronger and stockier lower-panel braces.

The hysteretic loops of axial force vs. axial displacement of braces 4 and 7 in different events are shown in Figs. 6.15 and 6.16, respectively. It is apparent that the stockier brace 7 had more efficient energy-dissipation hysteretic loops than brace 4, as well as a lower rate of strength deterioration. The rapid deterioration of tensile and compressive resistance of brace 4 that occurred during the "Ductility Level" event was caused by local buckling, which was responsible for tearing and final rupture of the brace. Brace 7 was more resistant to local buckling due to its smaller D/t ratio.

6.4.4. Energy Dissipation

The energy dissipation in the frame responses during the three major events is illustrated in Figs. 6.17 to 6.19, which show that most of the input energy from the ground motions was dissipated in the form of hysteretic damping. The viscous damping effect was relatively small when it was compared with the hysteretic energy dissipation, especially for the higher level events. The maximum amount of energy absorption in a single monotonic displacement occurred at about 3.8 sec. during each event, coinciding with the peak acceleration of the Taft

record (Fig. 6.5). The amount of energy absorbed during this the maximum excursion was about 7 kip-in. in the "Strength Level" event, and about 31 kip-in. in the "Maximum Credible" case. These energy-absorption trends satisfy the API "Ductility Level" design criterion [28], which recommends that a structure should be capable of absorbing at least 4 times the amount of energy required by the "Strength Level" criterion. Much of the absorbed energy was dissipated by inelastic deformations.

From Figs. 6.17 to 6.19, it is also apparent that the diagonal braces were responsible for nearly all the energy dissipation during the seismic events. During the "Strength" and "Ductility" level events, the inelastic deformations of the upper-panel braces contributed to most of the frame energy dissipation (Figs. 6.17 and 6.18). In the "Maximum Credible" event, the upper-panel braces ruptured, and the lower-panel ones took over the energy-dissipation mechanism (Fig. 6.19). The total amount of energy dissipated by the upper-panel braces in the three events was smaller than that by the lower-panel braces. Nevertheless, the upper-panel braces ruptured, while the lower-panel ones remained stable. This is in part due to the smaller D/t ratio, as well as to the more evenly distributed inelastic deformations, of the lower-panel diagonal braces.

6.5. Correlation With Previous Experimental Results

6.5.1. Shaking Table Tests

The comparison of pseudodynamic test results with those of shaking table tests [4] verifies the reliability of the pseudodynamic approach. Although a perfect correlation does not exist between the two experimental results, the inelastic seismic behaviors are similar and the failure modes of the two frames are identical. The most significant difference between the pseudodynamic and shaking table test specimens was in the lateral frame stiffnesses. The initial elastic stiffness of the shaking table test frame, computed from the period measured in a small level test, was 31% lower than the pseudodynamic frame's stiffness, and was considerably smaller than that predicted by analysis. Since the test frames were fabricated from brace members of

identical size specifications, the stiffness discrepancy was apparently caused by the flexibility of the base supports as well as the significant table-structure interaction (or rocking) observed during the shaking table tests. Due to the different stiffnesses, the pseudodynamic and shaking table frames had initial periods of 0.40 and 0.48 sec., respectively. This led to very different linear elastic responses in accordance with the response spectra in Fig. 6.13 and as shown in Fig. 6.20. In addition, it was not possible to obtain an exact material match so that the yield stress of the upper-panel braces in the pseudodynamic specimen was about 7 ksi (35%) greater than that in the shaking table frame. Consequently, a precise correlation of pseudodynamic and shaking table results would not be possible.

Table 6.3 Comparison of Experimental Results

Event Levels	Pseudodynamic Tests			Shaking Table Tests		
	Stiffness (kip/in.)	Max. Displ. (in.)	Max. Load (kip)	Stiffness (kip/in.)	Max. Displ. (in.)	Max. Load (kip)
Strength	24.6	0.8	18.0	17.4	0.6	9.5
Ductility	23.6	1.2	20.0	15.3	1.2	16.1
1 st Max. Cred.	11.4	2.4	21.0	11.2	2.4	28.5

In spite of these, it is useful to compare the stiffness degradation, maximum deck displacements, and maximum lateral loads experienced by the frames during the two separate experiments. These are listed in Table 6.3 and the displacement histories in the three major events of both experiments are compared in Figs. 6.20 to 6.22.

(i) "Strength Level" Event. Fig. 6.20 shows that the displacement histories obtained from the "Strength Level" events of the two experiments are significantly different. However, the peak displacement values are in agreement with the response spectra in Fig. 6.13. Due to the greater deck displacement and the less flexible base support, the maximum lateral load experienced by the frame in the pseudodynamic test was twice as much as that in the shaking table test. This led to considerable yielding of the upper-panel braces in the pseudodynamic experiment, but only localized yielding occurred in the shaking table specimen.

(ii) "Ductility Level" Event. The displacement histories in the "Ductility Level" events show better correlation than those in the previous case (Fig. 6.21). The peak displacements are very close. This is attributed to the considerable amount of energy dissipation in the pseudodynamic test, during which severe yielding and buckling of the upper-panel braces occurred. On the other hand, only relatively moderate yielding of the upper-panel braces occurred in the shaking table test specimen.

(iii) "Maximum Credible" Event. Due to the rapid deterioration of the pseudodynamic frame's stiffness during the "Maximum Credible" event, its overall stiffness approached that of the shaking table specimen (Table 6.3). Thus, the displacement responses of the two frames are very similar, as shown by Fig. 6.22. During this event, the upper-panel braces of the shaking table specimen buckled severely, while those of the pseudodynamic specimen ruptured. The final rupture of the braces in the former did not occur until the second "Maximum Credible" event. This shows that the shaking table specimen retained a greater load resistance than the pseudodynamic specimen. However, both frames retained good energy-dissipation capabilities.

The discrepancy between the experimental results is reasonable if the different dynamic characteristics of the two frames are taken into account. The more severe damage on the pseudodynamic frame is mainly due to its less flexible base support, which induced greater seismic loading on the test frame. Since the exact characteristics of the table-structure interaction are not clear, it can be difficult to obtain good correlations between analytical and shaking table test results. On the other hand, the base conditions of a pseudodynamic test specimen can be easily modeled from the measured support flexibility.

6.5.2. Quasi-Static Tests

The pseudodynamic test specimen was a 5/8 scale model of a frame previously tested by the conventional quasi-static method [8]. All the brace members of the pseudodynamic frame were appropriately scaled, such that the diagonal brace members of the two frames had very close D/t ratios. Therefore, the failure modes of the two frames were very similar.

In the quasi-static test, 18 cycles of predetermined displacements were imposed on the frame with gradually increasing amplitudes. At displacement ductility levels comparable to those in the "Strength Level", "Ductility Level", and "Maximum Credible" events in the pseudo-dynamic testing, the stiffness of the quasi-statically tested frame deteriorated to 97%, 79%, and 57% of its original value, respectively. At each stage, brace damages were less severe than those in the pseudodynamic tests. This was due to the larger number of displacement cycles experienced by the pseudodynamic test frame, and consequently, the greater deterioration of the braces. Therefore, the inelastic displacement history experienced by a frame has a significant influence on its seismic performance. Since the conventional quasi-static approach neglects the dynamic characteristics of a structure, the results of these tests are insufficient for assessing the potential seismic performance of a structure.

6.6. Analytical Correlations

Excellent analytical correlations were obtained for the pseudodynamic test results. Fig. 6.7b shows that the pseudodynamic test result is almost identical to the result of analytical simulation in the linear elastic range (1/4 - "Strength Level" event). Good correlations were also obtained for the "Strength Level", "Ductility Level", and "Maximum Credible" events, respectively, as shown in Figs. 6.23 to 6.25. In these analyses, the inelastic behavior of the diagonal braces was modeled by a postbuckling brace element developed by Bruce Maison [29]. This analytical model can closely mimic the inelastic postbuckling behavior of brace members under cyclic loading. The base support of the frame was modeled by elastic truss elements,

based on the base flexibility measured during the tests. The displacement histories obtained by analytical simulations matched very well with the pseudodynamic test results in the first two events (Figs. 6.23 and 6.24). In the "Maximum Credible" event, a slightly more significant displacement drift was observed in the analytical result (Fig. 6.25). In addition, the hysteretic loops of the frame and diagonal braces obtained by analytical simulations correlated well with the experimental results. A detailed discussion of the analytical procedure and results will be presented in a future report.

6.7. Concluding Remarks

The results of the tubular frame tests indicate the feasibility of the pseudodynamic method as an economical and reliable experimental technique to study the inelastic seismic behavior of structural systems. Based on these results as well as those from the previous experiments, the following conclusions can be obtained:

(1) The pseudodynamic method accounts for the dynamic characteristics of a test structure, so that the realism of the test results is comparable to that of shaking table results.

(2) The pseudodynamic method provides well-controlled experimental conditions. The problem of table-structure interaction which may occur in shaking table testing does not exist in pseudodynamic tests. In addition, the size and weight of a structure, and the magnitude of ground motions used in pseudodynamic testing are not so severely limited as in shaking table tests. Consequently, pseudodynamic testing with larger scale models can provide useful data for the verification and improvement of current analytical methods.

(3) From the difference between the pseudodynamic and shaking table test results, one can observe that the foundation stiffness of a test structure and the value of the structural period with respect to the frequency content of an earthquake record have a significant influence on the seismic response and the extent of structural damages developed. Consequently, these are important considerations in testing, design, and analysis of seismic-resistant structures; and several ground motions should be considered in design and analysis.

(4) The capability of an offshore tower to resist an "aftershock" depends on its post-damage structural properties as well as on its energy-dissipation capacity.

(5) The lateral load resistance and the hysteretic energy dissipation of the tubular x-braced frames were mainly contributed by the diagonal braces. The braces with smaller D/t ratios had greater energy-dissipation efficiency and durability under cyclic loadings. A good understanding of the post-buckling strength of the braces is important in the inelastic design and analysis of braced structures. The results of these experiments provide useful information to develop and evaluate analytical brace models.

(6) Based on the test results, a properly designed and constructed offshore structure can sustain intense seismic excitations and develop a significant energy-dissipation capacity. However, great uncertainties are associated with the determination of realistic environmental loadings (including seismic and wave actions) and structural boundary conditions (such as the soil-structure interaction). As mentioned above, these could have a significant influence on the dynamic response of a structure. Hence, further experimental and analytical studies are recommended to identify the exact influence of the above parameters on the inelastic performance of offshore structures.

(7) The pseudodynamic method seems to be a promising experimental technique for future studies. Hydrodynamic effects can be conveniently approximated in the pseudodynamic formulation by modifying the inertial and damping properties of a structure using appropriate inertia and drag coefficients, and by the determination of hydrodynamic loading from appropriate wave theories. The effects of soil-structure interaction can also be included using analytical substructures.

CHAPTER 7
CONCLUSIONS

The fundamental theory for the pseudodynamic test method has been examined in this report. It has been shown that this relatively new experimental method has its basic principles founded on well-established analytical techniques of structural dynamics. The method has, therefore, solid theoretical justification for the techniques used for formulating and solving the equations of motion for a test structure; but it also suffers the same inaccuracies which are usually encountered in analytical problems, such as errors introduced by discretization of structural systems and by numerical integration. In this respect, reliability criteria established for analytical procedures can be applied to the experimental method as well. In particular, the stability and accuracy criteria derived for the numerical integration methods should be observed in order to obtain reliable experimental results. In addition, the pseudodynamic method is more reliable than most analytical studies due to the direct measurement of stiffness properties from structural specimens during tests. Inaccuracies related to idealized nonlinear mathematical models of structures do not exist. Consequently, the pseudodynamic method provides a valuable means for increasing our understanding of nonlinear behavior of structures subjected to seismic excitations, and to assess and improve current analytical techniques for analyzing such systems.

Propagation of experimental errors appears to be the major source of inaccuracies in pseudodynamic testing. However, most of the experimental errors can be reduced to insignificant levels by the use of reliable test equipment and appropriate instrumentation techniques. Numerical techniques are also available to mitigate the effects of experimental errors. Although the pseudodynamic method uses the same experimental equipment as conventional quasi-static testing, it requires very precise control and feedback instruments due to the sensitivity of the method to experimental errors. On-line computer-control software also needs to be developed to implement the method. However, the costs of experimental facilities and test performance required for the pseudodynamic method are, generally, significantly less than those required for shaking table tests. From the analytical and experimental verification studies, the

capabilities and limitations of the method can be summarized as follows:

(1) The results of pseudodynamic tests can be as realistic and informative as those of shaking table tests for assessing the inelastic seismic performance of structural systems. In addition, it provides as well-controlled experimental conditions as quasi-static tests.

(2) Because of the simplified analytical assumptions used, the pseudodynamic method has its limitations as well. The method is most suitable for a structure which has a significant portion of its mass concentrated at a limited number of degrees of freedom. It is not adequate for structures which have uniformly distributed masses. In addition, the method would not be reliable for structures having nonlinear material properties that are highly sensitive to loading rates. Fortunately, this is not a problem for most structures subjected to seismic excitations. Due to the variety of damping mechanisms governing the elastic response of a structure, only an approximate equivalent viscous damping can be assumed for the test specimen. For this reason, linear elastic test results are generally less reliable than the results of inelastic tests, where structural damping is dominated by hysteretic energy dissipation which is automatically taken into account in pseudodynamic testing.

(3) The basic and summed-form central difference methods and the Newmark explicit method have been recommended for pseudodynamic application in previous studies. Actually these methods are mathematically identical, having the same stability and accuracy properties. Reliable numerical results can be obtained by these methods if $\Delta t/T$ is less than or equal to 0.05. For nonlinear systems, the Δt selected should be sufficiently small so that the nonlinear force-deformation relation can be adequately traced by the discretized displacement increments. In general, algorithms with frequency-proportional numerical damping, like the dissipative Newmark method, are more desirable in MDOF tests, because the spurious growth of higher frequency responses can suppressed by the numerical damping.

(4) In spite of the limitations and possible experimental errors, reliable pseudodynamic test results can be obtained if appropriate attention is directed to the selection of high performance test equipment, the use of proper experimental and numerical techniques, as well as the selection of appropriate test specimens. Most of the highly undesirable experimental errors can be checked or eliminated prior to a test.

Based on the previous observations, it appears that the pseudodynamic test method is a reliable procedure for evaluating the performance of a structure during severe seismic excitations. Use of the method is recommended for structures that satisfy the preceding guidelines. It is especially useful for large, heavy, and strong structures that cannot be tested on available shaking tables and for structures subjected to multiple components of excitations.

Future research work should be devoted to improve the performance of critical test equipment, such as the electro-hydraulic actuator-controller system, and to further the development of error resistant numerical algorithms and error correcting numerical techniques. This will reduce the potential adverse effects of error propagation and increase confidence in the method.

Pseudodynamic tests should be performed on structures constructed from different types of materials and on more complicated structural systems. This will clarify the applicability of the method and identify any potential limitations.

Furthermore, the analytical formulation of the pseudodynamic method should be extended to include substructuring and other numerical techniques such that a variety of structures or subassemblages of large structural systems can be tested under different boundary and loading conditions. Currently, only complete structural systems can be tested. By appropriate use of analytical substructuring concepts, structural subassemblages and components might be tested economically using realistic loading histories and boundary conditions. Application of the method to other problems of dynamics (hydrodynamic and areoelastic excitations) and to related problems such as frame instability should be explored.

REFERENCES

1. Takanashi, K., et al., "Nonlinear Earthquake Response Analysis of Structures by a Computer-Actuator On-Line System," *Bull. of Earthquake Resistant Structure Research Center,* Institute of Industrial Science, University of Tokyo, No. 8, 1975.

2. Bertero, V. V., et al., "Use of Earthquake Simulators and Large-Scale Loading Facilities," *Proceedings,* Workshop on ERCBC, University of California, Berkeley, 1978.

3. Karwinkler, H., "Experimental Research Needs," *Proceedings,* Workshop on ERCBC, University of California, Berkeley, 1978.

4. Ghanaat, Y. and Clough, R. W., "Shaking Table Tests of a Tubular Steel Frame Model," *UCB/EERC-82/02,* Earthquake Engineering Research Center, University of California, Berkeley, 1982.

5a. Galambos, T. V. and Mayes, R. L., "Dynamic Tests of a Reinforced Concrete Building," *Report No. 51,* Washington University, St Louis, 1978.

5b. Safford, B., "Development of Force Pulse Train Generators for the Study of Dynamic Response," Second ASCE-EMD Specialty Conference on Dynamic Response of Structures, Atlanta, 1981.

6. Lindberg, H., et al., "Simulation of Strong Earthquake Motion with Contained Explosion Line Source Arrays," Second ASCE-EMD Specialty Conference on Dynamic Response of Structures, Atlanta, 1981.

7. Townsend, W. H. and Anderson, J. C., "Analytical/Experimental Modeling of Exterior Beam-Column Connections," ACI Convention, Nov. 1978.

8. Zayas, V. A., Mahin, S. A., and Popov, E. P., "Cyclic Inelastic Behavior of Steel Offshore Structures," *UCB/EERC-80/27,* Earthquake Engineering Research Center, University of California, Berkeley, 1980.

9. Takanashi, K., et al., "Inelastic Response of H-Shaped Columns to Two Dimensional Earthquake Motions," *Bull. of Earthquake Resistant Structure Research Center,* Institute of Industrial Science, University of Tokyo, No. 13, 1980.

10. Okada, T., et al., "A Simulation of Earthquake Response of Reinforced Concrete Building Frames to Bi-Directional Ground Motion by IIS Computer-Actuator On-Line System," *Proceedings,* 7th World Conference on Earthquake Engineering, Istanbul, Turkey, 1980.

11. Watabe, M., et al., "Feasibility of Pseudo-Dynamic Testing System," *Progress Report on U.S. - Japan Large-Scale Aseismic Experiments for Building Structures,* Building Research Institute, Ministry of Construction, 13th Joint Meeting, U.S - Japan Panel on Wind and Seismic Effects, Tsukuba, 1981.

12. Okamoto, S., et al., "A Progress Report on the Full-Scale Seismic Experiment of a Seven Story Reinforced Concrete Building," Building Research Institute, Ministry of

Construction, Tsukuba, 1982.

13. Yamanouchi, H., et al., "Test Results of Full-Scale Six-Story Steel Building," Building Research Institute, Ministry of Construction, 4th Joint Technical Coordinating Committee Meeting, U.S. - Japan Cooperative Research Program, Tsukuba, Japan, 1983.

14. McClamroch, N. H., Serakos, J., and Hanson, R. D., "Design and Analysis of the Pseudo-Dynamic Test Method," *UMEE 81R3,* University of Michigan, Ann Arbor, 1981.

15. Shing, P. B. and Mahin, S. A., "Experimental Error Propagation in Pseudodynamic Testing," *UCB/EERC-83/12,* Earthquake Engineering Research Center, University of California, Berkeley, 1983.

16. Clough, R. W. and Penzien, J., *Dynamics of Structures,* McGraw Hill, 1975.

17. Bathe, K. and Wilson, E. L., *Numerical Methods in Finite Element Analysis,* Prentice Hall, 1976.

18. Newmark, N. M., "A Method of Computation for Structural Dynamics," *Journal of the Engineering Mechanics Division,* ASCE, No. EM3, Vol. 85, 1959.

19. Okada, T., "Computer-Actuator On-Line System at Institute of Industrial Science, University of Tokyo, with Emphasis on Numerical Integration Methods," *A Brief Note Submitted to Session 2,* First Planning Group Meeting, U.S. - Japan Cooperative Research Program Utilizing Large-Scale Testing Facilities, 1977.

20. Dahlquish, G., Björck, A., and Anderson, N., *Numerical Methods,* Prentice Hall, 1974.

21. Powers, W. F., "Preliminary Analysis of the Computer-Actuator On-Line System Difference Equation," University of Michigan, Ann Arbor, 1979.

22. Mahin, S. A. and Williams, M. E., "Computer Controlled Seismic Performance Testing," Second ASCE-EMD Specialty Conference on Dynamic Response of Structures, Atlanta, 1981.

23. Hilber, H. M., Hughes, T. J. R., and Taylor, R. L., "Improved Numerical Dissipation for Time Integration Algorithms in Structural Dynamics," *Earthquake Engineering and Structural Dynamics,* Vol. 5, 1977, pp. 283-292.

24. Park, K. C., "Evaluating Time Integration Methods for Nonlinear Dynamics Analysis," *Finite Element Analysis of Transient Nonlinear Structural Behavior,* Edited by Belystchko, T., Osias, J. R., and Marcal, P. V., Applied Mechanics Symposia Series, ASME, New York, 1975.

25. Hughes, T. J. R., "Stability, Convergence and Growth and Decay of Energy of the Average Acceleration Method in Nonlinear Structural Dynamics," *Computers and Structures,* Vol. 6, 1976, pp. 313-324.

26. Manjoine, M. J., "Influence of Rate of Strain and Temperature on Yield Stresses of Mild Steel," *Transactions,* ASME, Vol. 66, 1944, pp. A211-A218.

27. Hanson, R. D., "Comparison of Static and Dynamic Hysteresis Curves," *Journal of the Engineering Mechanics Division,* ASCE, No. EM5, Vol. 92, 1966, pp. 87-113.

28. American Petroleum Institute, "Recommended Practice for Planning, Designing, and Constructing Fixed Offshore Platforms," Dallas, Texas, 10th Ed., 1979.

29. Zayas, V. A., Shing, P. B., Mahin, S. A., and Popov, E. P., "Inelastic Structural Modeling of Braced Offshore Platforms for Seismic Loading," *UCB/EERC-81/04,* Earthquake Engineering Research Center, University of California, Berkeley, 1981.

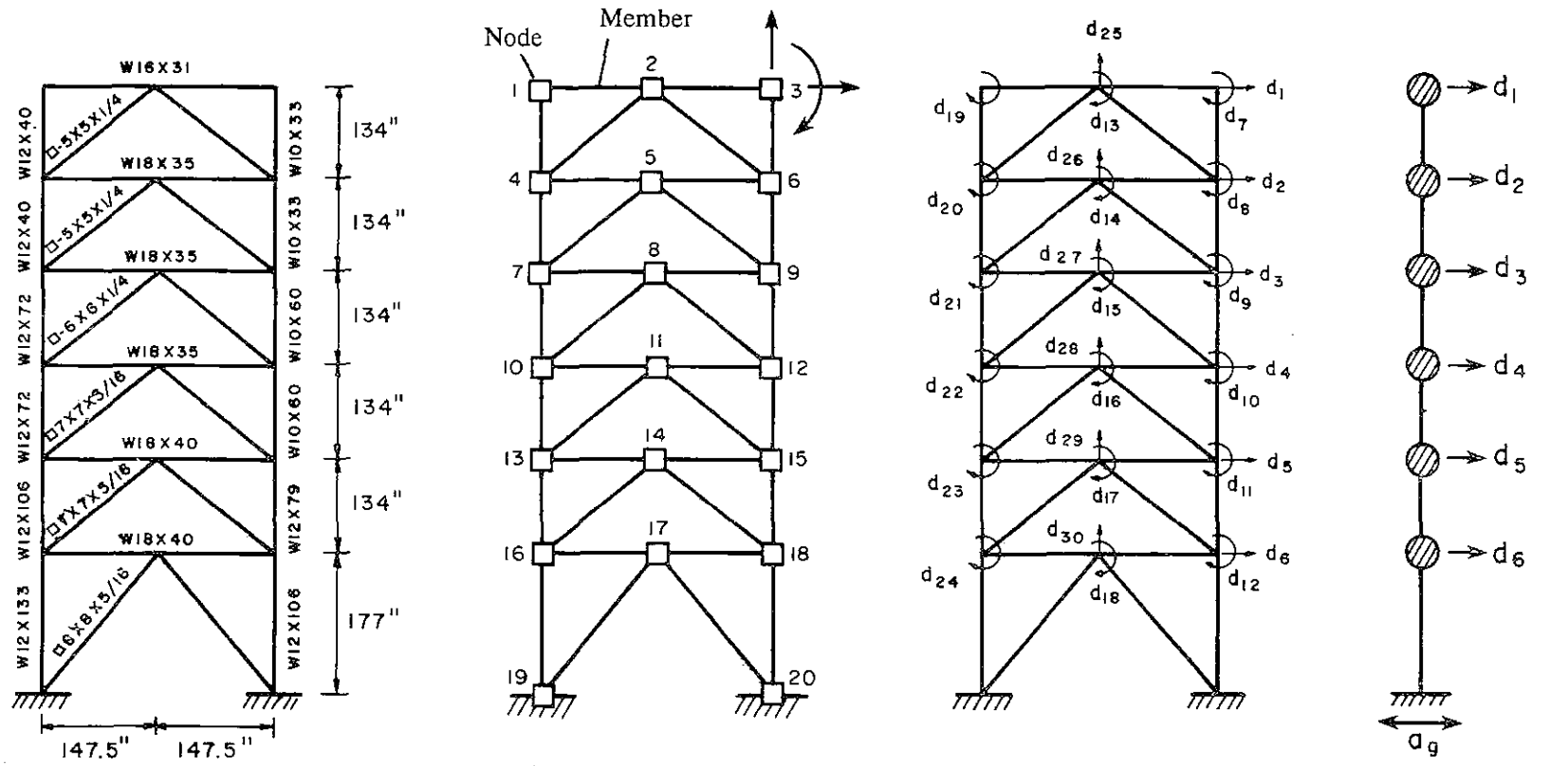

(a) Analyzed Frame

(b) Discrete-Parameter Frame Model

(c) Degrees of Freedom Considered

(d) Static Condensation

Fig. 2.1 Frame Idealization for Dynamic Analyses

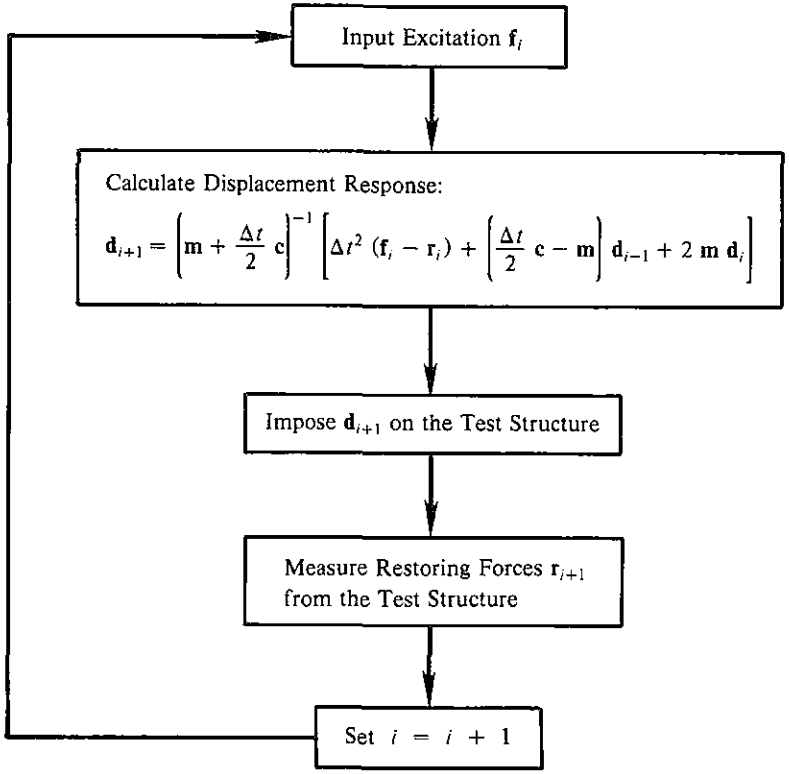

(a) Basic Central Difference Method

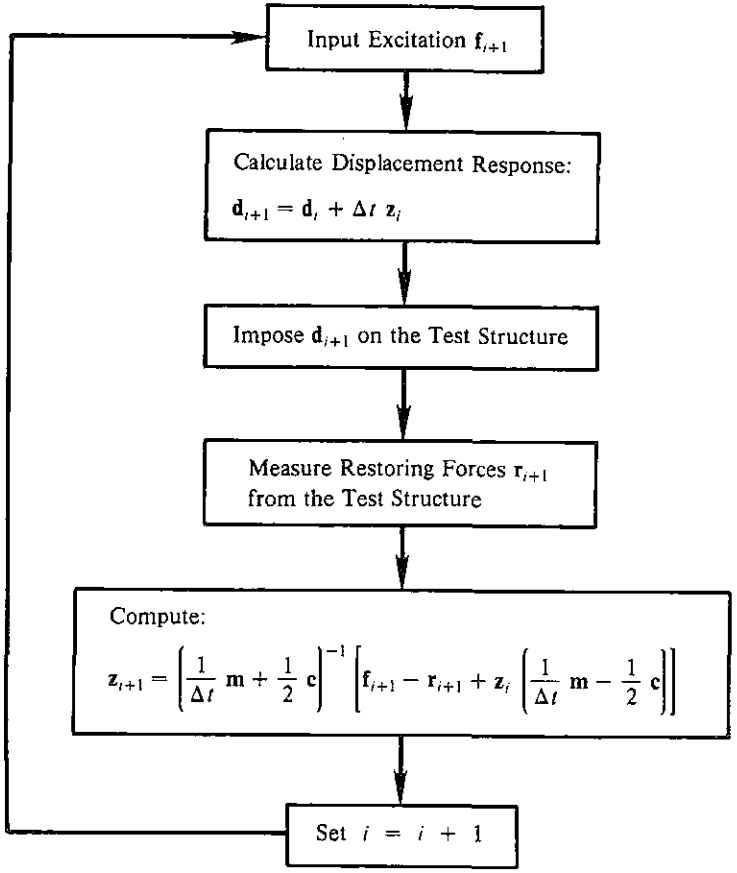

(b) Summed-Form Central Difference Method

Fig. 2.2 Numerical Algorithms for the Pseudodynamic Test Method

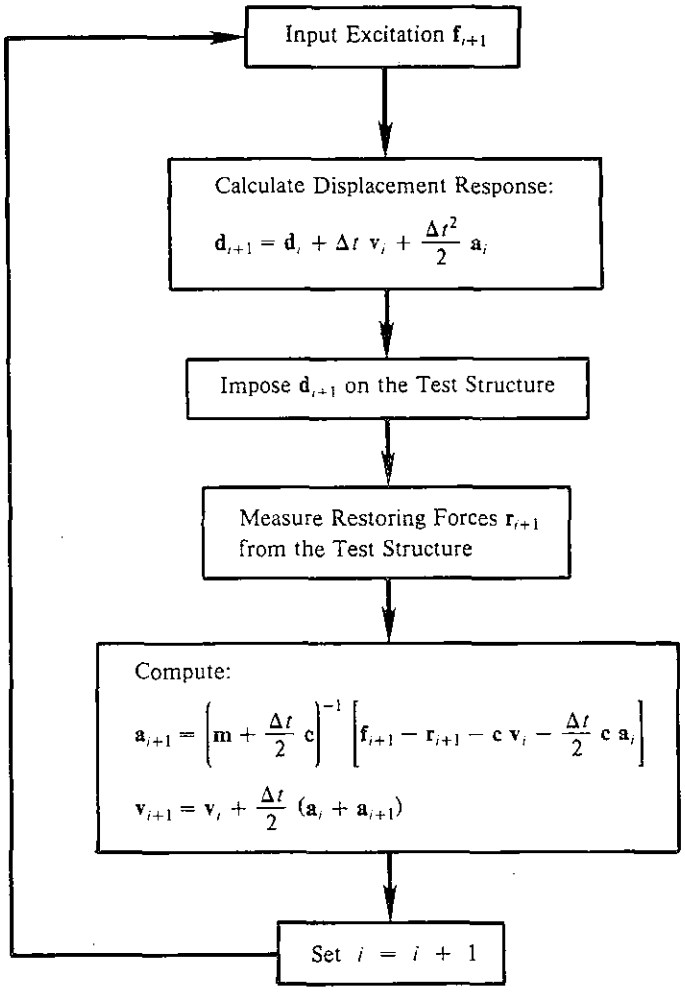

(c) Newmark Explicit Method

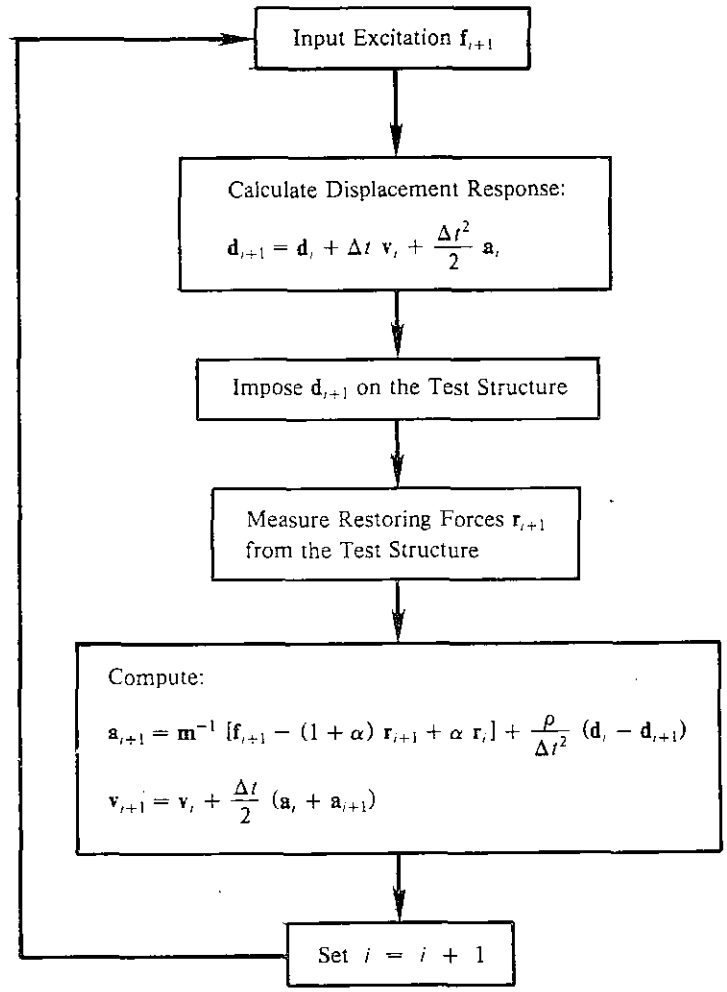

(d) Modified Newmark Explicit Method

Fig. 2.2 Numerical Algorithms for the Pseudodynamic Test Method

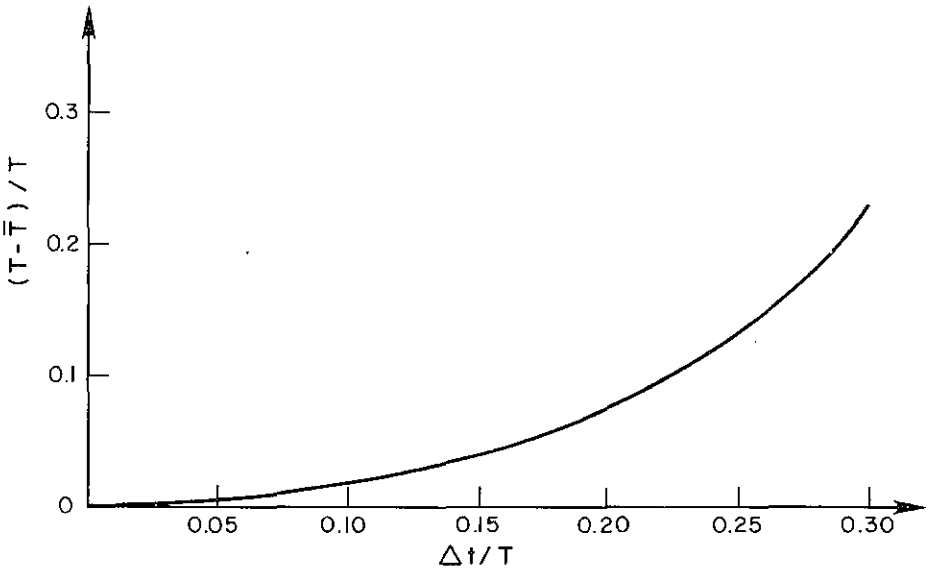

Fig. 3.1 Period Shrinkage by the Central Difference Method

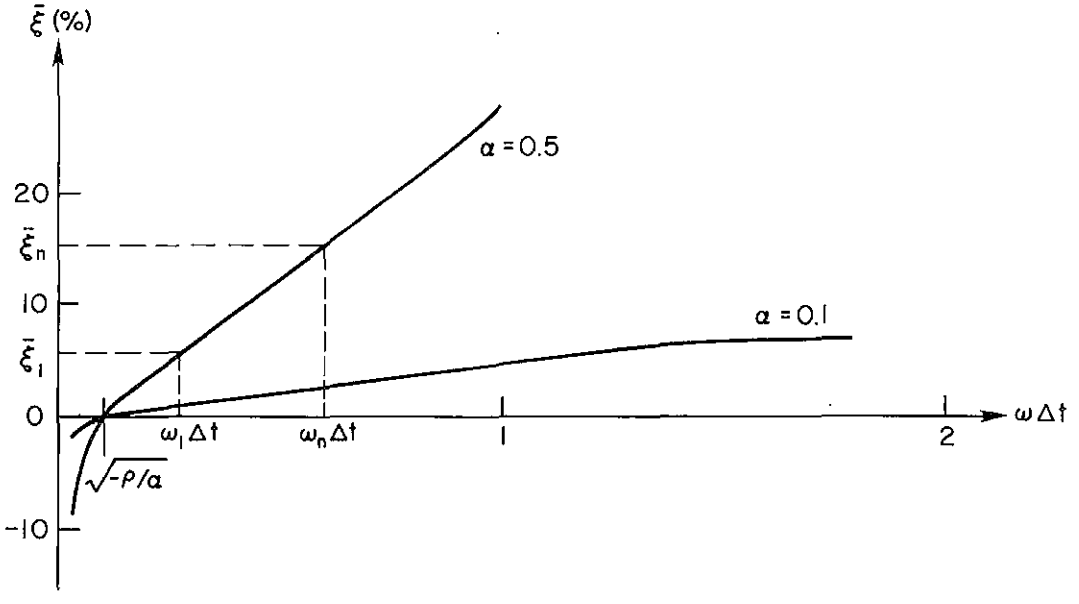

Fig. 3.2 Numerical Damping by the Modified Newmark Explicit Method

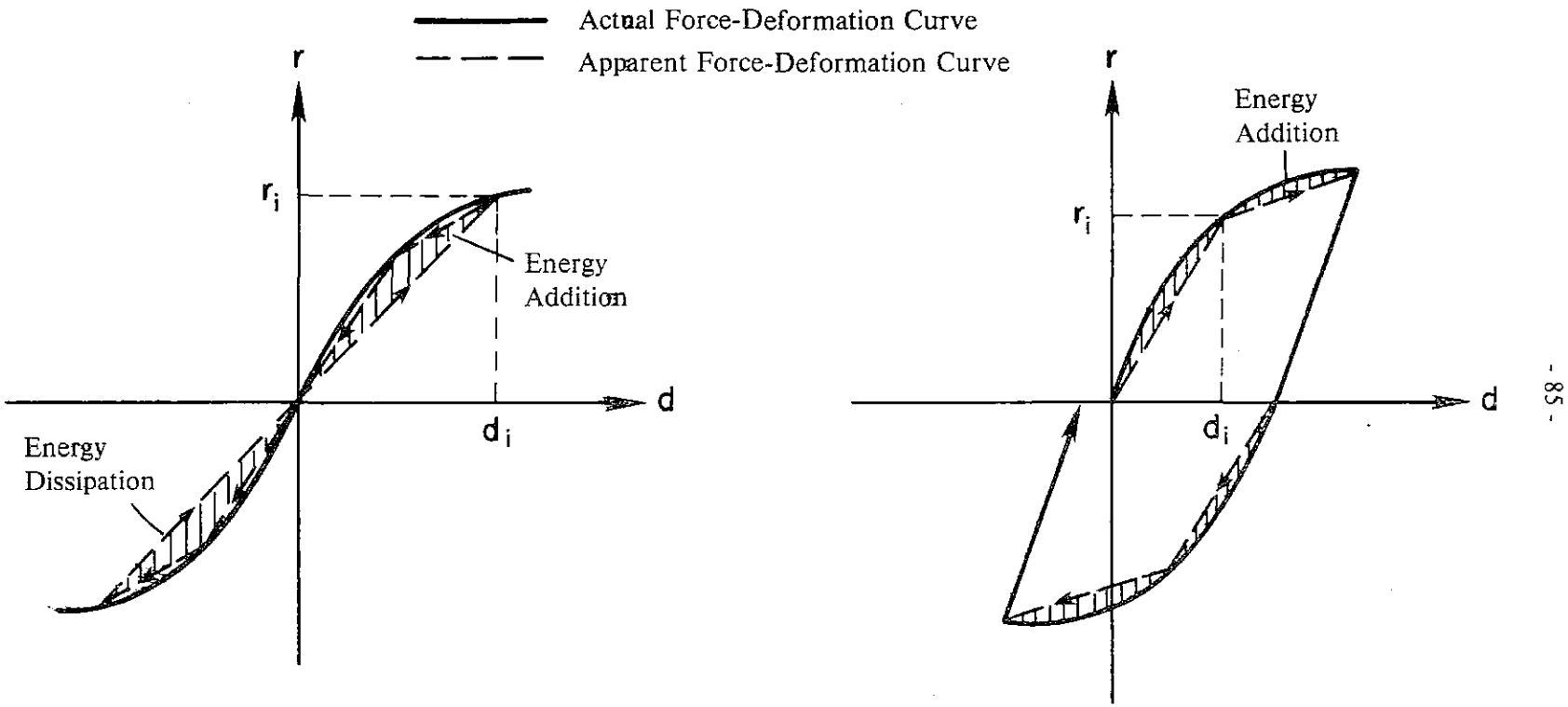

(a) Nonlinear Elastic System

(b) Inelastic System

Fig. 3.3 Erroneous Energy Effects in Solving the Equations of Motion of Nonlinear Systems by Means of Step-by-Step Integration

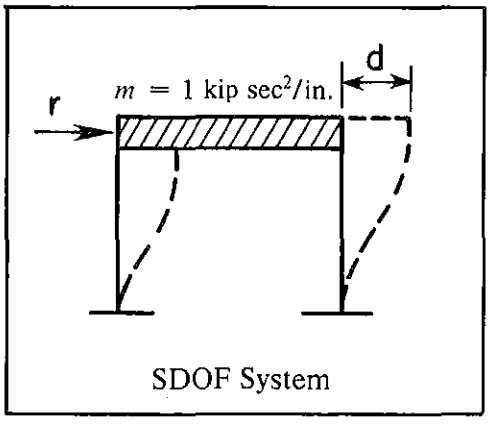

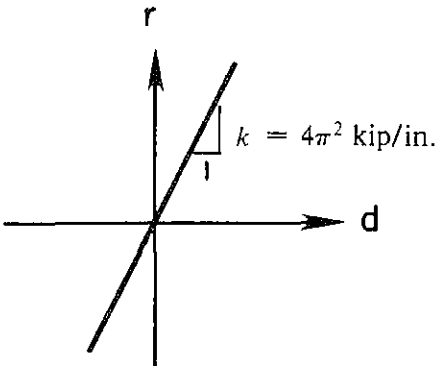

(i) Linear Elastic

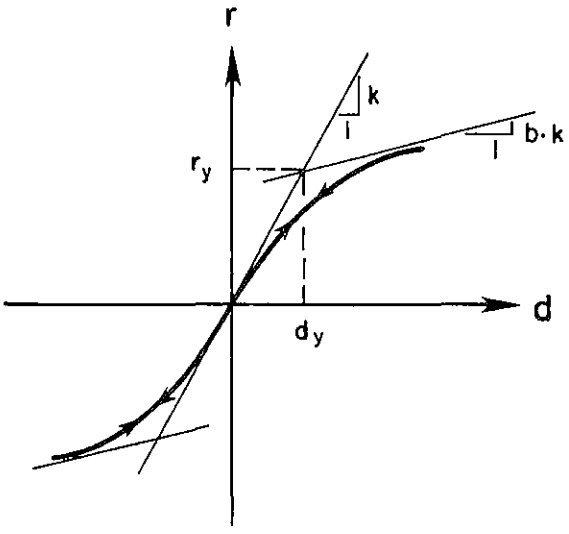

(ii) Nonlinear Elastic

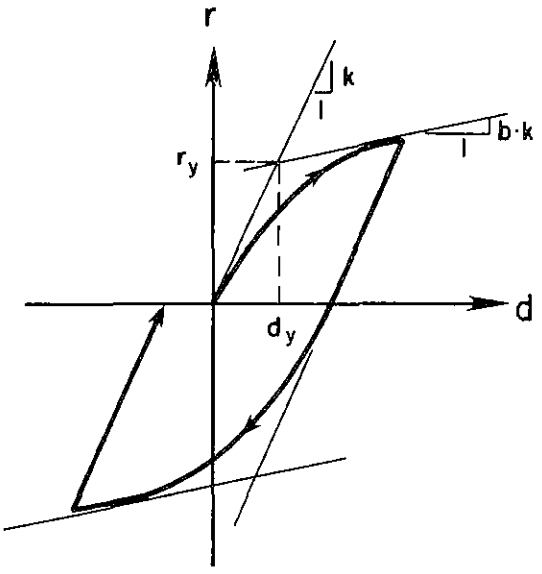

(iii) Inelastic

Menegotto-Pinto Model
(for Nonlinear Simulations)

$$\bar{r} = b\,\bar{d} + \frac{(1-b)\,\bar{d}}{(1+\bar{d}^{R})^{1/R}}$$

where

$\bar{r} = r/r_y$
$\bar{d} = d/d_y$
$k = r_y/d_y$

$d_y = 0.1$ in.
$r_y = 0.4\pi^2$ kip
$b = 0.02$
$R = 2$

Fig. 3.4 SDOF Numerical Simulations

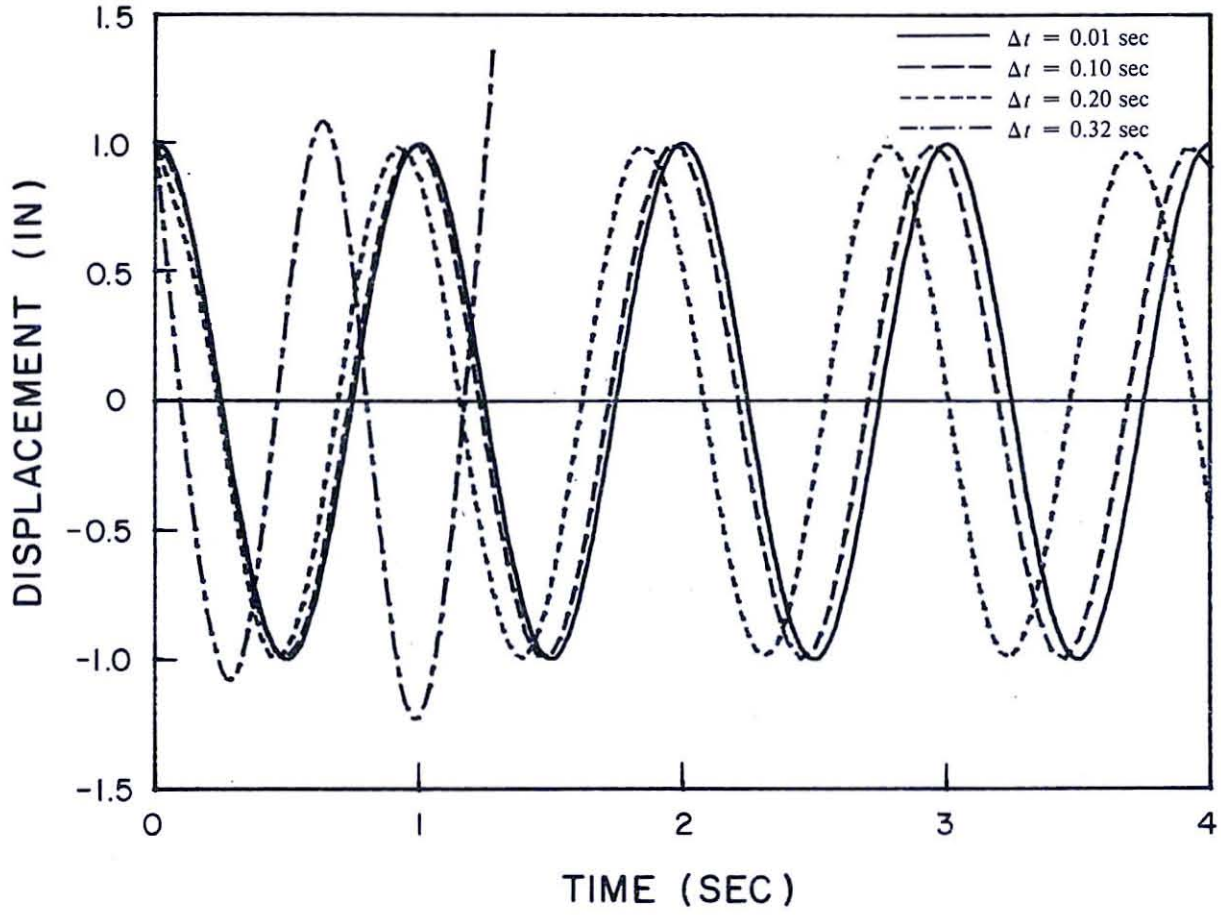

Fig. 3.5 Free-Vibration Response of a Linear Elastic SDOF System (Newmark Explicit Method)

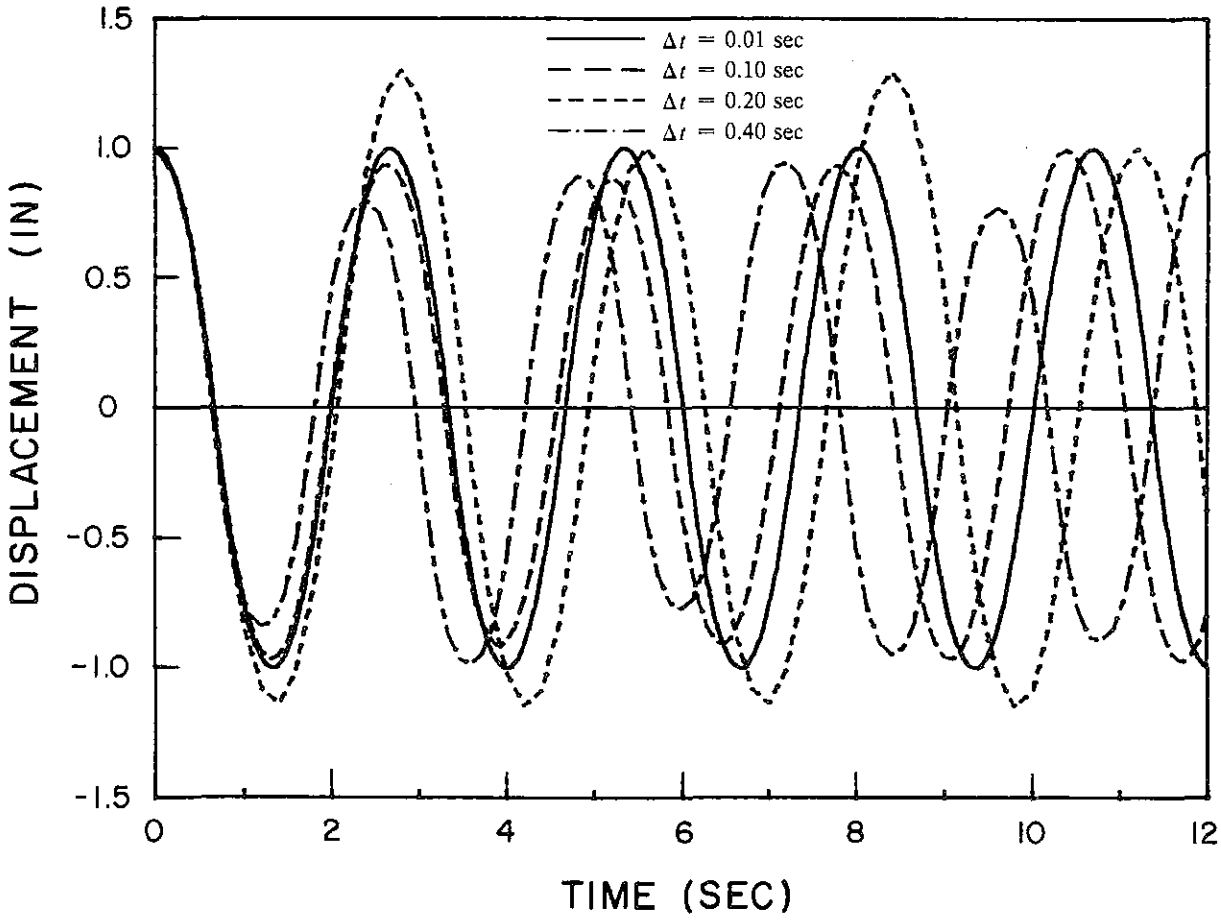

Fig. 3.6 Free-Vibration Response of a Nonlinear Elastic SDOF System (Newmark Explicit Method)

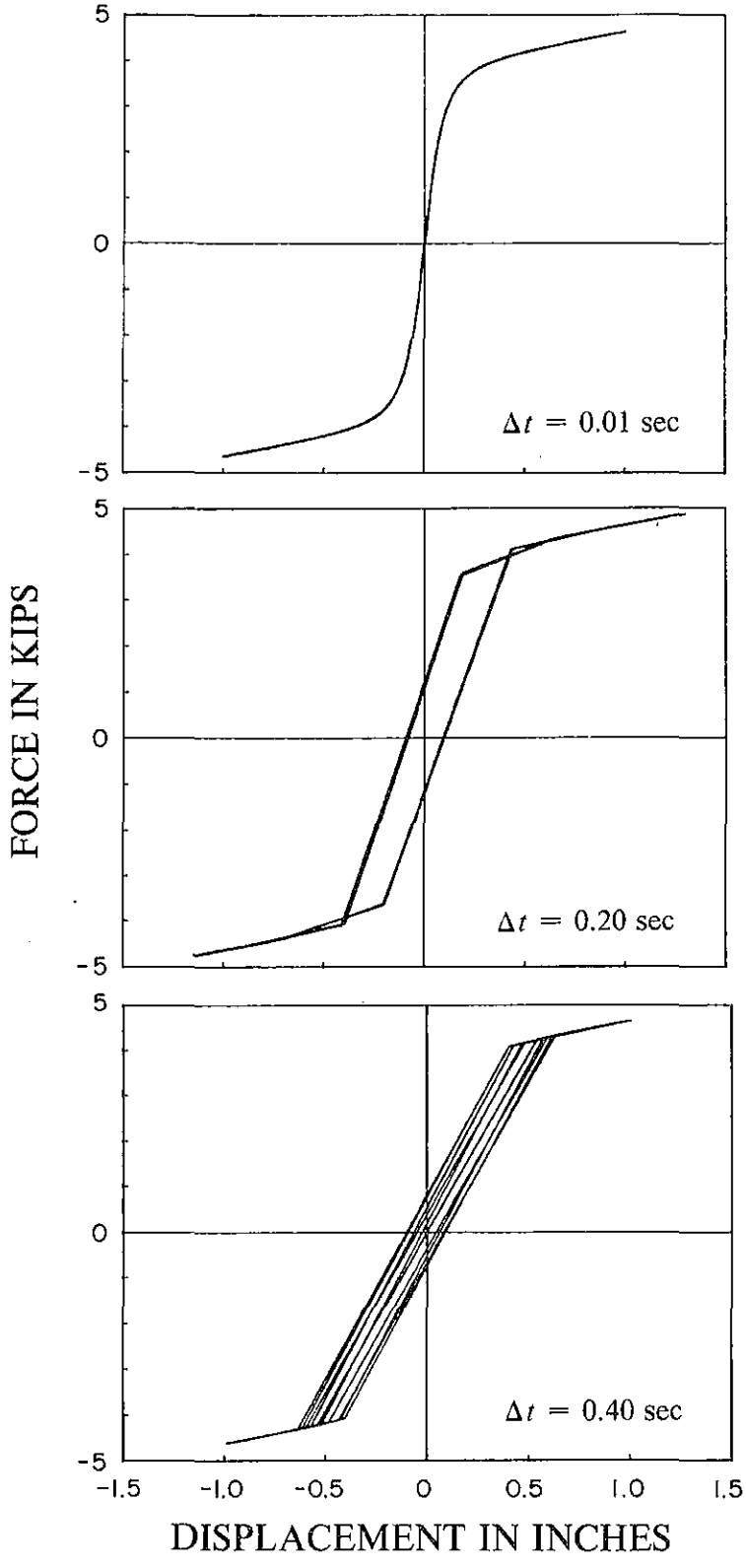

Fig. 3.7 Apparent Force-Deformation Curves of a Nonlinear Elastic System during Step-by-Step Integration

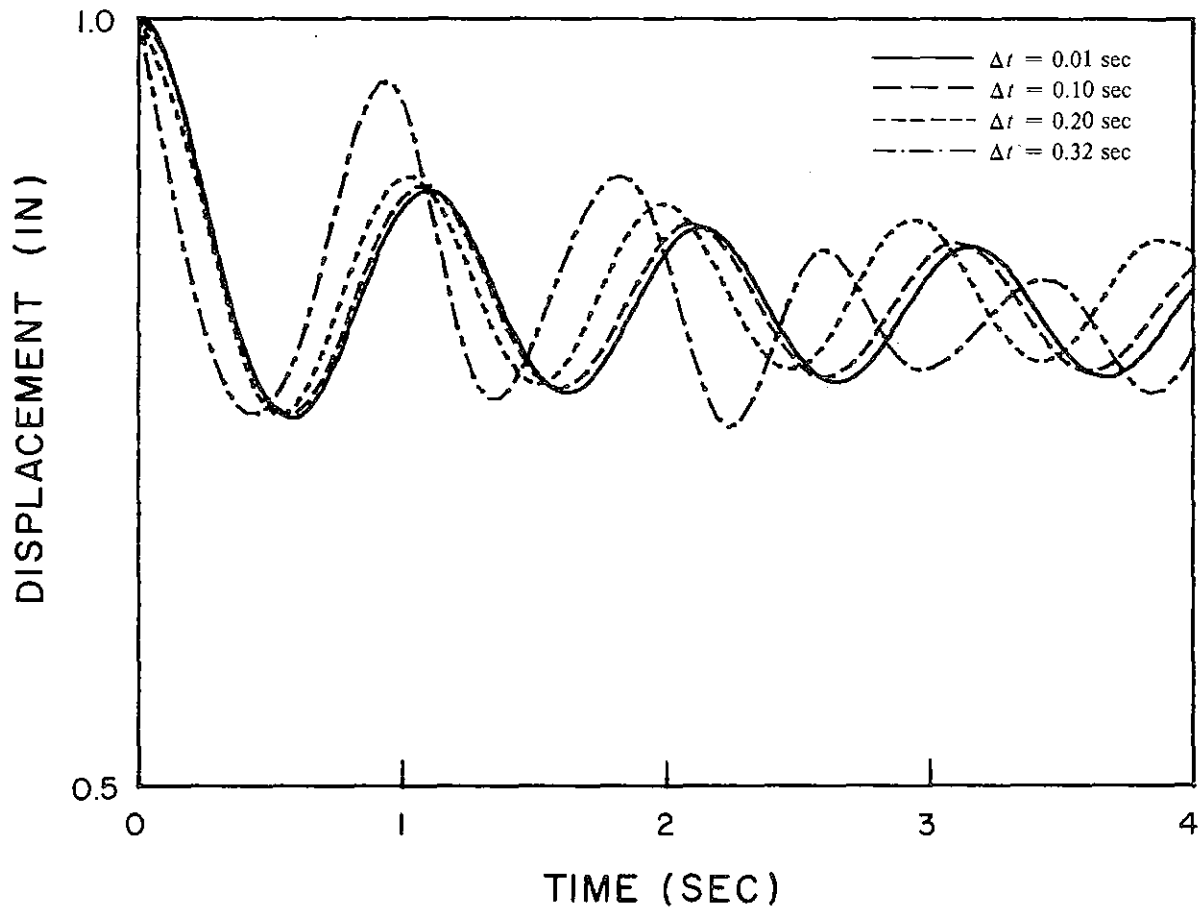

Fig. 3.8 Free-Vibration Response of an Inelastic SDOF System (Newmark Explicit Method)

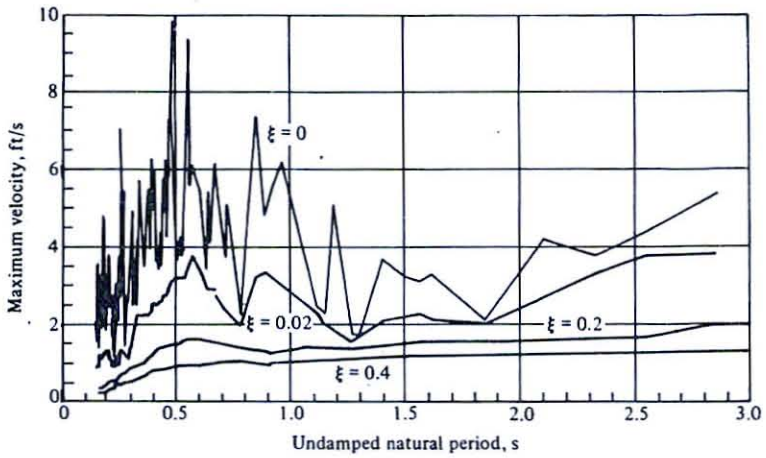

(a) Pseudo-Velocity Response Spectrum, El Centro Earthquake, May 18, 1940 (NS Component) [Ref. 16]

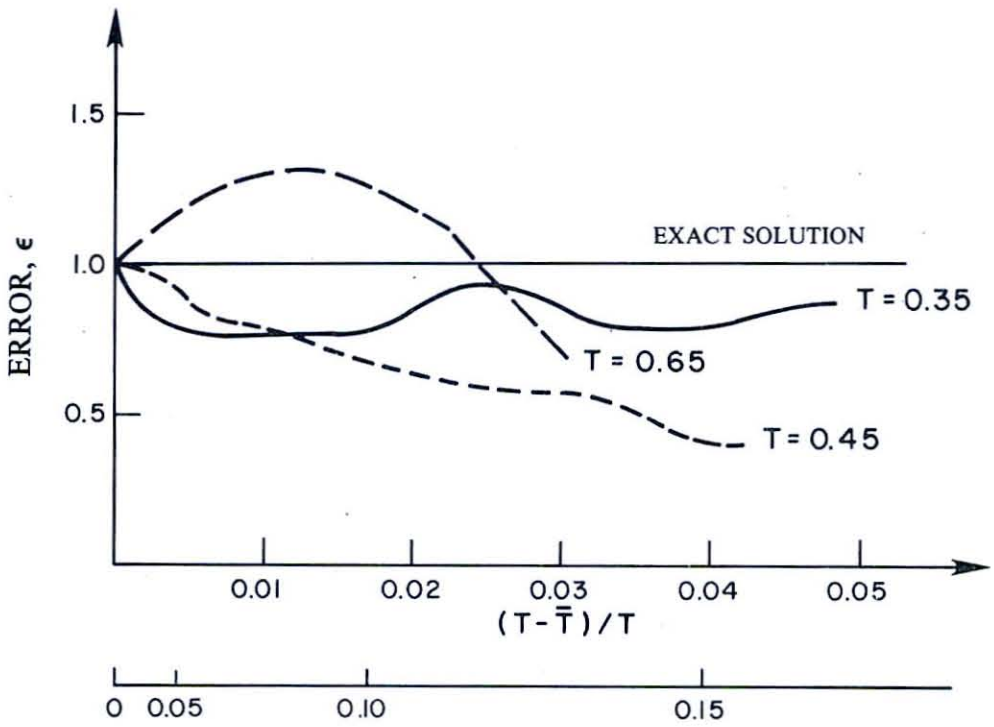

(b) Errors in Maximum Displacement Amplitudes due to Period Shrinkage (El Centro 1940)

Fig. 3.9 Effects of Frequency Distortion on Seismic Response Computations

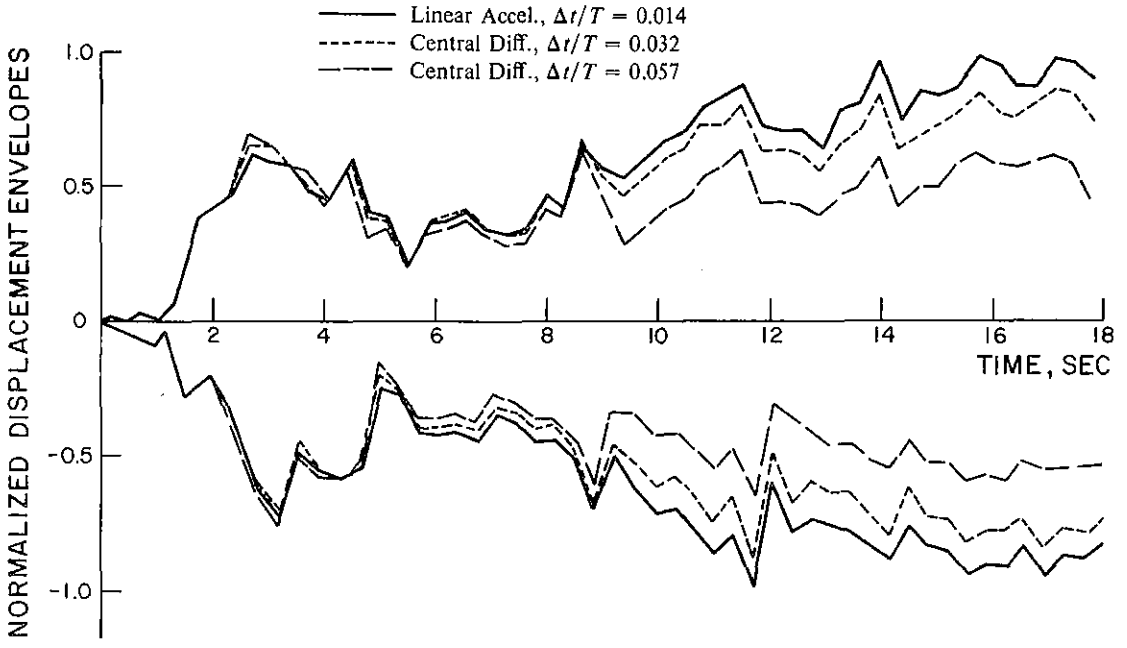

(a) $T = 0.35$ sec

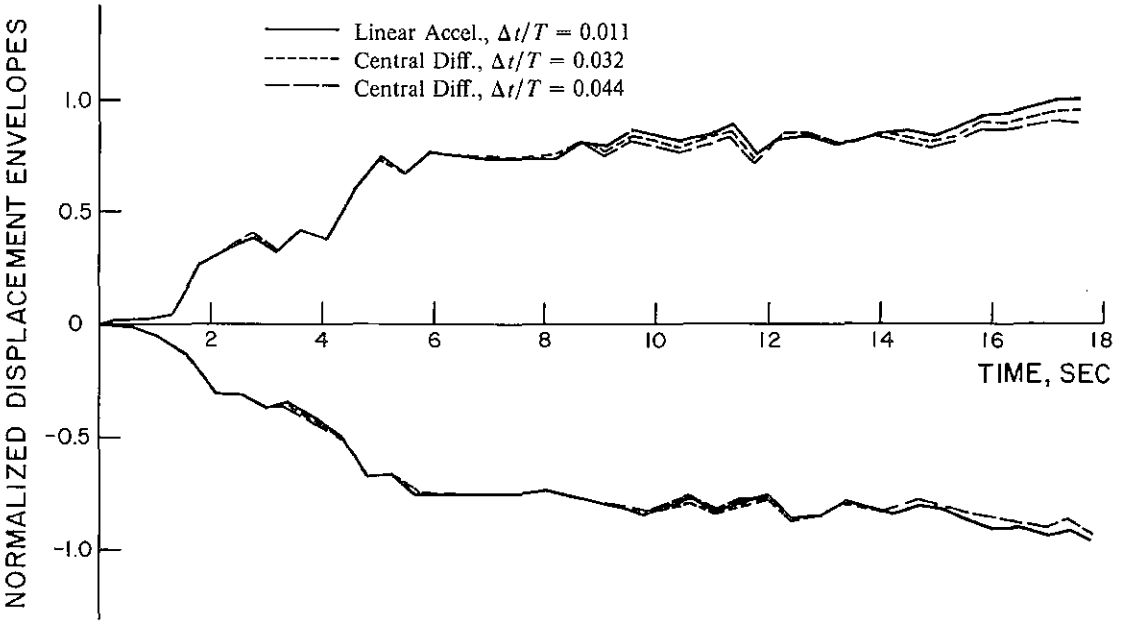

(b) $T = 0.45$ sec

Fig. 3.10 Response Envelopes of Linear Elastic SDOF Systems Subjected to the El Centro 1940 Earthquake (NS Component)

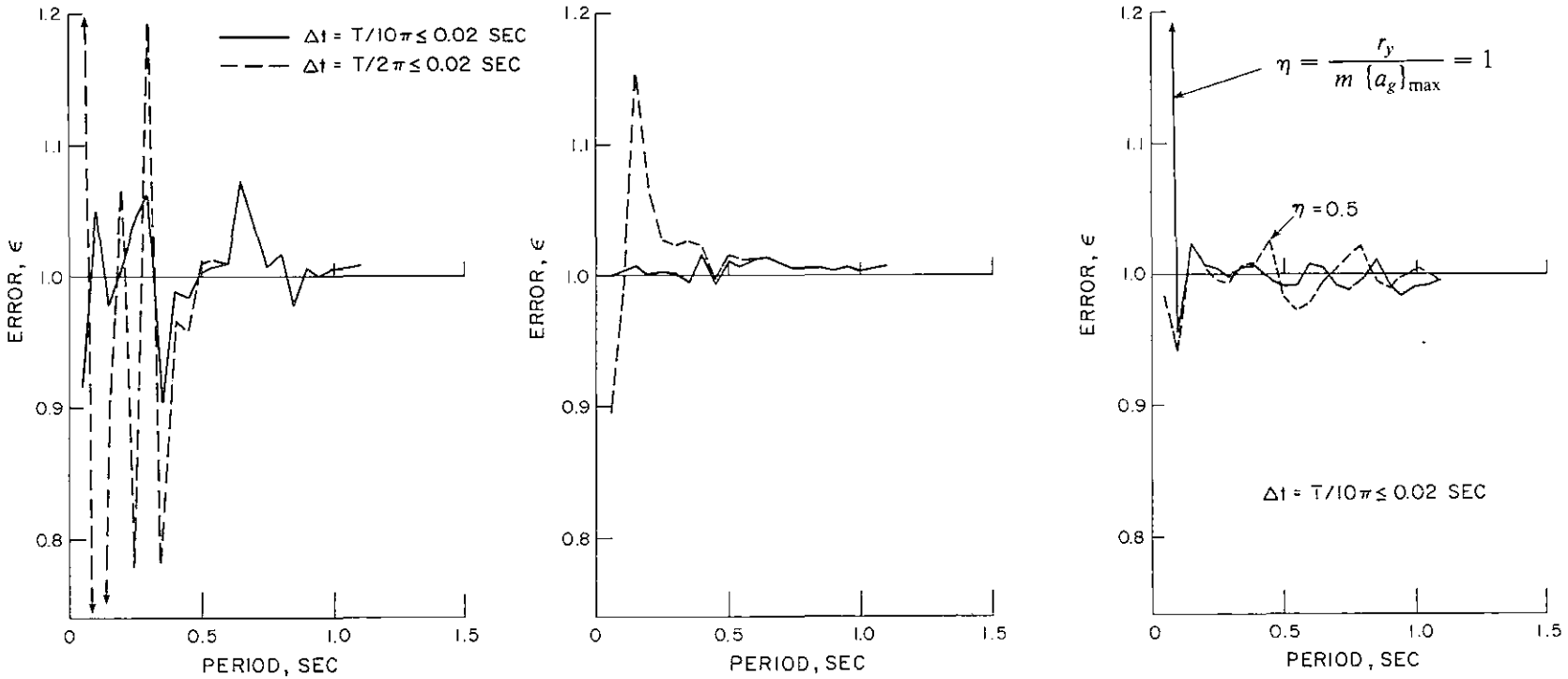

(a) Linear Elastic
No Damping

(b) Linear Elastic
5% Damping

(c) Elasto-Plastic
No Damping

Fig. 3.11 Error Spectra for Single-Degree-of-Freedom Systems
Subjected to the El Centro 1940 Earthquake

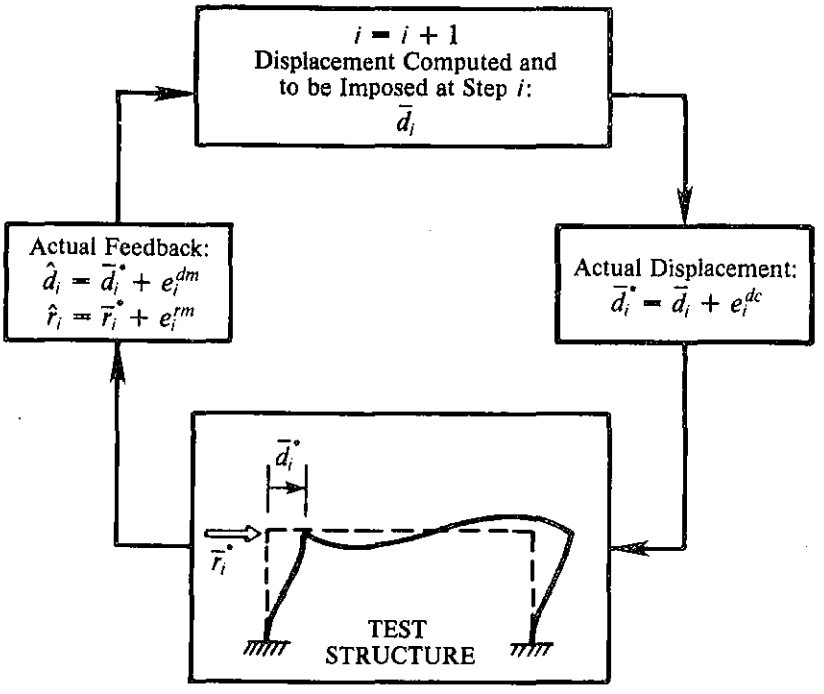

Fig. 3.12 Sources of Experimental Errors in Pseudodynamic Testing

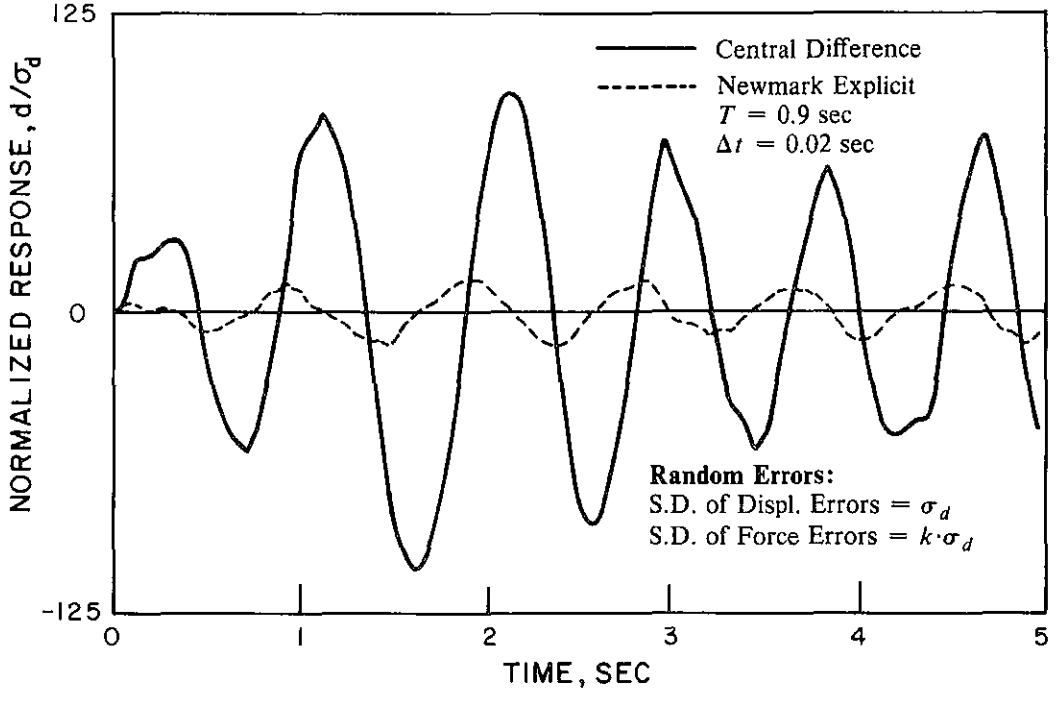

Fig. 3.13 Spurious Displacement Response of a Linear Elastic SDOF System Subjected to Random Feedback Errors during Numerical Integration

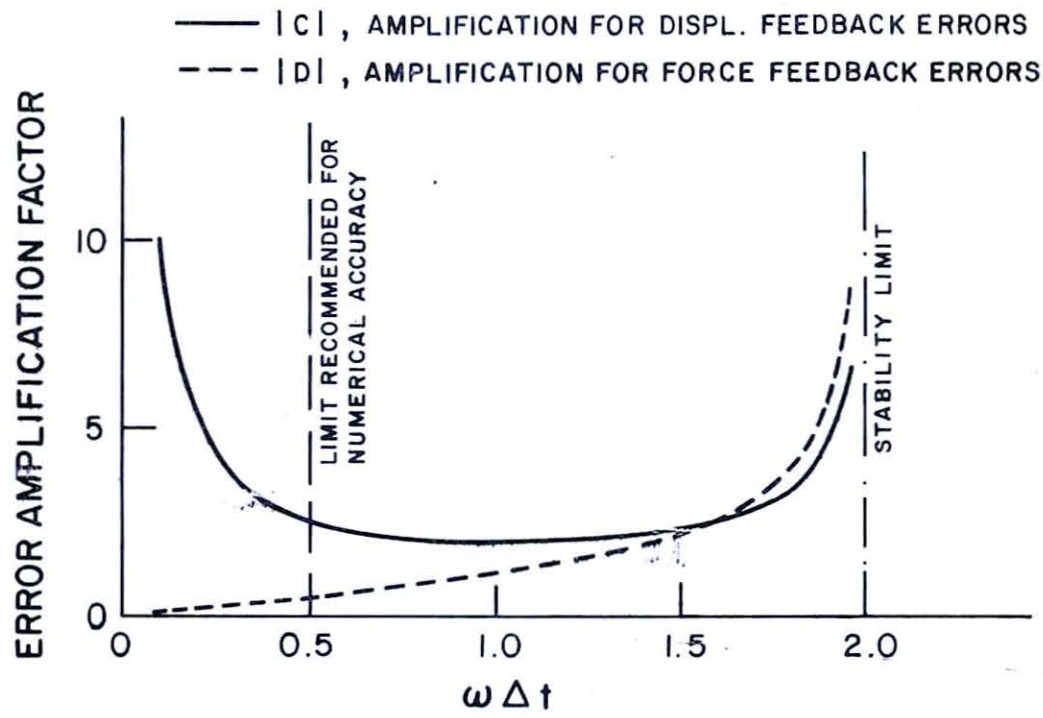

(a) Basic Central Difference Method

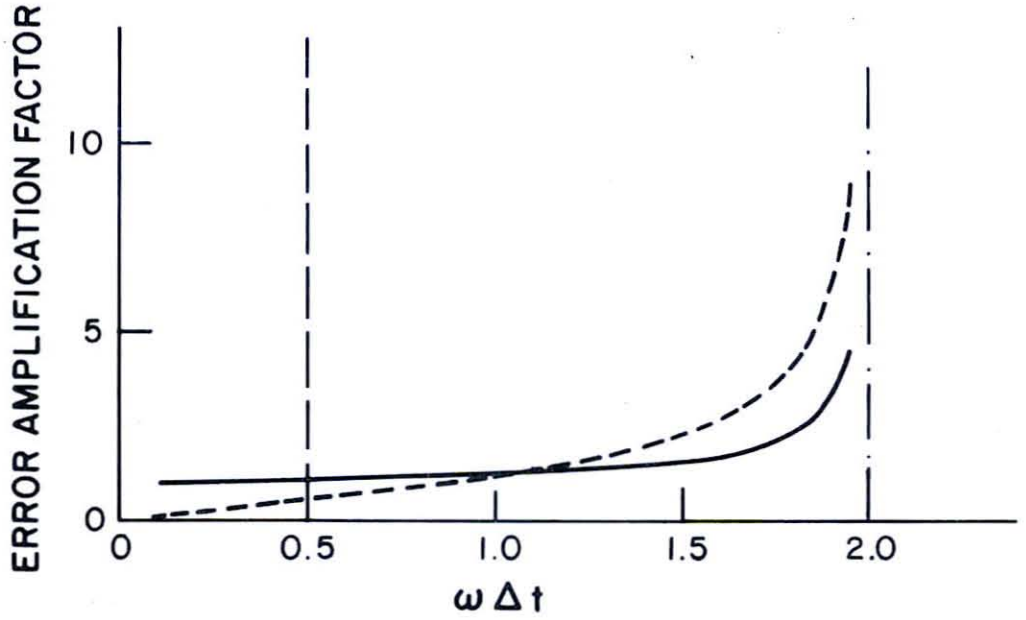

(b) Summed-Form Central Difference and Newmark Explicit Methods

Fig. 3.14 Comparisons of Cumulative Error Growth Among Different Integration Methods

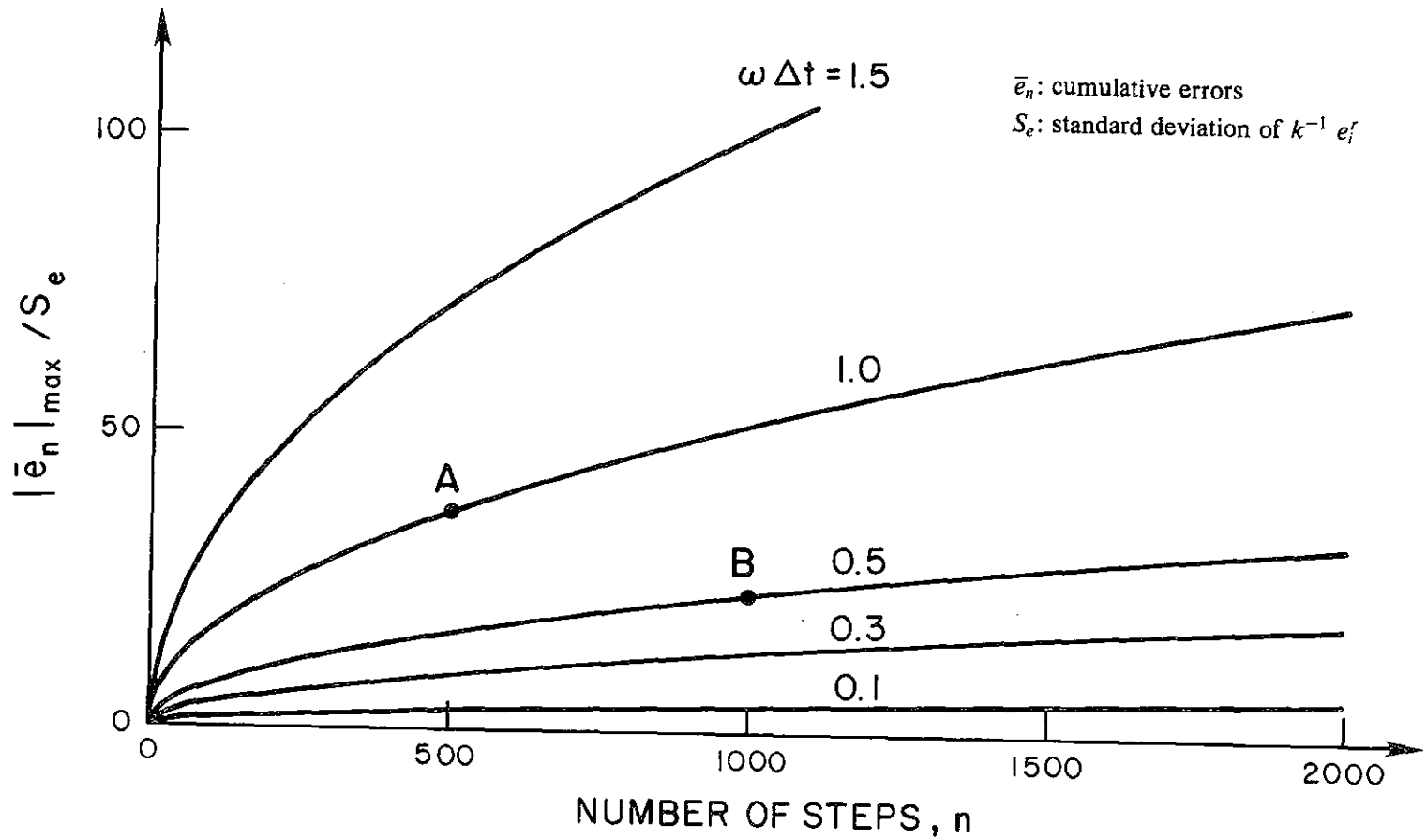

Fig. 3.15 Cumulative Error Bounds due to Random Force-Feedback Errors (e_i')

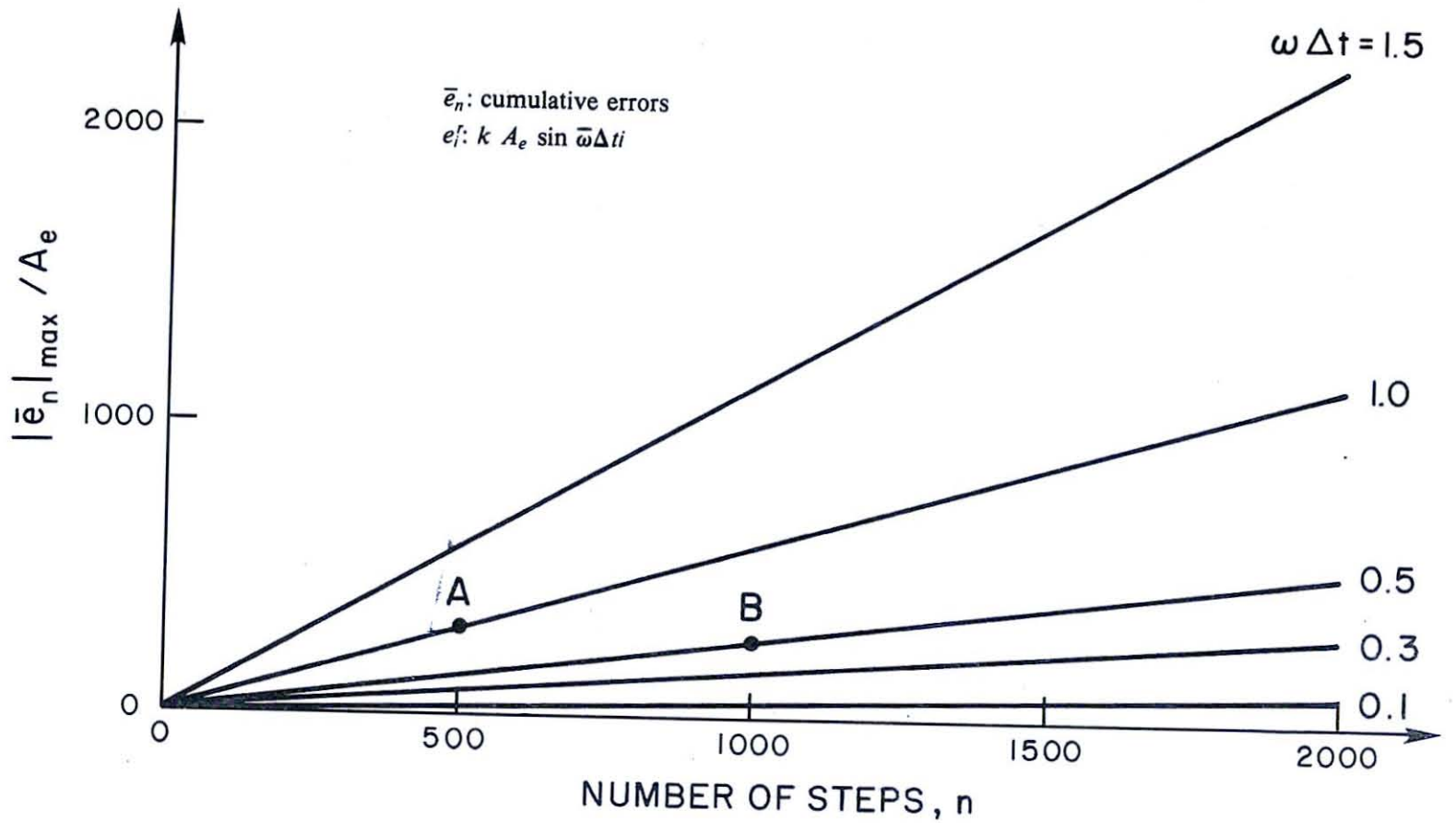

Fig. 3.16 Cumulative Error Bounds due to Sinusoidal Force-Feedback Errors (e_i') at Resonance Frequency ($\bar{\omega}$)

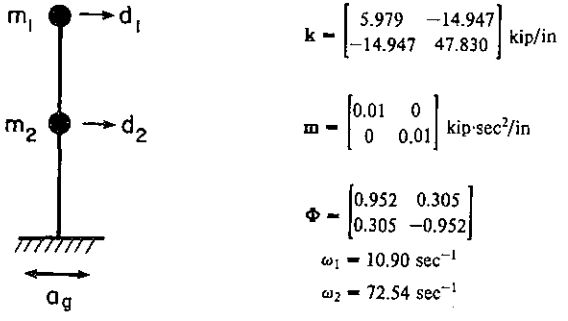

(a) Two-Degree-of-Freedom System

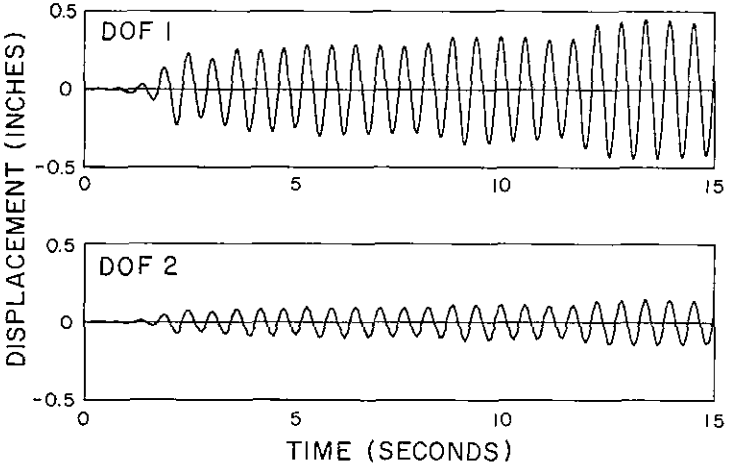

(b) Exact Numerical Solution

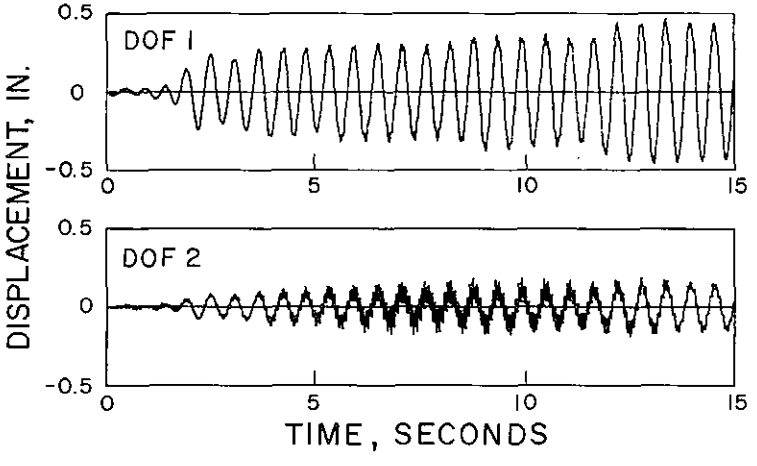

(c) Response with Random Errors

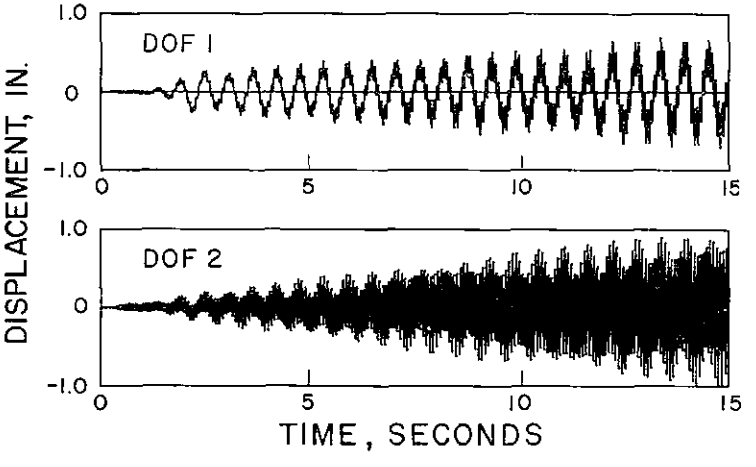

(d) Response with Systematic Errors

Fig. 3.17 Simulation of Experimental Error Effects using Newmark Explicit Method (Δt = 0.02 sec; a_g = 1940 El Centro (NS) with 0.02g Peak Acceleration)

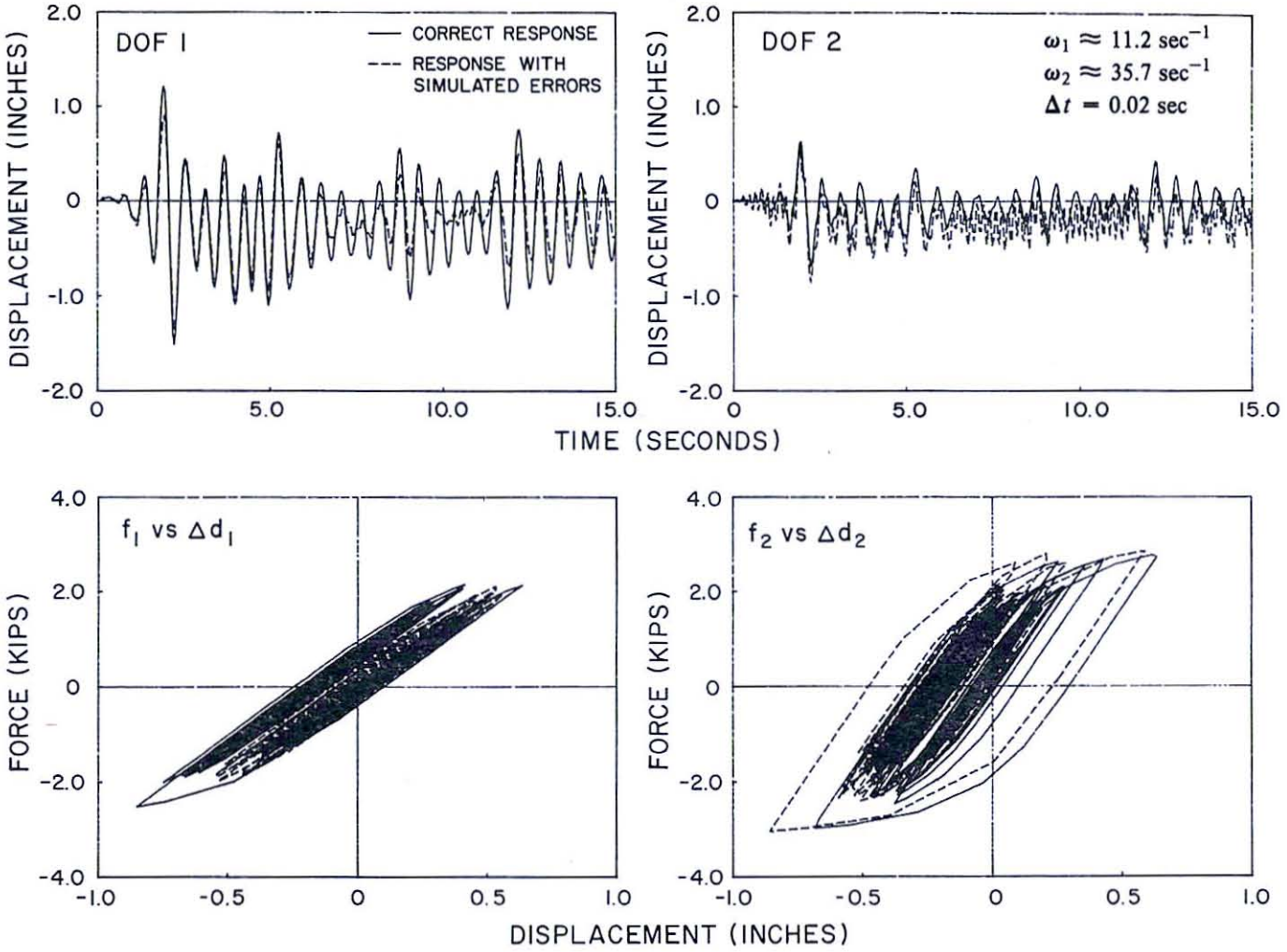

Fig. 3.18 Inelastic Responses of a Two-Story Shear Building with Systematic Errors (e_i') to El Centro 1940 (NS), 0.18g Ground Acceleration (Newmark Explicit Algorithm)

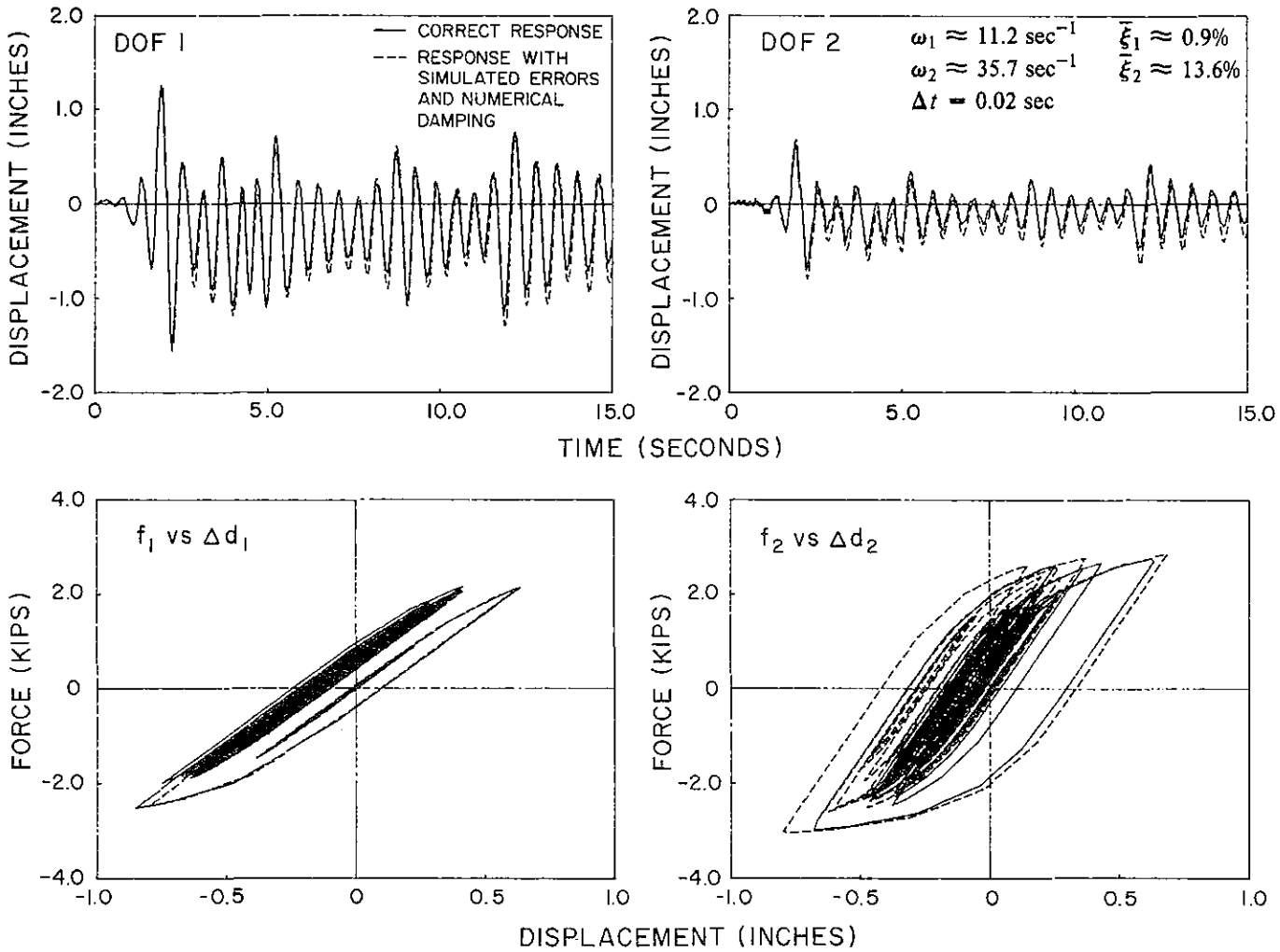

Fig. 3.19 Inelastic Responses of a Two-Story Shear Building with Systematic Errors (e_i') to El Centro 1940 (NS), 0.18g Ground Acceleration (Modified Newmark Algorithm, $\alpha = 0.4$, $\rho = -0.016$)

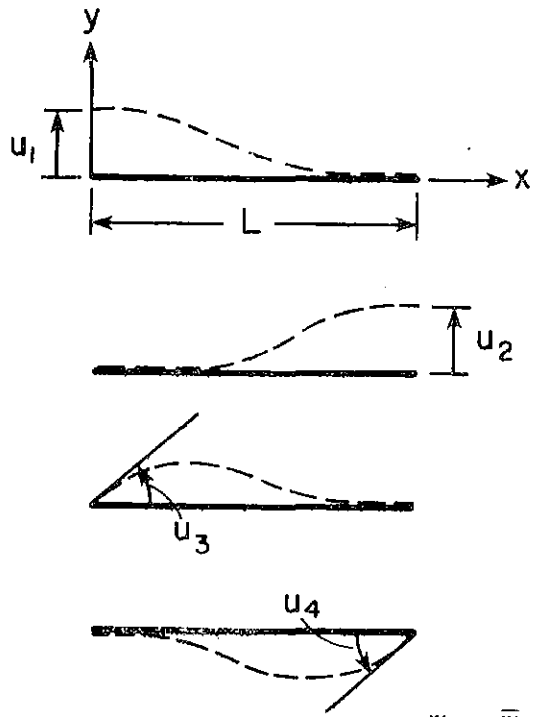

Shape Functions:

$$\psi_1 = 1 - 3\left(\frac{x}{L}\right)^2 + 2\left(\frac{x}{L}\right)^3$$

$$\psi_2 = 3\left(\frac{x}{L}\right)^2 - 2\left(\frac{x}{L}\right)^3$$

$$\psi_3 = x\left(1 - \frac{x}{L}\right)^2$$

$$\psi_4 = \frac{x^2}{L}\left(\frac{x}{L} - 1\right)$$

$$m_{ij} = \bar{m}\int_0^L \psi_i\,\psi_j\,dx$$

$$\mathbf{m} = \frac{\bar{m}\,L}{420}\begin{array}{c} \begin{matrix} \ddot{u}_1 & \ddot{u}_2 & \ddot{u}_3 & \ddot{u}_4 \end{matrix} \\ \begin{bmatrix} 156 & 54 & 22L & -13L \\ 54 & 156 & 13L & -22L \\ 22L & 13L & 4L^2 & -3L^2 \\ -13L & -22L & -3L^2 & 4L^2 \end{bmatrix} \end{array}$$

(a) Consistent-Mass Matrix

$$\mathbf{m} = \frac{\bar{m}\,L}{2}\begin{array}{c} \begin{matrix} \ddot{u}_1 & \ddot{u}_2 \end{matrix} \\ \begin{bmatrix} 1 & 0 \\ 0 & 1 \end{bmatrix} \end{array}$$

(b) Lumped-Mass Matrix

Fig. 4.1 Formulation of the Mass Matrix for a Beam Element

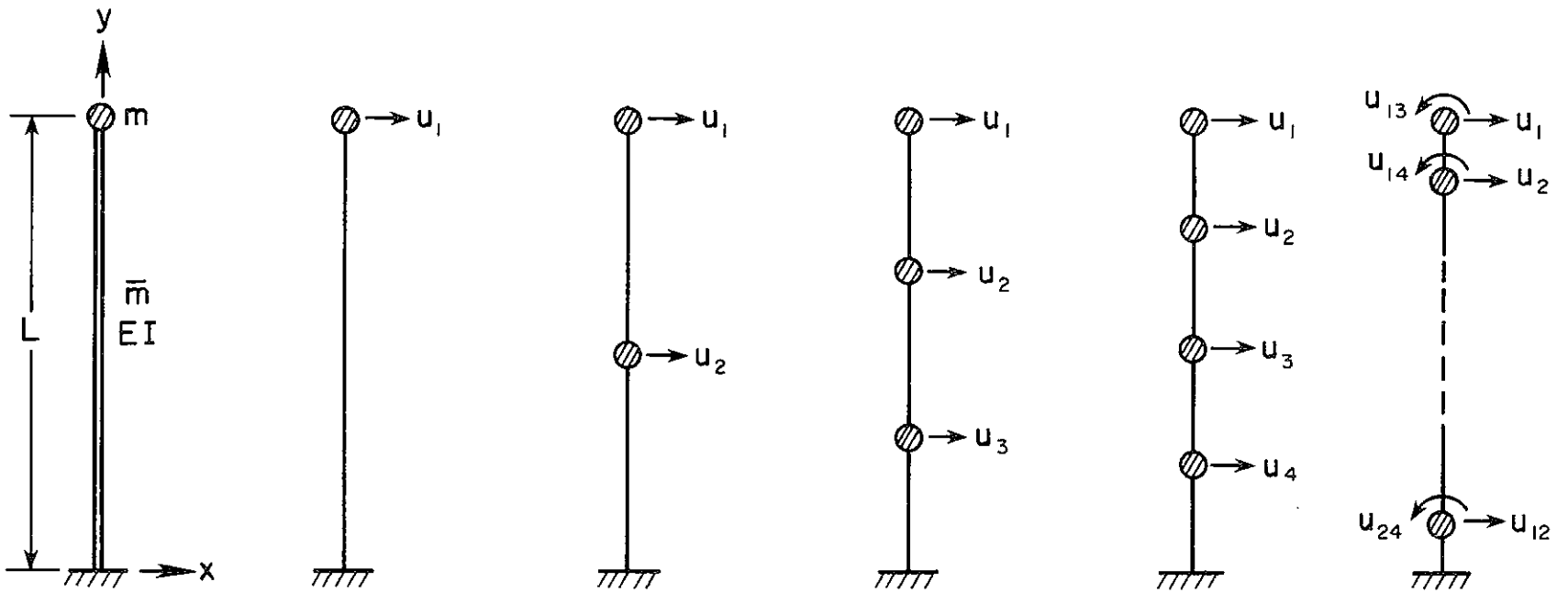

(a) Uniform Column (b) 1-DOF Lumped-Mass (c) 2-DOF Lumped-Mass (d) 3-DOF Lumped-Mass (e) 4-DOF Lumped-Mass (f) 24-DOF Consistent-Mass

Fig. 4.2 Discrete-Parameter Models for a Cantilever Column

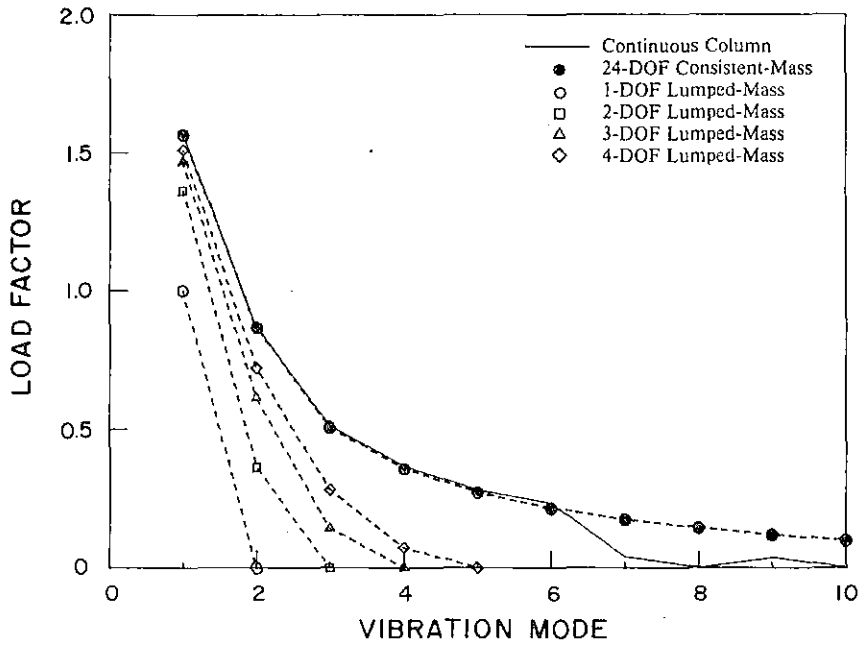

(a) Modal Participation

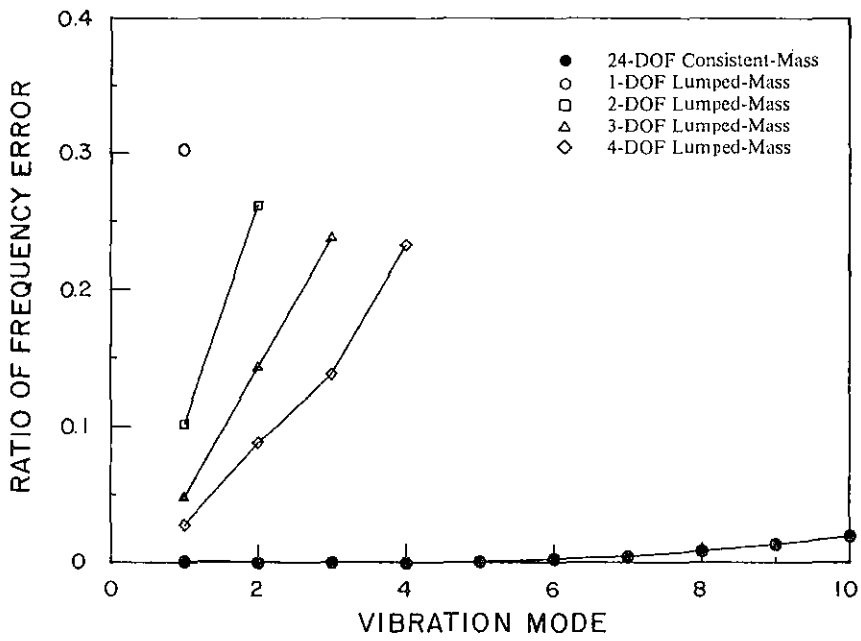

(b) Frequency Error

Fig. 4.3 Comparison of Discrete-Parameter Models for a Uniform Cantilever Column with No Mass Concentration

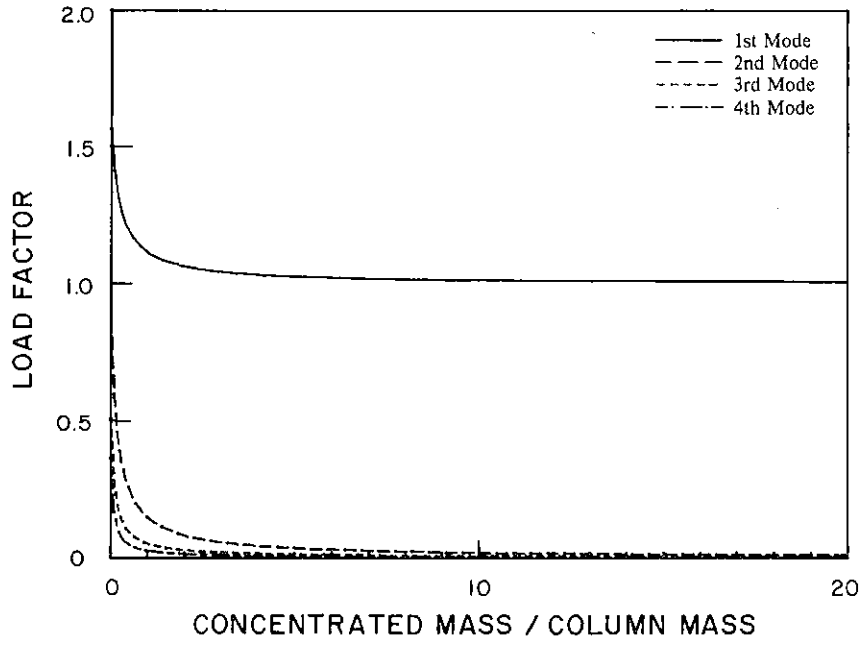

(a) Modal Participation

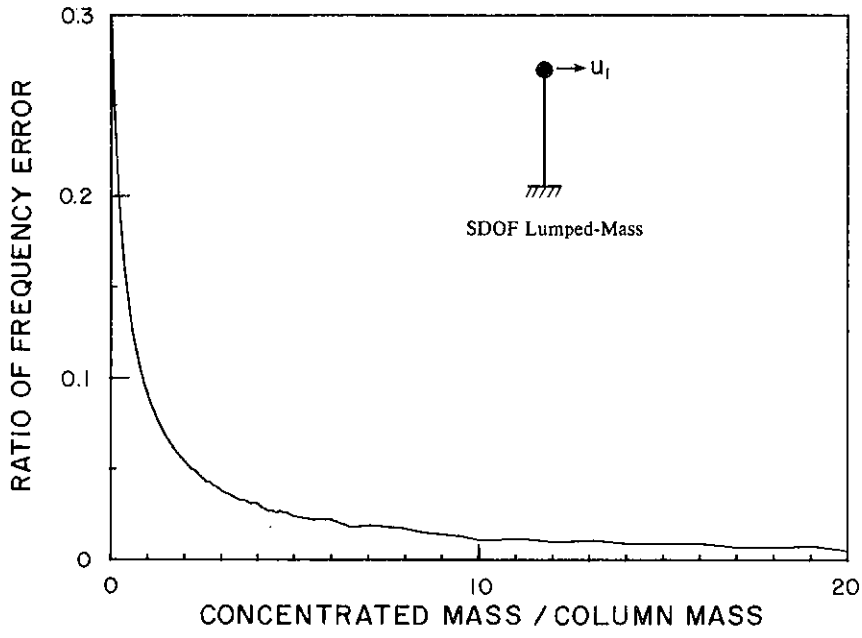

(b) Frequency Error

Fig. 4.4 Discrete-Parameter Representation of a Uniform Cantilever Column with a Single Concentrated Mass

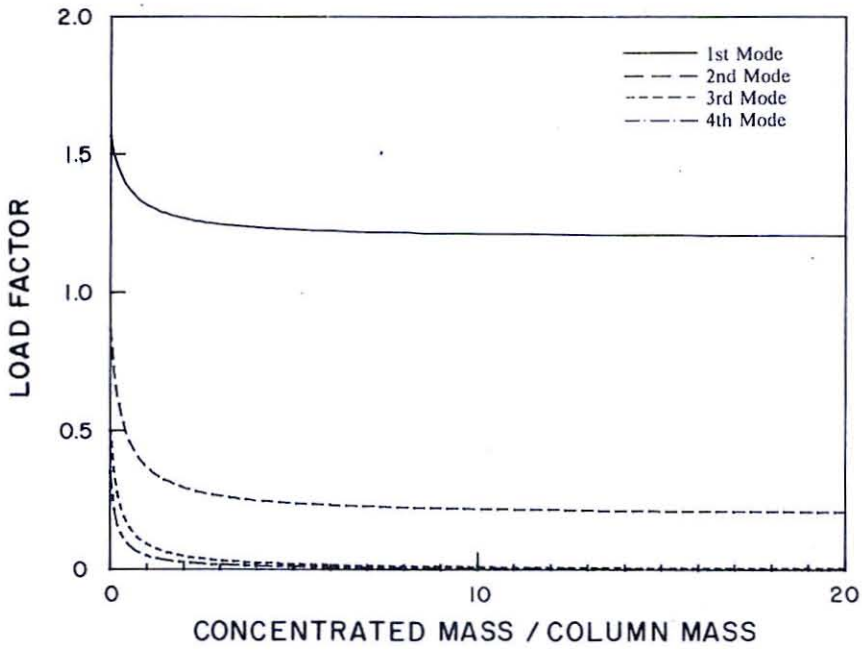

(a) Modal Participation

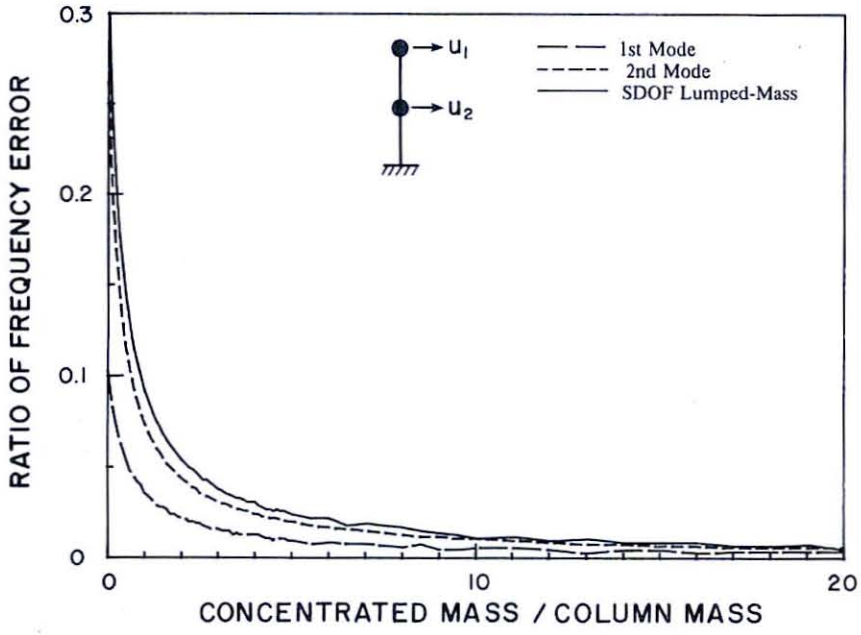

(b) Frequency Error

Fig. 4.5 Discrete-Parameter Representation of a Uniform Cantilever Column with Two Equal Concentrated Masses

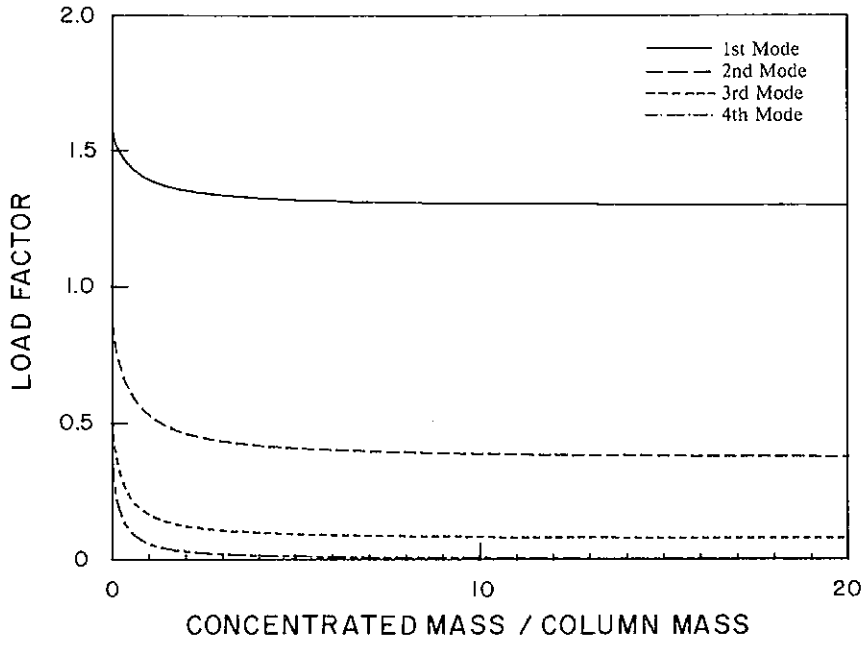

(a) Modal Participation

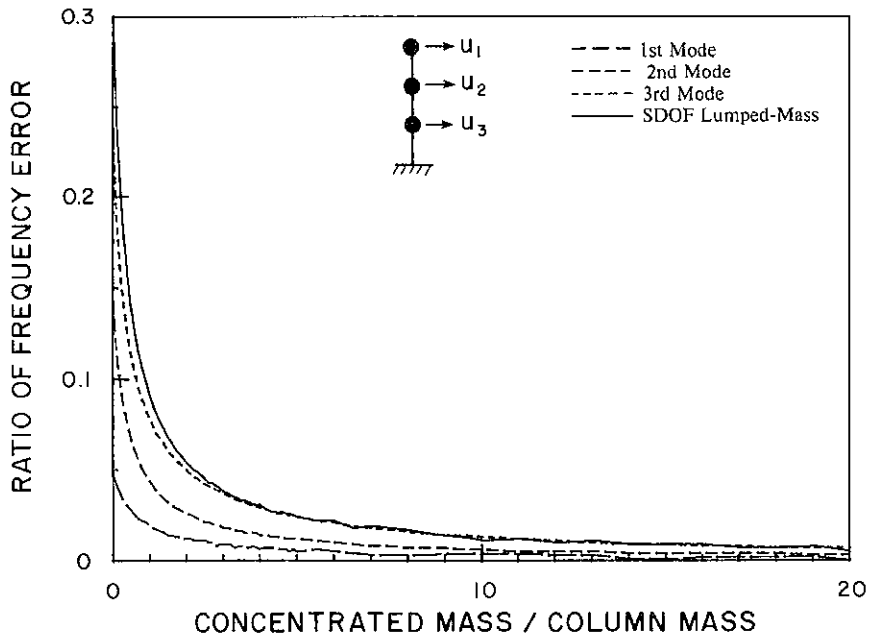

(b) Frequency Error

Fig. 4.6 Discrete-Parameter Representation of a Uniform Cantilever Column with Three Equal Concentrated Masses

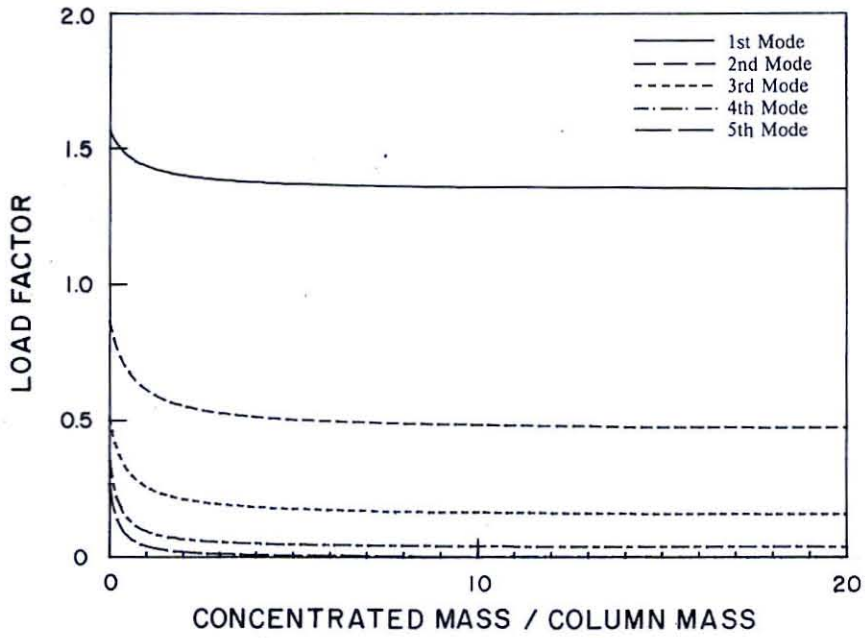

(a) Modal Participation

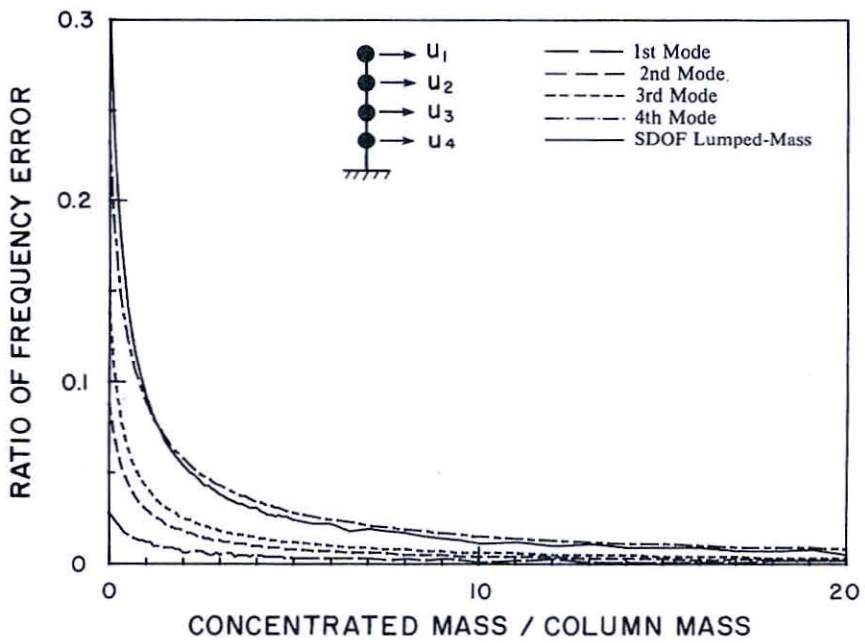

(b) Frequency Error

Fig. 4.7 Discrete-Parameter Representation of a Uniform Cantilever Column with Four Equal Concentrated Masses

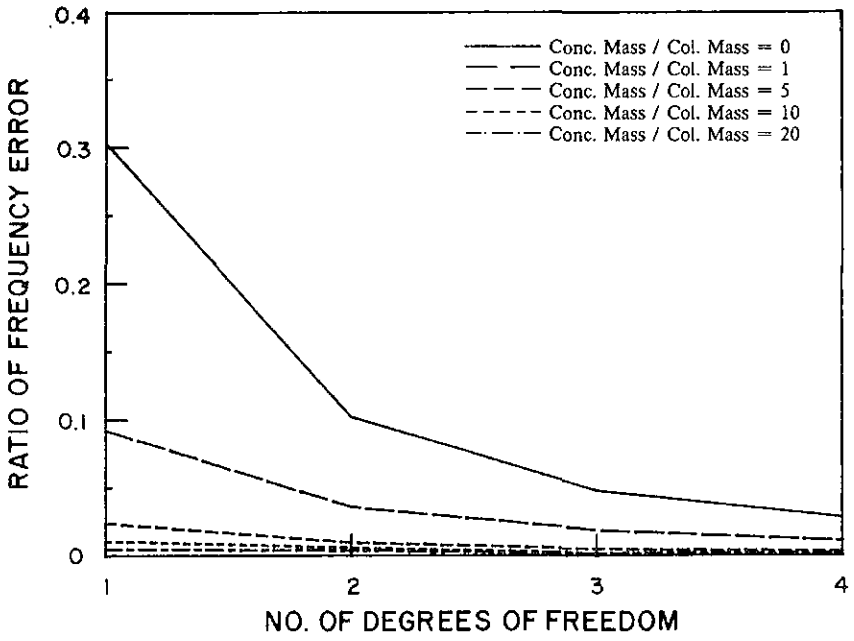

(a) 1st Mode Frequency

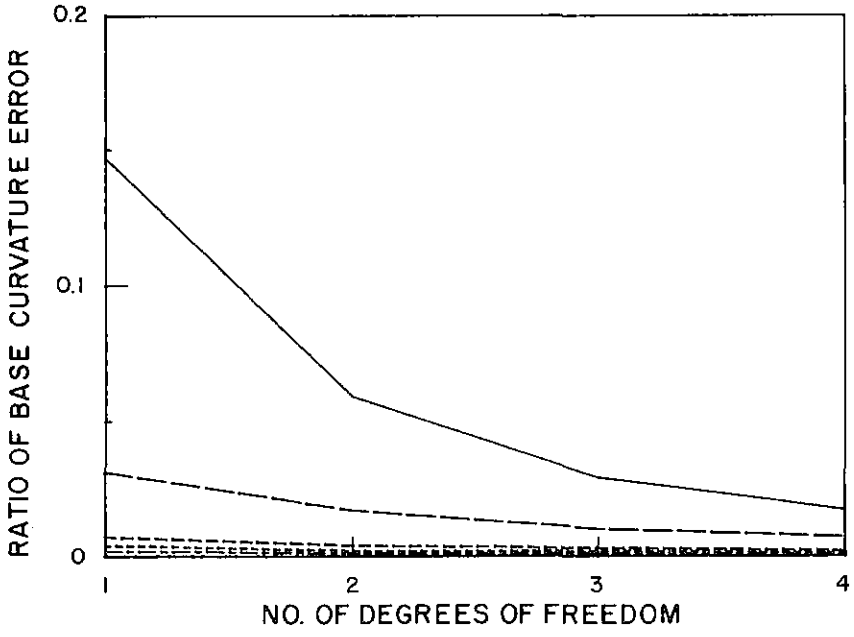

(b) Base Curvature due to 1st Mode Deformation

Fig. 4.8 Comparison of Frequency and Base Curvature Errors

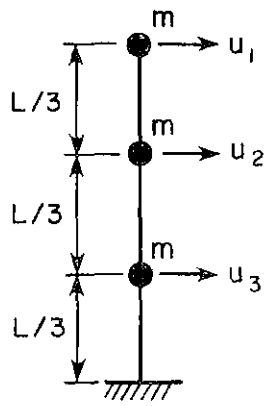

$$\mathbf{m} = \frac{\bar{m}\,L}{5670}\begin{matrix}\ddot{u}_1 & \ddot{u}_2 & \ddot{u}_3\end{matrix}\begin{bmatrix}702 & 243 & 0\\ 243 & 1404 & 243\\ 0 & 243 & 1404\end{bmatrix} + m\begin{bmatrix}1 & 0 & 0\\ 0 & 1 & 0\\ 0 & 0 & 1\end{bmatrix}$$

(a) Consistent-Mass Matrix without Rotational Inertia

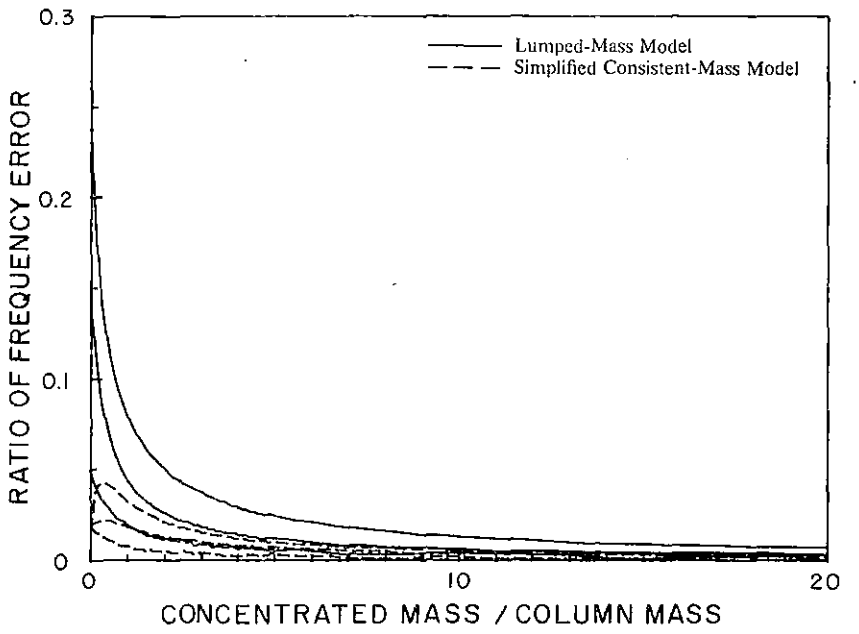

(b) Frequency Error

Fig. 4.9 Simplified Consistent-Mass Formulation

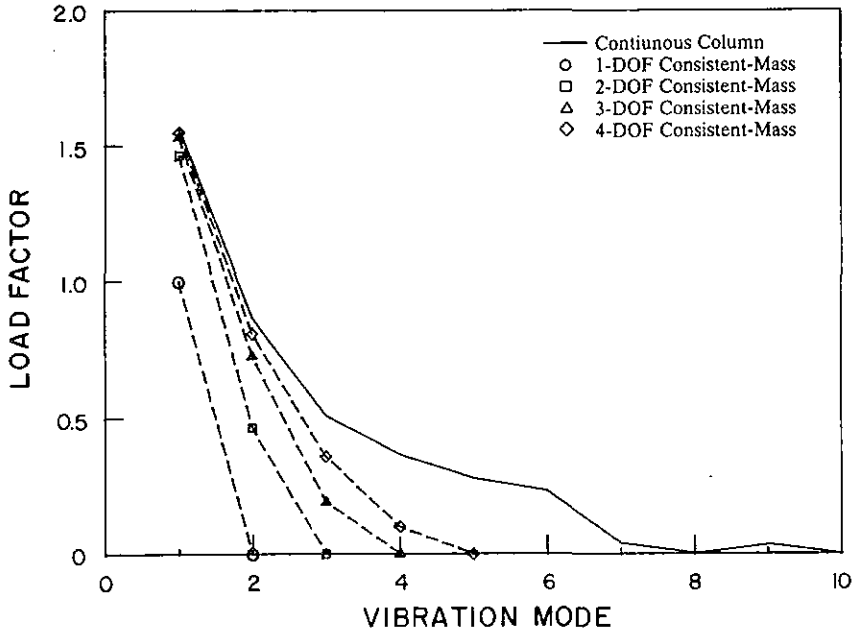

(a) Modal Participation

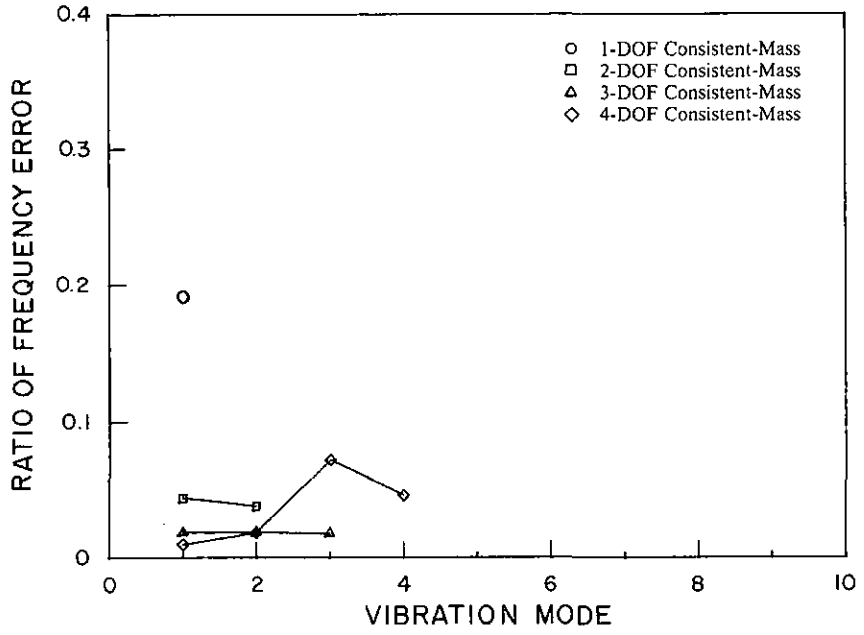

(b) Frequency Error

Fig. 4.10 Accuracy of Simplified Consistent-Mass Models

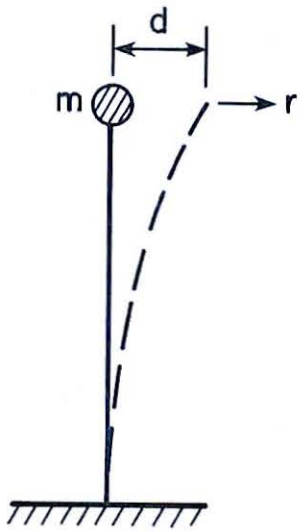

(a) SDOF System

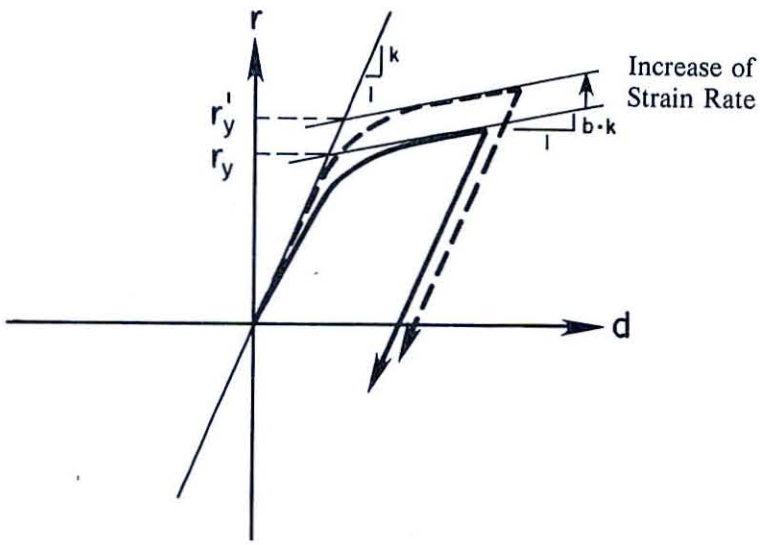

(b) Menegotto-Pinto Model

Fig. 4.11 Simulation of Strain-Rate Effects

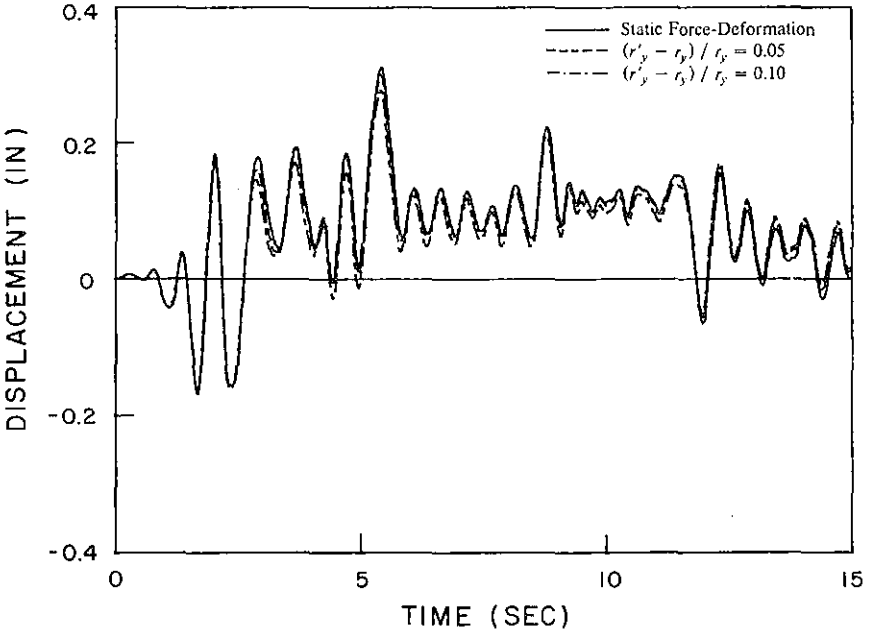

(a) Displacement History

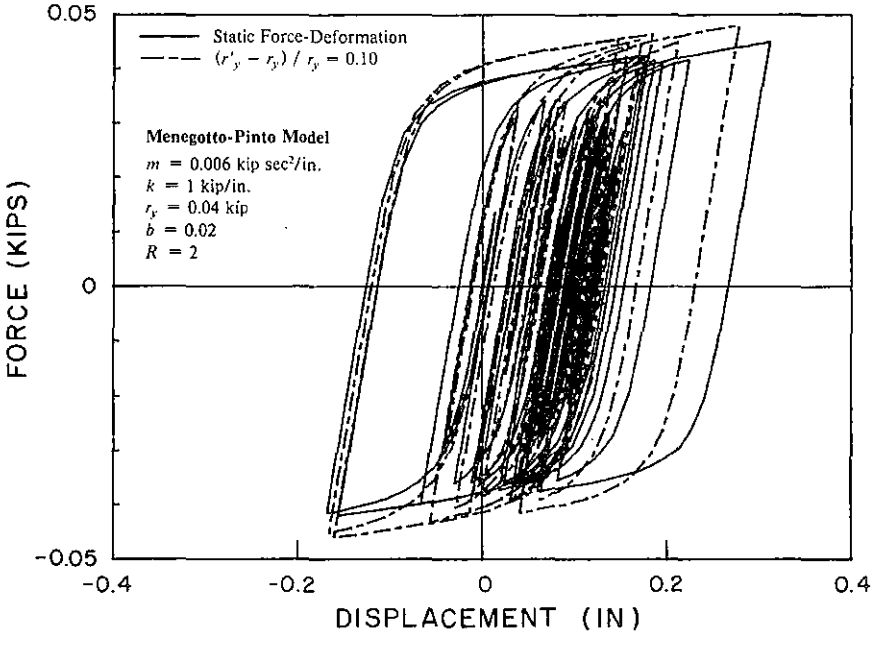

(b) Force-Deformation Hysteretic Loops

Fig. 4.12 Strain-Rate Effects on the Seismic Response of a SDOF System (El Centro 1940 (NS), 0.045g)

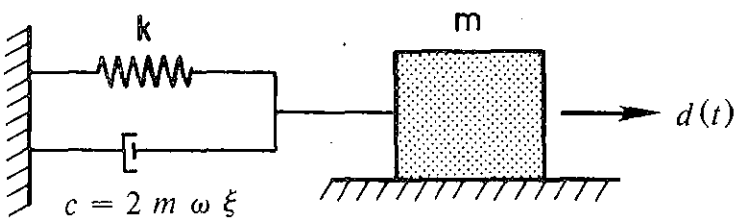

(a) SDOF System

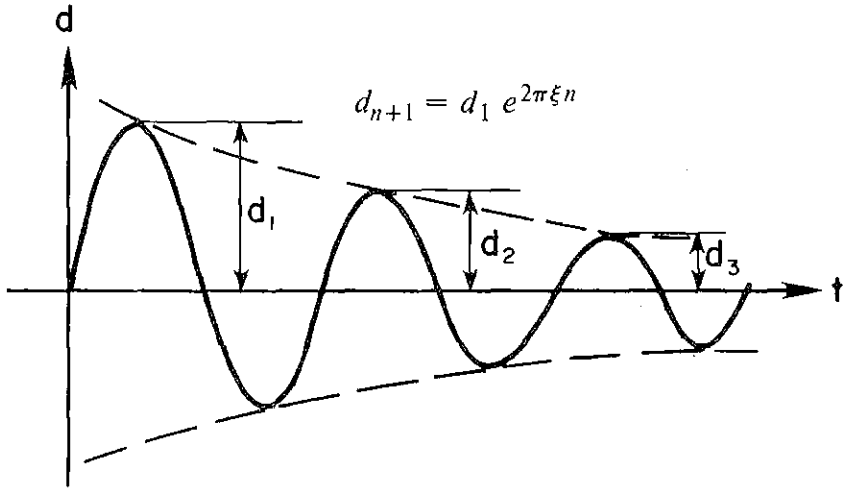

(b) Free-Vibration Response

Fig. 4.13 Viscous Damping

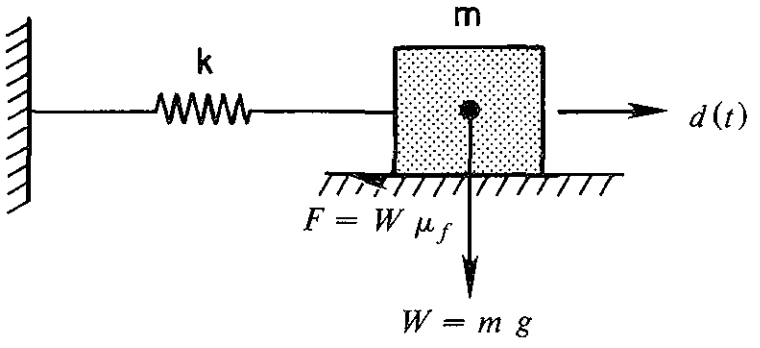

(a) SDOF System

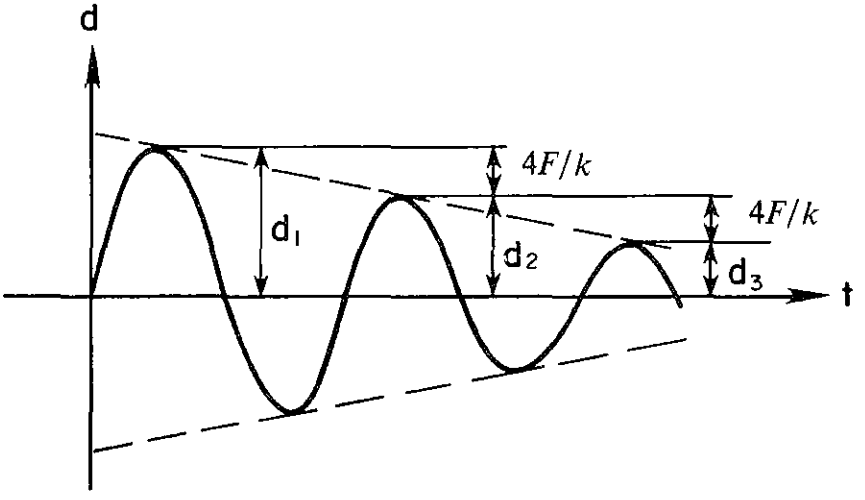

(b) Free-Vibration Response

Fig. 4.14 Coulomb Damping

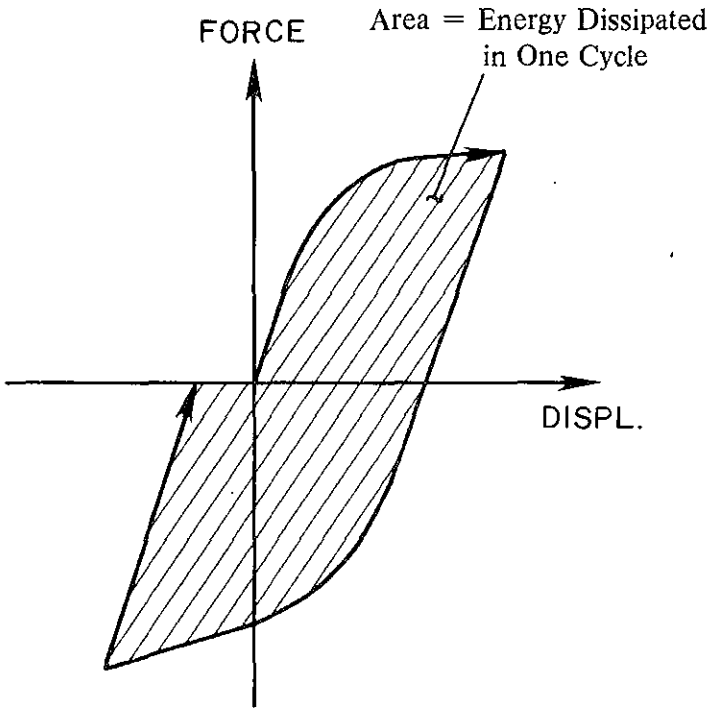

Fig. 4.15 Hysteretic Energy Dissipation

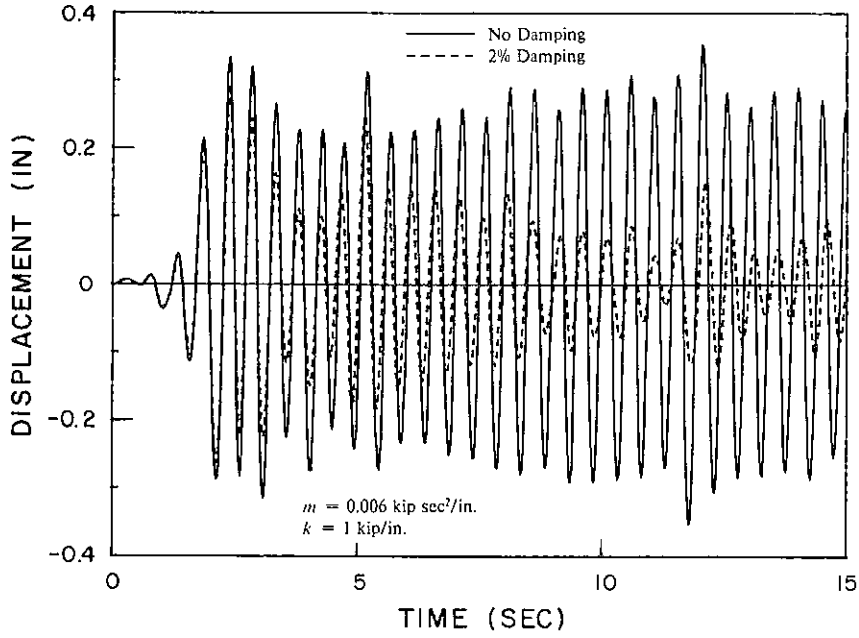

(a) Linear Elastic System

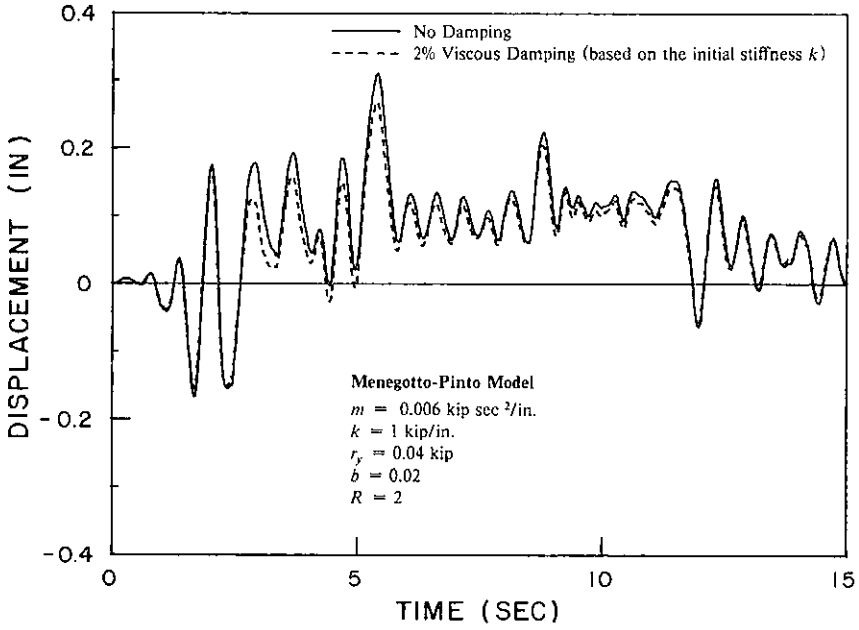

(b) Inelastic System

Fig. 4.16 Influence of Viscous Damping on Seismic Response (El Centro 1940 (NS), 0.045g)

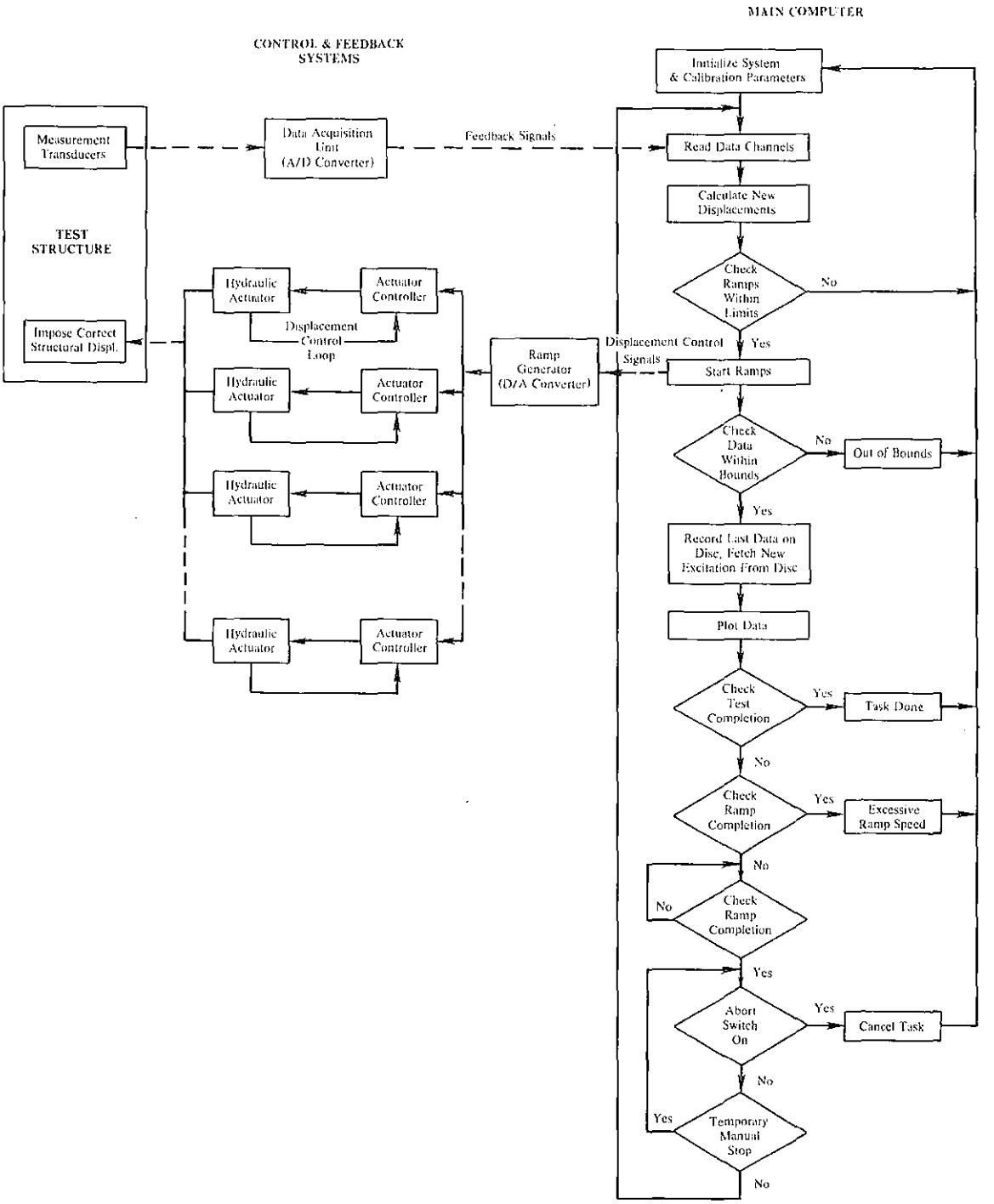

Fig. 5.1 Implementation Scheme for the Pseudodynamic Test Method

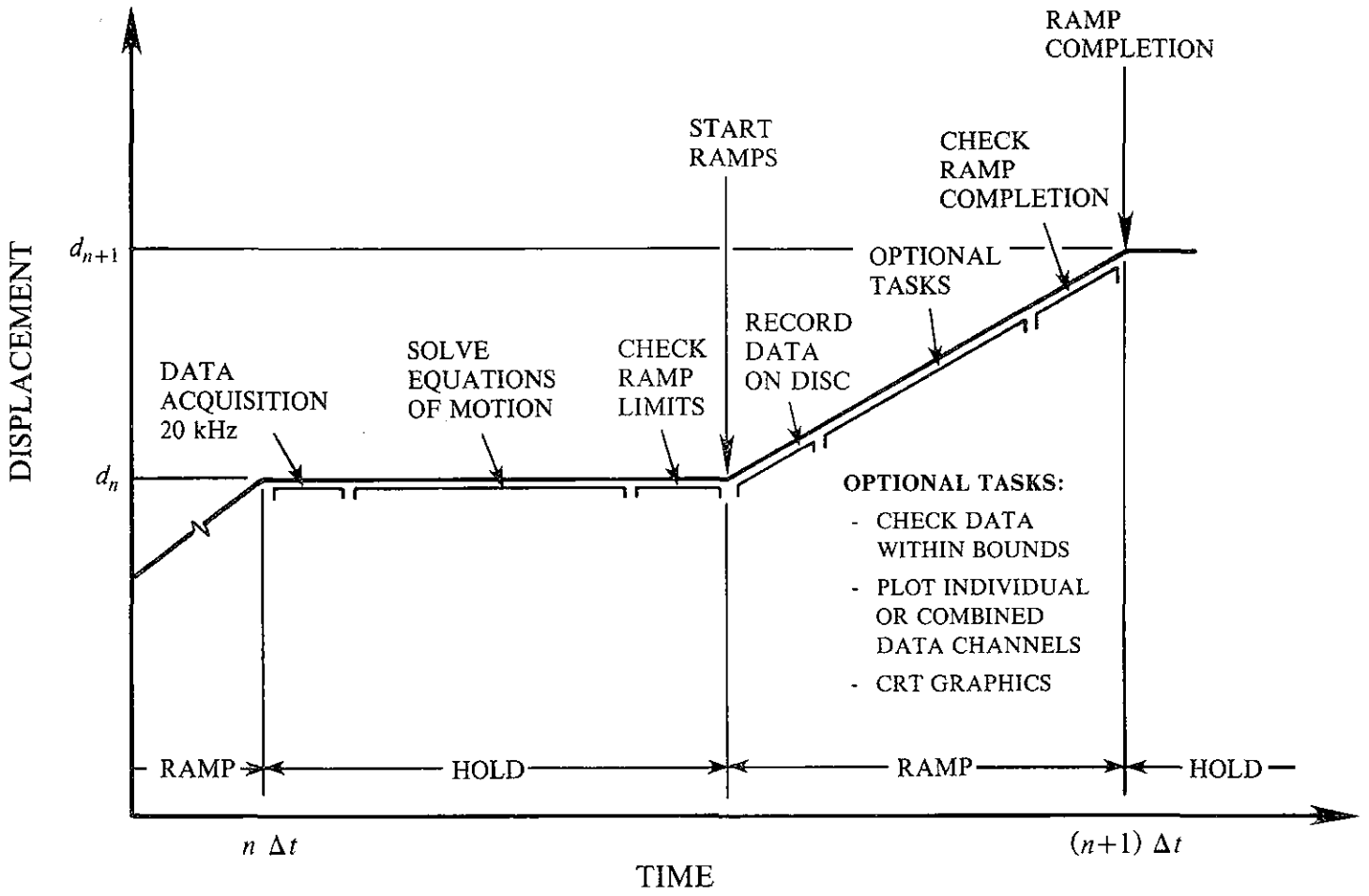

Fig. 5.2 Tasks Performed in Each Step of a Pseudodynamic Test

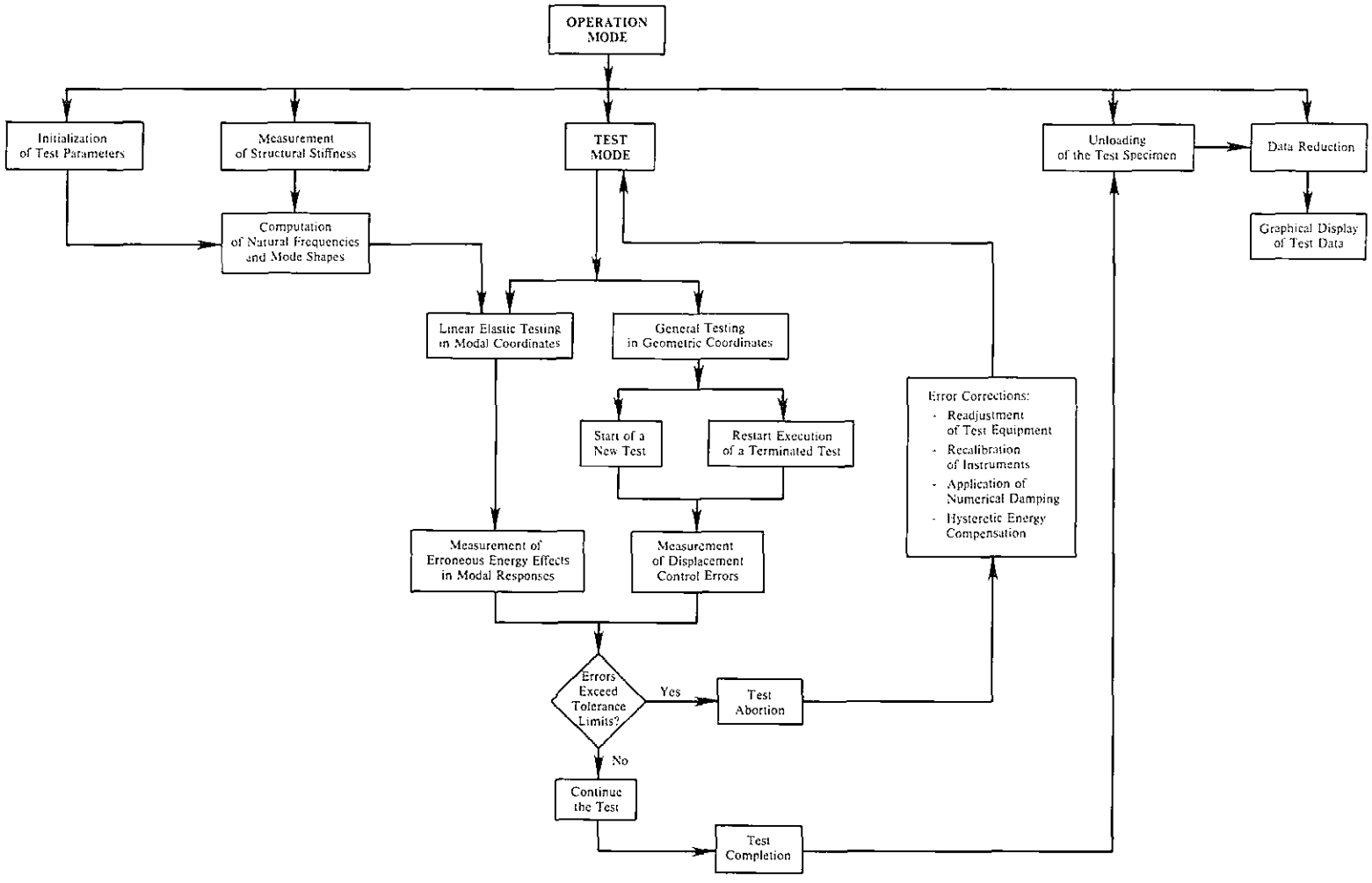

Fig. 5.3 Features of a Pseudodynamic Test Program

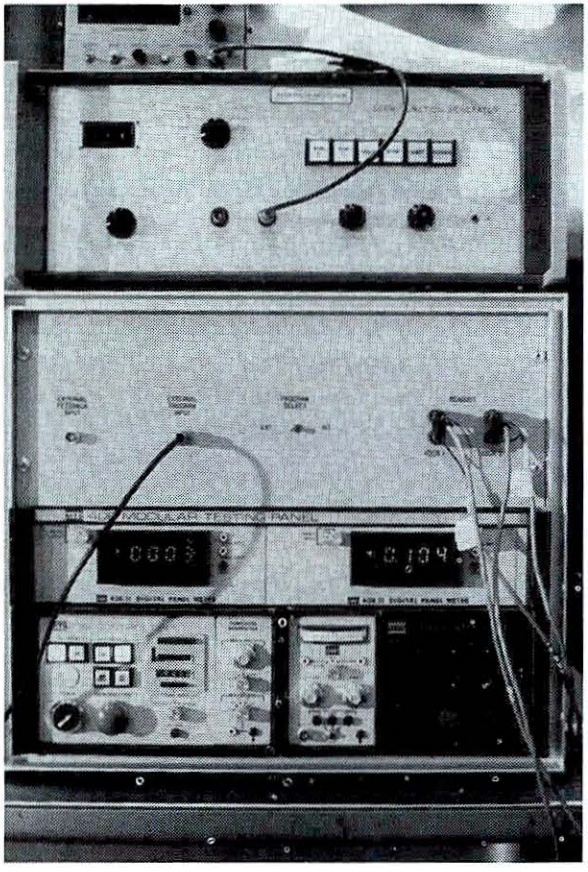

(a) Actuator Controller
(MTS Systems)

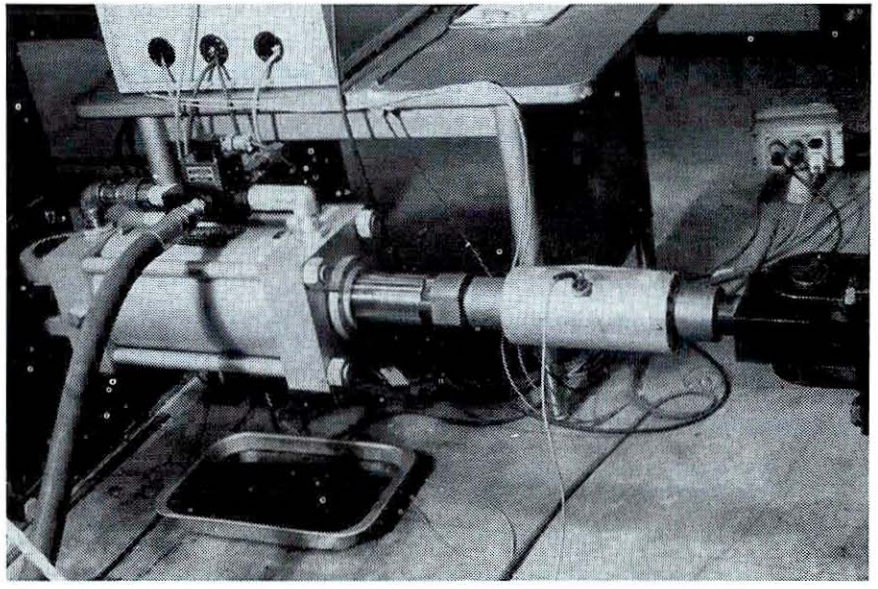

(b) Hydraulic Actuator

Fig. 5.4 Electro-Hydrualic Actuator-Controller System

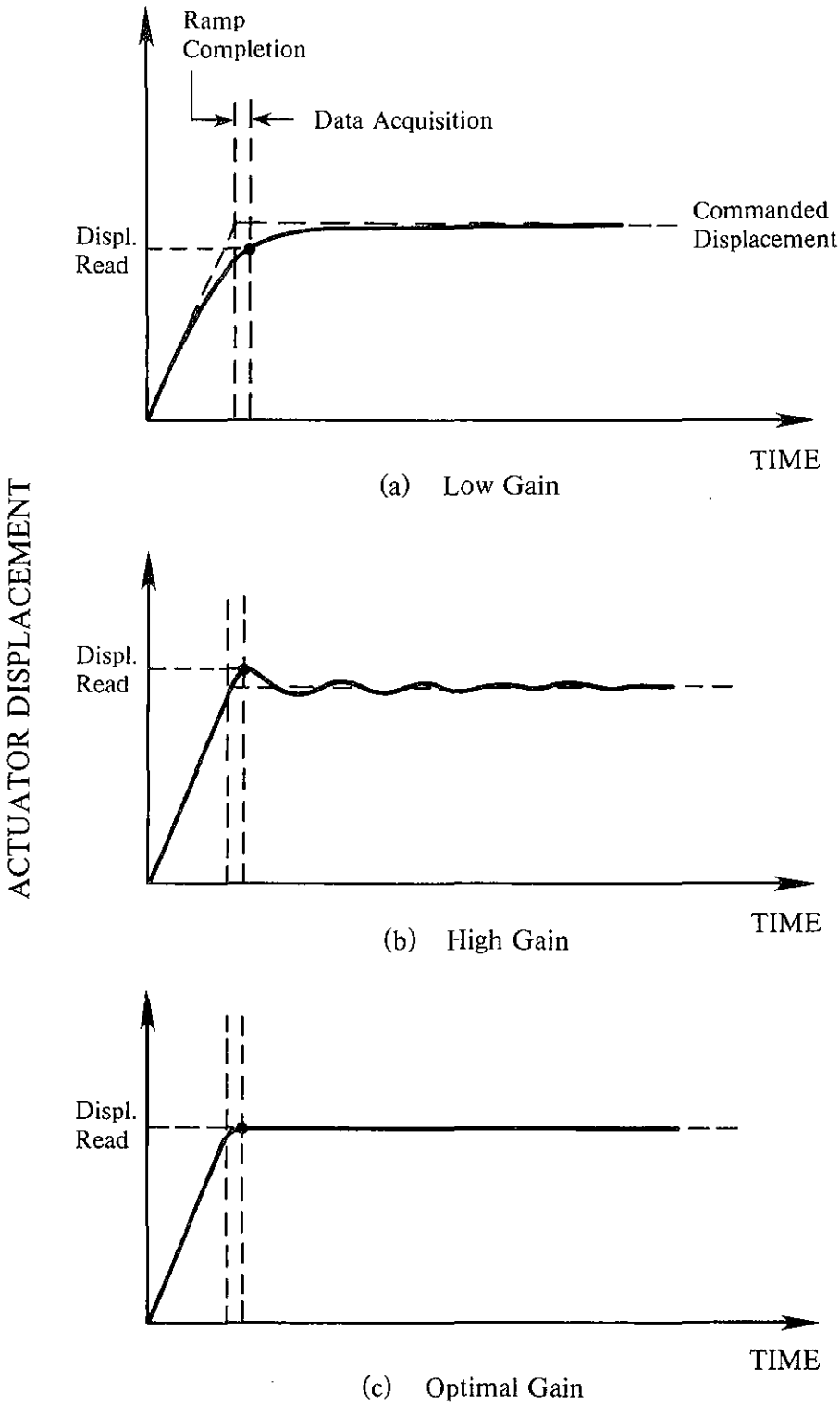

Fig. 5.5 Actuator Response

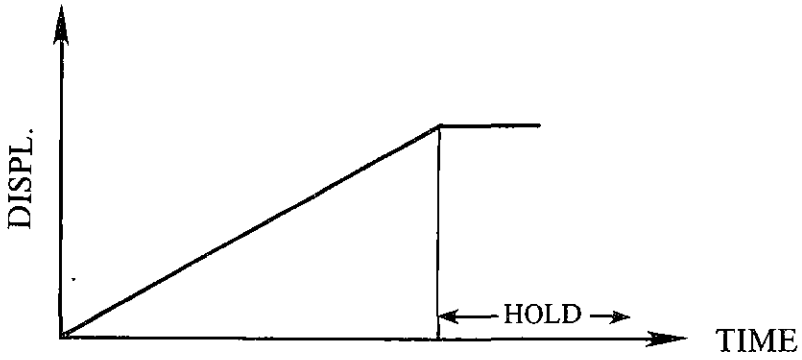

(a) Linear Ramp

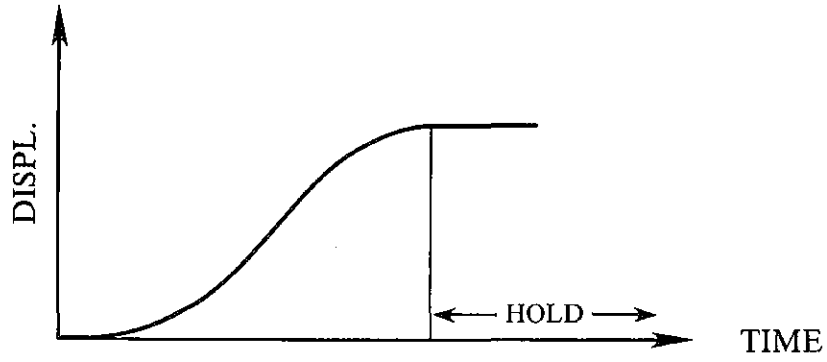

(b) Haver-Sine Ramp

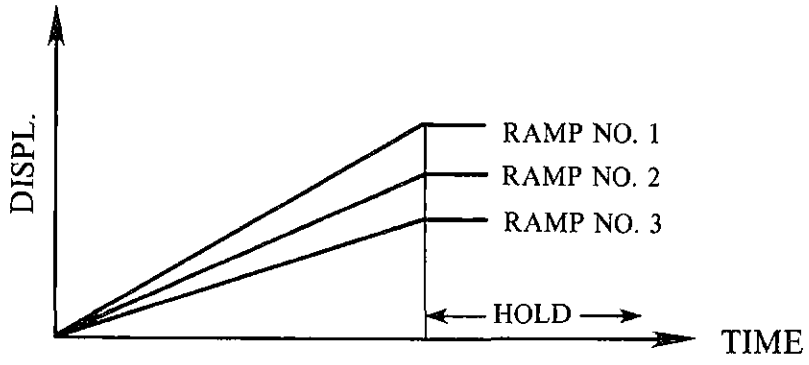

(c) Multiple Ramps

Fig. 5.6 Signals from a Ramp Generator

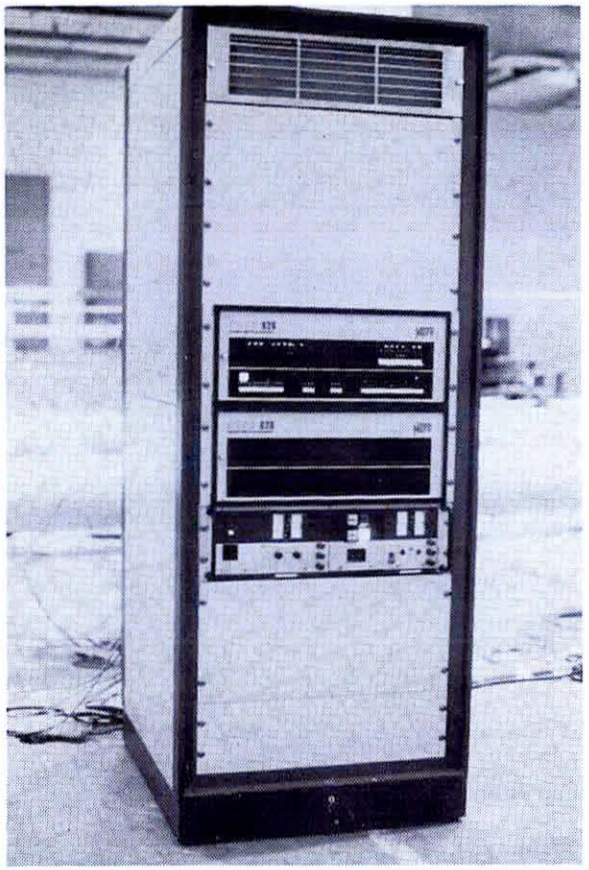

(a) Front Panel

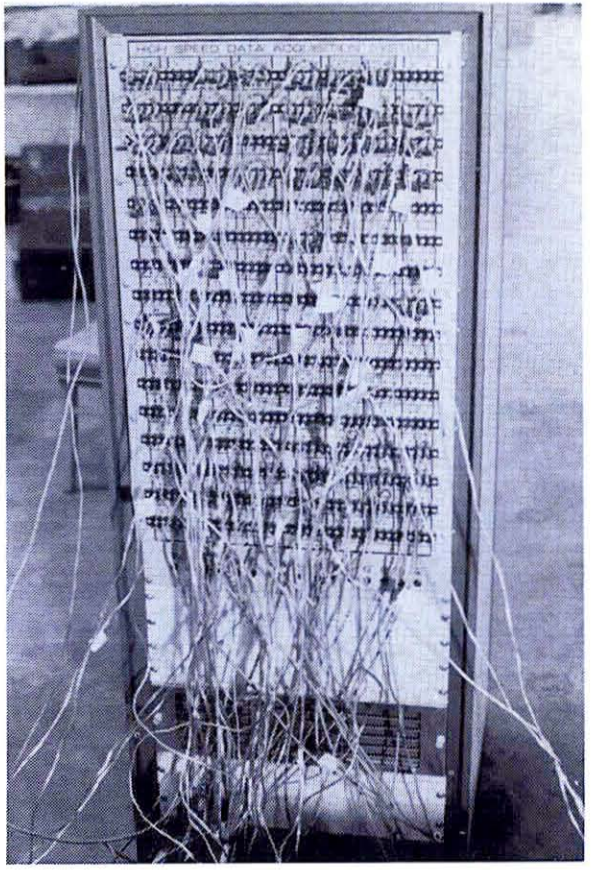

(b) Back Connectors
(128 Channels)

Fig. 5.7 High Speed Data Acquisition System

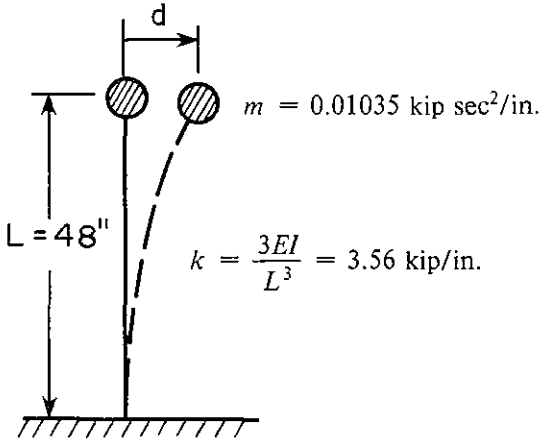

Fig. 5.8 SDOF Model

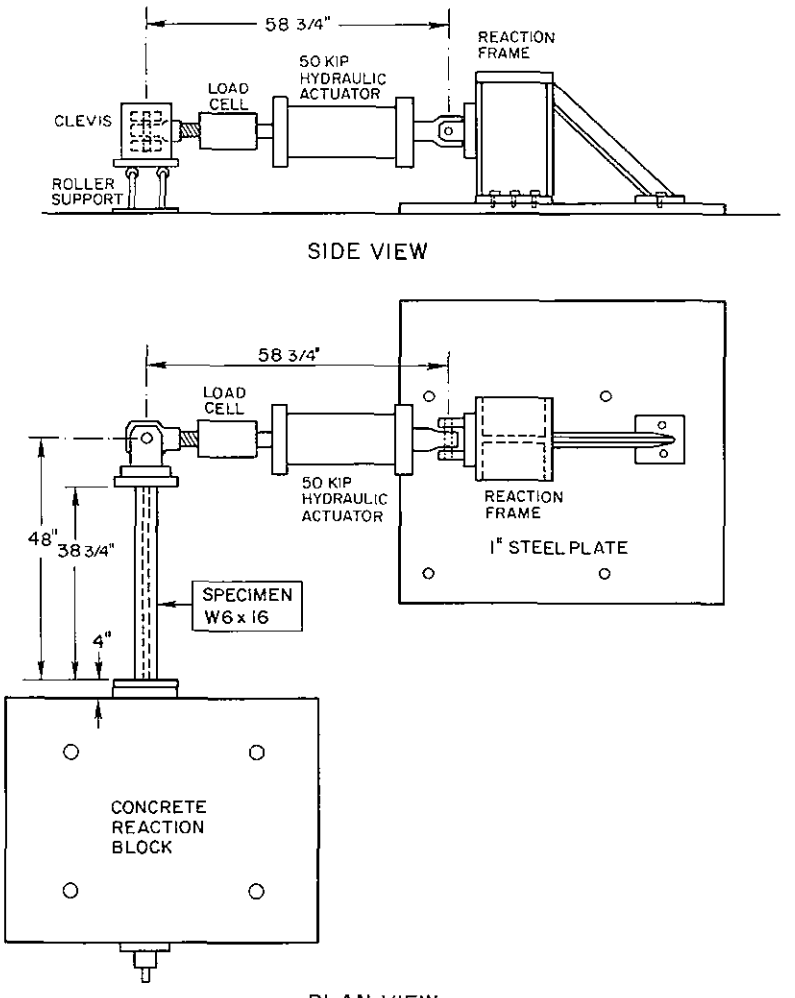

Fig. 5.9 SDOF Test Setup

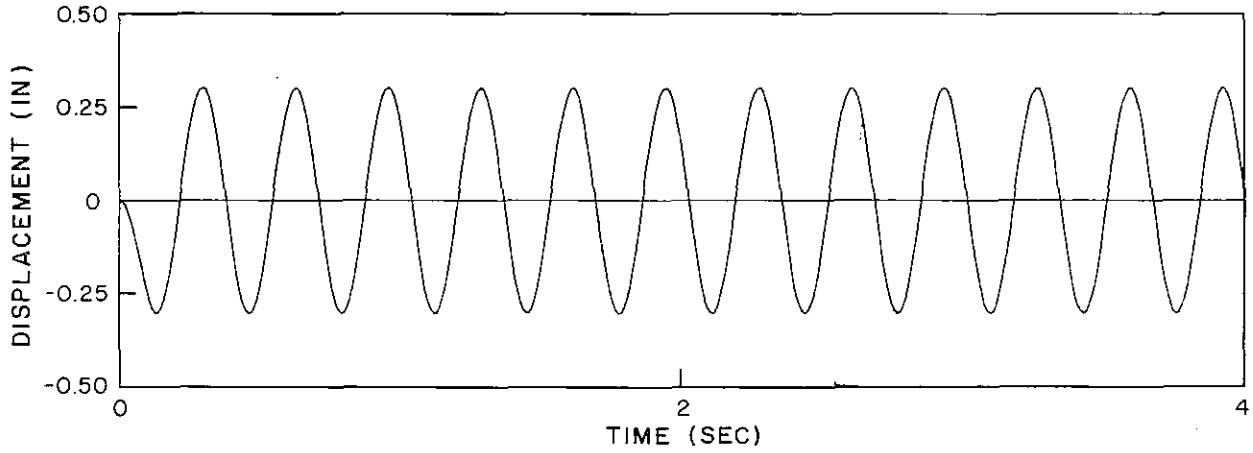

(a) Free-Vibration Response

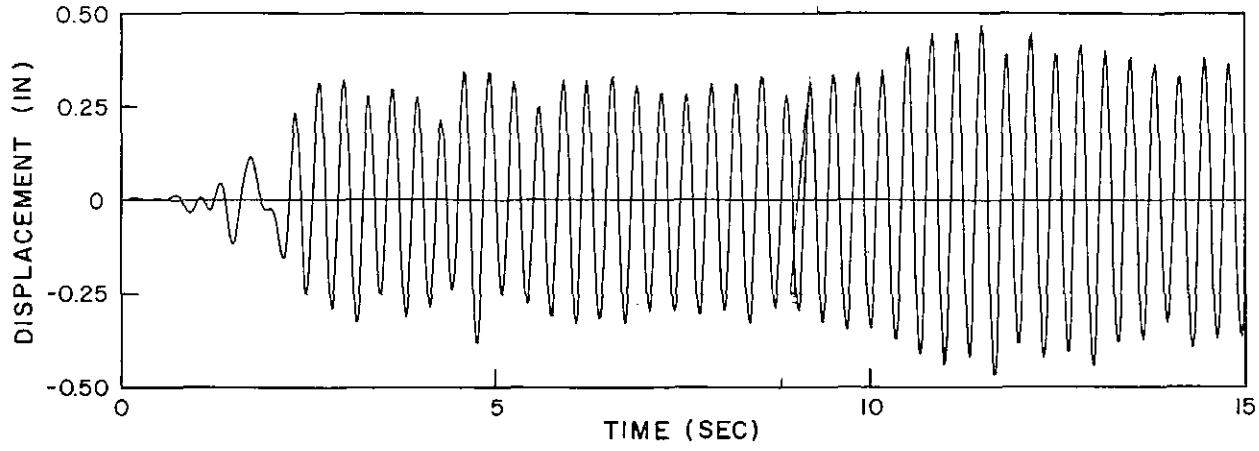

(b) Response to 0.1g El Centro

Fig. 5.10 Analytical Simulations (k = 3.75 kip/in., m = 0.01035 kip sec^2/in.)

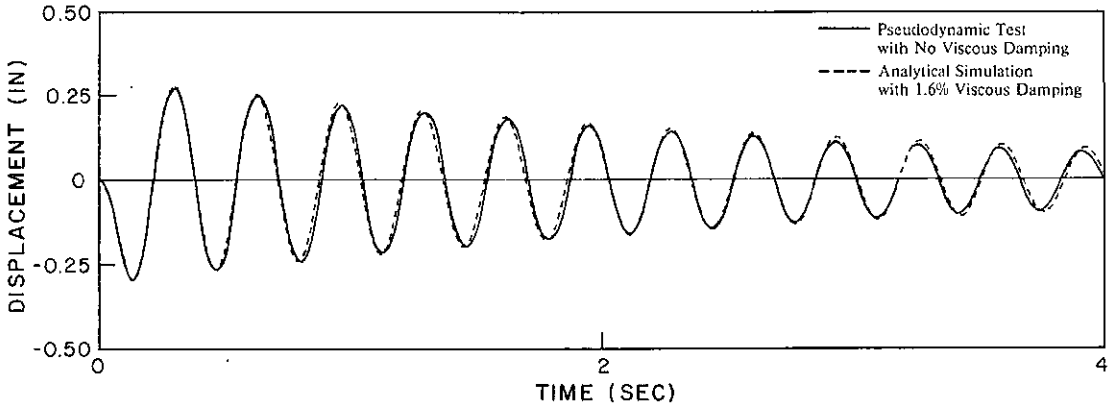

(a) Free-Vibration Response

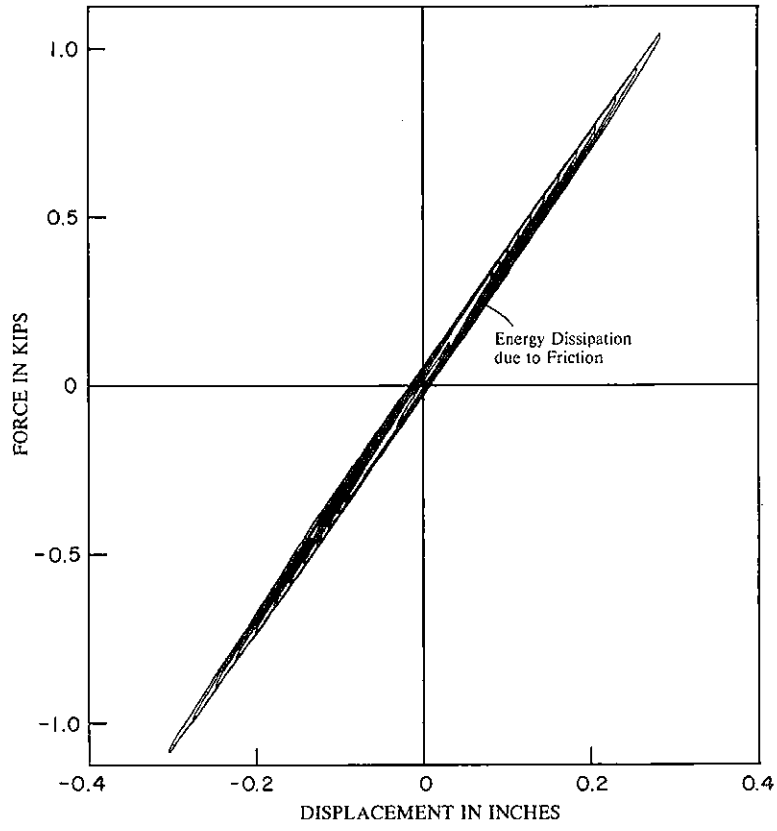

(b) Force-Displacement Curves Measured

Fig. 5.11 Pseudodynamic Free-Vibration Test

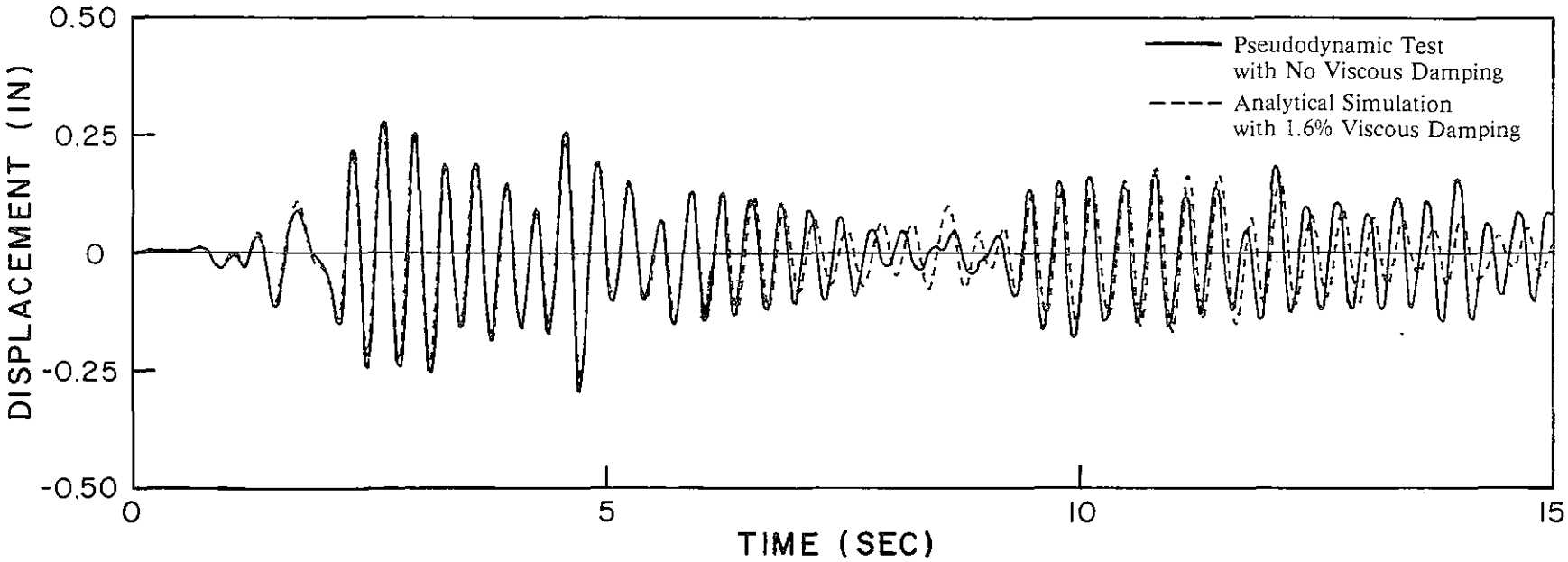

Fig. 5.12 Pseudodynamic Response to 0.1g El Centro Record

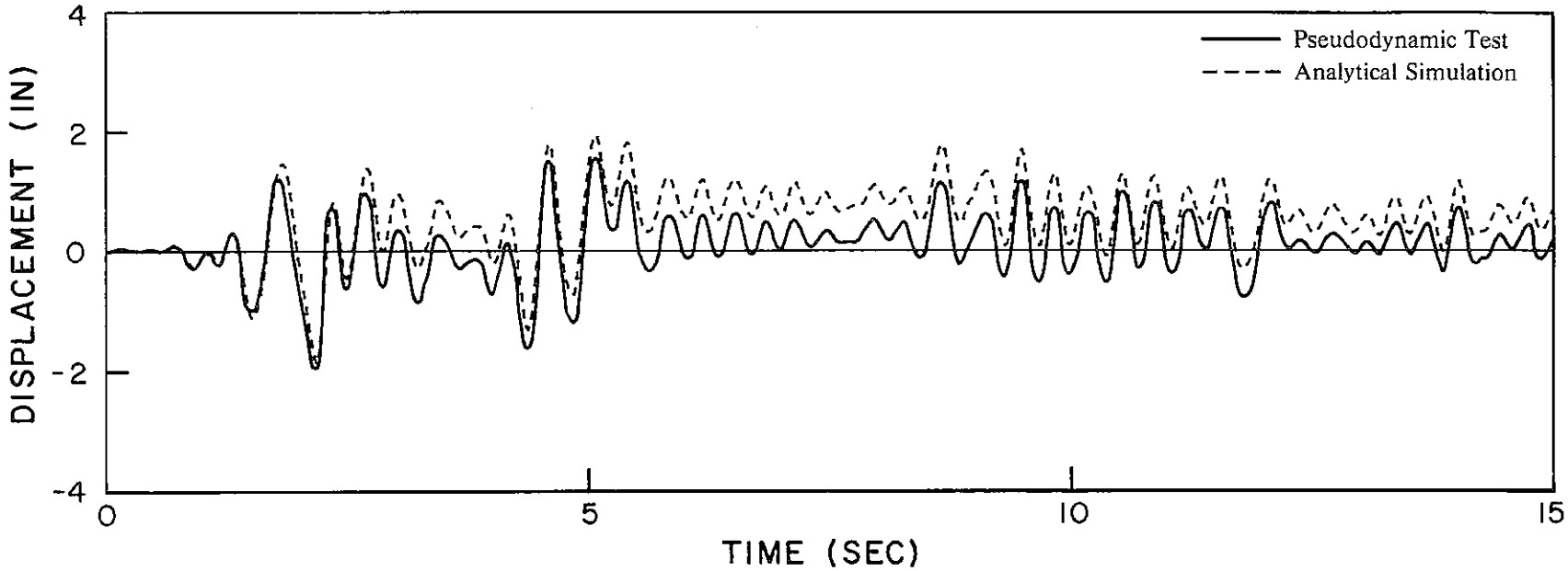

Fig. 5.13 Pseudodynamic Response to 0.8g El Centro Record

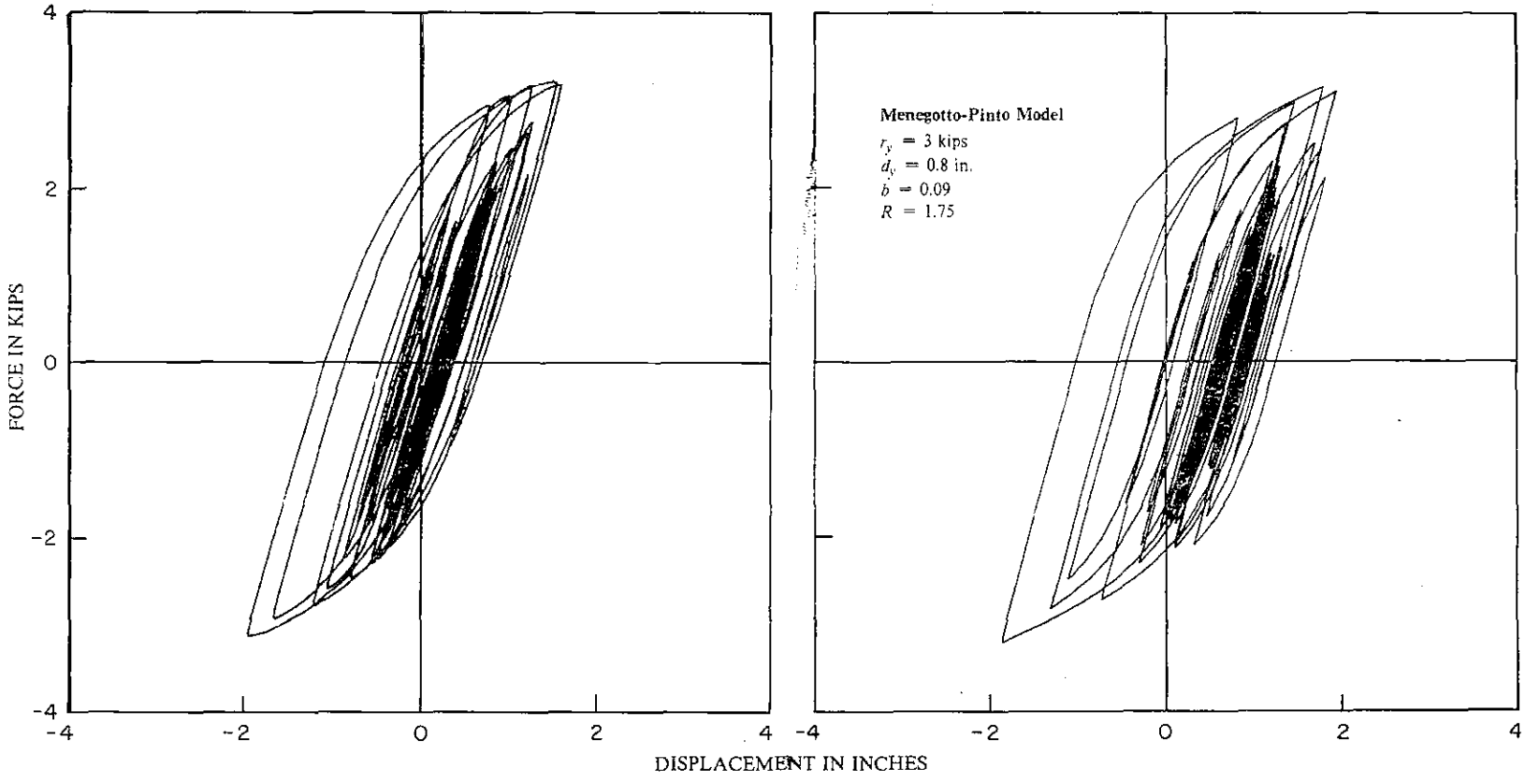

(a) Test Result

(b) Analytical Simulation

Fig. 5.14 Inelastic Hysteretic Curves

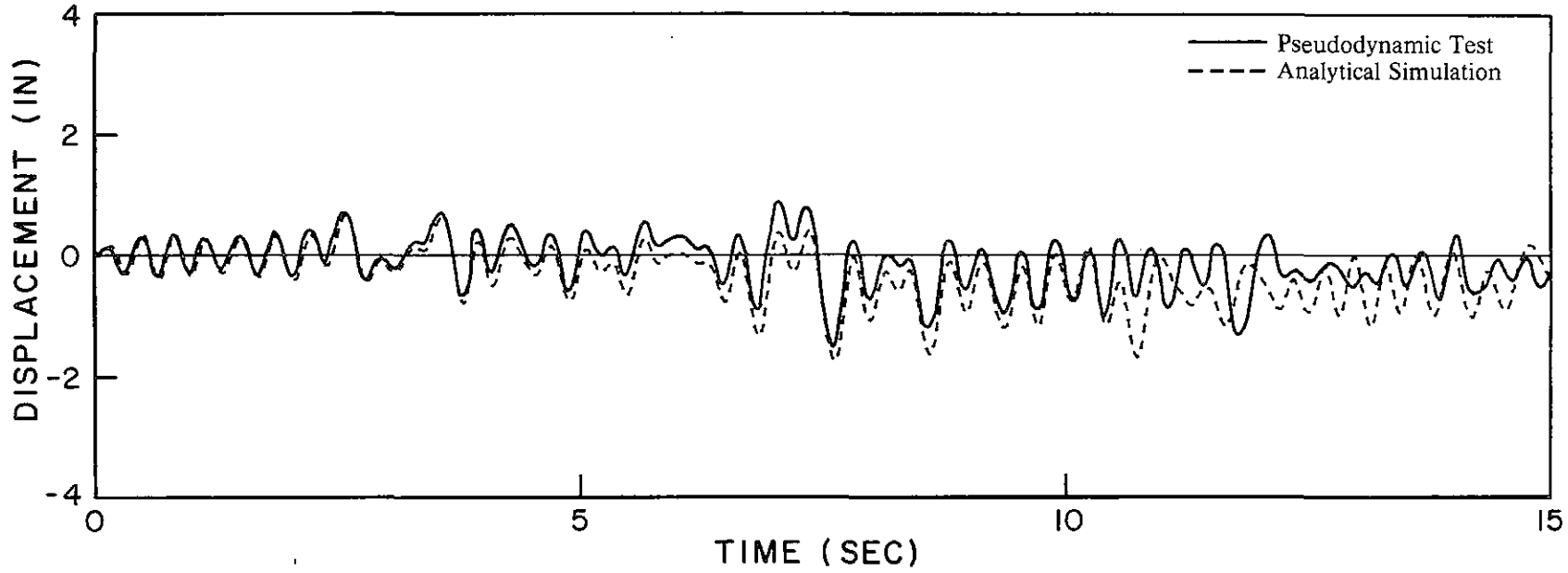

Fig. 5.15 Pseudodynamic Response to 0.45g Miyagi Oki Record

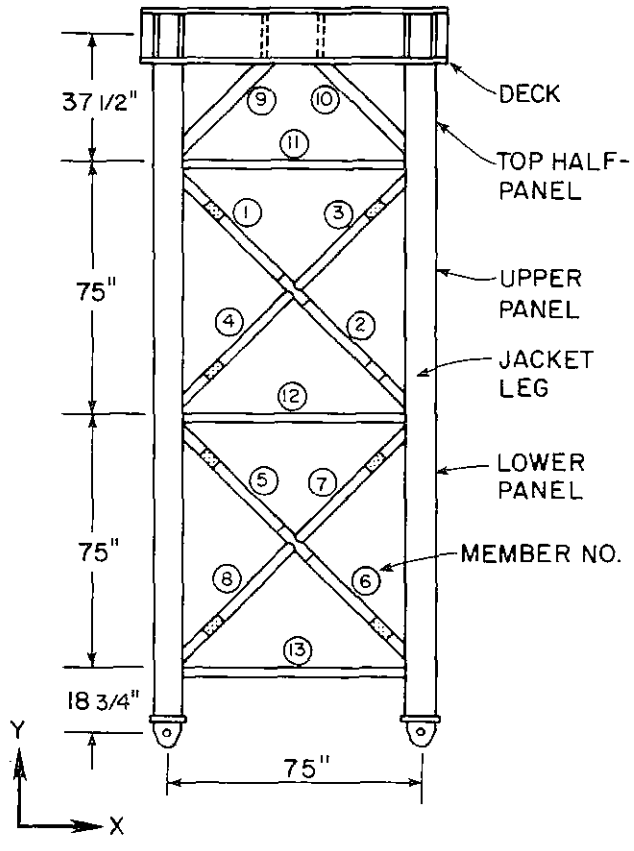

Fig. 6.1 Frame Configuration and Member Numbering

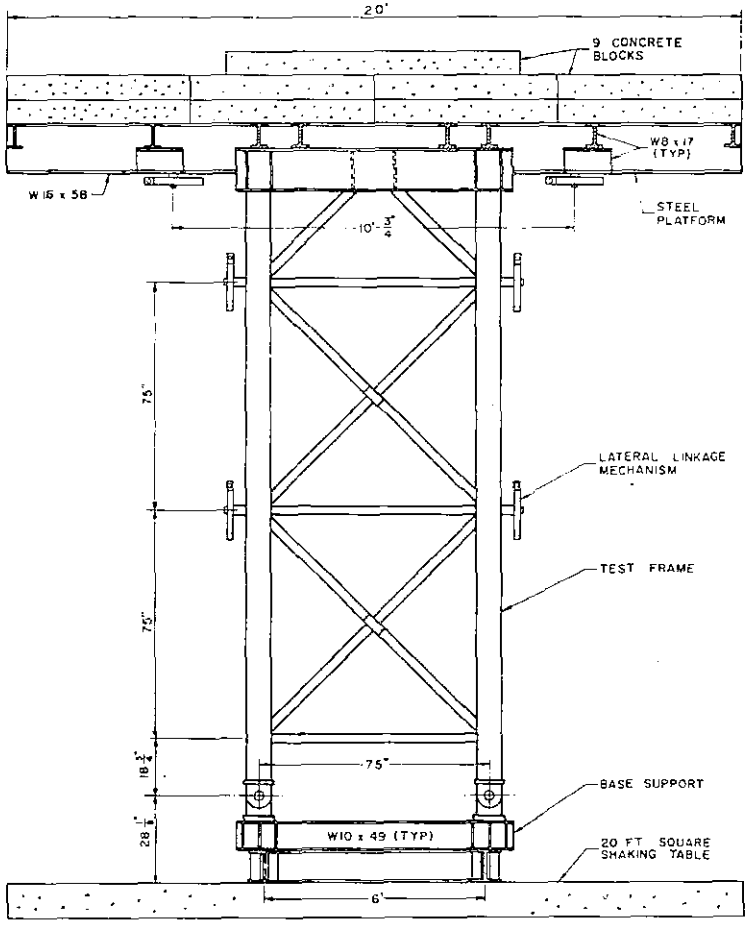

Fig. 6.2 Shaking Table Test Setup [Ref. 4]

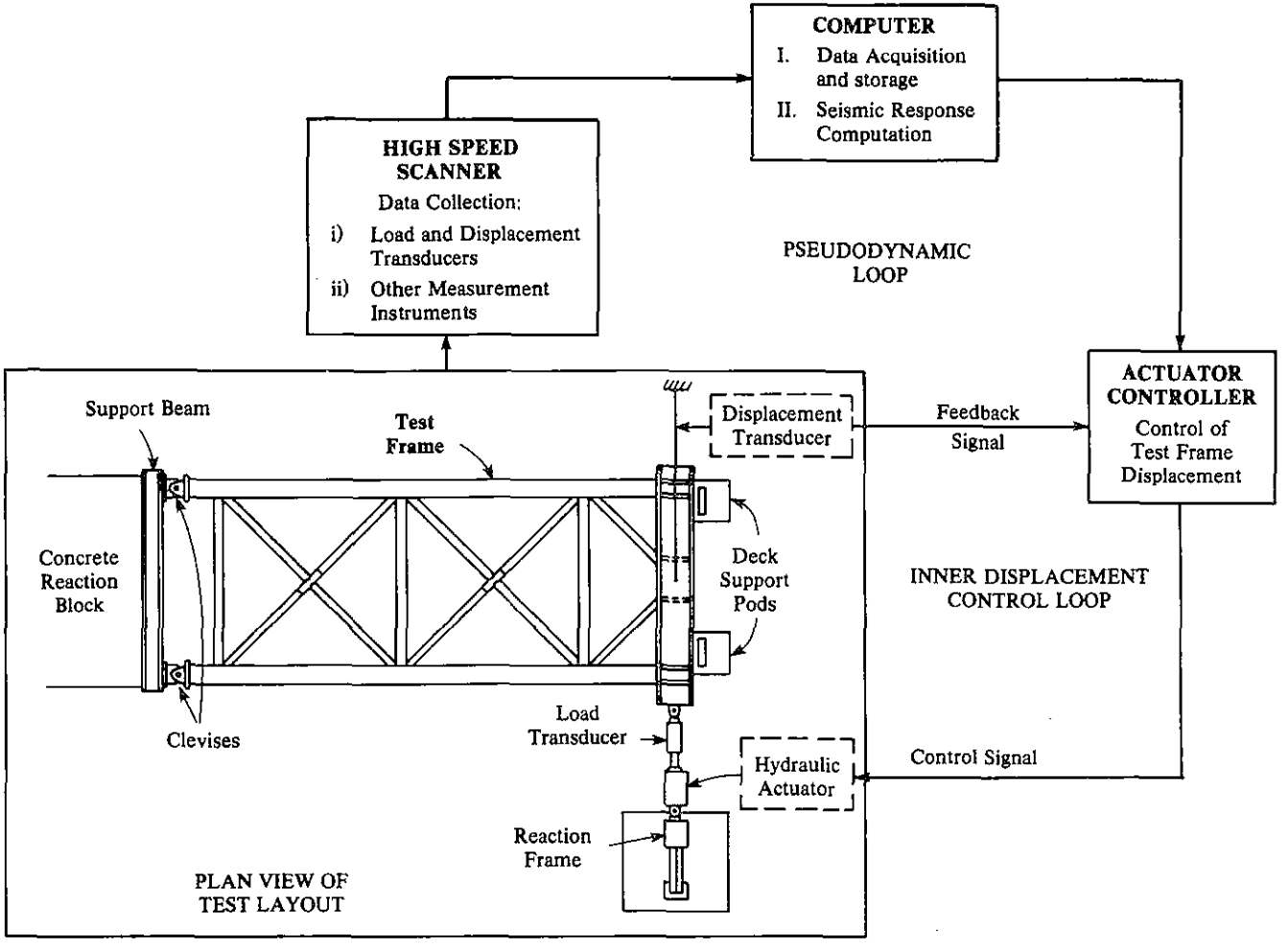

Fig. 6.3 Schematic of Pseudodynamic Test Setup

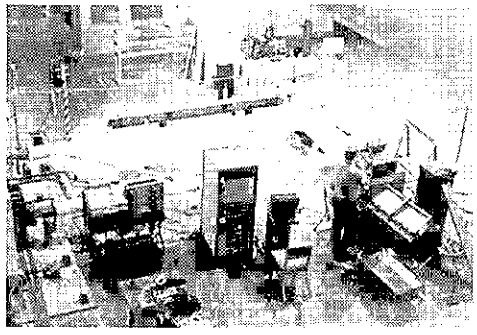

(a) Test Setup and Equipment

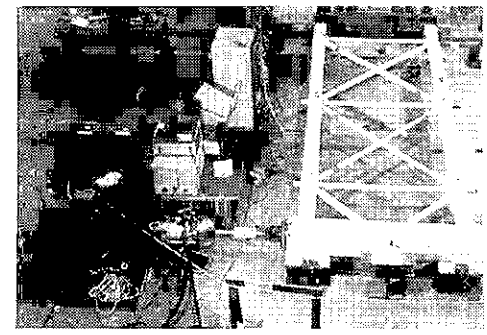

(b) Front View of Test Setup

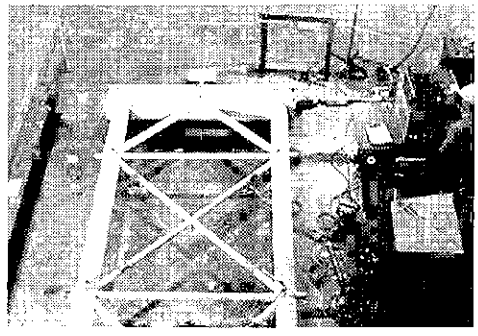

(c) Lateral Frame Displacement Transducers

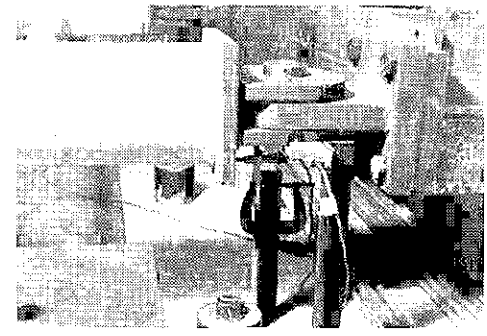

(d) LVDT's for Monitoring Clevis Movements

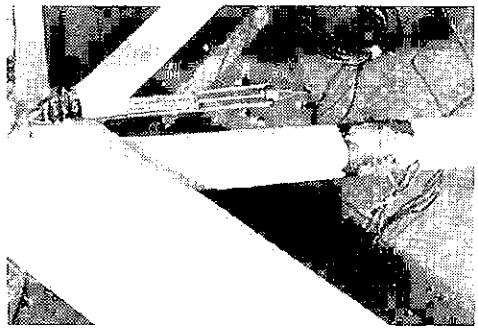

(e) Brace Axial Load and Displacement Transducers

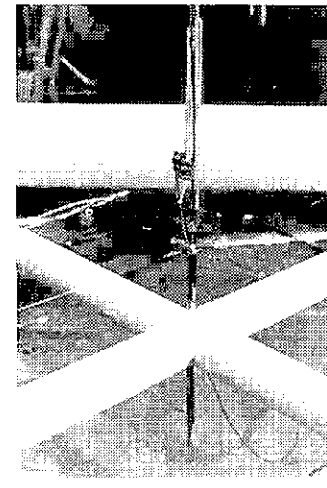

(f) Transducers Monitoring the Vertical Displacement of a Cross-Joint

Fig. 6.4 Photographs of Pseudodynamic Test Setup and Instrumentation

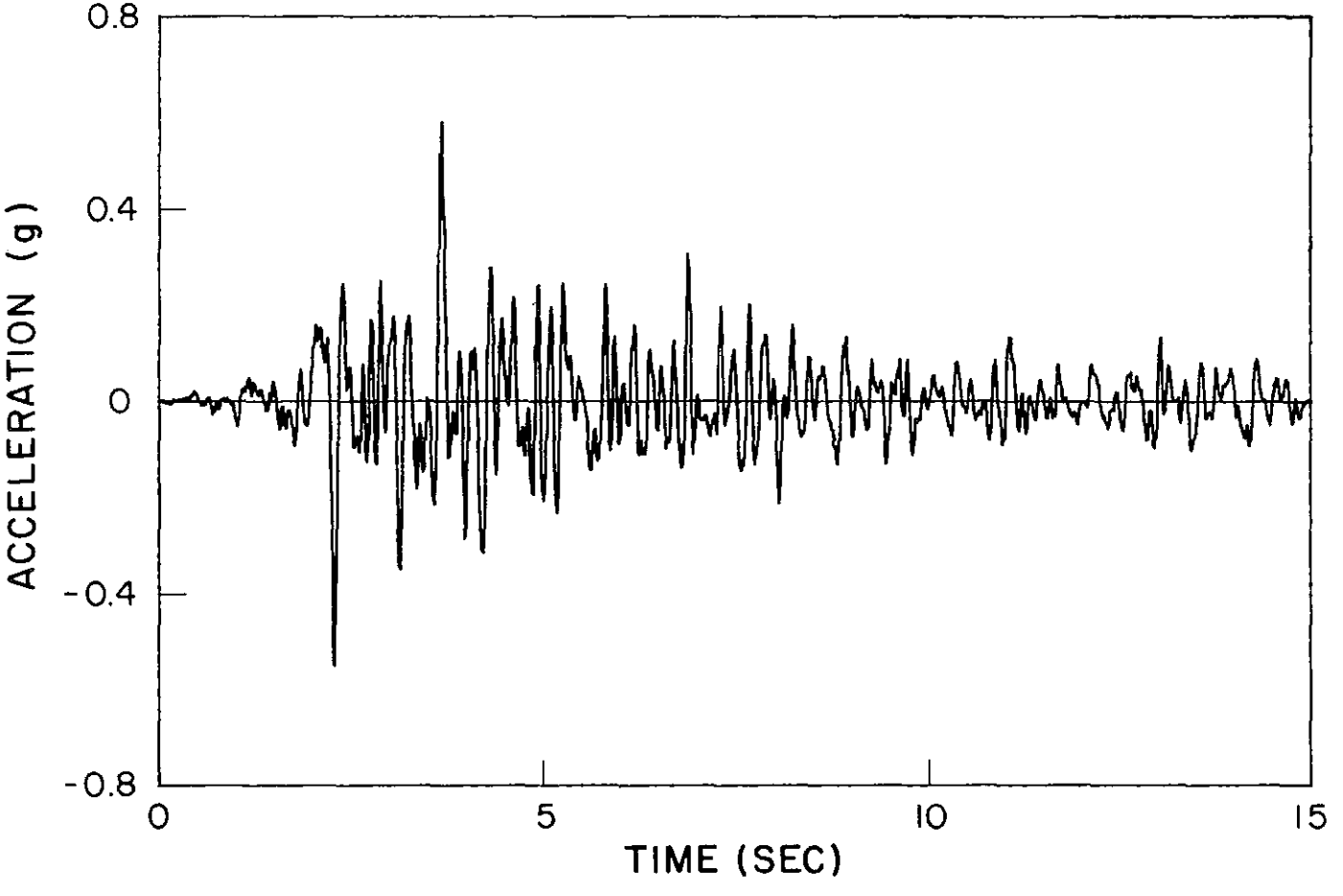

Fig. 6.5 Taft Accelerogram from Shaking Table Tests (Ductility Level)

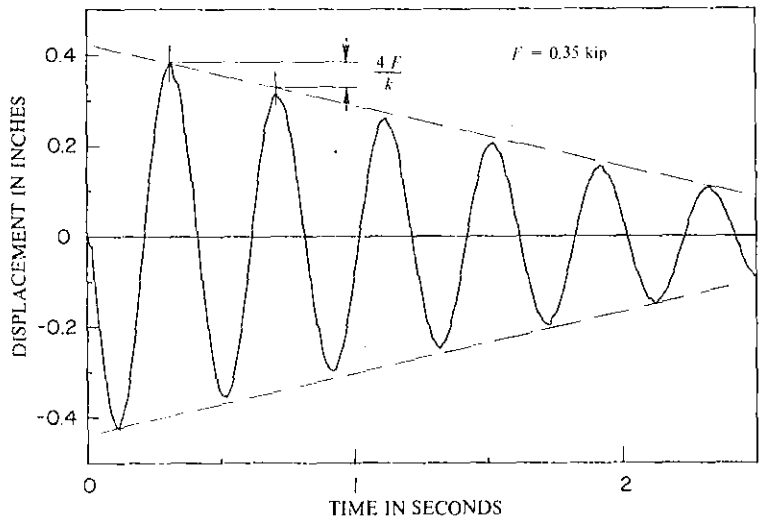

(a) Uncorrected Free-Vibration Response with Coulomb Damping

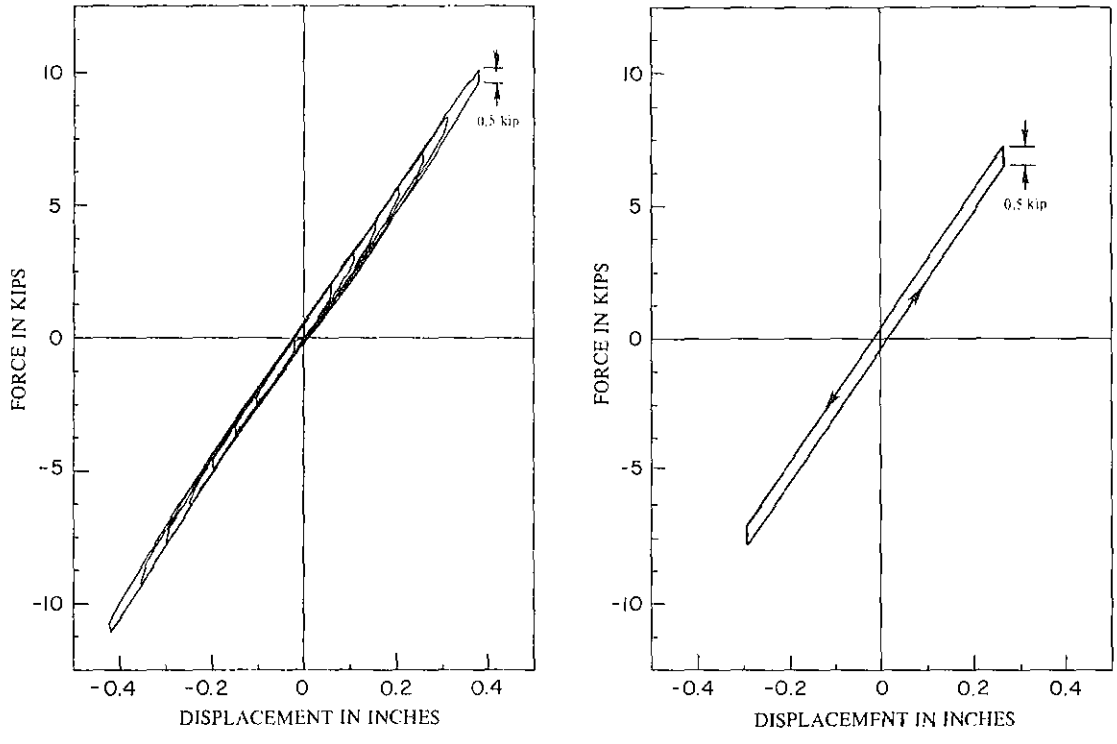

(b) Hysteretic Loops due to Friction

(c) Correction Hysteretic Loop

Fig. 6.6 Correction of Friction Force Effects in the Pseudodynamic Tests

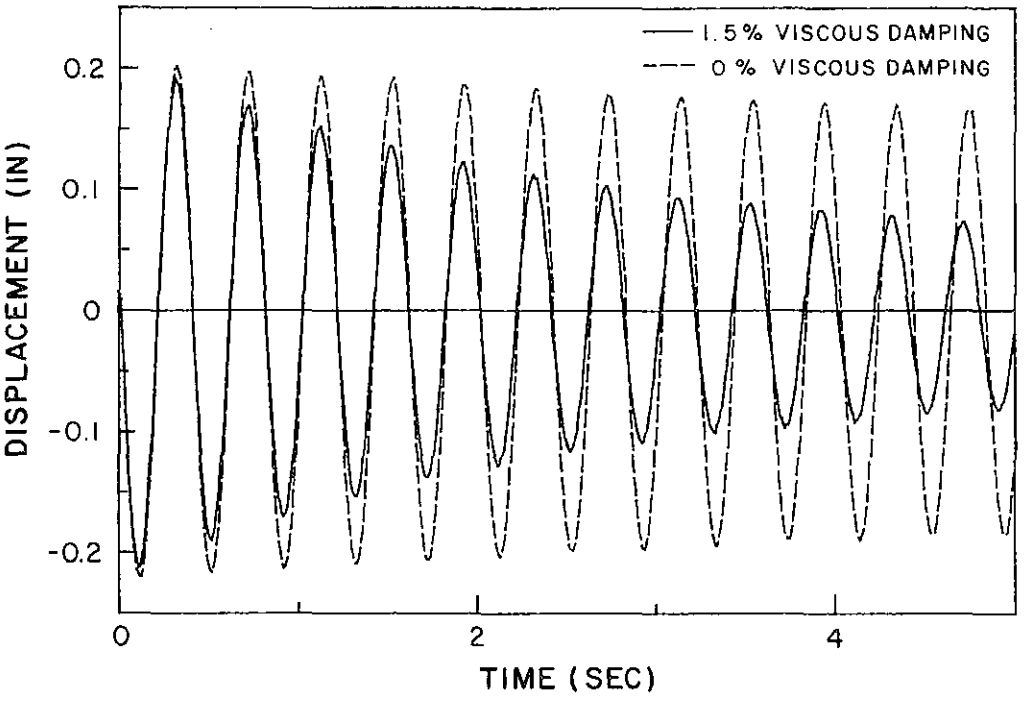

(a) Pseudodynamic Free Vibration with Correction for Friction

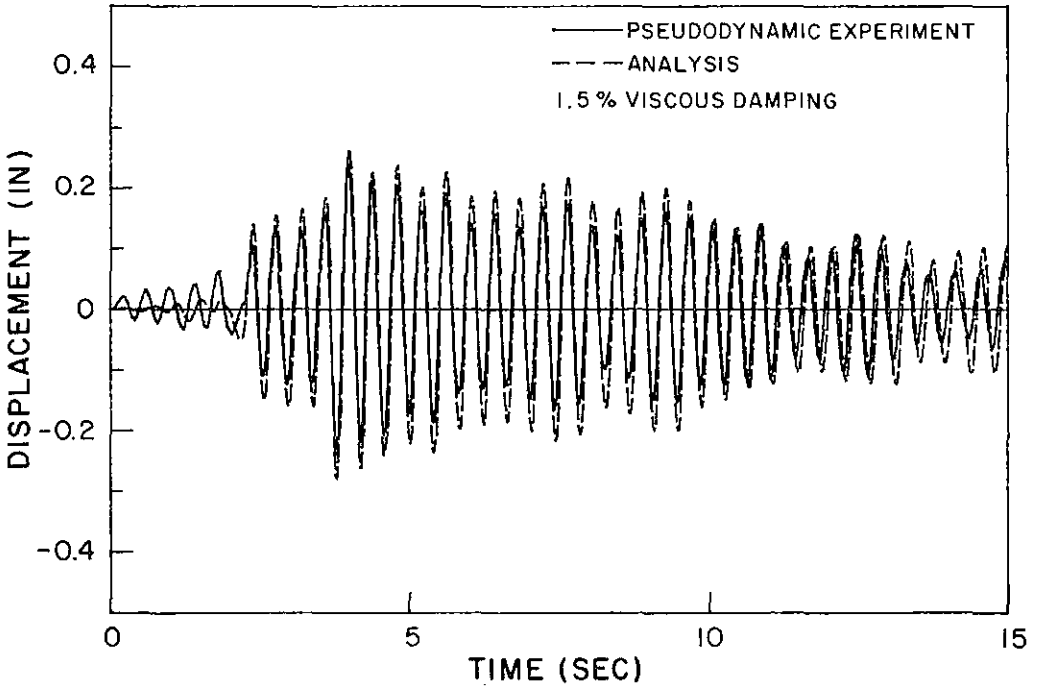

(b) Response to 0.069g Taft

Fig. 6.7 Verifcation Tests

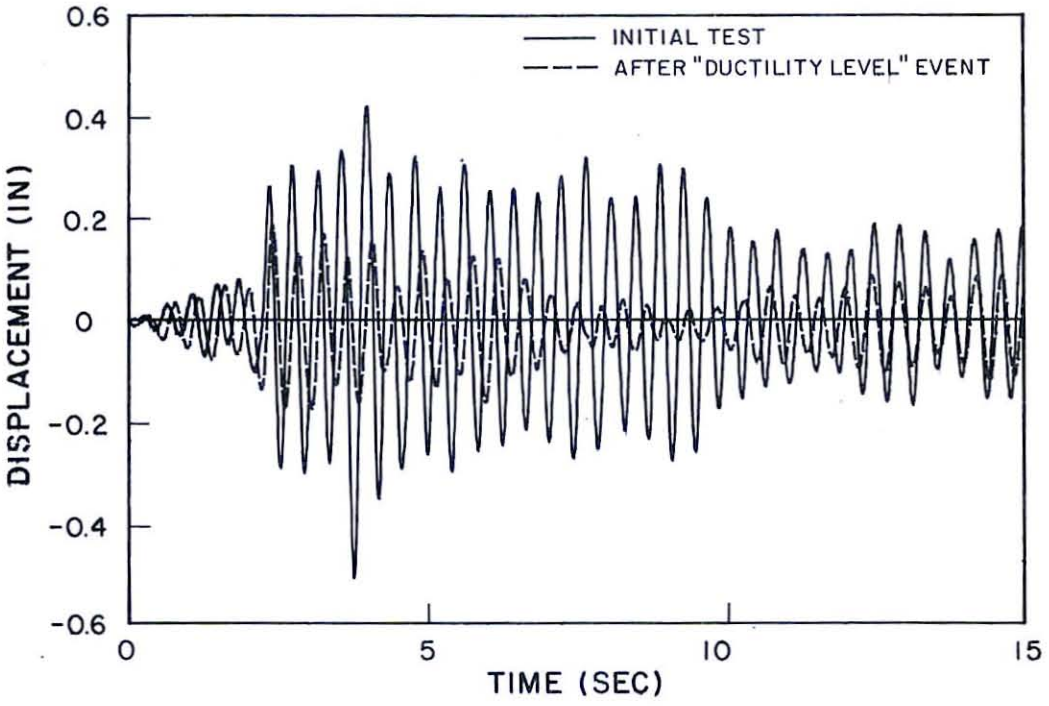

(a) Displacement History

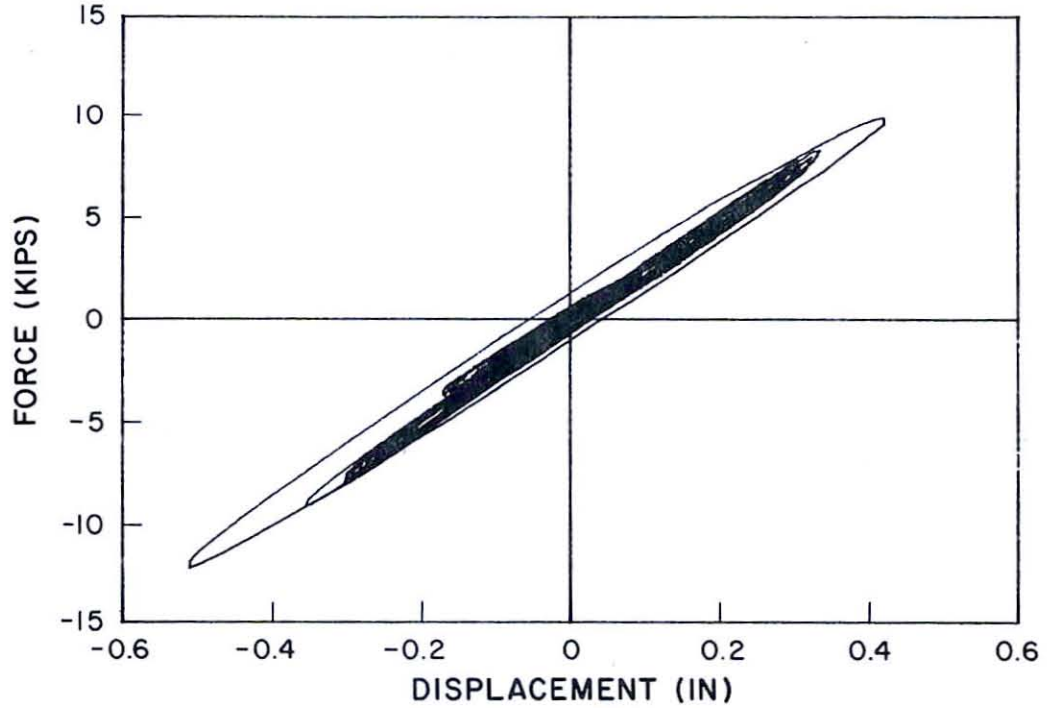

(b) Frame Hysteretic Loops

Fig. 6.8 Frame Response during the Half-"Strength Level" Event

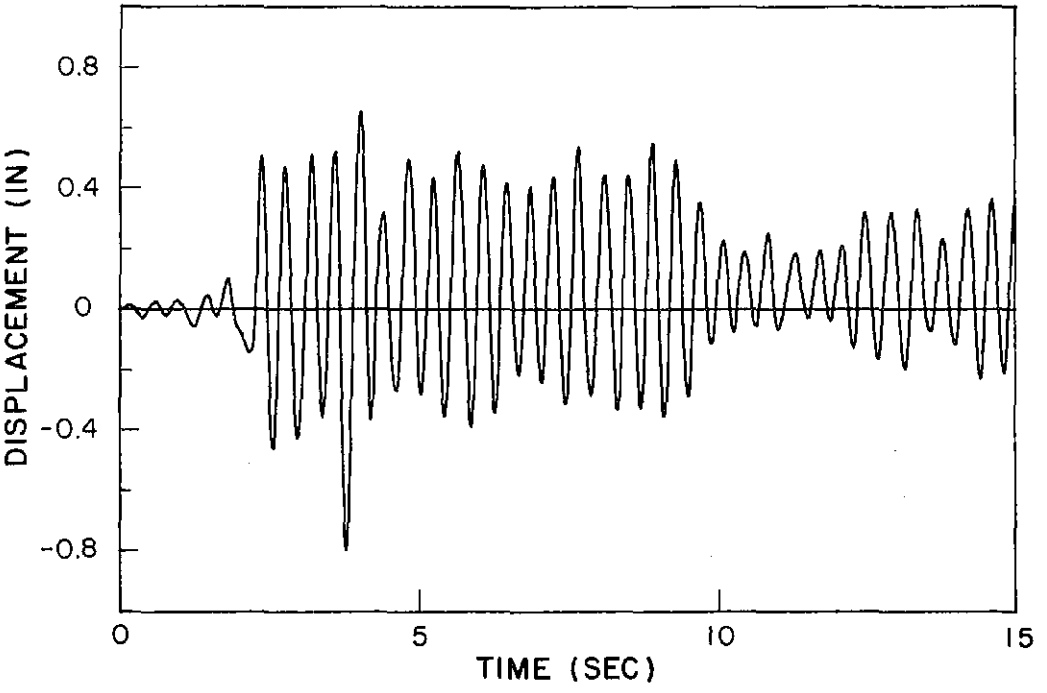

(a) Displacement History

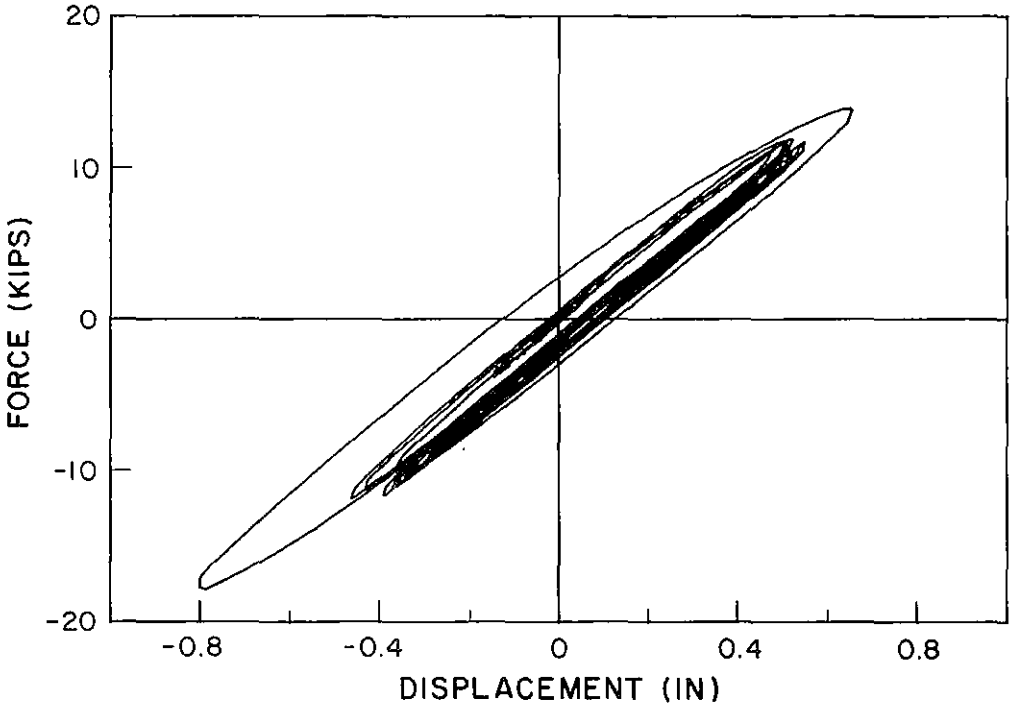

(b) Frame Hysteretic Loops

Fig. 6.9 Frame Response during the Strength Level Event

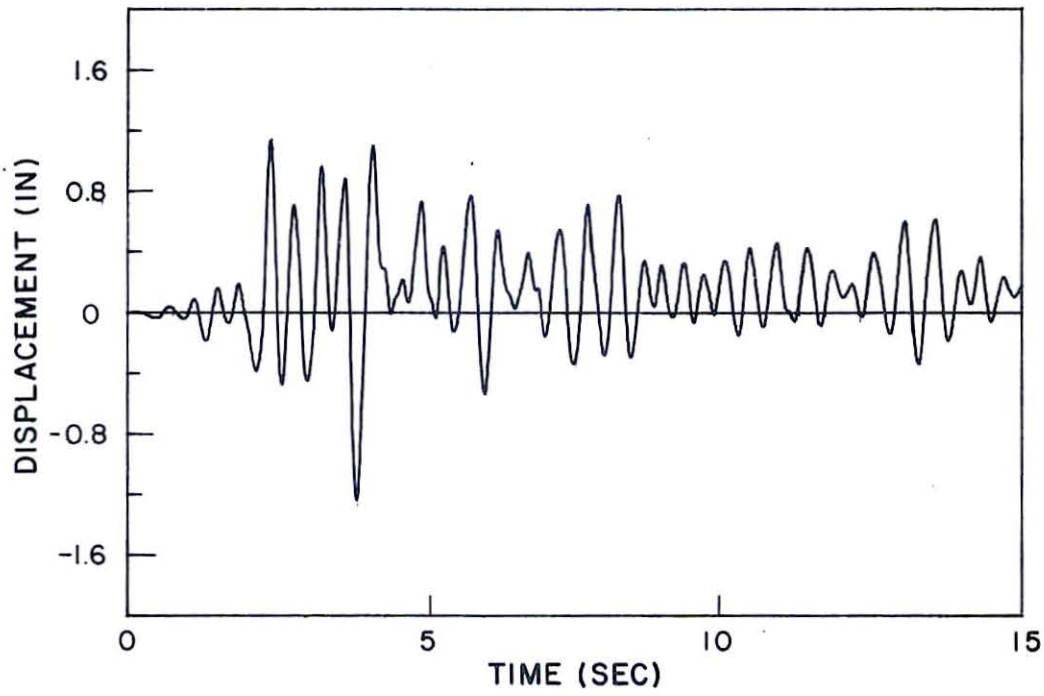

(a) Displacement History

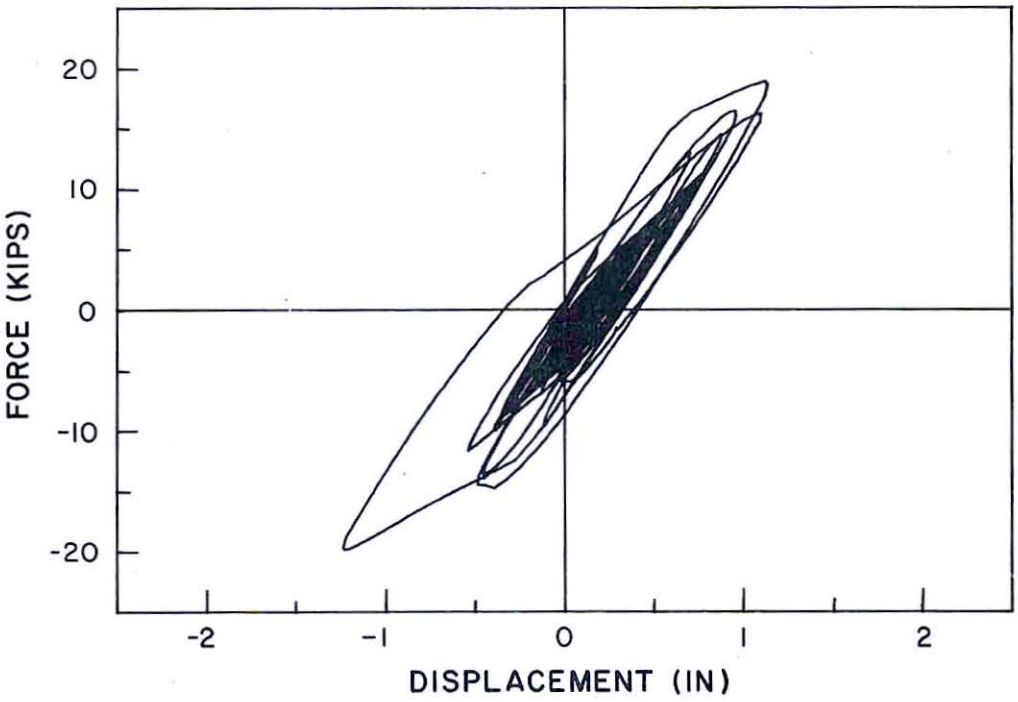

(b) Frame Hysteretic Loops

Fig. 6.10 Frame Response during the Ductility Level Event

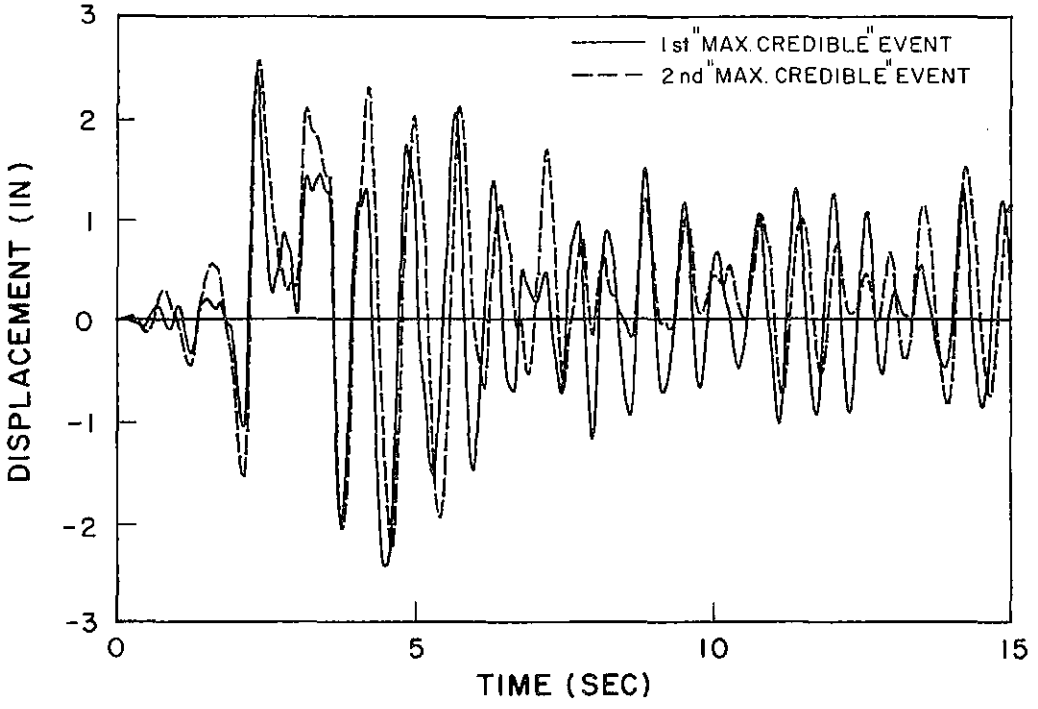

(a) Displacement History

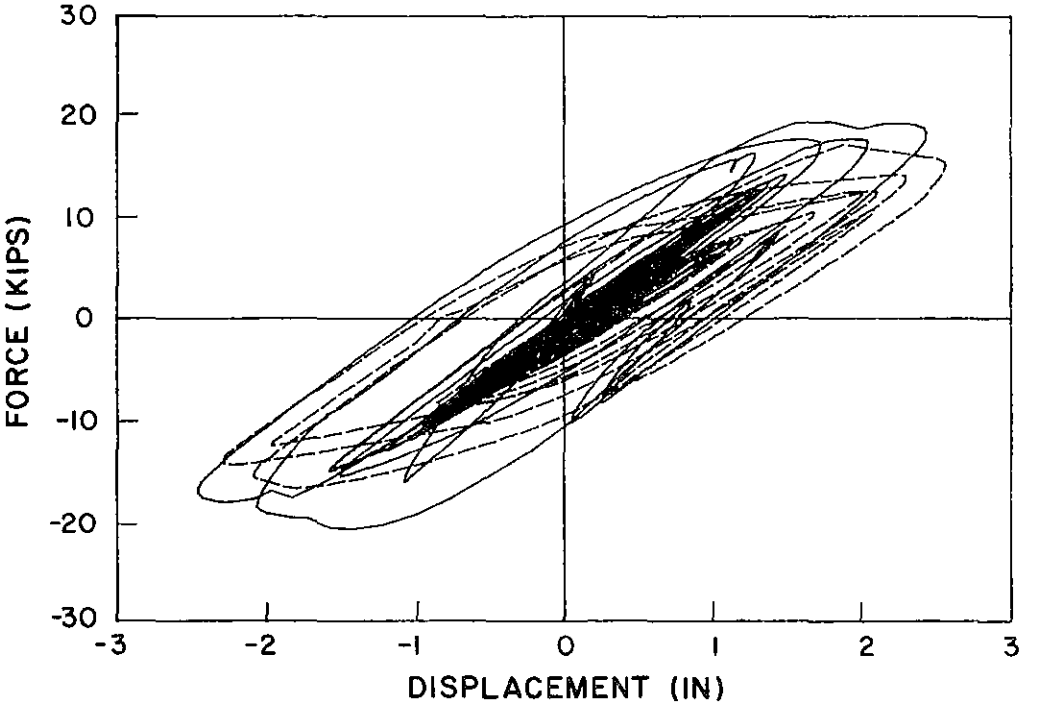

(b) Frame Hysteretic Loops

Fig. 6.11 Frame Response during the Maximum Credible Events

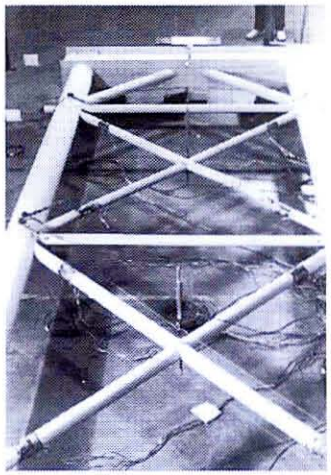

(a) Ductility Level Event

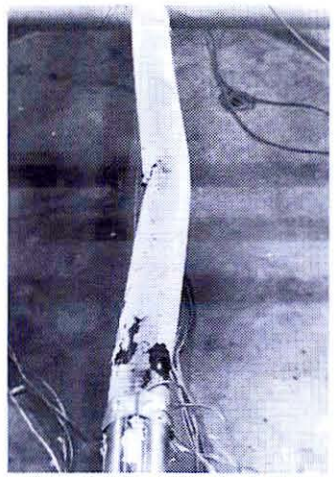

(b) Brace 2 in Ductility Level Event

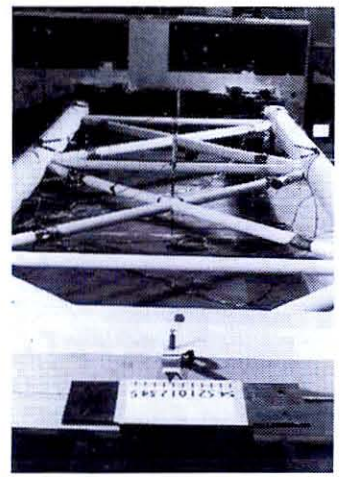

(c) 1st Maximum Credible Event

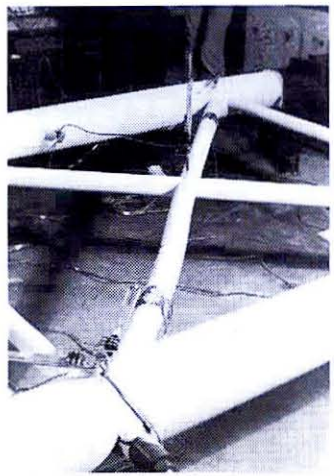

(d) Lower Panel Braces in 1st Maximum Credible Event

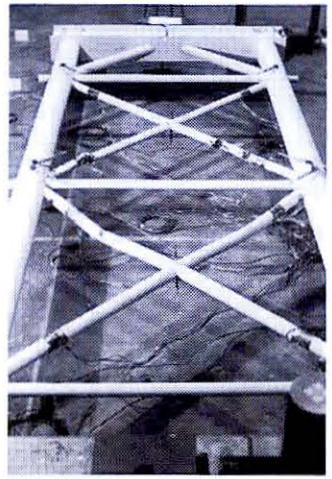

(e) 2nd Maximum Credible Event

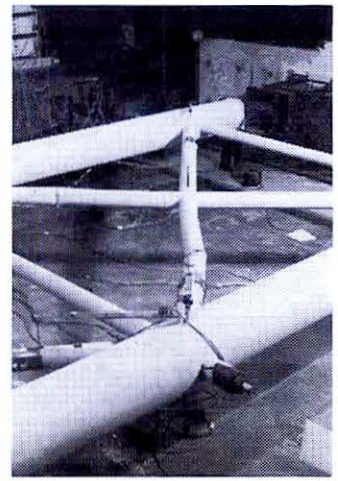

(f) Lower Panel Braces in 2nd Maximum Credible Event

Fig. 6.12 Photographs of Frame Damages during the Pseudodynamic Tests

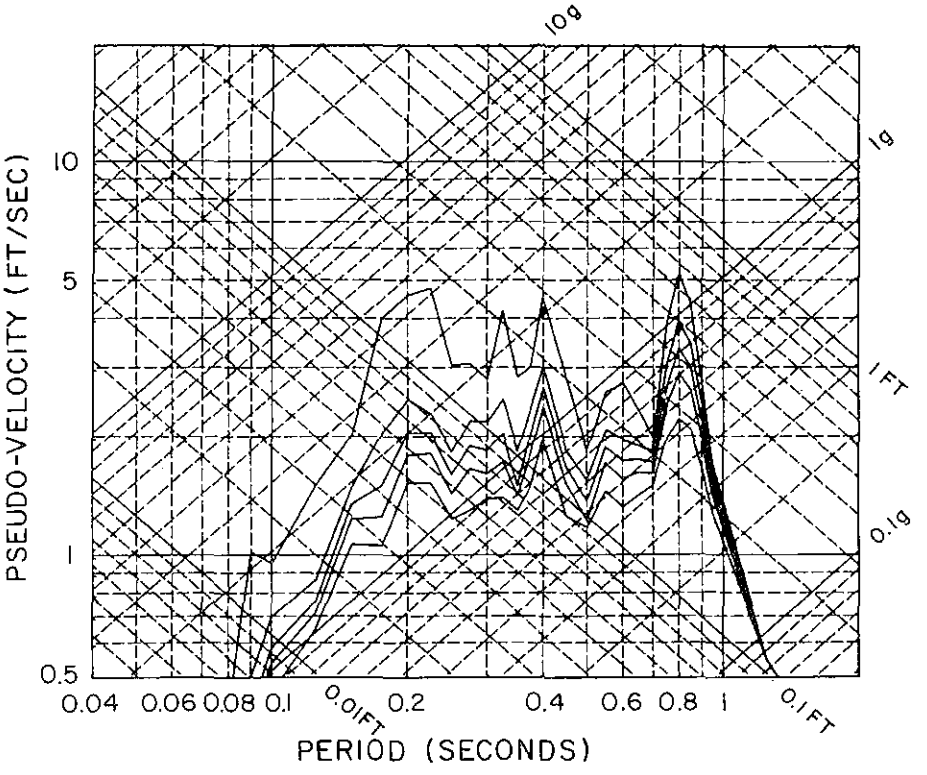

Damping Ratios: 0.0, 0.01, 0.02, 0.03, 0.05

Fig. 6.13 Response Spectra for the Taft Record (0.581g) [Ref. 4]

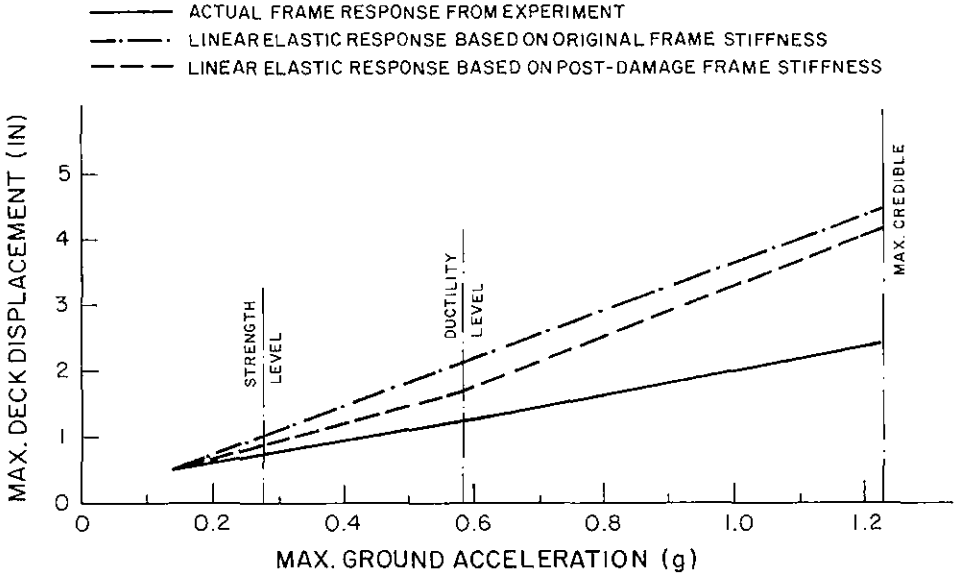

Fig. 6.14 Maximum Frame Displacement

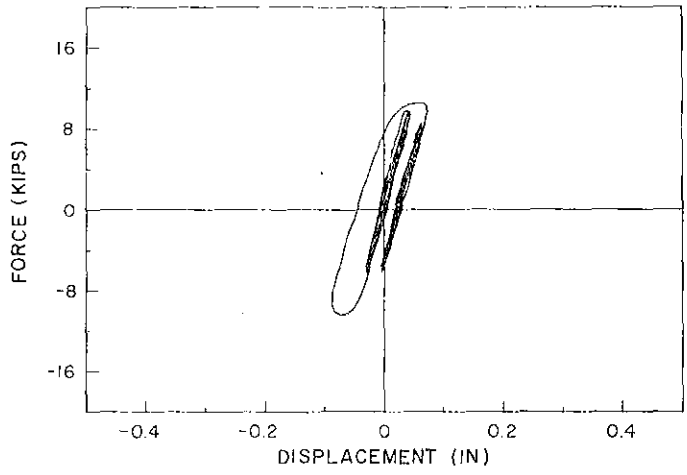

(a) Strength Level

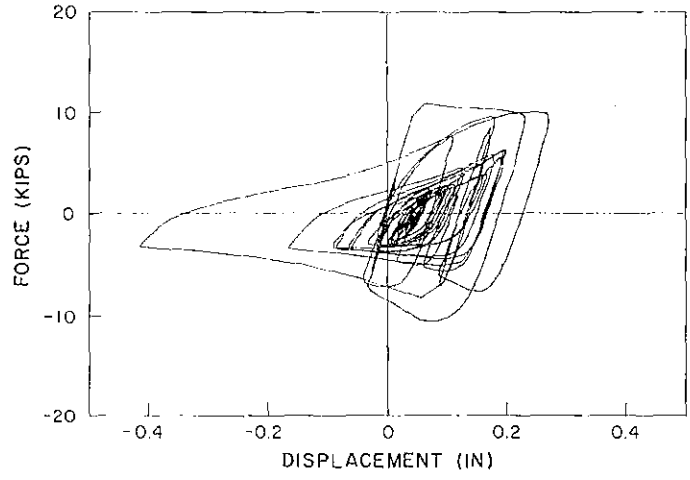

(b) Ductility Level

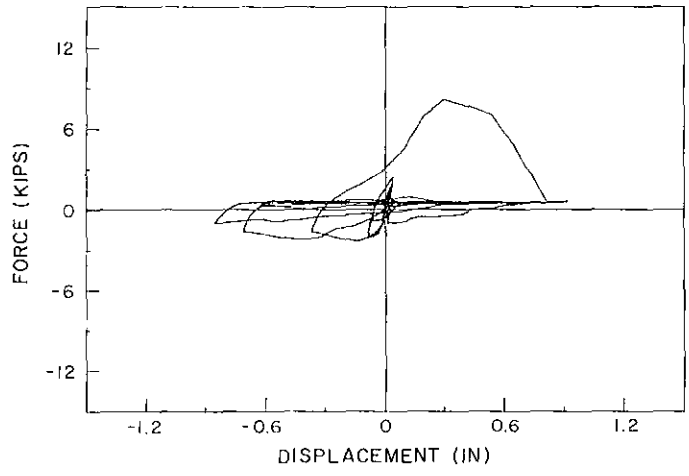

(c) 1st Maximum Credible

Fig. 6.15 Hysteretic Loops of Brace 4 (D/t = 51)

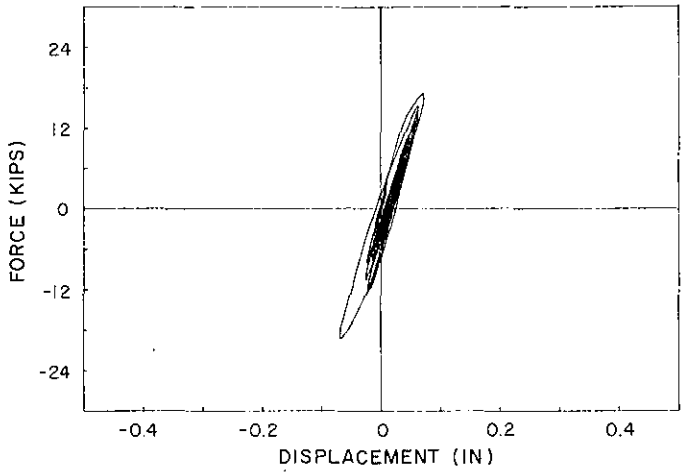

(a) Ductility Level

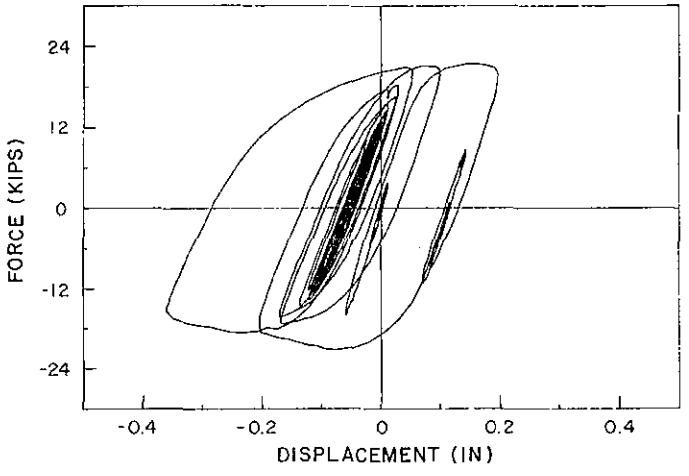

(b) 1st Maximum Credible

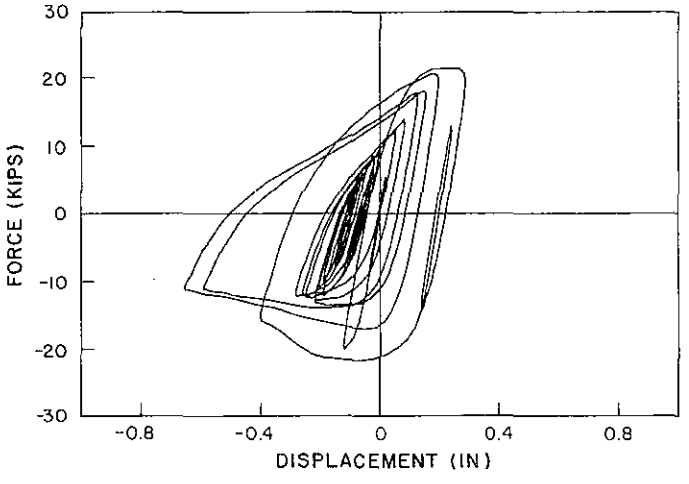

(c) 2nd Maximum Credible

Fig. 6.16 Hysteretic Loops of Brace 7 (D/t = 36)

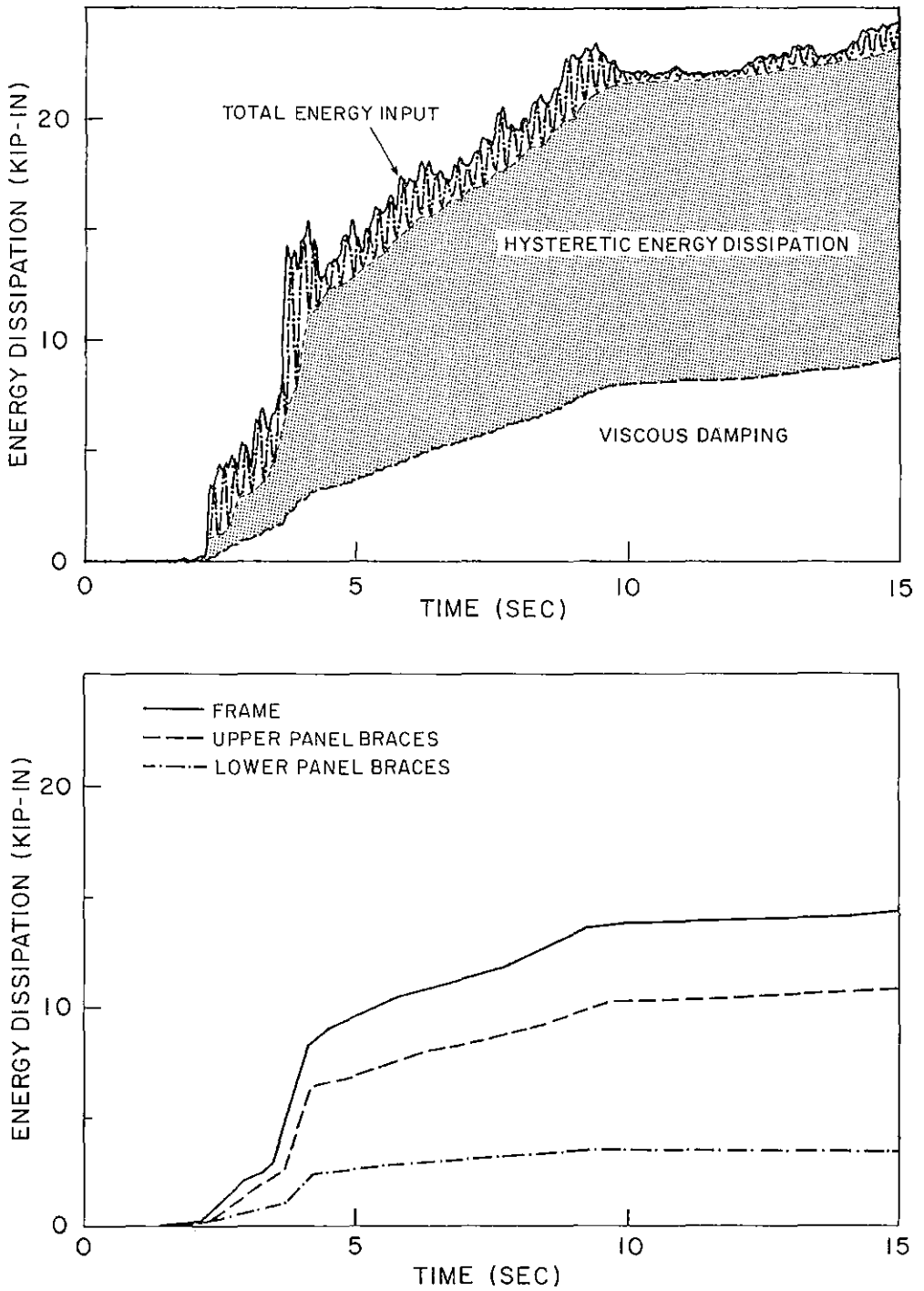

Fig. 6.17 Energy Dissipation during the Strength Level Event

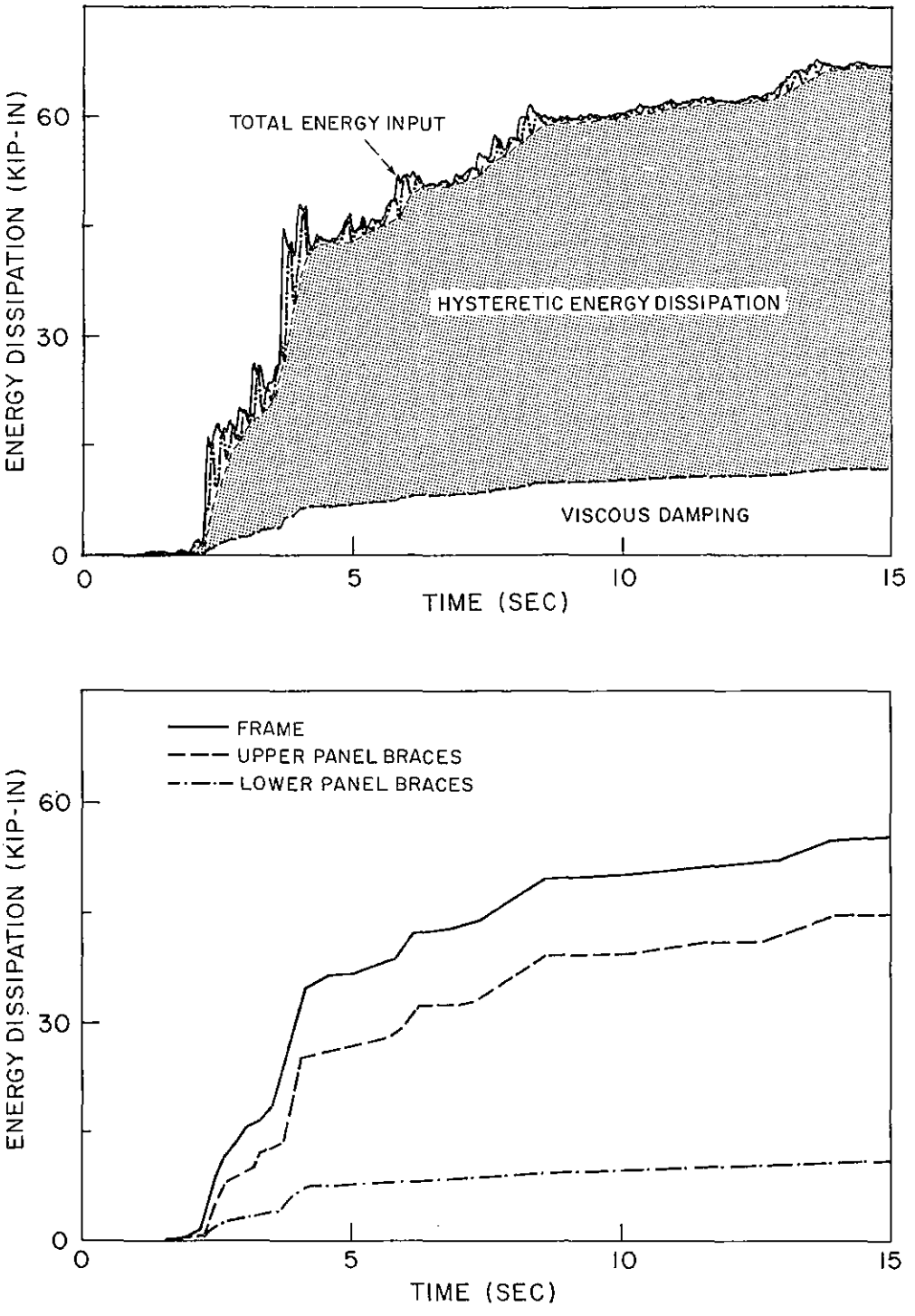

Fig. 6.18 Energy Dissipation during the Ductility Level Event

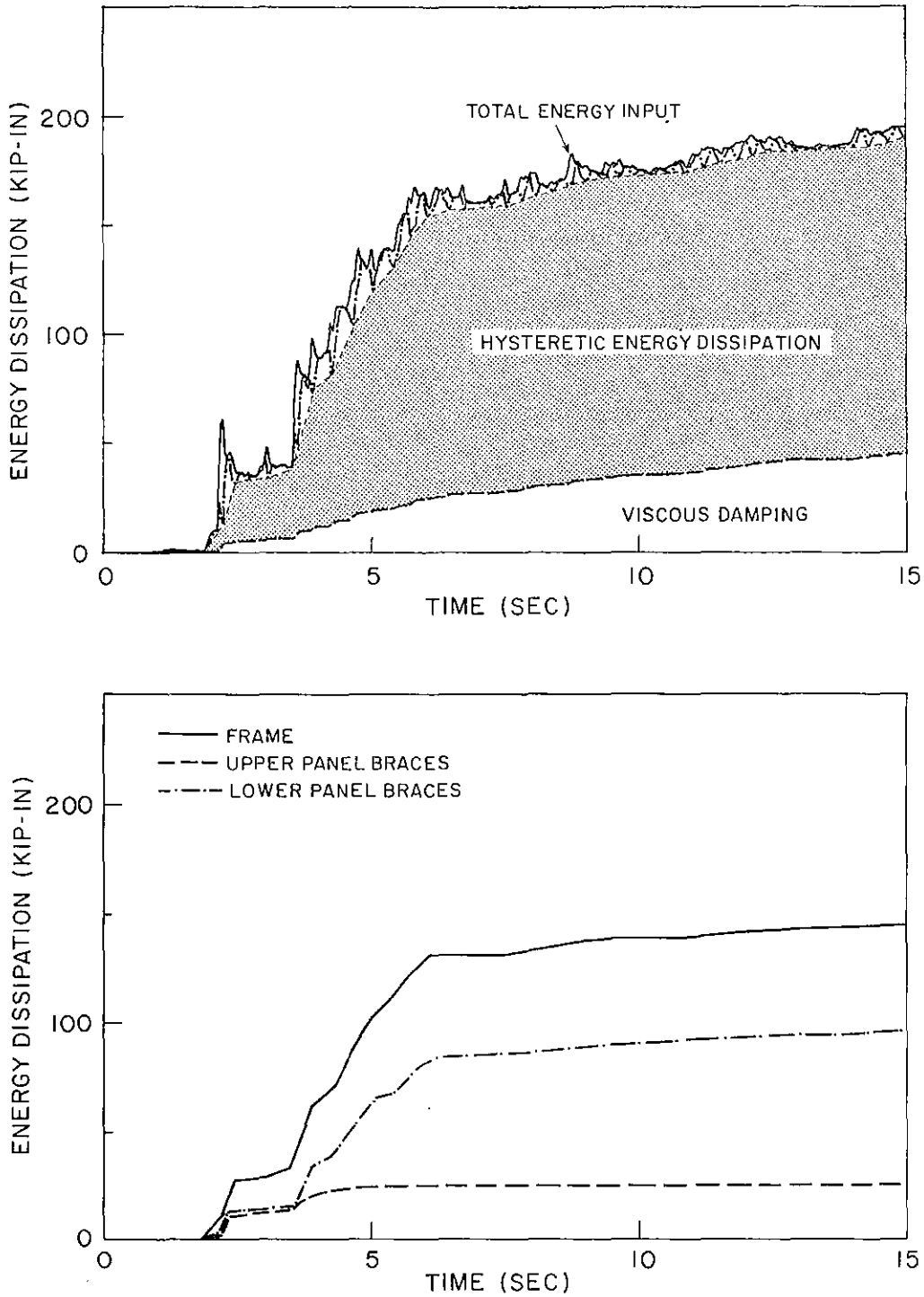

Fig. 6.19 Energy Dissipation during the 1st Maximum Credible Event

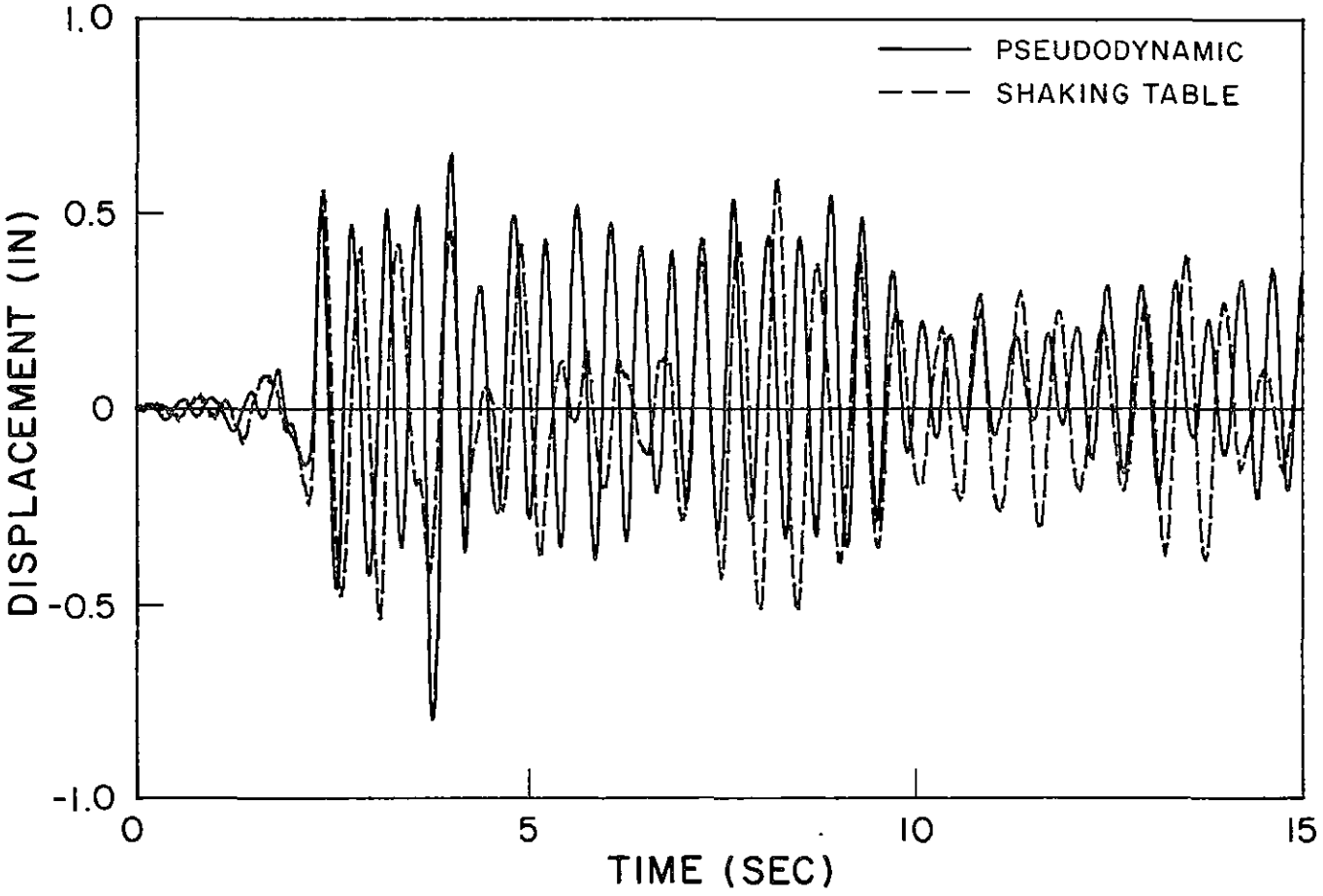

Fig. 6.20 Comparison of Pseudodynamic and Shaking Table Test Results in the Strength Level Event

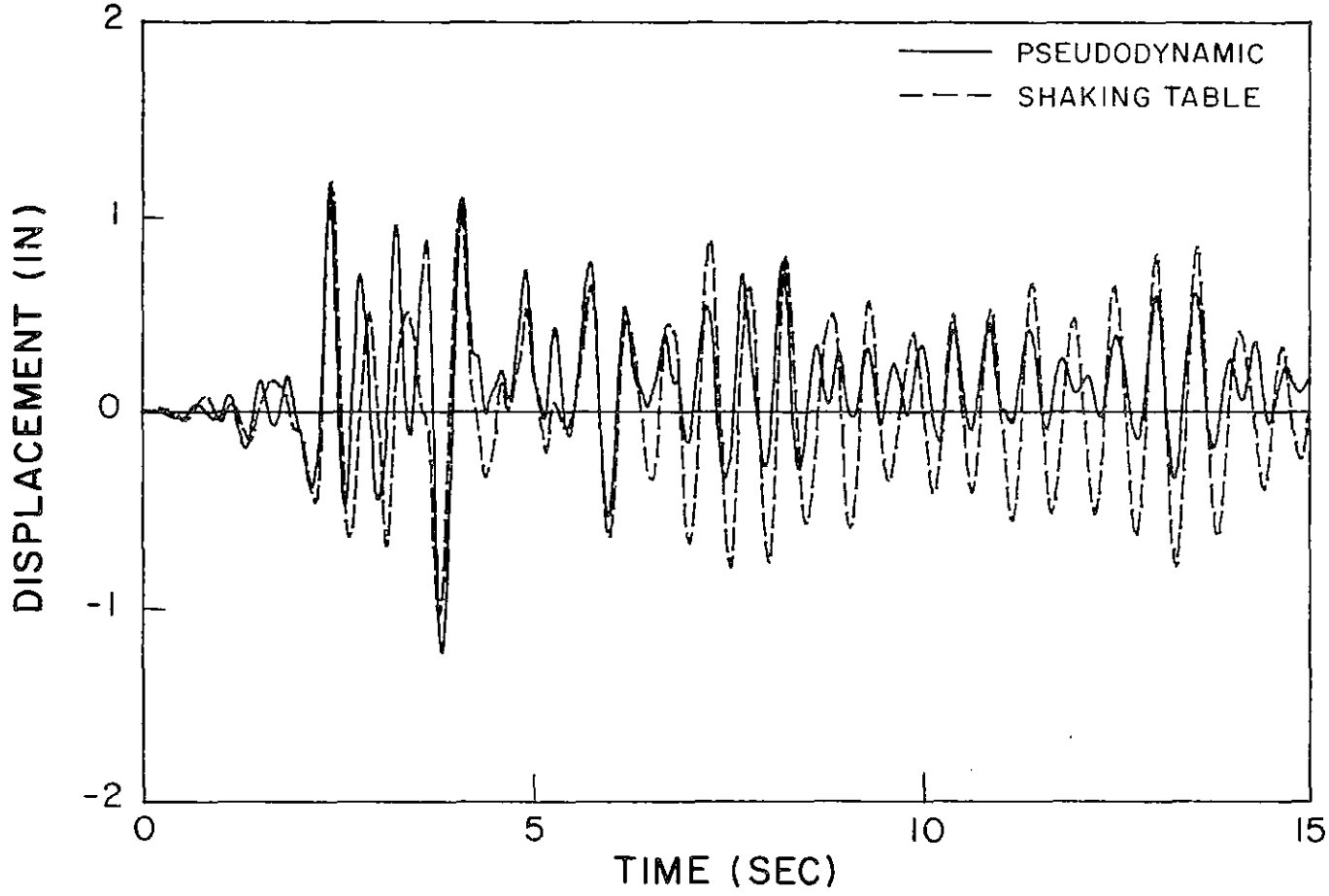

Fig. 6.21 Comparison of Pseudodynamic and Shaking Table Test Results in the Ductility Level Event

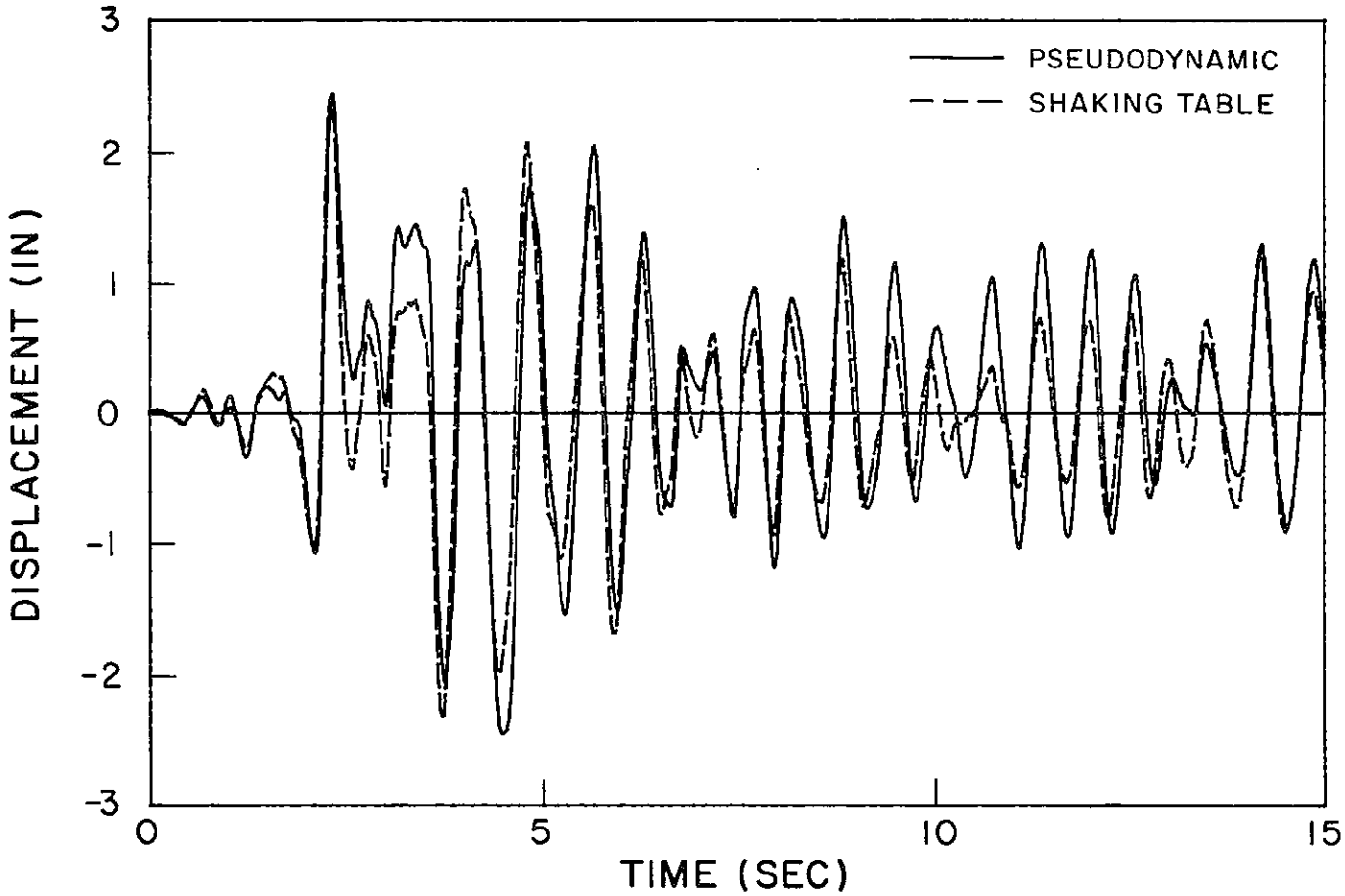

Fig. 6.22 Comparison of Pseudodynamic and Shaking Table Test Results in the 1st Maximum Credible Event

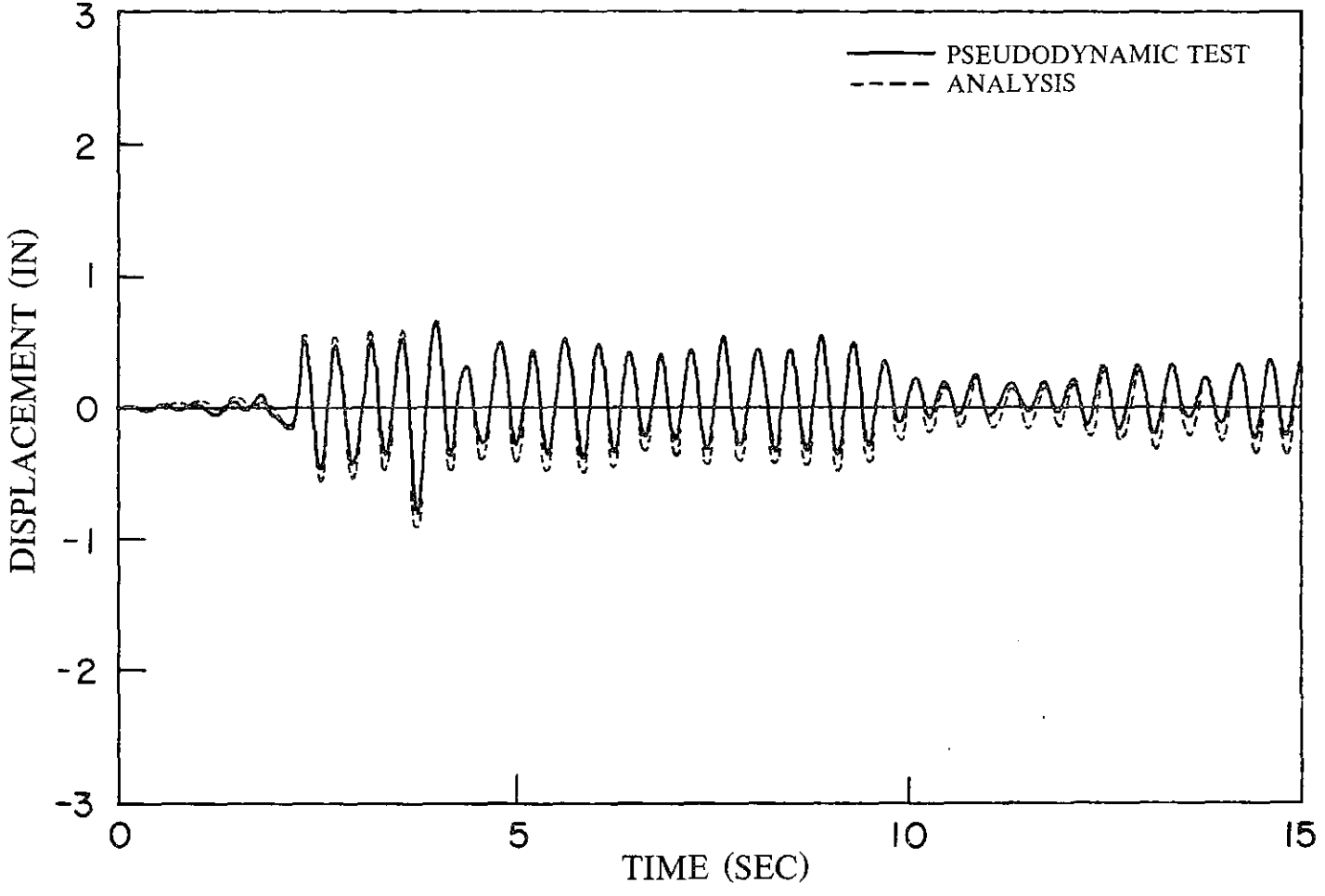

Fig. 6.23 Comparison of the Pseudodynamic Test Result with Analytical Simulation (Strength Level Event)

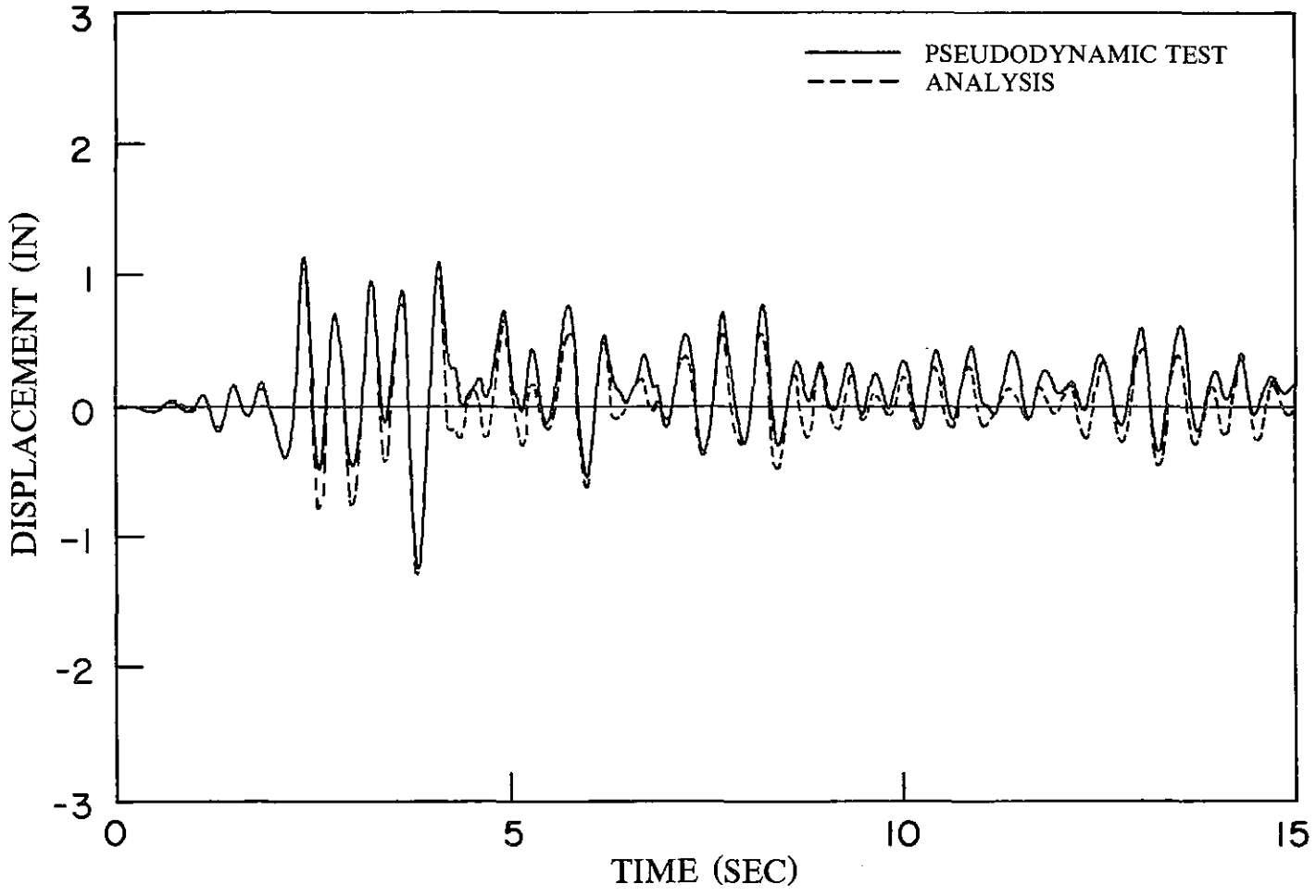

Fig. 6.24 Comparison of the Pseudodynamic Test Result with Analytical Simulation (Ductility Level Event)

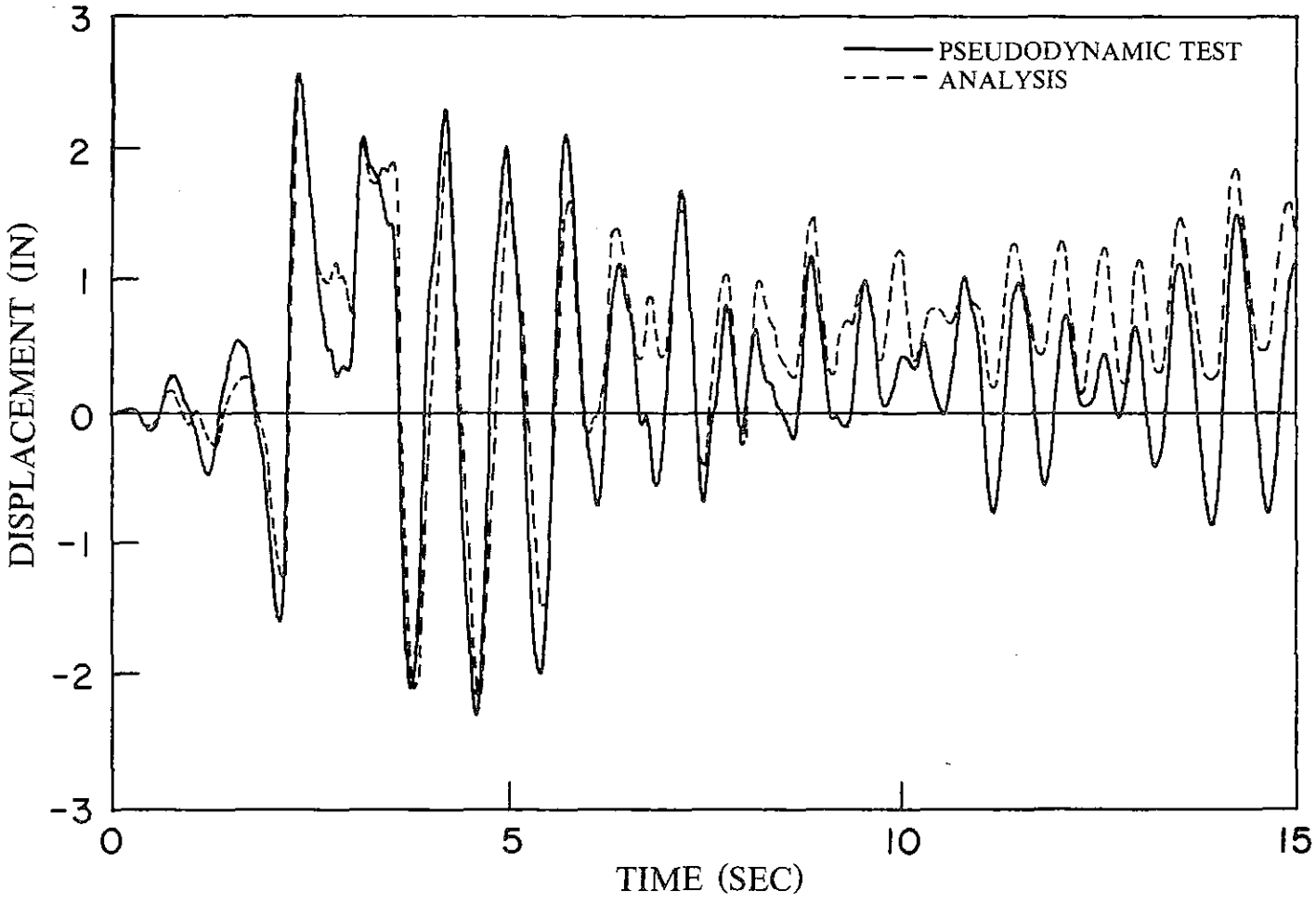

Fig. 6.25 Comparison of the Pseudodynamic Test Result with Analytical Simulation (2nd Maximum Credible Event)

EARTHQUAKE ENGINEERING RESEARCH CENTER REPORTS

NOTE: Numbers in parentheses are Accession Numbers assigned by the National Technical Information Service; these are followed by a price code. Copies of the reports may be ordered from the National Technical Information Service, 5285 Port Royal Road, Springfield, Virginia, 22161. Accession Numbers should be quoted on orders for reports (PB --- ---) and remittance must accompany each order. Reports without this information were not available at time of printing. The complete list of EERC reports (from EERC 67-1) is available upon request from the Earthquake Engineering Research Center, University of California, Berkeley, 47th Street and Hoffman Boulevard, Richmond, California 94804.

UCB/EERC-77/01 "PLUSH - A Computer Program for Probabilistic Finite Element Analysis of Seismic Soil-Structure Interaction," by M.P. Romo Organista, J. Lysmer and H.B. Seed - 1977 (PB81 177 651)A05

UCB/EERC-77/02 "Soil-Structure Interaction Effects at the Humboldt Bay Power Plant in the Ferndale Earthquake of June 7, 1975," by J.E. Valera, H.B. Seed, C.F. Tsai and J. Lysmer - 1977 (PB 265 795)A04

UCB/EERC-77/03 "Influence of Sample Disturbance on Sand Response to Cyclic Loading," by K. Mori, H.B. Seed and C.K. Chan - 1977 (PB 267 352)A04

UCB/EERC-77/04 "Seismological Studies of Strong Motion Records," by J. Shoja-Taheri - 1977 (PB 269 655)A10

UCB/EERC-77/05 Unassigned

UCB/EERC-77/06 "Developing Methodologies for Evaluating the Earthquake Safety of Existing Buildings," by No. 1 - B. Bresler; No. 2 - B. Bresler, T. Okada and D. Zisling; No. 3 - T. Okada and B. Bresler; No. 4 - V.V. Bertero and B. Bresler - 1977 (PB 267 354)A08

UCB/EERC-77/07 "A Literature Survey - Transverse Strength of Masonry Walls," by Y. Omote, R.L. Mayes, S.W. Chen and R.W. Clough - 1977 (PB 277 933)A07

UCB/EERC-77/08 "DRAIN-TABS: A Computer Program for Inelastic Earthquake Response of Three Dimensional Buildings," by R. Guendelman-Israel and G.H. Powell - 1977 (PB 270 693)A07

UCB/EERC-77/09 "SUBWALL: A Special Purpose Finite Element Computer Program for Practical Elastic Analysis and Design of Structural Walls with Substructure Option," by D.Q. Le, H. Peterson and E.P. Popov - 1977 (PB 270 567)A05

UCB/EERC-77/10 "Experimental Evaluation of Seismic Design Methods for Broad Cylindrical Tanks," by D.P. Clough (PB 272 280)A13

UCB/EERC-77/11 "Earthquake Engineering Research at Berkeley - 1976," - 1977 (PB 273 507)A09

UCB/EERC-77/12 "Automated Design of Earthquake Resistant Multistory Steel Building Frames," by N.D. Walker, Jr. - 1977 (PB 276 526)A09

UCB/EERC-77/13 "Concrete Confined by Rectangular Hoops Subjected to Axial Loads," by J. Vallenas, V.V. Bertero and E.P. Popov - 1977 (PB 275 165)A06

UCB/EERC-77/14 "Seismic Strain Induced in the Ground During Earthquakes," by Y. Sugimura - 1977 (PB 284 201)A04

UCB/EERC-77/15 Unassigned

UCB/EERC-77/16 "Computer Aided Optimum Design of Ductile Reinforced Concrete Moment Resisting Frames," by S.W. Zagajeski and V.V. Bertero - 1977 (PB 280 137)A07

UCB/EERC-77/17 "Earthquake Simulation Testing of a Stepping Frame with Energy-Absorbing Devices," by J.M. Kelly and D.F. Tsztoo - 1977 (PB 273 506)A04

UCB/EERC-77/18 "Inelastic Behavior of Eccentrically Braced Steel Frames under Cyclic Loadings," by C.W. Roeder and E.P. Popov - 1977 (PB 275 526)A15

UCB/EERC-77/19 "A Simplified Procedure for Estimating Earthquake-Induced Deformations in Dams and Embankments," by F.I. Makdisi and H.B. Seed - 1977 (PB 276 820)A04

UCB/EERC-77/20 "The Performance of Earth Dams during Earthquakes," by H.B. Seed, F.I. Makdisi and P. de Alba - 1977 (PB 276 821)A04

UCB/EERC-77/21 "Dynamic Plastic Analysis Using Stress Resultant Finite Element Formulation," by P. Lukkunapvasit and J.M. Kelly - 1977 (PB 275 453)A04

UCB/EERC-77/22 "Preliminary Experimental Study of Seismic Uplift of a Steel Frame," by R.W. Clough and A.A. Huckelbridge 1977 (PB 278 769)A08

UCB/EERC-77/23 "Earthquake Simulator Tests of a Nine-Story Steel Frame with Columns Allowed to Uplift," by A.A. Huckelbridge - 1977 (PB 277 944)A09

UCB/EERC-77/24 "Nonlinear Soil-Structure Interaction of Skew Highway Bridges," by M.-C. Chen and J. Penzien - 1977 (PB 276 176)A07

UCB/EERC-77/25 "Seismic Analysis of an Offshore Structure Supported on Pile Foundations," by D.D.-N. Liou and J. Penzien 1977 (PB 283 180)A06

UCB/EERC-77/26 "Dynamic Stiffness Matrices for Homogeneous Viscoelastic Half-Planes," by G. Dasgupta and A.K. Chopra - 1977 (PB 279 654)A06

UCB/EERC-77/27 "A Practical Soft Story Earthquake Isolation System," by J.M. Kelly, J.M. Eidinger and C.J. Derham - 1977 (PB 276 814)A07

UCB/EERC-77/28 "Seismic Safety of Existing Buildings and Incentives for Hazard Mitigation in San Francisco: An Exploratory Study," by A.J. Meltsner - 1977 (PB 281 970)A05

UCB/EERC-77/29 "Dynamic Analysis of Electrohydraulic Shaking Tables," by D. Rea, S. Abedi-Hayati and Y. Takahashi 1977 (PB 282 569)A04

UCB/EERC-77/30 "An Approach for Improving Seismic - Resistant Behavior of Reinforced Concrete Interior Joints," by B. Galunic, V.V. Bertero and E.P. Popov - 1977 (PB 290 870)A06

UCB/EERC-78/01 "The Development of Energy-Absorbing Devices for Aseismic Base Isolation Systems," by J.M. Kelly and D.F. Tsztoo - 1978 (PB 284 978)A04

UCB/EERC-78/02 "Effect of Tensile Prestrain on the Cyclic Response of Structural Steel Connections, by J.G. Bouwkamp and A. Mukhopadhyay - 1978

UCB/EERC-78/03 "Experimental Results of an Earthquake Isolation System using Natural Rubber Bearings," by J.M. Eidinger and J.M. Kelly - 1978 (PB 281 686)A04

UCB/EERC-78/04 "Seismic Behavior of Tall Liquid Storage Tanks," by A. Niwa - 1978 (PB 284 017)A14

UCB/EERC-78/05 "Hysteretic Behavior of Reinforced Concrete Columns Subjected to High Axial and Cyclic Shear Forces," by S.W. Zagajeski, V.V. Bertero and J.G. Bouwkamp - 1978 (PB 283 858)A13

UCB/EERC-78/06 "Three Dimensional Inelastic Frame Elements for the ANSR-I Program," by A. Riahi, D.G. Row and G.H. Powell - 1978 (PB 295 755)A04

UCB/EERC-78/07 "Studies of Structural Response to Earthquake Ground Motion," by O.A. Lopez and A.K. Chopra - 1978 (PB 282 790)A05

UCB/EERC-78/08 "A Laboratory Study of the Fluid-Structure Interaction of Submerged Tanks and Caissons in Earthquakes," by R.C. Byrd - 1978 (PB 284 957)A08

UCB/EERC-78/09 Unassigned

UCB/EERC-78/10 "Seismic Performance of Nonstructural and Secondary Structural Elements," by I. Sakamoto - 1978 (PB81 154 593)A05

UCB/EERC-78/11 "Mathematical Modelling of Hysteresis Loops for Reinforced Concrete Columns," by S. Nakata, T. Sproul and J. Penzien - 1978 (PB 298 274)A05

UCB/EERC-78/12 "Damageability in Existing Buildings," by T. Blejwas and B. Bresler - 1978 (PB 80 166 978)A05

UCB/EERC-78/13 "Dynamic Behavior of a Pedestal Base Multistory Building," by R.M. Stephen, E.L. Wilson, J.G. Bouwkamp and M. Button - 1978 (PB 286 650)A08

UCB/EERC-78/14 "Seismic Response of Bridges - Case Studies," by R.A. Imbsen, V. Nutt and J. Penzien - 1978 (PB 286 503)A10

UCB/EERC-78/15 "A Substructure Technique for Nonlinear Static and Dynamic Analysis," by D.G. Row and G.H. Powell - 1978 (PB 288 077)A10

UCB/EERC-78/16 "Seismic Risk Studies for San Francisco and for the Greater San Francisco Bay Area," by C.S. Oliveira - 1978 (PB 81 120 115)A07

UCB/EERC-78/17 "Strength of Timber Roof Connections Subjected to Cyclic Loads," by P. Gülkan, R.L. Mayes and R.W. Clough - 1978 (HUD-000 1491)A07

UCB/EERC-78/18 "Response of K-Braced Steel Frame Models to Lateral Loads," by J.G. Bouwkamp, R.M. Stephen and E.P. Popov - 1978

UCB/EERC-78/19 "Rational Design Methods for Light Equipment in Structures Subjected to Ground Motion," by J.L. Sackman and J.M. Kelly - 1978 (PB 292 357)A04

UCB/EERC-78/20 "Testing of a Wind Restraint for Aseismic Base Isolation," by J.M. Kelly and D.E. Chitty - 1978 (PB 292 833)A03

UCB/EERC-78/21 "APOLLO - A Computer Program for the Analysis of Pore Pressure Generation and Dissipation in Horizontal Sand Layers During Cyclic or Earthquake Loading," by P.P. Martin and H.B. Seed - 1978 (PB 292 835)A04

UCB/EERC-78/22 "Optimal Design of an Earthquake Isolation System," by M.A. Bhatti, K.S. Pister and E. Polak - 1978 (PB 294 735)A06

UCB/EERC-78/23 "MASH - A Computer Program for the Non-Linear Analysis of Vertically Propagating Shear Waves in Horizontally Layered Deposits," by P.P. Martin and H.B. Seed - 1978 (PB 293 101)A05

UCB/EERC-78/24 "Investigation of the Elastic Characteristics of a Three Story Steel Frame Using System Identification," by I. Kaya and H.D. McNiven - 1978 (PB 296 225)A06

UCB/EERC-78/25 "Investigation of the Nonlinear Characteristics of a Three-Story Steel Frame Using System Identification," by I. Kaya and H.D. McNiven - 1978 (PB 301 363)A05

UCB/EERC-78/26 "Studies of Strong Ground Motion in Taiwan," by Y.M. Hsiung, B.A. Bolt and J. Penzien - 1978 (PB 298 436)A06

UCB/EERC-78/27 "Cyclic Loading Tests of Masonry Single Piers: Volume 1 - Height to Width Ratio of 2," by P.A. Hidalgo, R.L. Mayes, H.D. McNiven and R.W. Clough - 1978 (PB 296 211)A07

UCB/EERC-78/28 "Cyclic Loading Tests of Masonry Single Piers: Volume 2 - Height to Width Ratio of 1," by S.-W.J. Chen, P.A. Hidalgo, R.L. Mayes, R.W. Clough and H.D. McNiven - 1978 (PB 296 212)A09

UCB/EERC-78/29 "Analytical Procedures in Soil Dynamics," by J. Lysmer - 1978 (PB 298 445)A06

UCB/EERC-79/01 "Hysteretic Behavior of Lightweight Reinforced Concrete Beam-Column Subassemblages," by B. Forzani, E.P. Popov and V.V. Bertero - April 1979(PB 298 267)A06

UCB/EERC-79/02 "The Development of a Mathematical Model to Predict the Flexural Response of Reinforced Concrete Beams to Cyclic Loads, Using System Identification," by J. Stanton & H. McNiven - Jan. 1979(PB 295 875)A10

UCB/EERC-79/03 "Linear and Nonlinear Earthquake Response of Simple Torsionally Coupled Systems," by C.L. Kan and A.K. Chopra - Feb. 1979(PB 298 262)A06

UCB/EERC-79/04 "A Mathematical Model of Masonry for Predicting its Linear Seismic Response Characteristics," by Y. Mengi and H.D. McNiven - Feb. 1979(PB 298 266)A06

UCB/EERC-79/05 "Mechanical Behavior of Lightweight Concrete Confined by Different Types of Lateral Reinforcement," by M.A. Manrique, V.V. Bertero and E.P. Popov - May 1979(PB 301 114)A06

UCB/EERC-79/06 "Static Tilt Tests of a Tall Cylindrical Liquid Storage Tank," by R.W. Clough and A. Niwa - Feb. 1979 (PB 301 167)A06

UCB/EERC-79/07 "The Design of Steel Energy Absorbing Restrainers and Their Incorporation into Nuclear Power Plants for Enhanced Safety: Volume 1 - Summary Report," by P.N. Spencer, V.F. Zackay, and E.R. Parker - Feb. 1979(UCB/EERC-79/07)A09

UCB/EERC-79/08 "The Design of Steel Energy Absorbing Restrainers and Their Incorporation into Nuclear Power Plants for Enhanced Safety: Volume 2 - The Development of Analyses for Reactor System Piping,""Simple Systems" by M.C. Lee, J. Penzien, A.K. Chopra and K. Suzuki "Complex Systems" by G.H. Powell, E.L. Wilson, R.W. Clough and D.G. Row - Feb. 1979(UCB/EERC-79/08)A10

UCB/EERC-79/09 "The Design of Steel Energy Absorbing Restrainers and Their Incorporation into Nuclear Power Plants for Enhanced Safety: Volume 3 - Evaluation of Commercial Steels," by W.S. Owen, R.M.N. Pelloux, R.O. Ritchie, M. Faral, T. Ohhashi, J. Toplosky, S.J. Hartman, V.F. Zackay and E.R. Parker - Feb. 1979(UCB/EERC-79/09)A04

UCB/EERC-79/10 "The Design of Steel Energy Absorbing Restrainers and Their Incorporation into Nuclear Power Plants for Enhanced Safety: Volume 4 - A Review of Energy-Absorbing Devices," by J.M. Kelly and M.S. Skinner - Feb. 1979(UCB/EERC-79/10)A04

UCB/EERC-79/11 "Conservatism In Summation Rules for Closely Spaced Modes," by J.M. Kelly and J.L. Sackman - May 1979(PB 301 328)A03

UCB/EERC-79/12 "Cyclic Loading Tests of Masonry Single Piers; Volume 3 - Height to Width Ratio of 0.5," by P.A. Hidalgo, R.L. Mayes, H.D. McNiven and R.W. Clough - May 1979(PB 301 321)A08

UCB/EERC-79/13 "Cyclic Behavior of Dense Course-Grained Materials in Relation to the Seismic Stability of Dams," by N.G. Banerjee, H.B. Seed and C.K. Chan - June 1979(PB 301 373)A13

UCB/EERC-79/14 "Seismic Behavior of Reinforced Concrete Interior Beam-Column Subassemblages," by S. Viwathanatepa, E.P. Popov and V.V. Bertero - June 1979(PB 301 326)A10

UCB/EERC-79/15 "Optimal Design of Localized Nonlinear Systems with Dual Performance Criteria Under Earthquake Excitations," by M.A. Bhatti - July 1979(PB 80 167 109)A06

UCB/EERC-79/16 "OPTDYN - A General Purpose Optimization Program for Problems with or without Dynamic Constraints," by M.A. Bhatti, E. Polak and K.S. Pister - July 1979(PB 80 167 091)A05

UCB/EERC-79/17 "ANSR-II, Analysis of Nonlinear Structural Response, Users Manual," by D.P. Mondkar and G.H. Powell July 1979(PB 80 113 301)A05

UCB/EERC-79/18 "Soil Structure Interaction in Different Seismic Environments," A. Gomez-Masso, J. Lysmer, J.-C. Chen and H.B. Seed - August 1979(PB 80 101 520)A04

UCB/EERC-79/19 "ARMA Models for Earthquake Ground Motions," by M.K. Chang, J.W. Kwiatkowski, R.F. Nau, R.M. Oliver and K.S. Pister - July 1979(PB 301 166)A05

UCB/EERC-79/20 "Hysteretic Behavior of Reinforced Concrete Structural Walls," by J.M. Vallenas, V.V. Bertero and E.P. Popov - August 1979(PB 80 165 905)A12

UCB/EERC-79/21 "Studies on High-Frequency Vibrations of Buildings - 1: The Column Effect," by J. Lubliner - August 1979 (PB 80 158 553)A03

UCB/EERC-79/22 "Effects of Generalized Loadings on Bond Reinforcing Bars Embedded in Confined Concrete Blocks," by S. Viwathanatepa, E.P. Popov and V.V. Bertero - August 1979(PB 81 124 018)A14

UCB/EERC-79/23 "Shaking Table Study of Single-Story Masonry Houses, Volume 1: Test Structures 1 and 2," by P. Gülkan, R.L. Mayes and R.W. Clough - Sept. 1979 (HUD-000 1763)A12

UCB/EERC-79/24 "Shaking Table Study of Single-Story Masonry Houses, Volume 2: Test Structures 3 and 4," by P. Gülkan, R.L. Mayes and R.W. Clough - Sept. 1979 (HUD-000 1836)A12

UCB/EERC-79/25 "Shaking Table Study of Single-Story Masonry Houses, Volume 3: Summary, Conclusions and Recommendations," by R.W. Clough, R.L. Mayes and P. Gülkan - Sept. 1979 (HUD-000 1837)A06

UCB/EERC-79/26 "Recommendations for a U.S.-Japan Cooperative Research Program Utilizing Large-Scale Testing Facilities," by U.S.-Japan Planning Group - Sept. 1979(PB 301 407)A06

UCB/EERC-79/27 "Earthquake-Induced Liquefaction Near Lake Amatitlan, Guatemala," by H.B. Seed, I. Arango, C.K. Chan, A. Gomez-Masso and R. Grant de Ascoli - Sept. 1979(NUREG-CR1341)A03

UCB/EERC-79/28 "Infill Panels: Their Influence on Seismic Response of Buildings," by J.W. Axley and V.V. Bertero Sept. 1979(PB 80 163 371)A10

UCB/EERC-79/29 "3D Truss Bar Element (Type 1) for the ANSR-II Program," by D.P. Mondkar and G.H. Powell - Nov. 1979 (PB 80 169 709)A02

UCB/EERC-79/30 "3D Beam-Column Element (Type 5 - Parallel Element Theory) for the ANSR-II Program," by D.G. Row, G.H. Powell and D.P. Mondkar - Dec. 1979(PB 80 167 224)A03

UCB/EERC-79/31 "3D Beam-Column Element (Type 2 - Parallel Element Theory) for the ANSR-II Program," by A. Riahi, G.H. Powell and D.P. Mondkar - Dec. 1979(PB 80 167 216)A03

UCB/EERC-79/32 "On Response of Structures to Stationary Excitation," by A. Der Kiureghian - Dec. 1979(PB 80166 929)A03

UCB/EERC-79/33 "Undisturbed Sampling and Cyclic Load Testing of Sands," by S. Singh, H.B. Seed and C.K. Chan Dec. 1979(ADA 087 298)A07

UCB/EERC-79/34 "Interaction Effects of Simultaneous Torsional and Compressional Cyclic Loading of Sand," by P.M. Griffin and W.N. Houston - Dec. 1979(ADA 092 352)A15

UCB/EERC-80/01 "Earthquake Response of Concrete Gravity Dams Including Hydrodynamic and Foundation Interaction Effects," by A.K. Chopra, P. Chakrabarti and S. Gupta - Jan. 1980(AD-A087297)A10

UCB/EERC-80/02 "Rocking Response of Rigid Blocks to Earthquakes," by C.S. Yim, A.K. Chopra and J. Penzien - Jan. 1980 (PB80 166 002)A04

UCB/EERC-80/03 "Optimum Inelastic Design of Seismic-Resistant Reinforced Concrete Frame Structures," by S.W. Zagajeski and V.V. Bertero - Jan. 1980(PB80 164 635)A06

UCB/EERC-80/04 "Effects of Amount and Arrangement of Wall-Panel Reinforcement on Hysteretic Behavior of Reinforced Concrete Walls," by R. Iliya and V.V. Bertero - Feb. 1980(PB81 122 525)A09

UCB/EERC-80/05 "Shaking Table Research on Concrete Dam Models," by A. Niwa and R.W. Clough - Sept. 1980(PB81 122 368)A06

UCB/EERC-80/06 "The Design of Steel Energy-Absorbing Restrainers and their Incorporation into Nuclear Power Plants for Enhanced Safety (Vol 1A): Piping with Energy Absorbing Restrainers: Parameter Study on Small Systems," by G.H. Powell, C. Oughourlian and J. Simons - June 1980

UCB/EERC-80/07 "Inelastic Torsional Response of Structures Subjected to Earthquake Ground Motions," by Y. Yamazaki April 1980(PB81 122 327)A08

UCB/EERC-80/08 "Study of X-Braced Steel Frame Structures Under Earthquake Simulation," by Y. Ghanaat - April 1980 (PB81 122 335)A11

UCB/EERC-80/09 "Hybrid Modelling of Soil-Structure Interaction," by S. Gupta, T.W. Lin, J. Penzien and C.S. Yeh May 1980(PB81 122 319)A07

UCB/EERC-80/10 "General Applicability of a Nonlinear Model of a One Story Steel Frame," by B.I. Sveinsson and H.D. McNiven - May 1980(PB81 124 877)A06

UCB/EERC-80/11 "A Green-Function Method for Wave Interaction with a Submerged Body," by W. Kioka - April 1980 (PB81 122 269)A07

UCB/EERC-80/12 "Hydrodynamic Pressure and Added Mass for Axisymmetric Bodies," by F. Nilrat - May 1980(PB81 122 343)A08

UCB/EERC-80/13 "Treatment of Non-Linear Drag Forces Acting on Offshore Platforms," by B.V. Dao and J. Penzien May 1980(PB81 153 413)A07

UCB/EERC-80/14 "2D Plane/Axisymmetric Solid Element (Type 3 - Elastic or Elastic-Perfectly Plastic) for the ANSR-II Program," by D.P. Mondkar and G.H. Powell - July 1980(PB81 122 350)A03

UCB/EERC-80/15 "A Response Spectrum Method for Random Vibrations," by A. Der Kiureghian - June 1980(PB81 122 301)A03

UCB/EERC-80/16 "Cyclic Inelastic Buckling of Tubular Steel Braces," by V.A. Zayas, E.P. Popov and S.A. Mahin June 1980(PB81 124 885)A10

UCB/EERC-80/17 "Dynamic Response of Simple Arch Dams Including Hydrodynamic Interaction," by C.S. Porter and A.K. Chopra - July 1980(PB81 124 000)A13

UCB/EERC-80/18 "Experimental Testing of a Friction Damped Aseismic Base Isolation System with Fail-Safe Characteristics," by J.M. Kelly, K.E. Beucke and M.S. Skinner - July 1980(PB81 148 595)A04

UCB/EERC-80/19 "The Design of Steel Energy-Absorbing Restrainers and their Incorporation into Nuclear Power Plants for Enhanced Safety (Vol 1B): Stochastic Seismic Analyses of Nuclear Power Plant Structures and Piping Systems Subjected to Multiple Support Excitations," by M.C. Lee and J. Penzien - June 1980

UCB/EERC-80/20 "The Design of Steel Energy-Absorbing Restrainers and their Incorporation into Nuclear Power Plants for Enhanced Safety (Vol 1C): Numerical Method for Dynamic Substructure Analysis," by J.M. Dickens and E.L. Wilson - June 1980

UCB/EERC-80/21 "The Design of Steel Energy-Absorbing Restrainers and their Incorporation into Nuclear Power Plants for Enhanced Safety (Vol 2): Development and Testing of Restraints for Nuclear Piping Systems," by J.M. Kelly and M.S. Skinner - June 1980

UCB/EERC-80/22 "3D Solid Element (Type 4-Elastic or Elastic-Perfectly-Plastic) for the ANSR-II Program," by D.P. Mondkar and G.H. Powell - July 1980(PB81 123 242)A03

UCB/EERC-80/23 "Gap-Friction Element (Type 5) for the ANSR-II Program," by D.P. Mondkar and G.H. Powell - July 1980 (PB81 122 285)A03

UCB/EERC-80/24 "U-Bar Restraint Element (Type 11) for the ANSR-II Program," by C. Oughourlian and G.H. Powell July 1980(PB81 122 293)A03

UCB/EERC-80/25 "Testing of a Natural Rubber Base Isolation System by an Explosively Simulated Earthquake," by J.M. Kelly - August 1980(PB81 201 360)A04

UCB/EERC-80/26 "Input Identification from Structural Vibrational Response," by Y. Hu - August 1980(PB81 152 308)A05

UCB/EERC-80/27 "Cyclic Inelastic Behavior of Steel Offshore Structures," by V.A. Zayas, S.A. Mahin and E.P. Popov August 1980(PB81 196 180)A15

UCB/EERC-80/28 "Shaking Table Testing of a Reinforced Concrete Frame with Biaxial Response," by M.G. Oliva October 1980(PB81 154 304)A10

UCB/EERC-80/29 "Dynamic Properties of a Twelve-Story Prefabricated Panel Building," by J.G. Bouwkamp, J.P. Kollegger and R.M. Stephen - October 1980(PB82 117 128)A06

UCB/EERC-80/30 "Dynamic Properties of an Eight-Story Prefabricated Panel Building," by J.G. Bouwkamp, J.P. Kollegger and R.M. Stephen - October 1980(PB81 200 313)A05

UCB/EERC-80/31 "Predictive Dynamic Response of Panel Type Structures Under Earthquakes," by J.P. Kollegger and J.G. Bouwkamp - October 1980(PB81 152 316)A04

UCB/EERC-80/32 "The Design of Steel Energy-Absorbing Restrainers and their Incorporation into Nuclear Power Plants for Enhanced Safety (Vol 3): Testing of Commercial Steels in Low-Cycle Torsional Fatigue," by P. Spencer, E.R. Parker, E. Jongewaard and M. Drory

UCB/EERC-80/33 "The Design of Steel Energy-Absorbing Restrainers and their Incorporation into Nuclear Power Plants for Enhanced Safety (Vol 4): Shaking Table Tests of Piping Systems with Energy-Absorbing Restrainers," by S.F. Stiemer and W.G. Godden - Sept. 1980

UCB/EERC-80/34 "The Design of Steel Energy-Absorbing Restrainers and their Incorporation into Nuclear Power Plants for Enhanced Safety (Vol 5): Summary Report," by P. Spencer

UCB/EERC-80/35 "Experimental Testing of an Energy-Absorbing Base Isolation System," by J.M. Kelly, M.S. Skinner and K.E. Beucke - October 1980(PB81 154 072)A04

UCB/EERC-80/36 "Simulating and Analyzing Artificial Non-Stationary Earthquake Ground Motions," by R.F. Nau, R.M. Oliver and K.S. Pister - October 1980(PB81 153 397)A04

UCB/EERC-80/37 "Earthquake Engineering at Berkeley - 1980," - Sept. 1980(PB81 205 674)A09

UCB/EERC-80/38 "Inelastic Seismic Analysis of Large Panel Buildings," by V. Schricker and G.H. Powell - Sept. 1980 (PB81 154 338)A13

UCB/EERC-80/39 "Dynamic Response of Embankment, Concrete-Gravity and Arch Dams Including Hydrodynamic Interaction," by J.F. Hall and A.K. Chopra - October 1980(PB81 152 324)A11

UCB/EERC-80/40 "Inelastic Buckling of Steel Struts Under Cyclic Load Reversal," by R.G. Black, W.A. Wenger and E.P. Popov - October 1980(PB81 154 312)A08

UCB/EERC-80/41 "Influence of Site Characteristics on Building Damage During the October 3, 1974 Lima Earthquake," by P. Repetto, I. Arango and H.B. Seed - Sept. 1980(PB81 161 739)A05

UCB/EERC-80/42 "Evaluation of a Shaking Table Test Program on Response Behavior of a Two Story Reinforced Concrete Frame," by J.M. Blondet, R.W. Clough and S.A. Mahin

UCB/EERC-80/43 "Modelling of Soil-Structure Interaction by Finite and Infinite Elements," by F. Medina - December 1980(PB81 229 270)A04

UCB/EERC-81/01 "Control of Seismic Response of Piping Systems and Other Structures by Base Isolation," edited by J.M. Kelly - January 1981 (PB81 200 735)A05

UCB/EERC-81/02 "OPTNSR - An Interactive Software System for Optimal Design of Statically and Dynamically Loaded Structures with Nonlinear Response," by M.A. Bhatti, V. Ciampi and K.S. Pister - January 1981 (PB81 218 851)A09

UCB/EERC-81/03 "Analysis of Local Variations in Free Field Seismic Ground Motions," by J.-C. Chen, J. Lysmer and H.B. Seed - January 1981 (AD-A099508)A13

UCB/EERC-81/04 "Inelastic Structural Modeling of Braced Offshore Platforms for Seismic Loading," by V.A. Zayas, P.-S.B. Shing, S.A. Mahin and E.P. Popov - January 1981(PB82 138 777)A07

UCB/EERC-81/05 "Dynamic Response of Light Equipment in Structures," by A. Der Kiureghian, J.L. Sackman and B. Nour-Omid - April 1981 (PB81 218 497)A04

UCB/EERC-81/06 "Preliminary Experimental Investigation of a Broad Base Liquid Storage Tank," by J.G. Bouwkamp, J.P. Kollegger and R.M. Stephen - May 1981(PB82 140 385)A03

UCB/EERC-81/07 "The Seismic Resistant Design of Reinforced Concrete Coupled Structural Walls," by A.E. Aktan and V.V. Bertero - June 1981(PB82 113 358)A11

UCB/EERC-81/08 "The Undrained Shearing Resistance of Cohesive Soils at Large Deformations," by M.R. Pyles and H.B. Seed - August 1981

UCB/EERC-81/09 "Experimental Behavior of a Spatial Piping System with Steel Energy Absorbers Subjected to a Simulated Differential Seismic Input," by S.F. Stiemer, W.G. Godden and J.M. Kelly - July 1981

UCB/EERC-81/10 "Evaluation of Seismic Design Provisions for Masonry in the United States," by B.I. Sveinsson, R.L. Mayes and H.D. McNiven - August 1981 (PB82 166 075)A08

UCB/EERC-81/11 "Two-Dimensional Hybrid Modelling of Soil-Structure Interaction," by T.-J. Tzong, S. Gupta and J. Penzien - August 1981(PB82 142 118)A04

UCB/EERC-81/12 "Studies on Effects of Infills in Seismic Resistant R/C Construction," by S. Brokken and V.V. Bertero - September 1981 (PB82 166 190)A09

UCB/EERC-81/13 "Linear Models to Predict the Nonlinear Seismic Behavior of a One-Story Steel Frame," by H. Valdimarsson, A.H. Shah and H.D. McNiven - September 1981(PB82 138 793)A07

UCB/EERC-81/14 "TLUSH: A Computer Program for the Three-Dimensional Dynamic Analysis of Earth Dams," by T. Kagawa, L.H. Mejia, H.B. Seed and J. Lysmer - September 1981(PB82 139 940)A06

UCB/EERC-81/15 "Three Dimensional Dynamic Response Analysis of Earth Dams," by L.H. Mejia and H.B. Seed - September 1981 (PB82 137 274)A12

UCB/EERC-81/16 "Experimental Study of Lead and Elastomeric Dampers for Base Isolation Systems," by J.M. Kelly and S.B. Hodder - October 1981 (PB82 166 182)A05

UCB/EERC-81/17 "The Influence of Base Isolation on the Seismic Response of Light Secondary Equipment," by J.M. Kelly - April 1981 (PB82 255 266)A04

UCB/EERC-81/18 "Studies on Evaluation of Shaking Table Response Analysis Procedures," by J. Marcial Blondet - November 1981 (PB82 197 278)A10

UCB/EERC-81/19 "DELIGHT.STRUCT: A Computer-Aided Design Environment for Structural Engineering," by R.J. Balling, K.S. Pister and E. Polak - December 1981 (PB82 218 496)A07

UCB/EERC-81/20 "Optimal Design of Seismic-Resistant Planar Steel Frames," by R.J. Balling, V. Ciampi, K.S. Pister and E. Polak - December 1981 (PB82 220 179)A07

UCB/EERC-82/01 "Dynamic Behavior of Ground for Seismic Analysis of Lifeline Systems," by T. Sato and A. Der Kiureghian - January 1982 (PB82 218 926)A05

UCB/EERC-82/02 "Shaking Table Tests of a Tubular Steel Frame Model," by Y. Ghanaat and R. W. Clough - January 1982 (PB82 220 161)A07

UCB/EERC-82/03 "Behavior of a Piping System under Seismic Excitation: Experimental Investigations of a Spatial Piping System supported by Mechanical Shock Arrestors and Steel Energy Absorbing Devices under Seismic Excitation," by S. Schneider, H.-M. Lee and W. G. Godden - May 1982 (PB83 172 544)A09

UCB/EERC-82/04 "New Approaches for the Dynamic Analysis of Large Structural Systems," by E. L. Wilson - June 1982 (PB83 148 080)A05

UCB/EERC-82/05 "Model Study of Effects of Damage on the Vibration Properties of Steel Offshore Platforms," by F. Shahrivar and J. G. Bouwkamp - June 1982 (PB83 148 742)A10

UCB/EERC-82/06 "States of the Art and Practice in the Optimum Seismic Design and Analytical Response Prediction of R/C Frame-Wall Structures," by A. E. Aktan and V. V. Bertero - July 1982 (PB83 147 736)A05

UCB/EERC-82/07 "Further Study of the Earthquake Response of a Broad Cylindrical Liquid-Storage Tank Model," by G. C. Manos and R. W. Clough - July 1982 (PB83 147 744)A11

UCB/EERC-82/08 "An Evaluation of the Design and Analytical Seismic Response of a Seven Story Reinforced Concrete Frame - Wall Structure," by F. A. Charney and V. V. Bertero - July 1982(PB83 157 628)A09

UCB/EERC-82/09 "Fluid-Structure Interactions: Added Mass Computations for Incompressible Fluid," by J. S.-H. Kuo - August 1982 (PB83 156 281)A07

UCB/EERC-82/10 "Joint-Opening Nonlinear Mechanism: Interface Smeared Crack Model," by J. S.-H. Kuo - August 1982 (PB83 149 195)A05

UCB/EERC-82/11 "Dynamic Response Analysis of Techi Dam," by R. W. Clough, R. M. Stephen and J. S.-H. Kuo - August 1982 (PB83 147 496)A06

UCB/EERC-82/12 "Prediction of the Seismic Responses of R/C Frame-Coupled Wall Structures," by A. E. Aktan, V. V. Bertero and M. Piazza - August 1982 (PB83 149 203)A09

UCB/EERC-82/13 "Preliminary Report on the SMART 1 Strong Motion Array in Taiwan," by B. A. Bolt, C. H. Loh, J. Penzien, Y. B. Tsai and Y. T. Yeh - August 1982 (PB83 159 400)A10

UCB/EERC-82/14 "Shaking-Table Studies of an Eccentrically X-Braced Steel Structure," by M. S. Yang - September 1982 (PB83 260 778)A12

UCB/EERC-82/15 "The Performance of Stairways in Earthquakes," by C. Roha, J. W. Axley and V. V. Bertero - September 1982 (PB83 157 693)A07

UCB/EERC-82/16 "The Behavior of Submerged Multiple Bodies in Earthquakes," by W.-G. Liao - Sept. 1982 (PB83 158 709)A07

UCB/EERC-82/17 "Effects of Concrete Types and Loading Conditions on Local Bond-Slip Relationships," by A. D. Cowell, E. P. Popov and V. V. Bertero - September 1982 (PB83 153 577)A04

UCB/EERC-82/18 "Mechanical Behavior of Shear Wall Vertical Boundary Members: An Experimental Investigation," by M. T. Wagner and V. V. Bertero - October 1982 (PB83 159 764)A05

UCB/EERC-82/19 "Experimental Studies of Multi-support Seismic Loading on Piping Systems," by J. M. Kelly and A. D. Cowell - November 1982

UCB/EERC-82/20 "Generalized Plastic Hinge Concepts for 3D Beam-Column Elements," by P. F.-S. Chen and G. H. Powell - November 1982 (PB03 247 981)A13

UCB/EERC-82/21 "ANSR-III: General Purpose Computer Program for Nonlinear Structural Analysis," by C. V. Oughourlian and G. H. Powell - November 1982 (PB83 251 330)A12

UCB/EERC-82/22 "Solution Strategies for Statically Loaded Nonlinear Structures," by J. W. Simons and G. H. Powell - November 1982 (PB83 197 970)A06

UCB/EERC-82/23 "Analytical Model of Deformed Bar Anchorages under Generalized Excitations," by V. Ciampi, R. Eligehausen, V. V. Bertero and E. P. Popov - November 1982 (PB83 169 532)A06

UCB/EERC-82/24 "A Mathematical Model for the Response of Masonry Walls to Dynamic Excitations," by H. Sucuoğlu, Y. Mengi and H. D. McNiven - November 1982 (PB83 169 011)A07

UCB/EERC-82/25 "Earthquake Response Considerations of Broad Liquid Storage Tanks," by F. J. Cambra - November 1982 (PB83 251 215)A09

UCB/EERC-82/26 "Computational Models for Cyclic Plasticity, Rate Dependence and Creep," by B. Mosaddad and G. H. Powell - November 1982 (PB83 245 829)A08

UCB/EERC-82/27 "Inelastic Analysis of Piping and Tubular Structures," by M. Mahasuverachai and G. H. Powell - November 1982 (PB83 249 987)A07

UCB/EERC-83/01 "The Economic Feasibility of Seismic Rehabilitation of Buildings by Base Isolation," by J. M. Kelly - January 1983 (PB83 197 988)A05

UCB/EERC-83/02 "Seismic Moment Connections for Moment-Resisting Steel Frames," by E. P. Popov - January 1983 (PB83 195 412)A04

UCB/EERC-83/03 "Design of Links and Beam-to-Column Connections for Eccentrically Braced Steel Frames," by E. P. Popov and J. O. Malley - January 1983 (PB83 194 811)A04

UCB/EERC-83/04 "Numerical Techniques for the Evaluation of Soil-Structure Interaction Effects in the Time Domain," by E. Bayo and E. L. Wilson - February 1983 (PB83 245 605)A09

UCB/EERC-83/05 "A Transducer for Measuring the Internal Forces in the Columns of a Frame-Wall Reinforced Concrete Structure," by R. Sause and V. V. Bertero - May 1983 (PB84 119 494)A06

UCB/EERC-83/06 "Dynamic Interactions between Floating Ice and Offshore Structures," by P. Croteau - May 1983 (PB84 119 486)A16

UCB/EERC-83/07 "Dynamic Analysis of Multiply Tuned and Arbitrarily Supported Secondary Systems," by T. Igusa and A. Der Kiureghian - June 1983 (PB84 118 272)A11

UCB/EERC-83/08 "A Laboratory Study of Submerged Multi-body Systems in Earthquakes," by G. R. Ansari - June 1983 (PB83 261 842)A17

UCB/EERC-83/09 "Effects of Transient Foundation Uplift on Earthquake Response of Structures," by C.-S. Yim and A. K. Chopra - June 1983 (PB83 261 396)A07

UCB/EERC-83/10 "Optimal Design of Friction-Braced Frames under Seismic Loading," by M. A. Austin and K. S. Pister - June 1983 (PB84 119 288)A06

UCB/EERC-83/11 "Shaking Table Study of Single-Story Masonry Houses: Dynamic Performance under Three Component Seismic Input and Recommendations," by G. C. Manos, R. W. Clough and R. L. Mayes - June 1983

UCB/EERC-83/12 "Experimental Error Propagation in Pseudodynamic Testing," by P. B. Shing and S. A. Mahin - June 1983 (PB84 119 270)A09

UCB/EERC-83/13 "Experimental and Analytical Predictions of the Mechanical Characteristics of a 1/5-scale Model of a 7-story R/C Frame-Wall Building Structure," by A. E. Aktan, V. V. Bertero, A. A. Chowdhury and T. Nagashima - August 1983 (PB84 119 213)A07

UCB/EERC-83/14 "Shaking Table Tests of Large-Panel Precast Concrete Building System Assemblages," by M. G. Oliva and R. W. Clough - August 1983

UCB/EERC-83/15 "Seismic Behavior of Active Beam Links in Eccentrically Braced Frames," by K. D. Hjelmstad and E. P. Popov - July 1983 (PB84 119 676)A09

UCB/EERC-83/16 "System Identification of Structures with Joint Rotation," by J. S. Dimsdale and H. D. McNiven - July 1983

UCB/EERC-83/17 "Construction of Inelastic Response Spectra for Single-Degree-of-Freedom Systems," by S. Mahin and J. Lin - July 1983

UCB/EERC-83/18 "Interactive Computer Analysis Methods for Predicting the Inelastic Cyclic Behaviour of Structural Sections," by S. Kaba and S. Mahin - July 1983

UCB/EERC-83/19 "Effects of Bond Deterioration on Hysteretic Behavior of Reinforced Concrete Joints," by F.C. Filippou, E.P. Popov and V.V. Bertero - August 1983

UCB/EERC-83/20 "Analytical and Experimental Correlation of Large-Panel Precast Building System Performance," by M.G. Oliva, R.W. Clough, M. Velkov, P. Gavrilovic and J. Petrovski - November 1983

UCB/EERC-83/21 "Mechanical Characteristics of Materials Used in a 1/5 Scale Model of a 7-Story Reinforced Concrete Test Structure," by V.V. Bertero, A.E. Aktan, H.G. Harris and A.A. Chowdhury - September 1983

UCB/EERC-83/22 "Hybrid Modelling of Soil-Structure Interaction in Layered Media," by T.-J. Tzong and J. Penzien - October 1983

UCB/EERC-83/23 "Local Bond Stress-Slip Relationships of Deformed Bars under Generalized Excitations," by R. Eligehausen, E.P. Popov and V.V. Bertero - October 1983

UCB/EERC-83/24 "Design Considerations for Shear Links in Eccentrically Braced Frames," by J.O. Malley and E.P. Popov - November 1983

UCB/EERC-84/01 "Pseudodynamic Test Method for Seismic Performance Evaluation: Theory and Implementation," by P.-S. Shing and S.A. Mahin - January 1984